Physical volcanology and hydrothermal alteration of the Rainy River Gold Project, northwest Ontario

A THESIS
SUBMITTED TO THE FACULTY OF THE GRADUATE SCHOOL
OF THE UNIVERSITY OF MINNESOTA
BY

Jakob Michael Wartman

IN PARTIAL FULFILLMENT OF THE REQUIREMENTS
FOR THE DEGREE OF
MASTER OF SCIENCE

Dr. Ron Morton

July 2011

Acknowledgements

I'd like to thank my advisors Dr. Morton and Dr. Hudak, who have been invaluable to my understanding of how to be become a good geologist and for their feedback and help along the way. There guidance has helped make this thesis possible and I don't know where I'd be without them. And to Dr. Siders for teaching the best class I have ever taken and I know in another life I would have been a physical chemist.

I'd like to thank everyone who has ever been a role model or a mentor to me in my geological education: Dr. Craddock, Dr. Kirby, Dr. Miller, Dr. Peterson and Jeff Thole. You've all helped form me into the person and the scientist I have become today.

I would also like to express my extreme gratitude to Rainy River Resources who made this project possible with their generous funding and their willingness to take on an American to work on their great project. Special thanks to the geologist at Rainy River, particularly Cory Hercun and Amy Shute who had great feedback and are some of the most astute field geologists I've met.

Finally, to my family, John, Gretchen and Sarah who gave me the foundation to achieve great things and Emily for always being there when I needed someone.

Abstract

The Rainy River Gold Project (RRGP) is located 75km northwest of Fort Frances, Ontario, within the Rainy River Greenstone Belt. This advanced stage exploration project has a NI43-101 compliant gold resource of 6.6 Moz indicated and inferred and 14.7 Moz indicated and inferred silver (from Rainy River Resources Press Release, February 2011) represented by low grade (<2g/t), low-moderate grade (2-10g/t), and high grade (>10g/t) gold mineralization. The nature of the gold mineralization in this deposit has been the subject of controversy, and several competing models have been proposed to explain its genesis. Initial exploration in 1967 suggested that the deposit was a shear zone-hosted resource. However, recently completed exploration drilling has now defined large, diffuse zones of gold mineralization in dacitic volcanic and volcaniclastic rocks, suggesting, in part, a syn-genetic genesis for the gold mineralization. While previous studies have examined structural regimes and timing of gold mineralization, this research focuses on the physical volcanology and hydrothermal alteration associated with the deposit.

Field mapping is difficult due to a paucity of outcrop, and geological correlations are complicated by polyphase deformation, hydrothermal alteration, and both regional, and locally contact, metamorphism. This study included comprehensive fieldwork involving mapping of all available outcrops and compiling them at a 1:25,000 scale and exploration drill core logging along three sections totaling ~9000 m of core. Fieldwork, supplemented with petrographic studies of 210 thin sections and lithogeochemical investigations comprising 69 samples, has enabled distinction of stratigraphy, volcanic facies, and hydrothermal alteration assemblages, and enabled processes associated with hydrothermal metasomatism to be evaluated.

Drill core is locally intensely altered and deformed, resulting in many of the units having false pyroclastic textures (Allen, 1988). Despite this, strata associated with the RRGP contain some well-preserved primary textures. These primary textures indicate that the volcanic facies in the deposit include coherent dacitic flows and associated syn-volcanic intrusions with autoclastic breccias, hyaloclastites, peperites, and syn- to post-depositional resedimented volcaniclastic deposits. The coherent dacitic flows are

massive, range in thickness up to 150 m, and in lateral extent for 2500 meters. Coherent dacite flows grade into a heterogeneous facies, characterized by pods and lobes of coherent dacite, enveloped by autoclastic breccia and hyaloclastite. Flows are interspersed with strongly altered volcaniclastic sediments that are locally punctuated by peperites. Volcanic facies reconstruction indicates the presence of lobe-hyaloclastite dome/flow complex fed, and locally intruded by, synvolcanic dacite hypabyssal intrusions. An apparent feeding fissure is centered to the west of the main area of mineralization.

Hydrothermal alteration is widespread throughout the deposit and is marked by silicification, chloritization, sericitization, and carbonitization (as well as minor epidote and local biotite alteration). Quartz, sericite and chlorite are ubiquitous in the deposit. The isocon method developed by Grant (1986) and the box plot method developed by Large et al. (2001) were utilized to quantify the chemical alteration resulting from the hydrothermal alteration in RRGP rocks. Alteration assemblages are dominantly stratabound, and their distribution is related to original rock permeability, with flow tops, autoclastic breccias, and volcaniclastic sediments being most strongly altered. Shear-zones also preserve stronger alteration intensities.

Gold mineralization appears to have initially occurred within a synvolcanic, low-sulfidation (Simmons et al., 2005) epithermal system. Elevated gold values are strongly correlated with highly permeable units and increased alteration intensity, suggesting enhanced mineralization in areas that experienced higher water: rock ratios. Post-volcanic remobilization of the gold appears to have occurred, as the highest gold values in the deposit are spatially related to shear-zones and associated quartz-carbonate-epidote veins.

Table of Contents

List of Tables

List of Figures

1.0 Introduction

The Rainy River Gold Project (RRGP) in northwestern Ontario (Fig. 1) is a gold deposit hosted in a ~700 m thick felsic succession of dacitic lava flows and associated breccias and mafic tuffs. Within this felsic succession Rainy River Resources Ltd. (RRRL) has defined an NI 43-101 compliant indicated and inferred resource of 6.6 Moz gold and 14.7 Moz indicated and inferred silver (from Rainy River Resources Press Release, February 2011). The genesis of the felsic succession and associated gold mineralization has been the subject of controversy, and several competing models have been proposed to explain its origin. Mineralization around the RRGP has attracted exploration since 1967, and was first explored and evaluated as a shear zone-hosted resource (Cole et al., 2009). Subsequent drilling, however, defined large, diffuse zones of gold mineralization in the dacitic volcanic rocks (Cole et al., 2009). This pervasive, low-grade, disseminated style of mineralization more closely fits an epithermal deposit model than the typical Superior Province orogenic gold model (Cooke and Simmons, 2000). The deposit continues to be developed and evaluated by RRRL.

1.1 Purpose of study

Because of the controversy surrounding the nature of the gold mineralization, there is much to be gained by studying the physical volcanology and hydrothermal alteration associated with the deposit, especially as understanding the volcanic processes may lead to a better understanding of gold genesis. The volcanology and facies architecture at the RRGP have previously been described only briefly as parts of studies that focused on: 1) the structure and kinematics of the deposit (e.g. Ayers, 1997; Siddorn, 2007; and Cole et al., 2009); and 2) the composition of gold and associated sulfides (Schandl, 2006). Paucity of outcrop and locally intense deformation makes stratigraphic correlation between areas difficult and has hampered regional scale reconstruction of the facies architecture. However, expanded drilling by RRRL, now with a core repository of over 500,000 m from 750+ exploration drill holes, has provided valuable information on the lithologies and stratigraphy of the RRGP. Using the extensive core library and the available outcrops the purpose of this thesis is to:

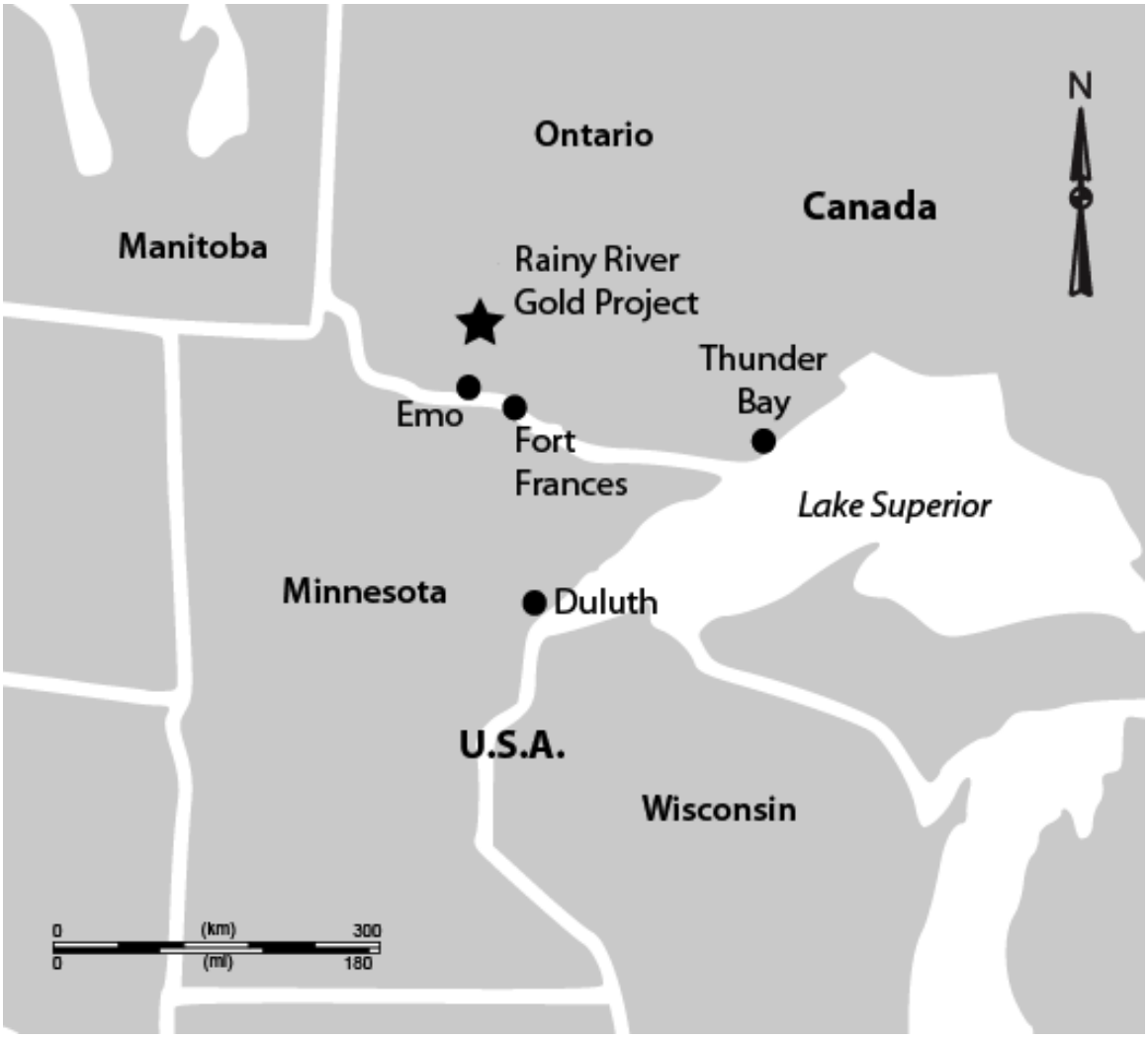

Figure 1. Location map of the RRGP.

1. determine the detailed stratigraphy, lithological facies, and hydrothermal alteration mineral assemblages associated with the deposit,
2. determine the physical volcanology of the deposit based on stratigraphic units and lithological facies,
3. define mineralogically and spatially the hydrothermal alteration in and around the ore body,
4. formulate a model for the genesis of the deposit and compare it to previously established models of gold formation.

1.2 Location

The RRGP is centered in Richardson Township, 50 km northwest of Fort Frances, Ontario and 250 km northwest of Duluth, MN (Fig. 1). Access is available year round on Provincial Road 600 located 8 km west of the Trans-Canada Highway. The area around the RRGP is largely held by RRRL with minor holdings by Bayfield Ventures Corporation. The area is sparsely populated and is part of the Canadian northeastern hardwood region, on the southern margin of the boreal forest (Cullen et al., 2005).

The RRGP is located within the Severn Upland of the Canadian Shield and divided into two main physiographical regions by the Rainy Lake-Lake of the Woods Moraine (Cullen et al., 2005). To the north and east is a Precambrian highland, only sparsely covered by glacial drift with relief of 90 m or more, resulting in substantial outcrops (Mackie et al., 2003). Areas to the west and south of the RRGP have been significantly affected by late-Wisconsin glaciation and are typically overlain by 20-40 m of glacial till, which causes poor drainage and poor outcrop exposure (Mackie et al., 2003). Most of the RRGP is located within a lowland area and due to substantial amounts of glacial till (20-40 m), only ~2% of the RRGP area contains outcrop exposures (Bajc, 1991).

1.3 Regional geology

The RRGP is part of the larger Rainy River Greenstone Belt (RRGB), located between Lake of the Woods and Rainy Lake in the western portion of the Wabigoon

Subprovince of the Canadian Shield (Stott, 2007). The Wabigoon Subprovince is a volcanic-plutonic belt interposed between the sedimentary-plutonic Quetico Belt to the south and the English River Belt to the north (Stott, 2007). This subprovince trends east to west from northwestern Minnesota to central Ontario, a distance of ~900 km (Stott, 2007). The Wabigoon comprises a wide variety of volcanic assemblages with affinities ranging from ultramafic to felsic (Blackburn, 1981) and has been previously interpreted as representing ocean floor or plateau and arc-like environments (Percival, 2006). Typically, felsic volcanic and volcaniclastic rocks overlay massive to pillowed ultramafic to mafic lava flows and are succeeded in stratigraphic height by clastic and chemical sediments (Blackburn, 1981). A large number of granitoid batholiths and diapirs intrude the Wabigoon and form synformal structures in the supracrustal rocks creating large shear zones (Condie, 1981). All of the rocks within the Wabigoon preserve some sense of alteration, and have been dominantly metamorphosed to greenschist facies, although amphibolites facies rocks exist locally (Condie, 1981).

1.4 Previous work

Bedrock geology of the RRGB was compiled by Blackburn (1981) using geophysical surveys and the results of Ontario Geological Survey (OGS) drill programs to complete OGS Map 243 at a 1:253,440 scale (Fig. 2). Previous deposit scale work by RRRL and Nuinsco Resources has grouped the rocks into nine broad units (Mackie et al., 2003 and Cullen et al., 2005) and 45 individual lithologies varying from “tholeiitic, high-iron and magnesium basalt flows” to “pebble conglomerates.” Many of these divisions have been strongly influenced by pseudo-textures. No previous petrographic analysis on all individual lithologies has been done, and lithogeochemistry has previously been limited to major and minor element analysis.

Several previous studies have defined major structural features of the deposits, and regionally, a well-defined penetrative fabric is observed. The foliation is commonly similar to the strike and dip of the volcanic rocks, striking ~300 degrees with a dip 50-70 degrees to the south (Cole et al., 2009). In all lithologies within the main mineralized zones there is a steep southwest plunging lineation present, and kinematic indicators

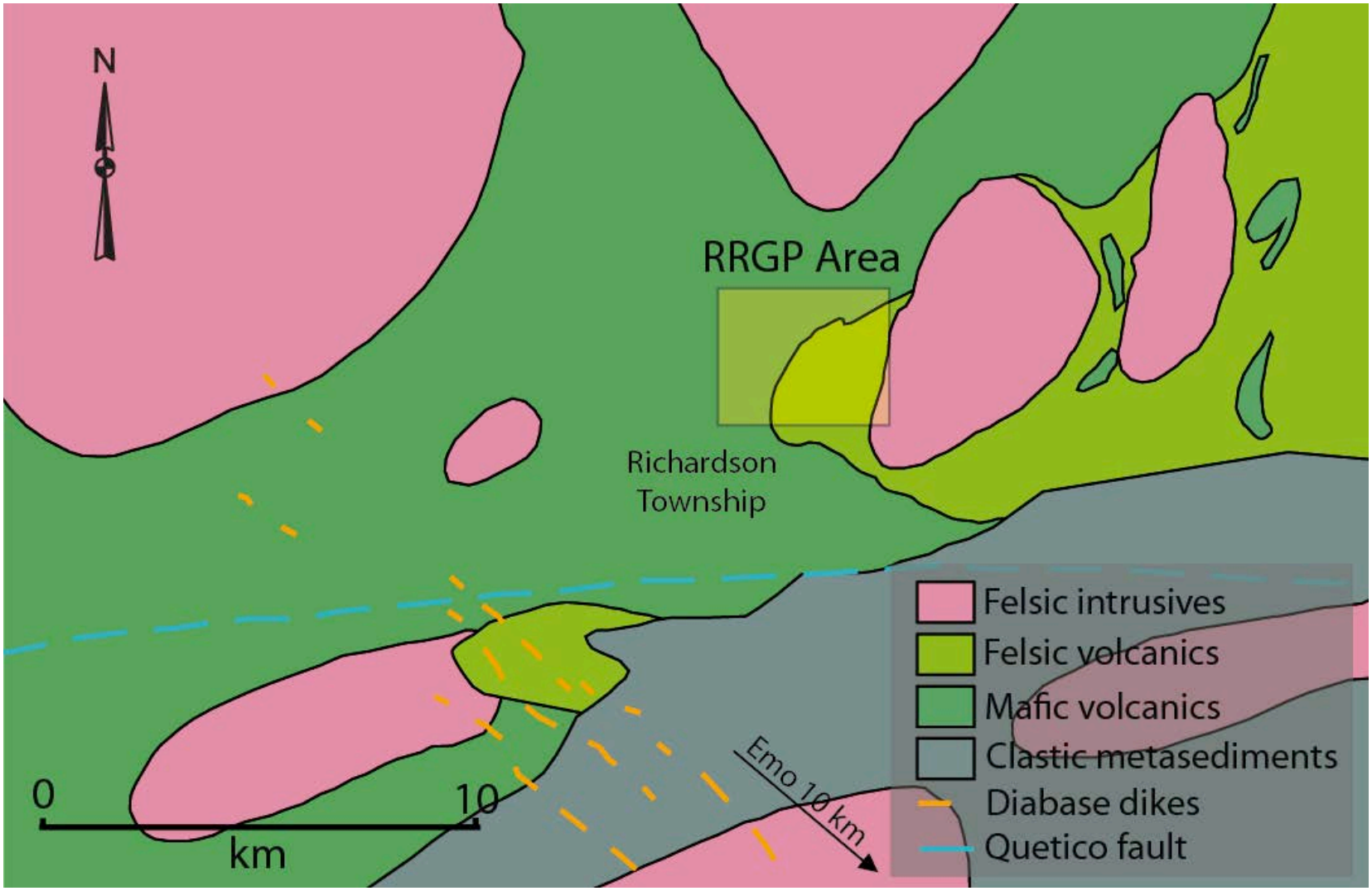

Figure 2. Regional geology of the RRGP area compiled by the OGS in Map 2443. The location of the RRGP area is highlighted. Map modified from Blackburn (1981).

suggest a south reverse-sinistral movement (Siddorn, 2007). This area has also been offset by late, north-south brittle faulting (Ayers, 1997). A study of the immediate area's structure by Siddorn (2007) showed that:

1. auriferous mineralization is aligned with the regional foliation,
2. gold mineralization had a strong overprint from shear deformation,
3. fold axes of auriferous quartz veins and sulfide zones are rotated sub-parallel to the stretching lineation,
4. fold axes and stretching lineation are sub-parallel to the plunge of the gold mineralization;
5. sulfide mineralization is deformed by late stage folding.

A study conducted by Schandl (2006) defined a paragenetic sequence of mineralization and the composition and mineralogy of gold mineralization in the deposit, noting that:

1. gold mineralization is hosted in pyrite-rich volcaniclastic rocks of dacitic composition,
2. auriferous rocks have been extensively altered,
3. gold and electrum occur as inclusions in pyrite, and disseminated in sphalerite, carbonates (ankerite and dolomite) or fine-grained silicates
4. gold mineralization took place during two separate episodes:
    a. an early period when hydrothermal fluids enriched in metalliferous ions precipitated gold and electrum—possibly contemporaneous with early hydrothermal alteration,
    b. a latter event associated with metamorphism and the recrystallization of minerals which resulted in concentrating the gold.

The identification of two different periods of gold mineralization, one early and one late, has lead to two separate genetic models to explain the gold mineralization. Initially, Nuinsco Resources interpreted the gold mineralization to be epigenetic in origin due to its spatial relationship to sheared rocks. This orogenic model was based on gold mineralization constrained to quartz-carbonate style veins within the deposit. According to this model, the ore was formed by gold-rich aqueous fluids percolating through the

rocks during brittle deformational periods (Groves et al., 2003). However, as exploration progressed, large diffuse zones of gold mineralization were found within the deposit. The subsequent model was based on an epithermal-like volcanogenic massive sulfide (VMS) model because of the strong sodium depletion, potassium enrichment, gold-pyrite association, a high gold to silver ratio, as well as ubiquitous sphalerite, and chalcopyrite (Cullen et al., 2005). Gold mineralization in this model is directly linked to volcanism, and the precipitation of metalliferous sulfides in zones at or near a volcanic center (Franklin et al., 2005).

1.5 Methods

Fieldwork occurred in two stages during an eight week period from May to August during 2010. The first stage involved field mapping of all the outcrops in the RRGP area. Twenty-five outcrops were mapped and compiled at a 1:25,000 scale. Mapping was used to identify rock units, structures, alteration, and primary textures. Before mapping, outcrops were cleaned with water and bleach to elucidate the textures within the rocks. Additionally, a GPS unit was used to accurately locate outcrops. Mapping was compiled in NAD83 UTM 15N. Samples were collected from each outcrop.

The second stage consisted of logging diamond drill core from the RRGP area. Three transects were selected to provide a complete view of the stratigraphy. A total of 14 drill holes and ~9000 m of diamond drill core were logged from these three transects. In addition to the three transects, four periphery holes were reconnaissance logged to observe changes near the flanks of the RRGP. Core was logged and samples taken based on both alteration and lithology. Data gathered from mapping and core logging was digitized into ArcMap and Interdex to create final maps and cross sections of the lithologies and alteration of the area around the RRGP (Plates 1 and 2).

One hundred and eighty-five standard thin sections, 11 large format thin sections and 31 polished sections were made from the samples collected from outcrops and diamond drill core (see Appendix I). These thin sections and polished sections were used for petrographic analysis to delineate and identify volcanic rock types, volcanic textures,

fragment types, mineralogy, and alteration mineralogy. Due to the fine-grained nature of many of the volcanic and sedimentary rocks, the petrographic analysis was supplemented with scanning electron microscopy studies at the University of Minnesota Duluth.

Sixty-nine samples chosen to be representative of the various rock units and alteration assemblages were analyzed for whole rock lithogeochemical analyses at ALS Chemex in Thunder Bay, Ontario. The samples were evaluated for major elements, minor elements, and a suite of trace elements (see Appendix II). Using the isocon method developed by Grant (1986) and the box plot developed by Large et al. (2001) these analyses provided information regarding the metasomatic changes associated with alteration processes.

2.0 Volcanology

2.1 Introduction

Many mineralized ancient volcanic terranes have undergone strong hydrothermal alteration followed by polyphase deformation. These processes often make identifying primary textures and original volcanic rock types difficult (Allen, 1988). Alteration and deformation can produce pseudo-textures and have been noted in several prominent Archean areas including Benambra (Allen, 1988), Rouyn-Noranda (De Rosen-Spence et al., 1980), Thalanga (Paulick and McPhie, 1999) and the Mt. Keith region (Rosengren et al., 2008). The RRGP is similar to these areas as it is hosted in rocks which are polyphase deformed and have undergone mid- to upper-greenschist facies metamorphism (Mackie et al., 2003). The RRGP displays a high variability in preservation of primary textures and in the degree of alteration and deformation; schistose to mylonitic fabrics and locally intense alteration overprints are common (Figs. 3, 4, and 5).

In spite of the deformation and alteration, the units within the RRGP preserve a number of primary textures that allow the rocks to be divided into nine separate units (see Table 1). The most useful primary feature in the RRGP is the presence of quartz crystals (phenocrysts in the dacite lava flows and dacite dikes and sills) because of ubiquitous groundmass recrystallization and the destruction and replacement of many other original features. Other important primary textures used to differentiate units include fragments, phenocrysts (e.g. plagioclase feldspar), and amygdules.

Overall, the felsic succession is ~700 m in stratigraphic thickness and is overlain and underlain by homogeneous, massive to pillowed basalt lava flows. The rocks strike ~300 degrees with dip between 50-70 degrees to the south, and top to the south. The felsic volcanic succession thins to the west and east and is effectively terminated by massive to pillowed basalt lava flows. Gold mineralization at the RRGP is concentrated in the dacitic lava flows with lesser amounts in dacitic intrusions, mafic derived sediments, lapilli tuffs, and sedimentary rocks. Economic mineralization occurs in a 450 m thick section of dacitic lava flows.

Typically, fresh felsic successions can be classified using TAS diagrams-total alkalis vs. silica (LeBas et al., 1986) or TiO_2 vs. Al_2O_3 discrimination plots (Whitford et

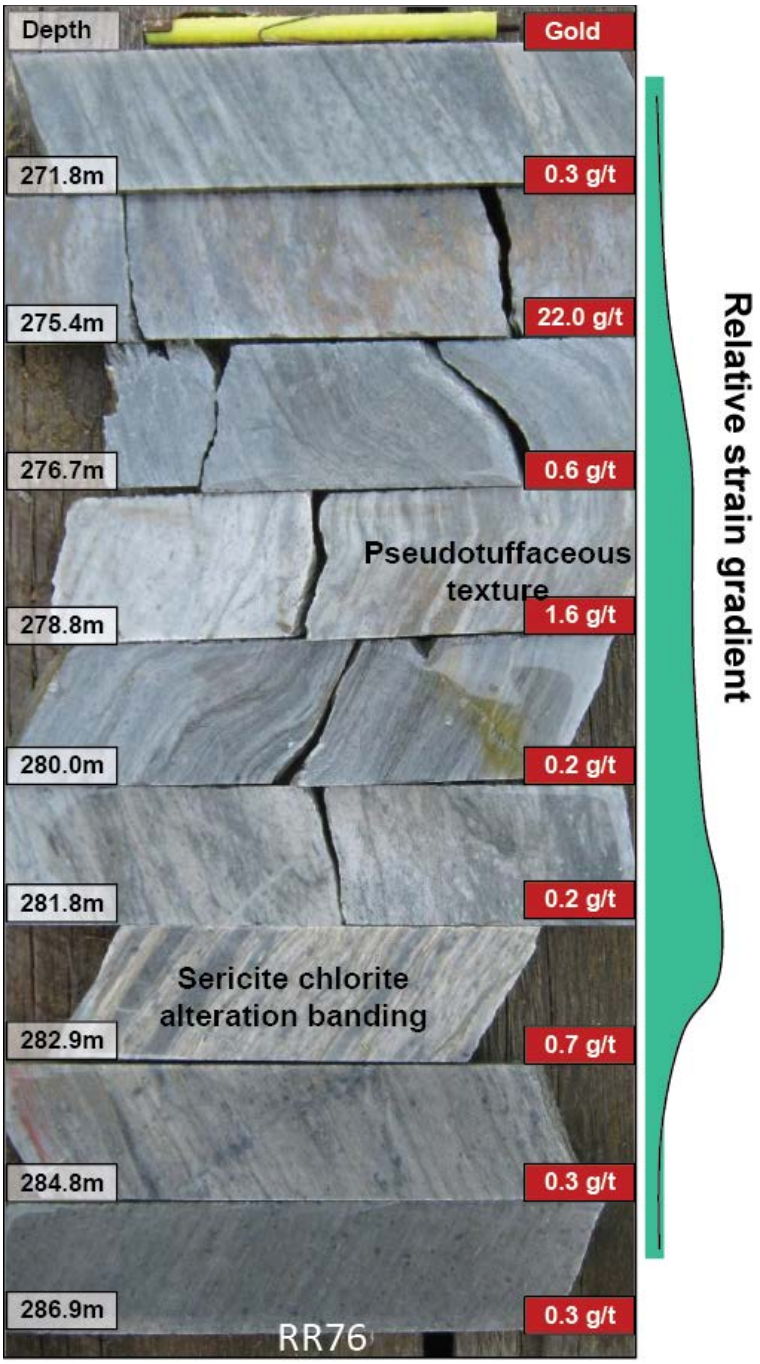

Figure 3. Psuedo-tuffaceous textures resulting from intense shearing of a dacitic lava flow in diamond drill hole RR76. Banding and apparent layering are caused by alternating chlorite and sericite domains. Image from Hrabi and Vos (2010). Pencil magnet for scale.

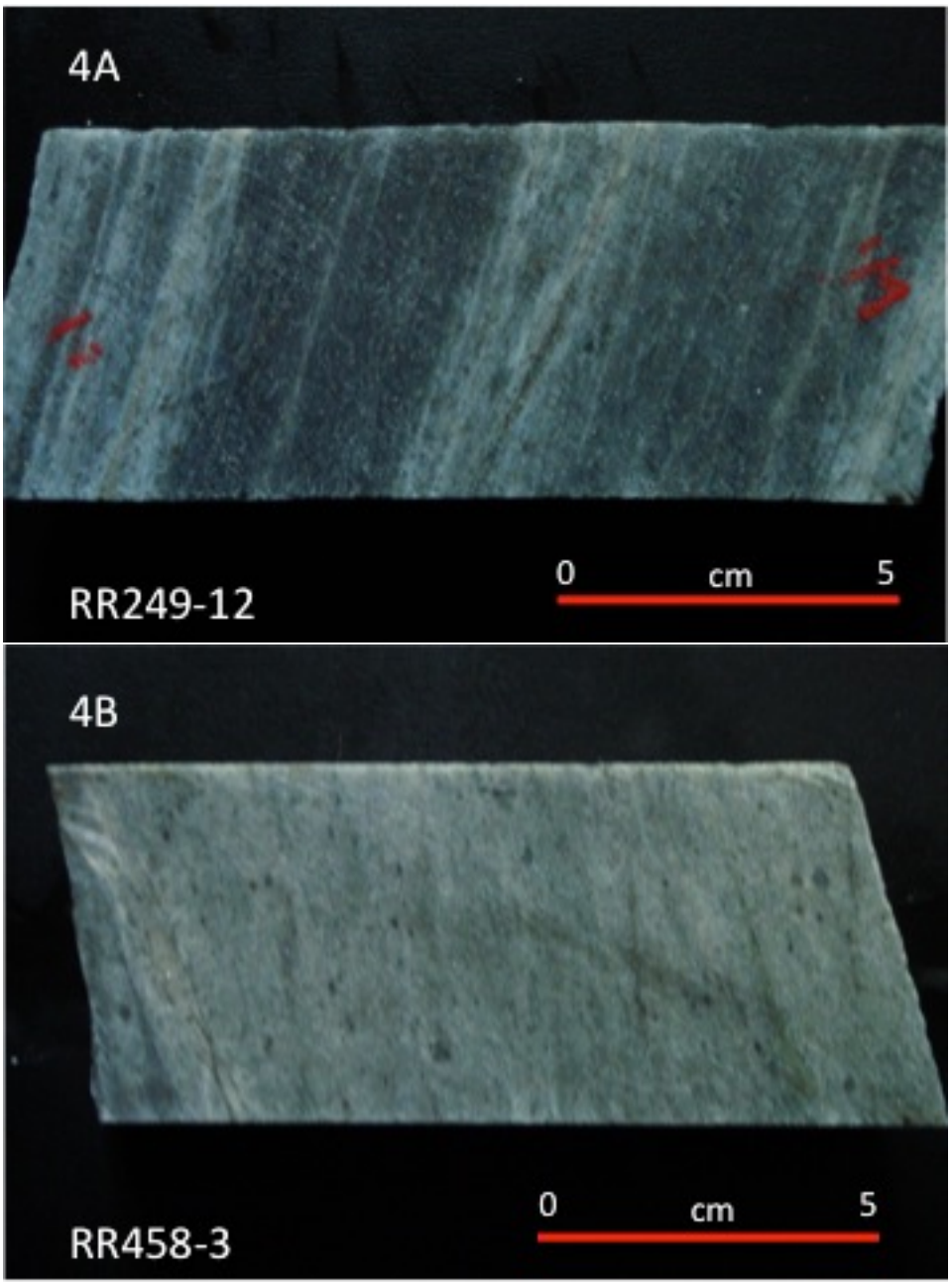

Figure 4. Difference in appearance of the dacitic lava flows in diamond drill core. Fig. 4A shows alternating sericite rich bands, which gives the rock a banded appearance in hand sample RR249-12. Fig. 4B is moderately silicified and sericitized, which results in the light tan color and homogeneous textures. The sample in Fig. 4A was originally interpreted as a tuff; the sample in Fig. 4B was interpreted as a quartz crystal tuff.

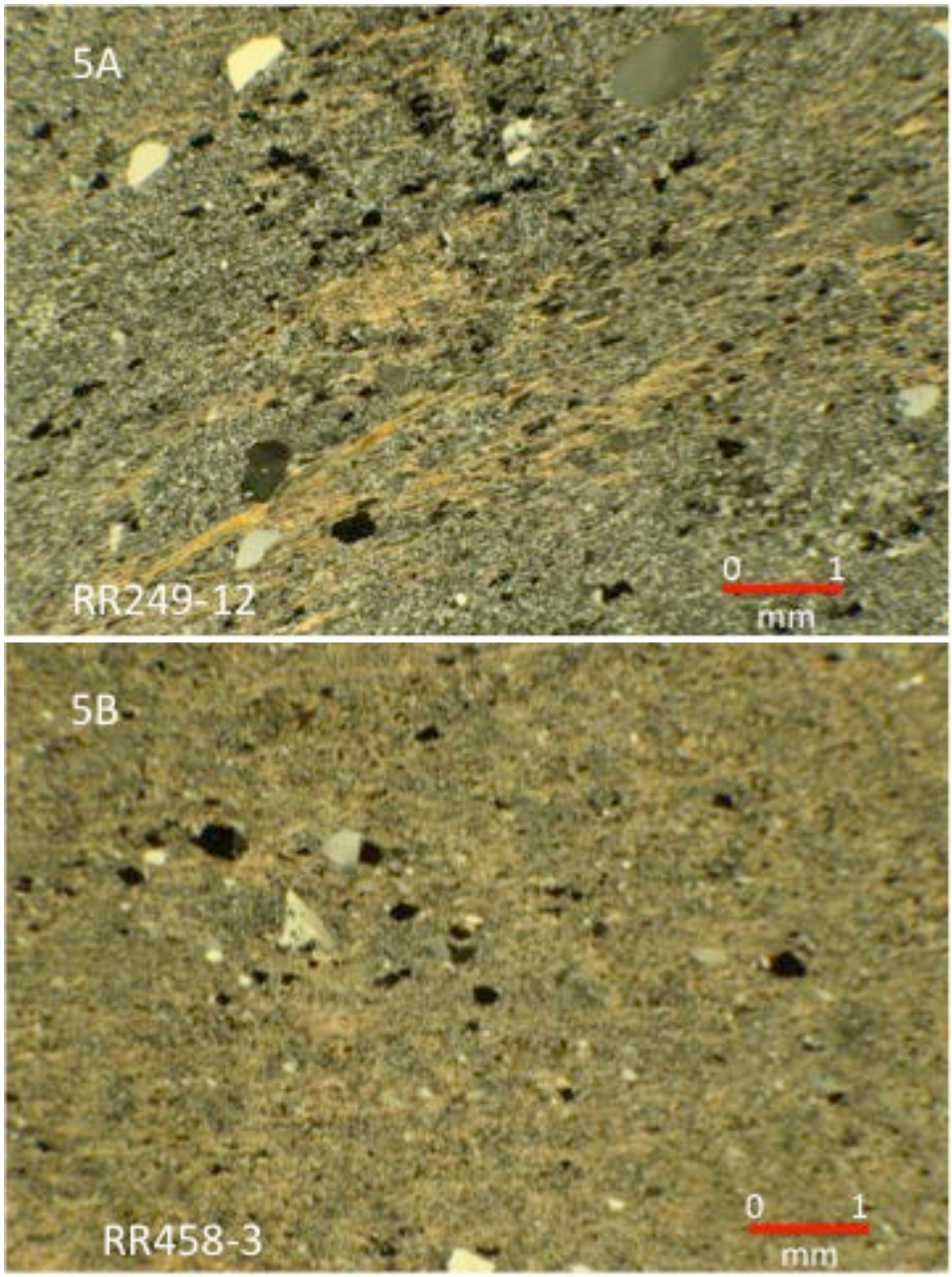

Figure 5. Photomicrographs of Figs. 4A and 4B hand samples. Well-foliated sericite bands in Fig. 5A give the hand sample a pseudo-tuffaceous texture. Disseminated sericite and quartz in Fig. 5B give the hand sample in Fig. 4B the homogeneous tan appearance. Subhedral, 0.3-1.0 mm quartz phenocrysts are disseminated throughout both samples and the groundmass is similarly made up of equigranular microcrystalline quartz and very fine-grained sericite.

Facies	Interpretation	Geometry
Basalt lava flows	Subaqueous massive and pillowed basalt lava flows	Thick horizons; laterally extensive; dominates the non-felsic stratigraphy of the RRGB; observed contacts with felsic units rare because of lack of outcrops, sharp in drill core
Mafic tuff	Mass flows related to gravitational instabilities or slumping of autoclastic units of the basalt lava flows	Two thick packages: 1) underlays the felsic succession of RRGP; and 2) separates dacite flows; other thin, 5-20 m thick units of mafic sediments intercalated with dacitic lava flows; can have: 1) sharp contacts with dacitic intrusions; or 2) gradational contacts with peperites
Dacite lava flows	Subaqueous lava flows	Horizons <10 to 150 m thick; multiple flows can be stacked; in contact with hyaloclastite, polymict lapilli tuffs, and monomictic lapilli tuffs; sharp to irregular or brecciated contacts; rare narrow cross-cutting mafic dykes
Dacite sills and dikes	Synvolcanic sills and dykes	Horizons <10 to 50 m thick; some with sharp contacts with adjacent mafic tuffs; contacts can occur as 1-2 m chilled margins when in contact with mafic tuffs or gradational with peperites; tabular to lobate
In situ monomict clast supported dacite lapilli tuff	Hyaloclastite produced by quench fragmentation	Laterally limited; horizons <1-25 m thick; closely associated with dacite lava flows; sharp to irregular upper and lower contacts
Dacite-sediment lapilli tuff	Peperites formed from the disintegration of a magma intruding a wet unconsolidated sediment	Variable layers between 5-10 m thick; gradational between dacitic sills and dikes and mafic tuffs; units are discontinuous and laterally confined
Monomict matrix supported lapilli tuff	Resedimented dacitic lava flows or hyaloclastite	Mostly thin, 4-10 m thick; sharp contacts with dacitic lava flows; laterally confined
Polymict clast to matrix supported lapilli tuff	Debris-flow deposits	Sharp contact between dacitic lava flows; laterally confined; 3 to 10 m thick; typically grades into sediments or dacitic lava flows
Sedimentary rocks	Sedimentation in a low-energy setting during times of volcanic quiescence	Thin, 1-4 m thick; argillite to sandstone and has a limited lateral extent; typically capped by polymict lapillis and dacitic lava flows

Table 1. Lithological units of the RRGP.

Textures	Textures/mineralogy
Massive to pillowed flows; sheet flows; pillows are typically bun-mattress shaped 0.3-1.5 m in size; quartz-filled amygdules increase towards rim	Aphyric to rare porphyritic (0-3% fine-grained augite); groundmass has been strongly altered with chlorite, actinolite, epidote and carbonate; 2-4%, 0.2-1.0 mm quartz-filled amygdules in pillows
Heterogeneous; made up of very fine- to fine-grained matrix material with rare mafic lapilli clasts	Matrix is dominated by chlorite, carbonate with some recrystallized quartz; mafic lapilli clasts are basalt and can be strongly amygdaloidal
Massive; rarely brecciated; variably altered and deformed; zones of strong alteration/deformation can result in pseudo-tuffs or pseudo-breccias; degree of alteration can result in homogeneous to heterogeneous appearance; quartz, calcite or pyrite-filled amygdules, highly amygdaloidal units (>40%) are likely flow tops	Sparsely to strongly porphyritic, 0-20% quartz crystals (0.15-2.5 mm, subhedral-rounded), with rare 0-5% feldspar phenocrysts (0.05-1.0 mm-lath-like to tabular), feldspar phenocrysts are absent or relict due to strong sericite alteration; very-fine to fine-grained groundmass of quartz, sericite with variable chlorite and carbonate; chunky to equigranular groundmass, rare spherulitic textures
Massive; typically less altered than dacitic lava flows; rarely pseudo-tuffaceous or pseudo-brecciated	Porphyritic, 0-25% quartz phenocrysts (0.5-5 mm, subround-round), with variable 0-25% feldspar phenocrysts (0.05-1.0 mm-lath-like to tabular); similar groundmass to dacitic lava flows
Clast-supported with angular, jigsaw fit to curviplanar clasts; variably elongate with foliation-depending on level of deformation; clast size is highly variable from millimeter to centimeter scale (1 mm-5 cm)	Clasts have identical composition to the associated dacitic lava flows; typically aphyric to sparsely porphyritic; rare amygdules; breccia matrix of ash-sized particles of dacite; matrix is strongly altered with secondary chlorite, epidote, and carbonate
Original textures are hard to distinguish given the amount of alteration in these units; highly variable appearance in hand sample based on alteration; strongly brecciated, size varies between 3 cm-1 m; deformation and alteration make breccia hard to observe in hand sample	Variable in appearance; typically strongly altered; monomict lapilli clasts; variable amount of quartz crystals, mostly absent but up to 3% (0.2-1.5 mm)-quartz typically has a strong violet color; matrix is "chunky" to inequigranular composed of dominantly secondary minerals i.e. chlorite and carbonate; chlorite can give samples mafic look in hand sample
Made up of 1-3 cm monomict clasts; clasts are elongate with foliation	Similar to in situ lapilli composition; clasts have identical composition to the associated dacite units; typically aphyric to sparsely porphyritic; breccia matrix of ash-sized particles of dacite; rare cherty clasts interbedded (<3%); rare spherulitic textures
Beds of polymict clasts; clasts are strongly elongate due to deformation; massive to graded; matrix-supported	Subround to round lapilli clasts, most 0.5-2.5 cm in diameter; clasts range from dacite to siltstone to sandstone; clasts are variably altered; dacitic lapilli sized clasts can (rare) preserve spherulitic textures; poorly sorted
Laminated; interbedded with thin beds of pyrite	Argillites composed almost entirely of opaque carbon particles with layered pyrite, and as sandstone made up of fine grained quartz with rare coarse grained disseminated pyrite

Table 1. cont.

al., 1989). However, these plots cannot be used to accurately evaluate the original geochemical characteristics of rocks that have undergone syn- or post-volcanic metasomatism. Immobile trace elements, i.e. high field strength elements (HFSE, Ti, Zr, Hf, Nb; Jenner, 1996) can be used to designate original rock types for such rocks. Winchester and Floyd (1977) diagrams, which utilize immobile trace elements, indicate that the mafic units range from basaltic to andesitic (Fig. 6) and the felsic units are dacitic (Fig. 7).

Additional classification within the volcanology section includes: 1) bedding types and bedding nomenclature which follows the classification outlined by McPhie et al. (1993); 2) volcaniclastic rocks are described according to Fisher (1960, 1966); and 3) pillow nomenclature follows Dimroth (1978).

2.2 Lithological Units

Because of syn- and post-volcanic alteration and metamorphism, many primary textures in the RRGP have been destroyed or modified. Primary features that remain include: quartz crystals, fragments, phenocrysts, and amygdules (a result of an infilled vesicle) that allow the lithological facies to be distinguished. These primary textures indicate the major rock types associated with the RRGP are dacitic sills and dikes which have intruded mafic derived tuffs, and dacitic lava flows with subordinate dacite lapilli tuffs and sedimentary rock.

In addition to primary textures and features, interfacies relationships are important in distinguishing units. These relationships are of particular importance when distinguishing dacitic sills and dikes from dacitic lava flows. Dacitic sills and dikes and dacitic lava flows are compositionally identical, but can be defined by primary textures and contact relationships.

The nine defined volcanic units are discussed below in stratigraphic order (from oldest to the youngest lithologies). All units have undergone regional mid- to upper-greenschist grade metamorphism (Mackie et al., 2003); for simplicity the prefix meta- has been dropped from naming convention.

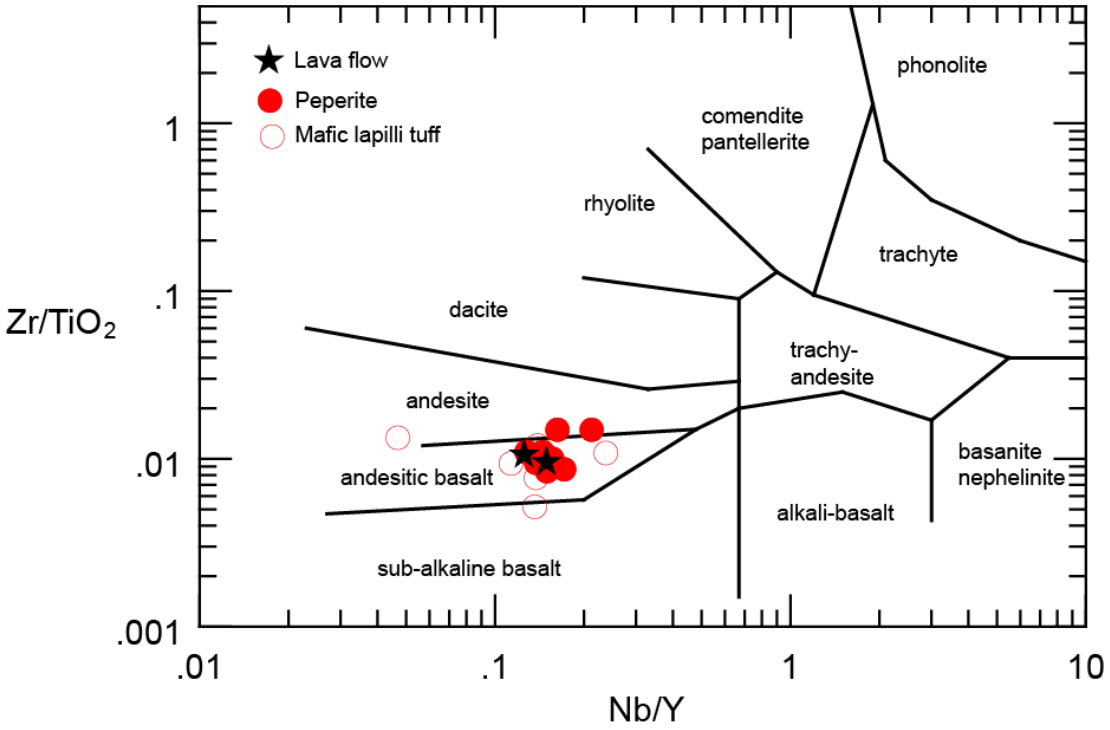

Figure 6. Winchester and Floyd (1977) immobile trace element lithological classification of mafic volcanic rocks at the RRGP.

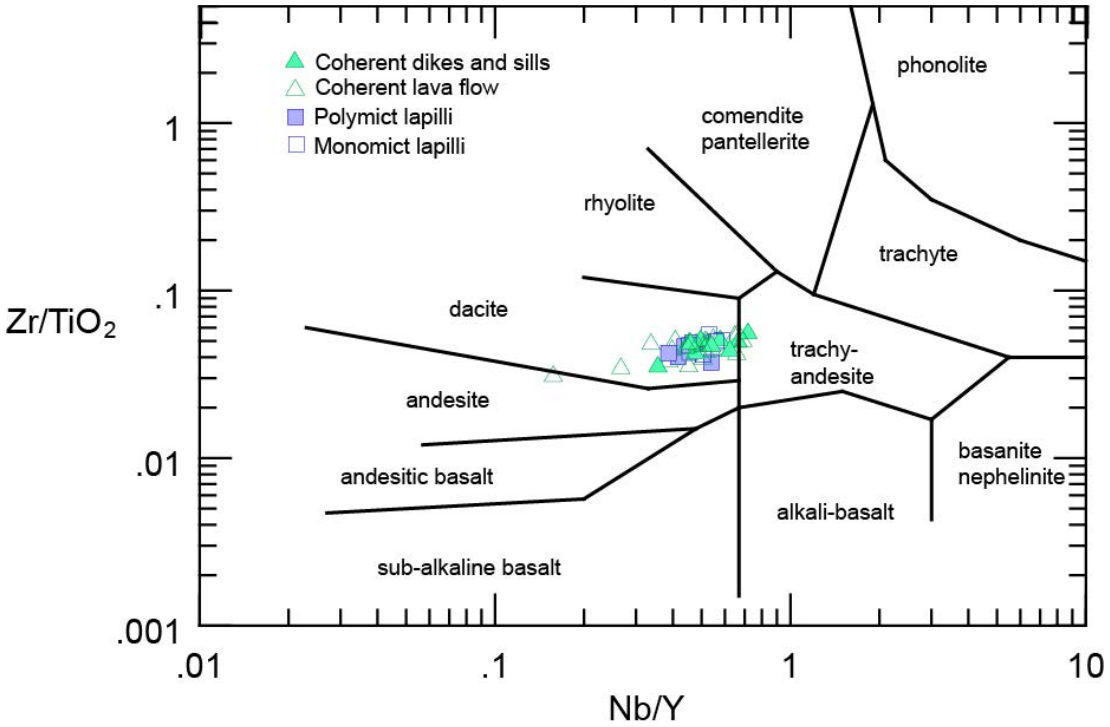

Figure 7. Winchester and Floyd (1977) immobile trace element lithological classification of felsic volcanic rocks at the RRGP.

2.2.1 Footwall and hanging wall massive to pillowed basalts

Basalts can be divided into two lava flow facies: 1) massive facies; and 2) pillowed facies. The felsic succession at the RRGP is underlain and overlain by compositionally similar basalt lava flows (Plate 1). The footwall contact between massive basalts and mafic tuffs does not outcrop, but is sharp in diamond drill core exploration holes collared to the north. The hanging wall contact has not been observed in either outcrop or drill core.

Individual massive flow thicknesses are difficult to determine because of outcrop paucity. Massive flows are nonamygdaloidal and, like the cores of the pillowed flows, display patchy epidote-quartz alteration, imparting a patchy green-grey color which occurs on a cm to meter scale. In outcrop, foliation is highly variable from nonfoliated to intensely foliated.

Pillowed lavas are typically poorly preserved, and composed of closely packed, 0.5-1.5 m wide (Fig. 8), bun to mattress shapes, with 1-2 cm wide, selvages. Selvages are now composed of fine-grained actinolite and chlorite with minor pyrite. Hyaloclastite granules range from 0.5-1.5 cm in diameter and occur along rims and/or as interpillow matrix. Near pillow margins, 2-4%, 0.2-1.0 mm quartz-filled amygdules occur.

In thin section, both massive and pillowed basalt facies can contain 0-3% fine-grained subhederal augite set in a very fine-grained equigranular groundmass composed of 20-25% chlorite, 15-20% actinolite, 25-35% epidote and 10-15% carbonate. Rare, fine-grained anhedral to cubic pyrite is disseminated through the basalt flows.

2.2.2 Mafic tuffs

Mafic tuffs occur at three discrete stratigraphic levels: 1) at the base of the volcanic succession creating the “cap zone” separating the footwall basalts from the felsic volcanics; 2) stratigraphically higher in a ~150 m interval separating dacitic lava flows (Fig. 9); and 3) interbedded in small 5-15 m lenses within dacitic lava flows (Plate 1). The mafic tuffs are intercalated with the dacite-sediment lapilli tuffs and dacitic intrusions, with gradational contacts with the dacite-sediment lapilli tuffs and sharp

Figure 8. Cleaned and bleached outcrop of flat lying basalt pillow lava, ~3 km west of the RRGP (all outcrop figure locations are labeled on Plate 1). Geo-tool rock hammer for scale.

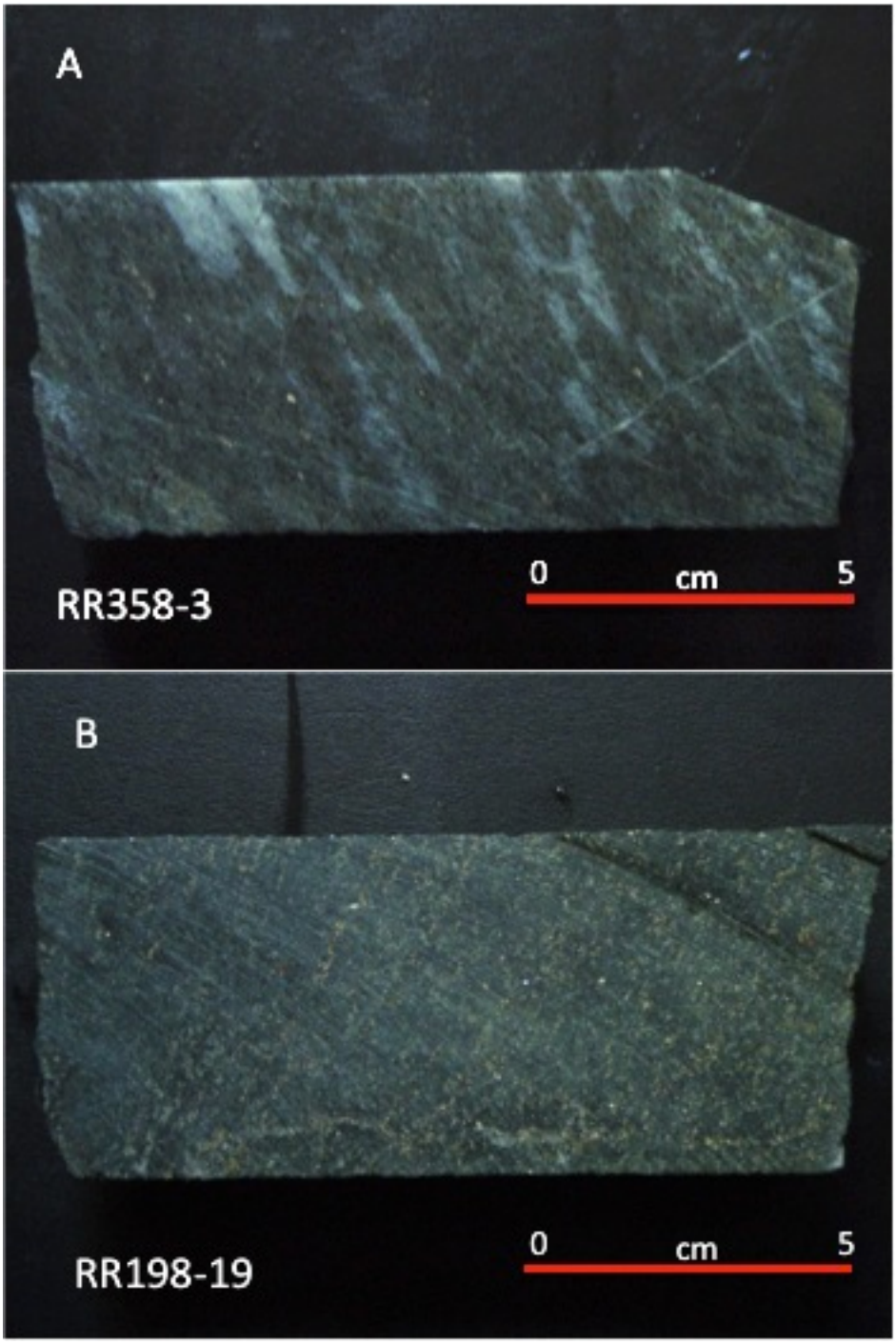

Figure 9. Two drill core samples of mafic tuff from different stratigraphic heights. Sample in Fig. 9A is from a depth of 98 m and sample in Fig. 9B is from the "cap zone" at 1222.3 m. Sample RR358-3 in Fig. 9A has abundant chlorite and carbonate disseminated in the matrix and is strongly sheared. Sample RR198-19 in Fig. 9B is from the cap zone with abundant pyrite disseminated in the matrix.

contacts with dacitic intrusions. In outcrop, mafic tuffs are dark grey to black, and often have a surface sulfide staining because of the abundance of pyrite in the matrix (Fig. 10). The unit locally contains 5-20% amygdaloidal mafic lapilli-sized clasts that strongly resemble basalt hyaloclastite. Clasts are enclosed by a very-fine grained matrix (Fig. 11). In both outcrop and diamond drill core, secondary alteration minerals have replaced most primary textures.

In thin section the mafic tuffs are very fine- to fine-grained with a matrix that ranges from equigranular to chunky. Mineral composition of the mafic tuff varies widely with quartz ranging from 10-45%, sericite 0-30%, chlorite 10-45%, ankerite and dolomite (typically disseminated with some vein filling) 5-35%, epidote 0-30%, and ferroactinolite 0-30%. Samples locally contain abundant (5-35%), fine- to medium-grained euhedral cubic pyrite, which is disseminated throughout the groundmass.

2.2.3 Dacitic dikes and sills

The mafic tuffs have been intruded by dacitic dikes and sills (Fig. 12). These intrusions vary in thickness from 5 to 25 m, and are mostly tabular to lobate and laterally confined. Contacts vary from sharp to gradational. Sharp contacts between dacitic intrusions and mafic tuffs are characterized by 1-2 m chilled margins whereas gradational contacts are common with dacite-sediment lapilli tuff. Internally the dacitic dikes and sills are massive. These units are typically less altered than dacitic lava flows.

The dacitic intrusions are similar to dacitic lava flows in mineralogical and chemical composition (Fig. 7). Quartz crystals (2-25%) vary in size from <1-5 mm (Fig. 13). Rare (0-5%), euhedral, twinned plagioclase feldspar phenocrysts range in size from 1 to 4 mm, and are often strongly sericitized. The groundmass is typically equigranular, and is composed of microcrystalline quartz and plagioclase feldspar with 5-40% sericite, 0-20% chlorite, 0-10% ankerite and dolomite; other accessory minerals include tourmaline, rutile, and zircon. Fine-grained cubic pyrite (locally up to 10%) is disseminated in many samples.

2.2.4 Dacite-sediment lapilli tuff (peperites)

Figure 10. Outcrop of mafic tuff. Outcrop has dark reddish-brown sulfide staining from presence of oxidized pyrite. 15 cm pencil for scale.

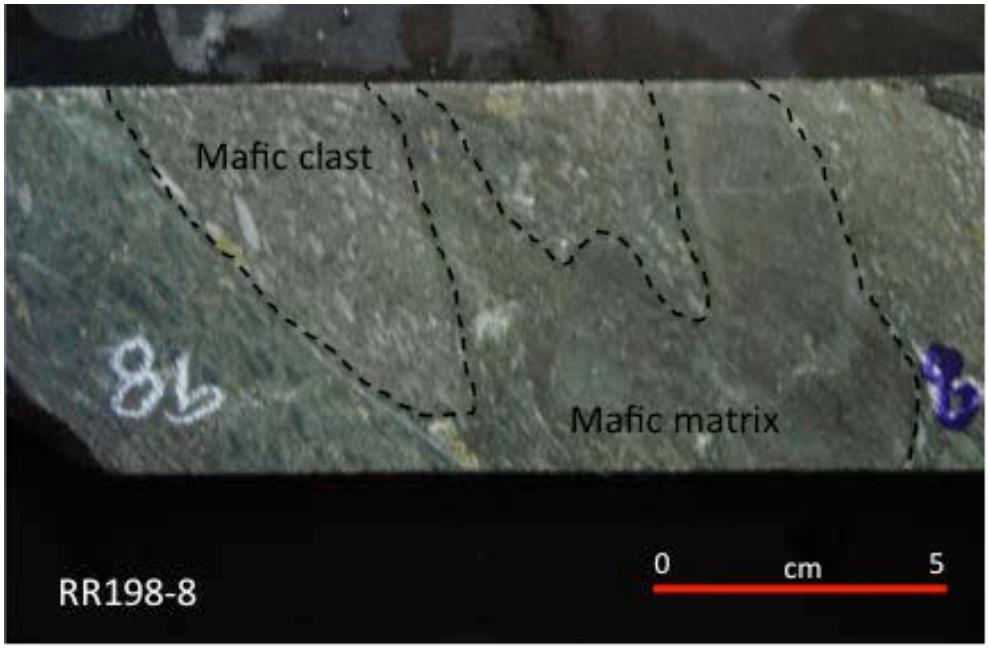

Figure 11. Diamond drill core sample of mafic lapilli tuff containing amygdaloidal mafic lapilli clasts. The clasts strongly resemble mafic hyaloclastite. The matrix is composed of very-fine grained chlorite and carbonate.

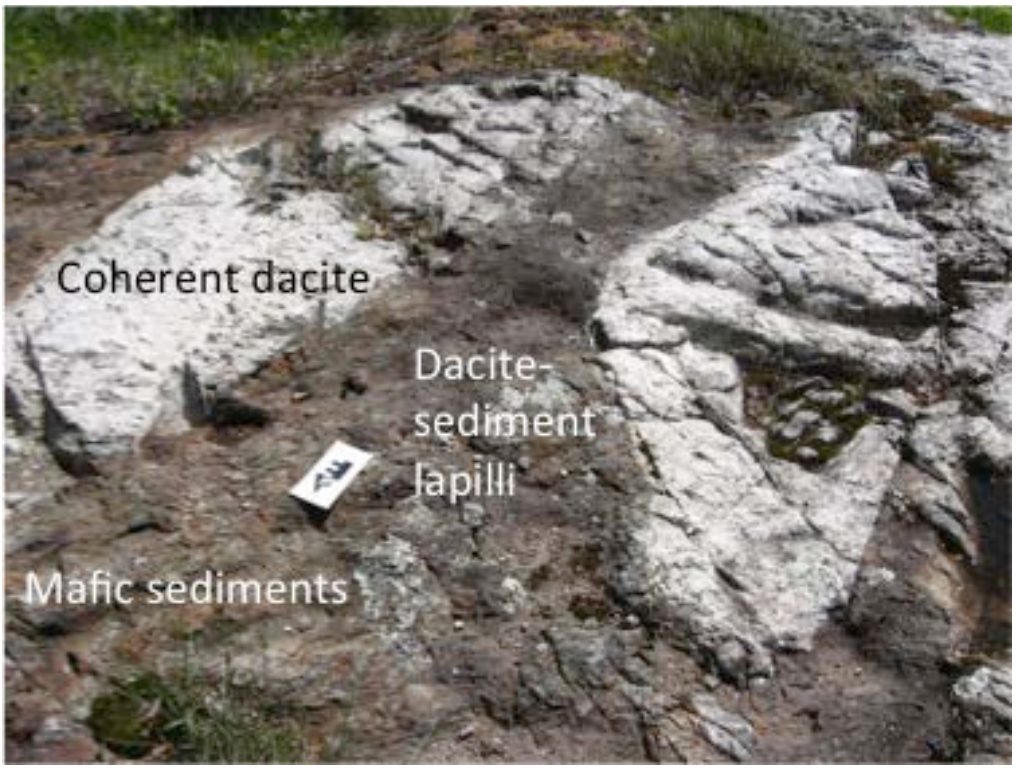

Figure 12. Cleaned outcrop of dacitic intrusion with mafic tuff and dacite-sediment lapilli tuffs. These units were originally logged as boulders resulting from caldera collapse (Ayers, 1997). Scale card is 15 cm long.

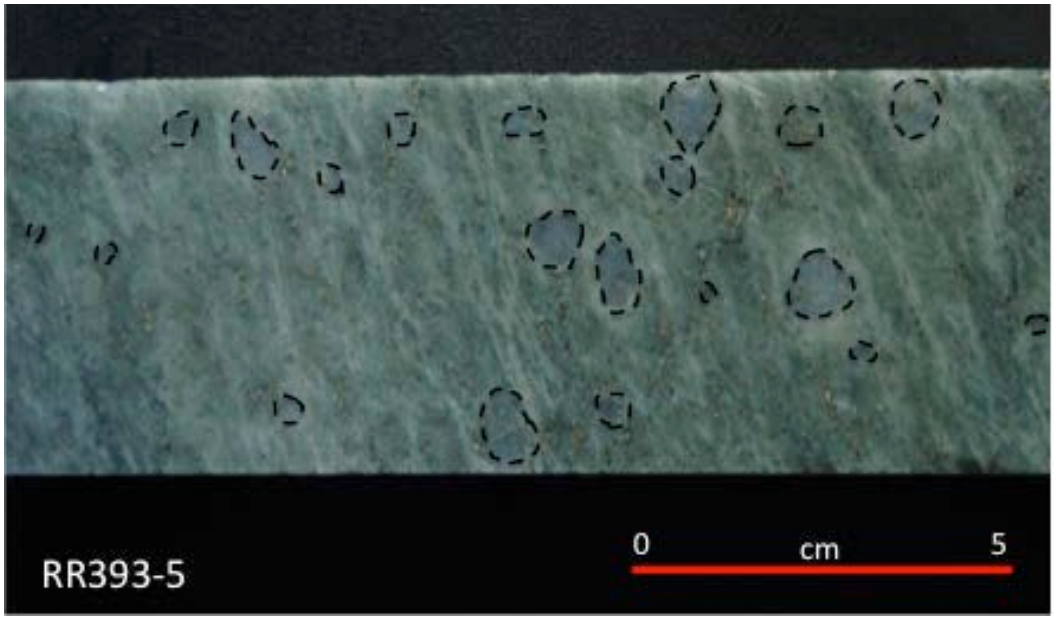

Figure 13. dacite dike or sill in hand sample. The sample contains ~15%, 1-8 mm quartz crystals (outlined). Groundmass is light green because of the abundance of sericite and quartz in the groundmass.

The dacite-sediment lapilli tuffs at the RRGP are composed of dacitic clasts in a mafic matrix and are highly variable in both hand sample and thin section. This unit occurs stratigraphically between dacitic intrusions and mafic tuffs and exhibits gradational contacts with both, grading from 60-70% dacitic lapilli clasts near dacitic intrusive units to matrix-dominated near contacts with the mafic tuff (Fig. 14). These lapilli tuffs are laterally limited and difficult to trace between outcrops and drill holes. The unit has been strongly altered and primary textures, including brecciated clasts, are often difficult to recognize. The dacite-sediment lapilli tuffs are interpreted to be peperites. Peperite is a genetic term applied to a rock of igneous fragments disseminated in a sedimentary matrix formed by the *in-situ* disintegration of magma intruded into unconsolidated wet sediments (White, 2000).

Lapilli clasts within the peperites are compositionally similar to the dacitic intrusions. The clasts are made up of a microcrystalline quartz matrix which contains 1-5%, 1-3 mm, subhedral to euhedral quartz crystals. Clasts range from 0.5-5 cm in size and are curviplanar to poorly rounded. The clasts are set in a matrix similar to the mafic tuff, which is composed of fine grained carbonate, chlorite, and quartz. The units are typically extensively altered.

2.2.5 Dacitic lava flows

Dacitic lava flows are the most abundant unit within the felsic succession. Dacitic lava flows are evenly quartz-phyric (quartz crystals are not graded), and are laterally extensive, traced over 1500 m. While compositionally identical to dacitic intrusions and homogeneous in outcrop (Fig. 15) the presence of hyaloclastites, flow banding, and amygdules distinguish the dacitic lava flows from dacitic intrusions. Most other primary textures have been destroyed by alteration and deformation. Likewise, alteration has obscured most individual flow boundaries, but several individual flows, ranging in thickness from 10-200 m, can be separated by changes in quartz crystal and amygdule content. Dacitic lava flows are interlayered with lapilli tuffs, intervals of sedimentary rocks, and rare lenses of mafic tuff. The contacts between breccias can be gradational whereas contacts with sedimentary rocks and the mafic tuffs are sharp. Sections of dacitic

Figure 14. Outcrop of dacite-sediment lapilli tuff and mafic tuff. The matrix of the mafic sedimentary tuff has sulfide staining. Clasts within the lapilli tuff are equivalent to the dacites in composition. Yellow field notebook used for scale is 15 cm long.

Figure 15. Outcrop of dacitic lava flow. Outcrop is homogeneous with 3-5%, 0.4-1.5 mm rounded quartz crystals evenly disseminated throughout the unit. Scale card is 15 cm long.

lava flows containing >40% amygdules are interpreted as flow tops. The amygdules are 0.3-1.5 mm and are filled by quartz +/- carbonate +/- pyrite.

In the dacitic lava flows quartz crystals (0-15%) vary in size from <1-5 mm, are typically round-subhedral, and are often embayed with undulose extinction (Fig. 16). Quartz crystals are set in a groundmass composed of 35-60% microcrystalline quartz and plagioclase feldspar, 10-40% sericite, 0-25% chlorite, and 0-15% carbonate. Epidote and zoisite/clinozoisite may also be disseminated in the groundmass (0-5%). Accessory minerals are tourmaline, rutile, and zircon. Amygdules vary in modal proportion from 0-45% (highest in flow tops) and range in size from 0.3-3 mm in diameter. Locally, amygdules are elongate parallel to foliation (Fig. 17). Amygdules are composed of recrystallized quartz that is coarser than the surrounding groundmass. Fine-grained cubic pyrite (0-20%) is locally disseminated throughout many samples. Rare sphalerite and chalcopyrite (0-2%) can occur as open space fillings or disseminations associated with veins.

2.2.6 In-situ monomict clast supported dacite lapilli tuff (hyaloclastites)

In-situ monomict clast supported dacite lapilli tuffs are well-preserved in two diamond drill holes (RR198 and RR458). These units are interpreted as hyaloclastites, volcaniclastic rocks formed by the nonexplosive granulation of magma flowing into water (Schmincke, 2004). These lapilli tuffs occur stratigraphically above dacitic lava flows with sharp stratigraphic thicknesses of 0.4-5 m. These monomict clast-supported lapilli tuffs can grade into monomict lapilli tuffs or into dacitic lava flows. Clasts range in size from 1 mm to 5 cm, with larger clasts characterized by angular- to blocky-shapes with curviplanar margins. Smaller clasts tend to have a shard-like morphology (Fig. 18). Locally the fragments have a jigsaw-fit morphology, which indicates the lapilli has not been resedimented from its original site of fragmentation (Rosengren et al., 2008). Monomict clast-supported lapilli tuffs are laterally limited and impossible to correlate between diamond drill holes.

In thin section, clasts are identical to the dacitic lava flows. The clasts are typically aphyric to sparsely porphyritic with 0-6% subhedral to round quartz crystals

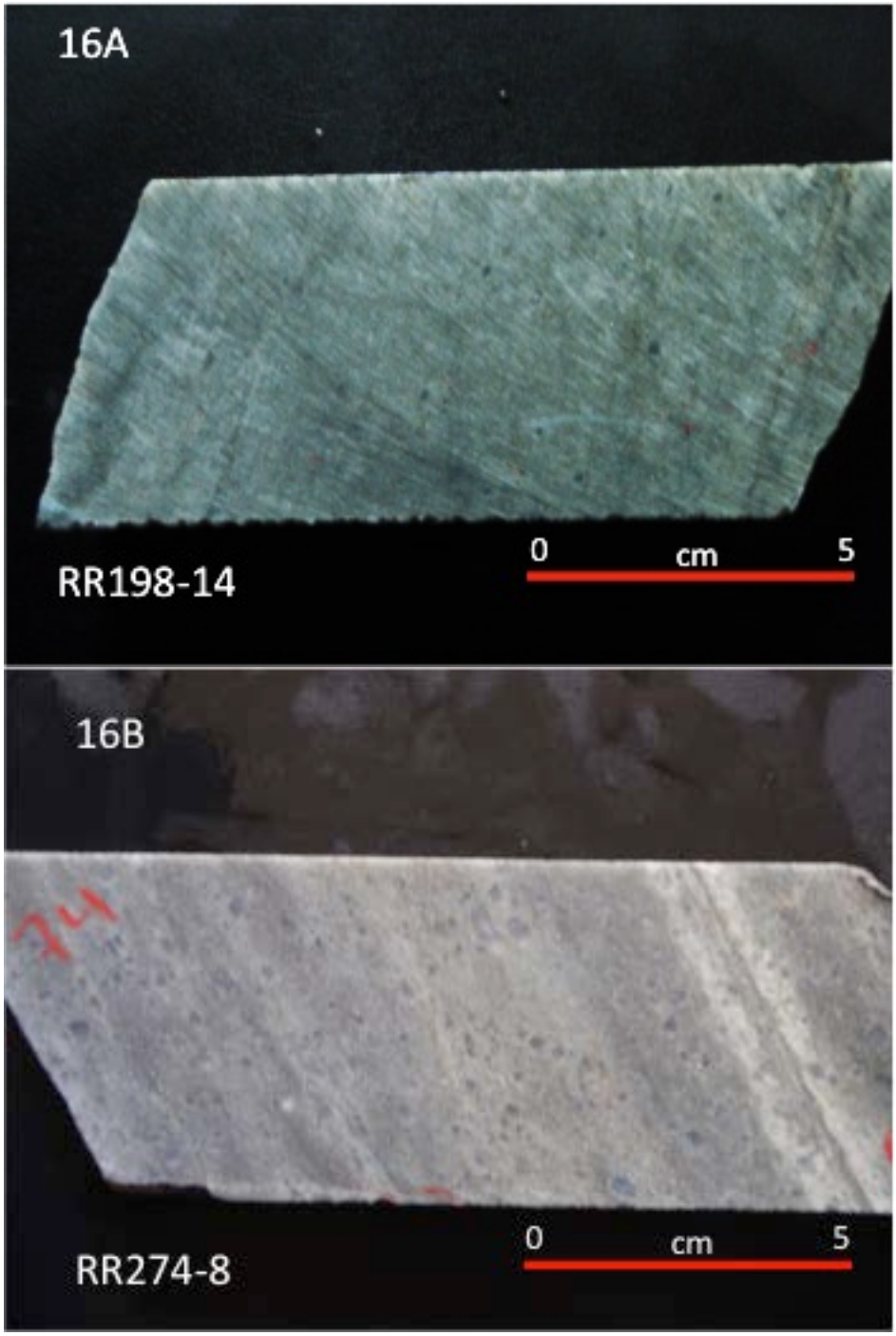

Figure 16. Two drill core samples of dacitic lava flows illustrating the differences in quartz crystal content. Differences in quartz crystal abundance can be used to distinguish different lava flows. Sample RR198-14 in Fig. 16A has more abundant chlorite in its groundmass giving the light green color with 2%, 0.2-.0.5 mm quartz crystals. Sample RR274-8 in Fig. 16B is dominated by sericite and quartz with 8%, 0.5-1.5 mm quartz crystals.

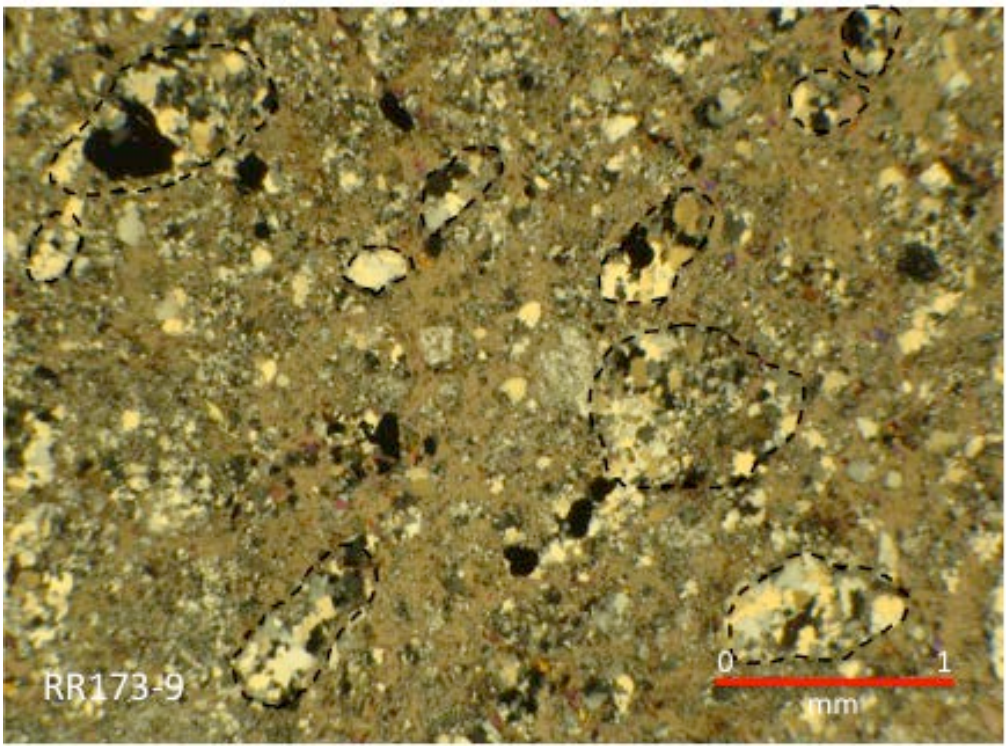

Figure 17. Recrystallized quartz amygdules within a sample representing a dacitic lava flow top. Note the open space filling pyrites (opaque angular minerals) associated with the quartz amygdules.

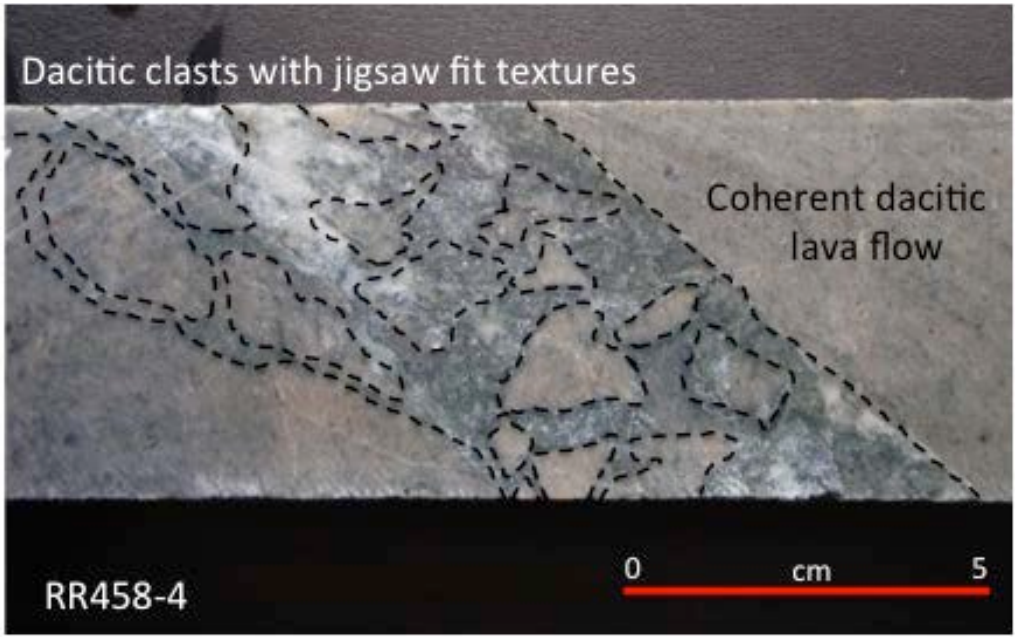

Figure 18. Drill core sample of hyaloclastite. The clasts with curivplanar and jigsaw fit margins are identical in composition to the surrounding dacitic lava flows. Secondary minerals have recrystallized the interstitial tuff between the individual clasts.

within a very-fine grained microcrystalline groundmass identical to the dacites. Clasts can contain 0-15%, 0.5-1.6 mm, recrystallized quartz-filled amygdules. The matrix to the clasts is composed of microcrystalline quartz with abundant sericite and chlorite.

2.2.7 Monomict matrix-supported lapilli tuffs

Monomict clast- to matrix-supported lapilli tuffs were observed in several diamond drill holes within the RRGP. This volcaniclastic facies is between 4-18 m thick, is laterally restricted, and has sharp contacts with dacite and gradational contacts with hyaloclastites (Fig. 19). Monomict lapilli tuffs exhibit good sorting with clasts varying from 80% at the basal contact to 25% at the upper contacts. The clasts are 0.5-3 cm in size and are well-rounded to slightly elongate. The monomict lapilli tuffs are distinguished from the hyaloclastites based on clast shape and contacts with dacitic lava flows.

Petrographically the clasts are monomict and mineralogically resemble the composition of the clasts within hyaloclastites or dacitic lava flows. Quartz crystals (1-4%) are disseminated in a groundmass of microcrystalline quartz with sericite and chlorite. The interstitial matrix is very fine-grained and is compositionally identical to the clasts—albeit finer. The cores of the clasts contain 0.2-1.3 cm quartz spherulites which are noted by their circular shape and radial extinction. The spherulites formed by high temperature devitrification of volcanic glass (Schmincke, 2004).

2.2.8 Polymict clast- to matrix-supported lapilli tuffs

This facies is diverse and varies between diamond drill holes. It is most abundant in outcrops to the east of the study area near the Black Hawk Stock. Polymict lapilli tuffs occur interbedded with dacitic lava flows, hyaloclastite, and sedimentary rock. The rocks are poorly bedded and typically have sharp lower contacts. Polymict lapilli tuffs vary in thickness from 10-40 m, and in lateral extent from local to laterally extensive. The facies varies from having a strongly clast-supported framework with 95% clasts to matrix dominated sections composed of 25% clasts (Fig. 20).

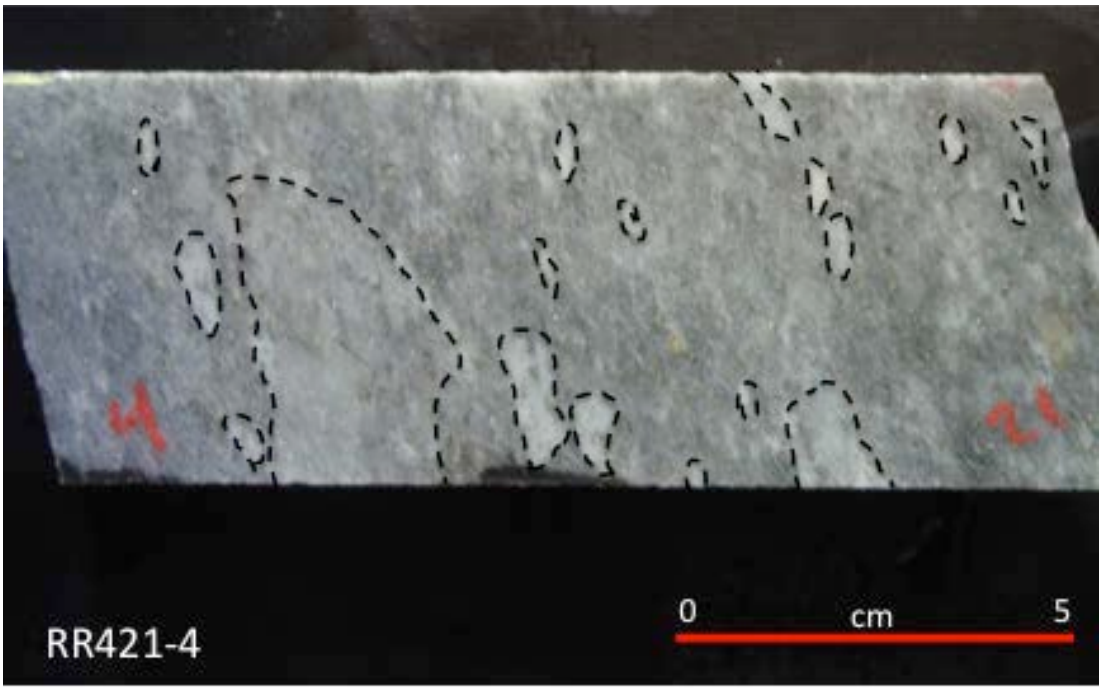

Figure 19. Drill core sample of monomictic lapilli tuff. The clasts are dacitic in composition and elongated parallel to the foliation. The majority of the clasts are <1-2 cm with rare clasts up to 4 cm long.

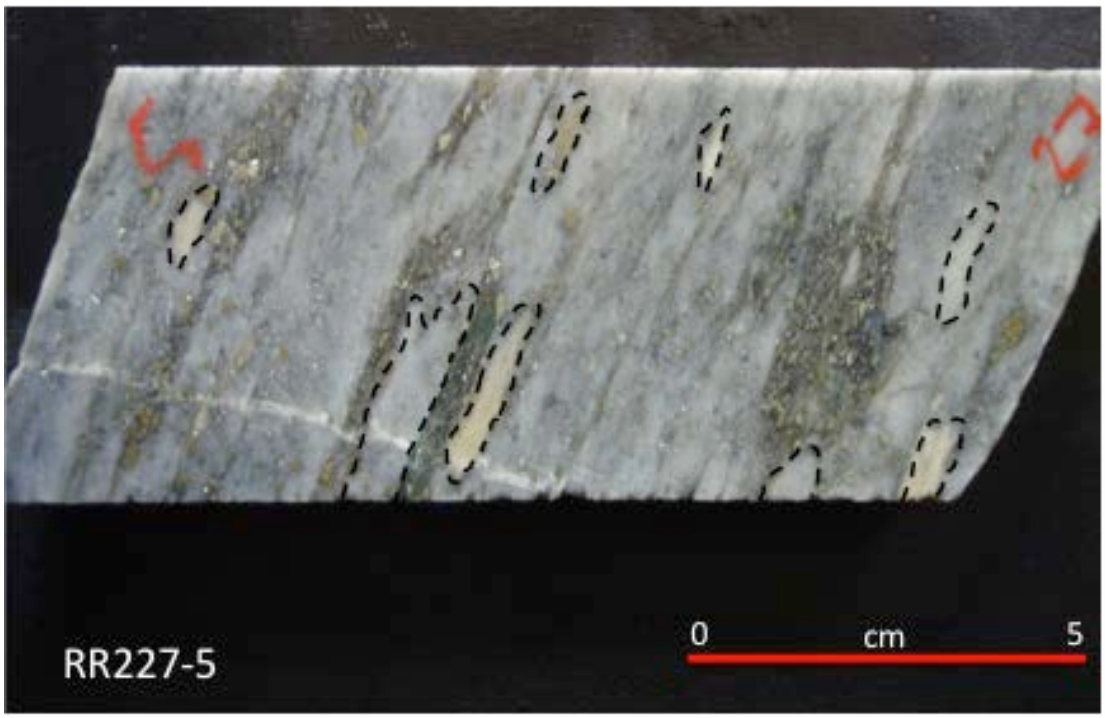

Figure 20. Drill core sample of polymict lapilli tuff. The 1-3 cm diameter polymict clasts are dacitic with subordinate tan clasts. Note elongation of the clasts parallel to the well-defined foliation.

Clasts range in appearance from dacite to "cherty" tan clasts and are mineralogically composed of microcrystalline quartz and feldspar. Like the monomict lapilli tuffs, rare dacitic clasts contain spherulitic textures. The majority of clasts are dacitic in composition and are mineralogically similar to the clasts within the monomict lapilli tuffs. The interstitial matrix has been highly altered and recrystallized to quartz, sericite and chlorite.

2.2.9 Sedimentary Rocks

Sedimentary facies are minor components of the felsic succession of the RRGP. Two different rock types make up the sedimentary unit—pyritic black argillites and fine-grained sandstones. The argillites are finely laminated, strongly foliated, folded (Fig. 21) and are less than 3 m thick. Pyrite layers and nodules are often surrounded by "tear-shaped" tails of shale indicating the shale has been deformed around the pyrite (Rosengren et al., 2008). The sandstone is similar in thickness and distribution to the shale. Sedimentary rocks are interbedded with dacitic lava flows and breccias and are poorly correlated between diamond drill holes.

The pyritic argillite units are composed of 70% very-fine grained organic carbon with 30% secondary minerals including sericite and chlorite, and cubic to anhedral pyrite. The unit is finely-bedded, and fine-grained with minor sulfides disseminated throughout the groundmass. The sandstone composition is nearly exclusively medium-grained quartz with minor sericite and chlorite.

2.3 Types and distribution of gold mineralization

Because of the very-fine grained nature of the gold mineralization, assays are necessary to understand its distribution. Gold is associated with all lithologies within the RRGP area, ranging from 5 ppb to 200,000+ ppb, with 90% of assayed samples falling under 300 ppb. However, while gold is disseminated within all units, practically all economic concentrations—80% of assays >1500 ppb—or 1.5 g/ton—occur in the dacitic lava flows. Within individual dacitic lava flows gold values vary based on the original permeability of the rocks and the amount of structural deformation. Zones of higher

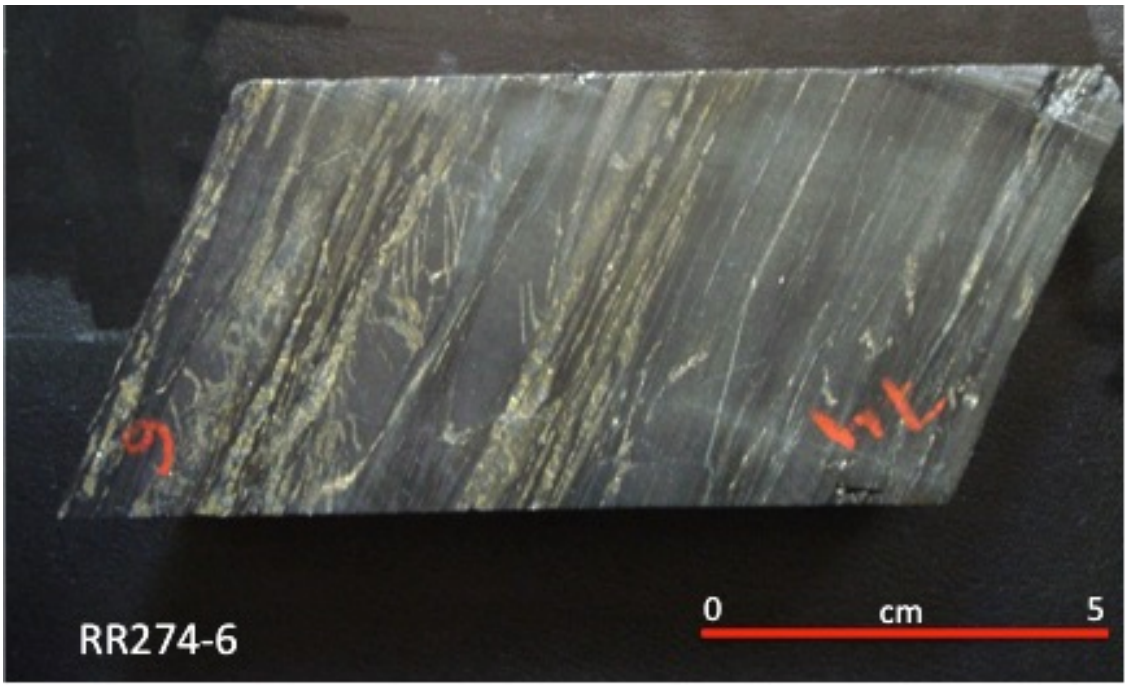

Figure 21. Drill core sample of argillite. The argillite is strongly foliated.

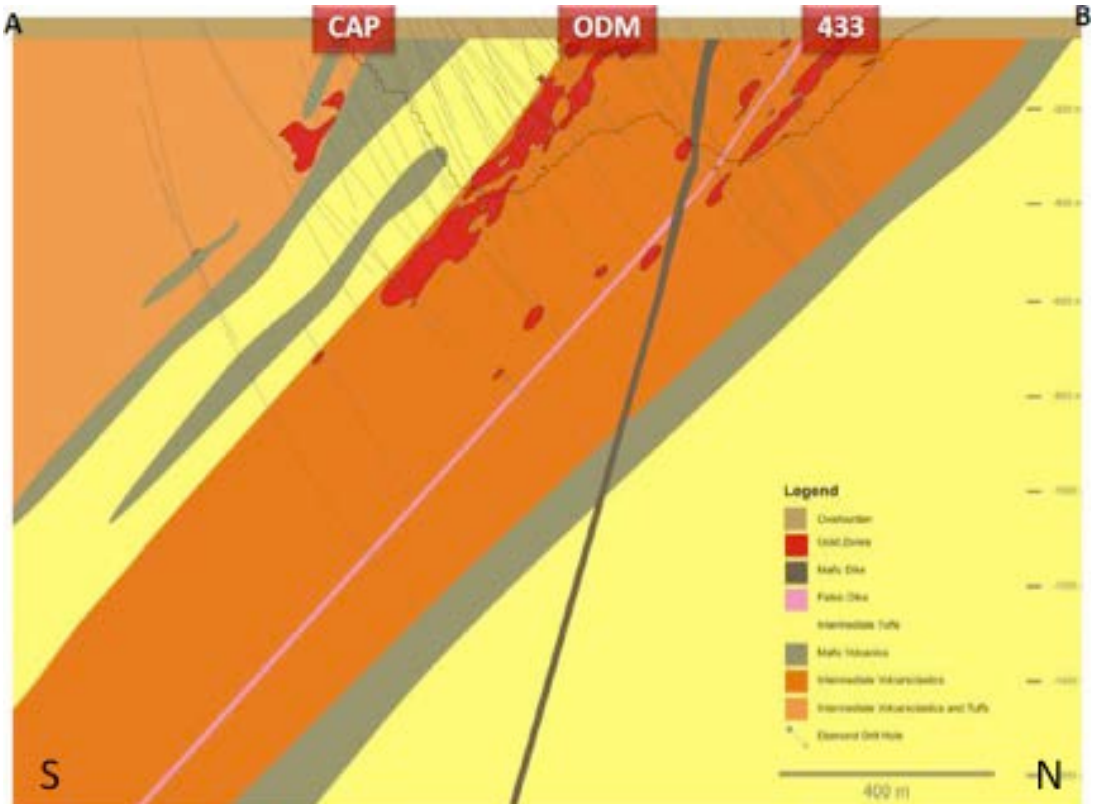

Figure 22. Distribution of gold zones at the RRGP. From Rainy River Resources Press Release (2010).

primary permeability (i.e. flow tops and breccias related to dacitic lava flows) and areas of intense deformation have elevated gold values, up to 10,000x greater than gold values in the surrounding rock.

Economic gold mineralization at the RRGP has been constrained to three different zones referred to as the Cap, ODM/17 and 433 zones (see Fig. 22). Gold within the RRPG occurs in three styles of mineralization: low grade (<2 g/t), low to moderate grade (2-10 g/t) and high grade (>10 g/t), and these can be correlated with changes in alteration assemblages and intensities. Low-grade gold mineralization is characterized as disseminated, associated with pyrite and in tightly folded pyrite stringer veins in moderately altered rocks (Fig. 23). In thin section the gold-bearing pyrite grains have anhedral shapes and are often associated with minor amount of chalcopyrite—either disseminated in the matrix or as chalcopyrite veinlets (Schandl, 2006).

Moderate gold grades are characterized by folded and foliated pyrite-sphalerite and pyrite stringer veins (Fig. 24). These zones are associated with more intense alteration and are typically associated with areas of silicification. Sphalerite fills fractures in pyrite, and gold and electrum occur together in carbonate and sphalerite veins (Schandl, 2006). Moderate gold grades are also associated with sphalerite aggregates that are intergrown with carbonate and epidote veins (Schandl, 2006).

Higher grade gold mineralization is often associated with pyrite-chalcopyrite veins and most visible gold is strongly associated with chalcopyrite and quartz veins as well as areas of strong silicification (Fig. 25). These chalcopyrite-gold veins can crosscut foliation, but also occur as weakly deformed veins generally sub-parallel to foliation or tightly folded (Hrabi and Vos, 2010).

The RRGP also contains an indicated and inferred value of over 14 million oz silver. Silver occurs most commonly as electrum and in very-fine grained galena (containing 1-2 weight % silver; Schandl 2006). The distribution of silver is, like gold, constrained to the most intensely altered and permeable units of the RRGP (Fig. 26). Elevated values of gold, however, do not guarantee high silver values. Other metals including Cu, Zn, As and Hg show similar patterns to gold and silver (Fig. 27), being strongly concentrated within the most intensely altered and permeable units. Metal values

Figure 23. Two styles of low grade gold mineralization at the RRGP. Sample in Fig. 23A is characterized by tightly folded pyrite stringer veins and disseminated gold in moderately altered rocks (Fig. 23A is modified from Hrabi and Vos, 2010). Sample RR173-9 in Fig. 23B is dominated by gold hosted in open space filling pyrite associated with quartz filled amygdules.

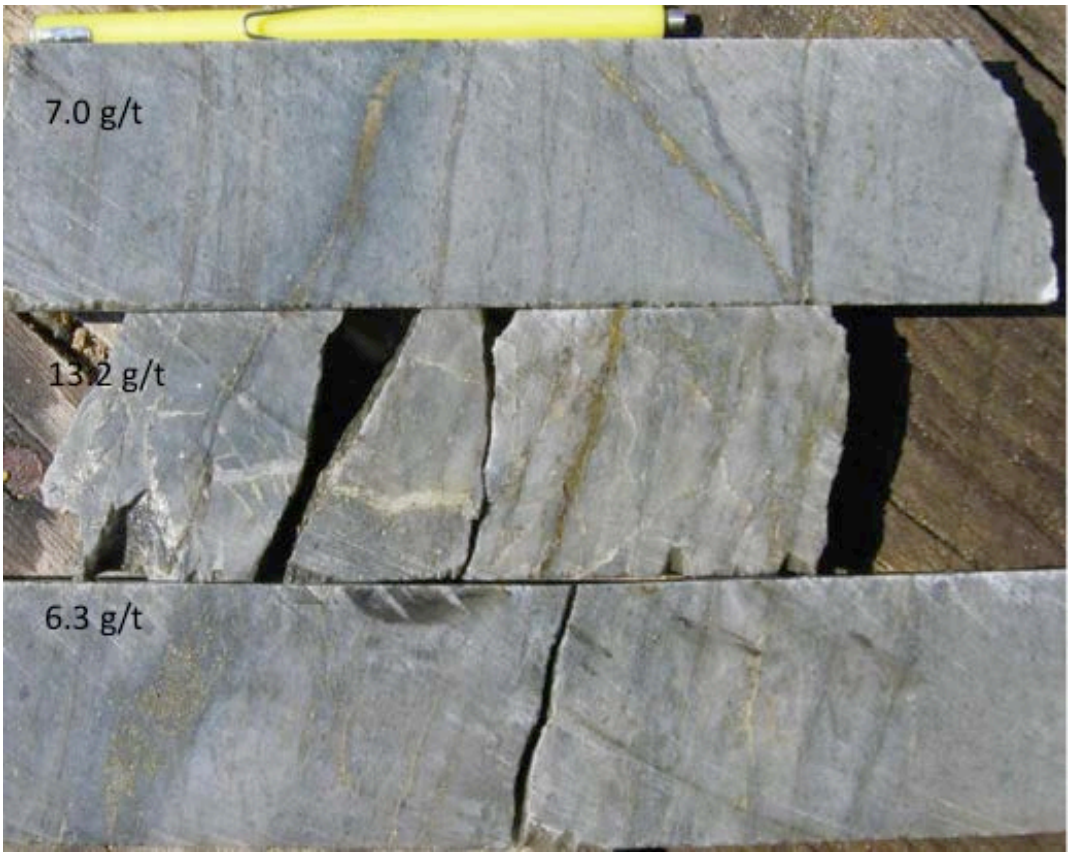

Figure 24. Medium grade gold mineralization characterized by folded and foliated pyrite-sphalerite and pyrite stringer veins. Modified from Hrabi and Vos (2010).

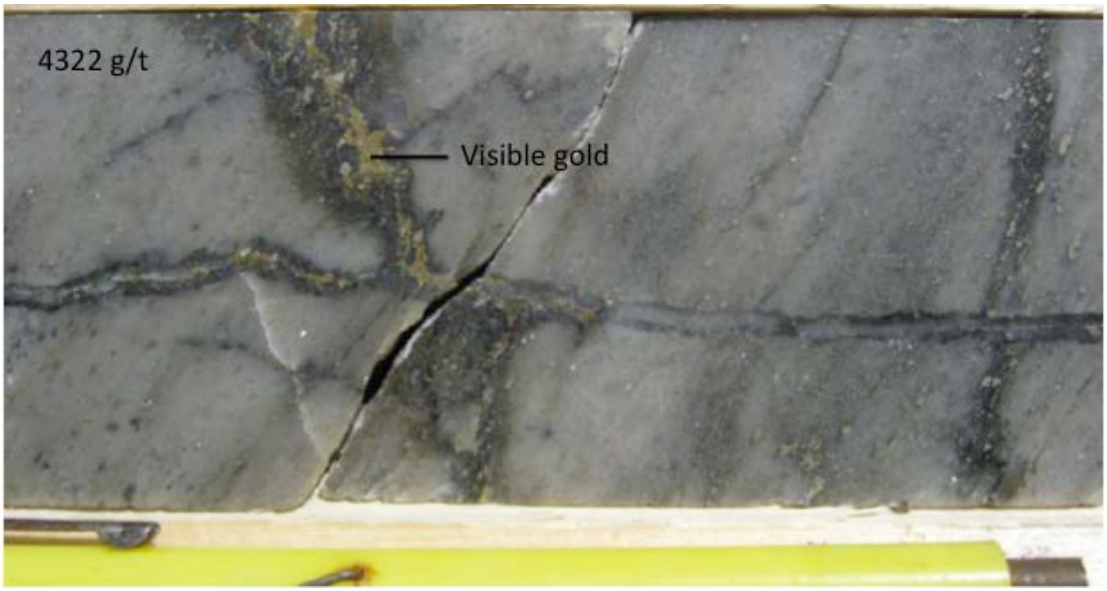

Figure 25- High grade gold mineralization in which visible gold is associated with chalcopyrite and quartz in stringers. Modified from Hrabi and Vos (2010).

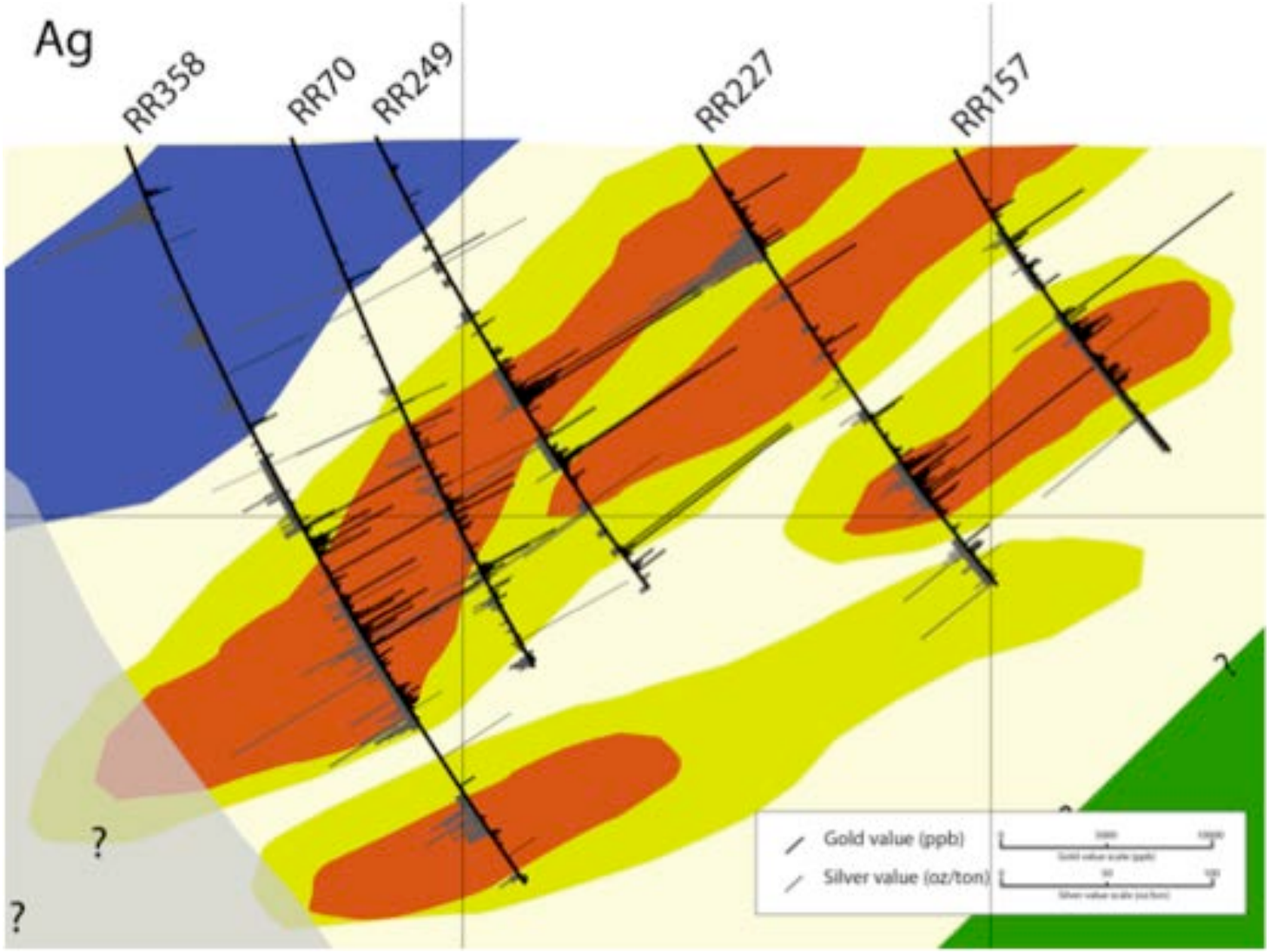

Figure 26- Relative gold and silver values on the east section line (refer to Fig. 55 for explanation of background color).

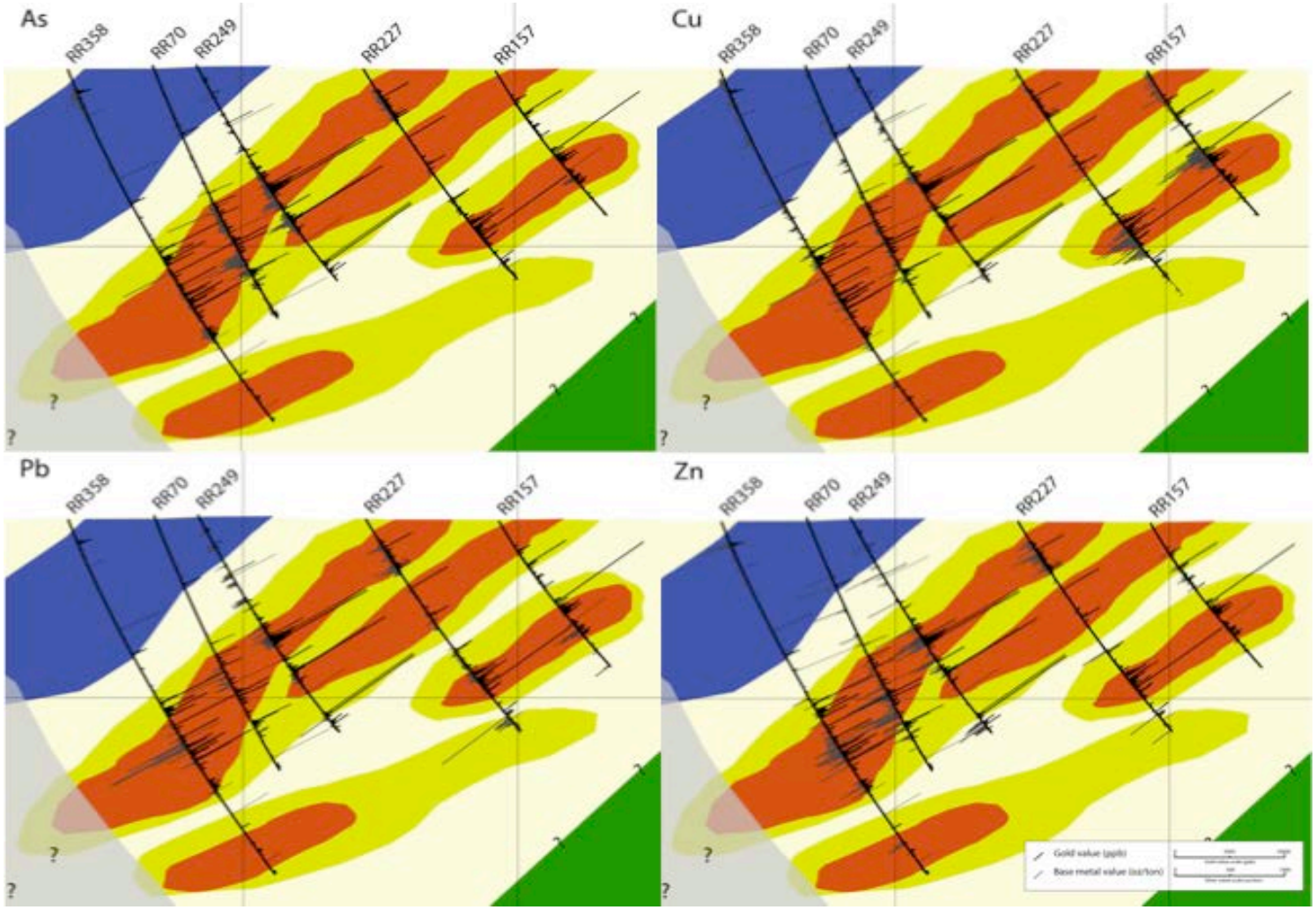

Figure 27- Relative metal values on the east section line (refer to Fig. 55 for explanation of background color). Increases in Cu correspond to areas with higher amounts of chalcopyrite and increases in Zn correspond to areas with higher amounts of sphalerite.

are correlative and the relationship between Cu and Zn is seen in drill core samples with chalcopyrite and sphalerite often associated with visible gold.

2.4 Post-volcanic Intrusive Units

2.4.1 Black Hawk Stock

The Black Hawk Stock (BHS) is a quartz monzonite intrusive body located 3 km east of the RRGP (Plate 1). The stock has a map area ~25 km^2 and truncates the felsic succession in the east where it occurs in association with topographic highs. In thin section the BHS is relatively unaltered and composed of medium- to coarse-grained subhedral quartz, euhedral orthoclase and plagioclase feldspar and subhedral hornblende. In the RRGP there are quartz monzonite sills and dikes that are compositionally identical to the Black Hawk Stock that crosscut the felsic volcanic succession. While the BHS and the dikes are barren, the BHS dikes are often related to gold mineralization in the surrounding wall rocks. These dikes have been locally referred to as the "rainbow dikes" because of their color variability and association with elevated gold values.

2.4.2 Quartz-feldspar porphyry dikes

Quartz-feldspar porphyry dikes (QFPs) are abundant within the RRGP area and crosscut all facies. QFPs are distinguished from dacites because of their coarser grain size and relatively minor alteration. Porphyritic euhedral quartz varies from 10-35% and unaltered plagioclase feldspar ranges from 15-30%. The quartzofeldspathic groundmass is fine-grained and microcrystalline.

2.4.3 Diabase dikes

Fine-grained diabase dikes are common near the RRGP. These diabase dikes crosscut stratigraphy and have sharp contacts with the surrounding units. Geochemically they are homogeneous and similar to the footwall basalts. These units are differentiated from the basalts based on their grain size and chill margins with the surrounding rocks, as well as their cross-cutting geometries.

2.4.4 Mafic-ultramafic intrusions

Several high standing outcrops of gabbro occur near the RRGP. These are coarse-grained and made up of pyroxene, plagioclase, and amphibole with minor olivine. The rocks are nonfoliated and relatively unaltered. Within the RRGP there is a tabular body of pyroxenite composed of coarse-grained pyroxene and minor amphibole. Like the gabbros the pyroxenite is nonfoliated and not altered. The pyroxenite hosts minor net-texture sulfide mineralization. The pyroxenite intrusion has been proposed to be related to the midcontinent rift system, and was previously evaluated as a host of economic quantities of Ni-Cu (pers. comm. Rayner, 2010).

2.5 Stratigraphic reconstruction

The felsic succession of the RRGP is dominated by dacitic lava flows with subordinate breccias and sediments (Plate 1). The felsic succession represents ~700 m of stratigraphy striking east-west and dipping 50-70 degrees to the south. Because of the paucity of outcrop and polyphase deformation, the stratigraphy has previously been poorly defined. Mapping and construction of cross sections along three section lines (Plate 1, Figs. 28, 29 and 30) helps in understanding and defining the spatial distribution of the lithologies. Additionally, three generalized stratigraphic columns of the three section lines have been created to show representative units at various stratigraphic heights (Figs. 28b, 29b, 30). This is important in understanding their modes of emplacement and establishing a genetic model for the RRGP.

The felsic succession at the RRGP is underlain by basalt lava flows (Fig. 31). Footwall basalts are in contact with a thick package of mafic tuffs that have been intruded by lobate to tabular, 5-15 m thick dacitic intrusions. Contacts between the intrusions and surrounding mafic tuff can be sharp, with chilled boundaries, or gradational with peperites. The mafic tuff unit is sharply overlain by dacitic lava flows. This sequence of flows is ~350 m thick with individual flows defined by flow tops or where there is a change in the modal percentage of quartz crystals. Additionally, dacitic lava flows are interlayered with breccias and sedimentary rocks as well as thin lenses of mafic tuffs. These lower dacitic flows are intercepted in all drill holes.

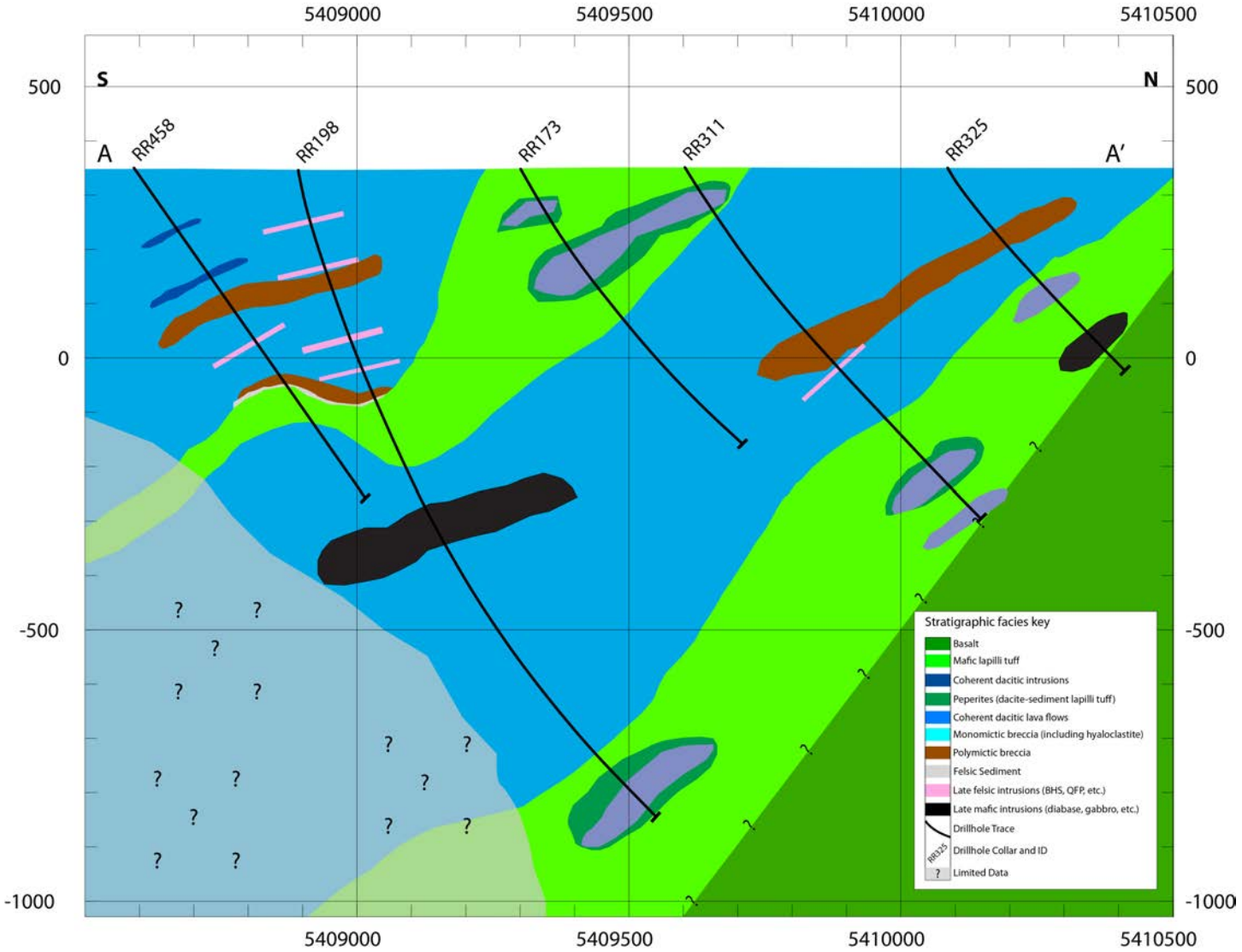

Figure 28. Lithological cross section along the west section line.

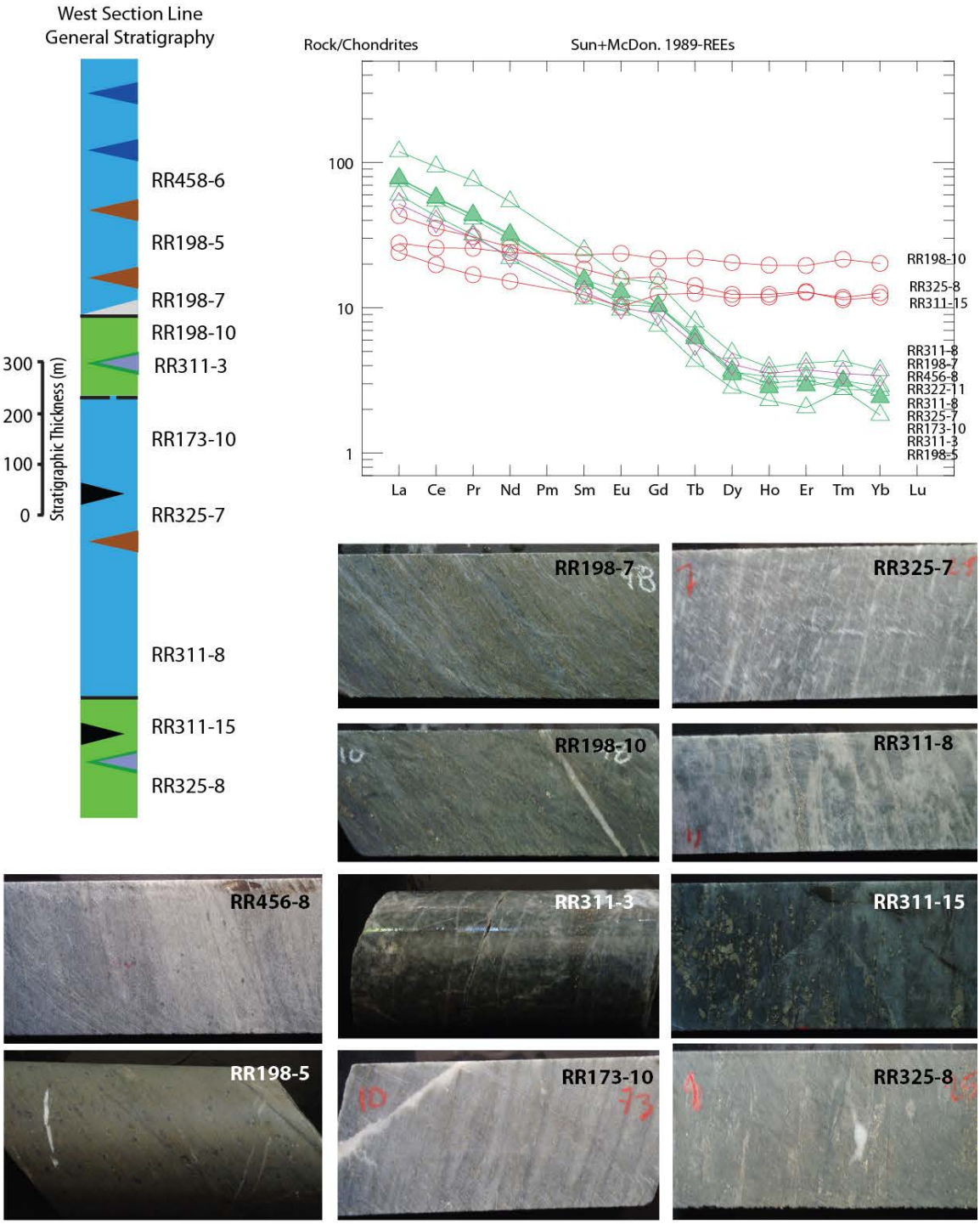

Figure 28b. Schematic diagram showing the different lithologies associated with different stratigraphic height along the west section line. Stratigraphic height corresponds to sample images and REE trace element plot. Core samples are ~5.0 cm wide.

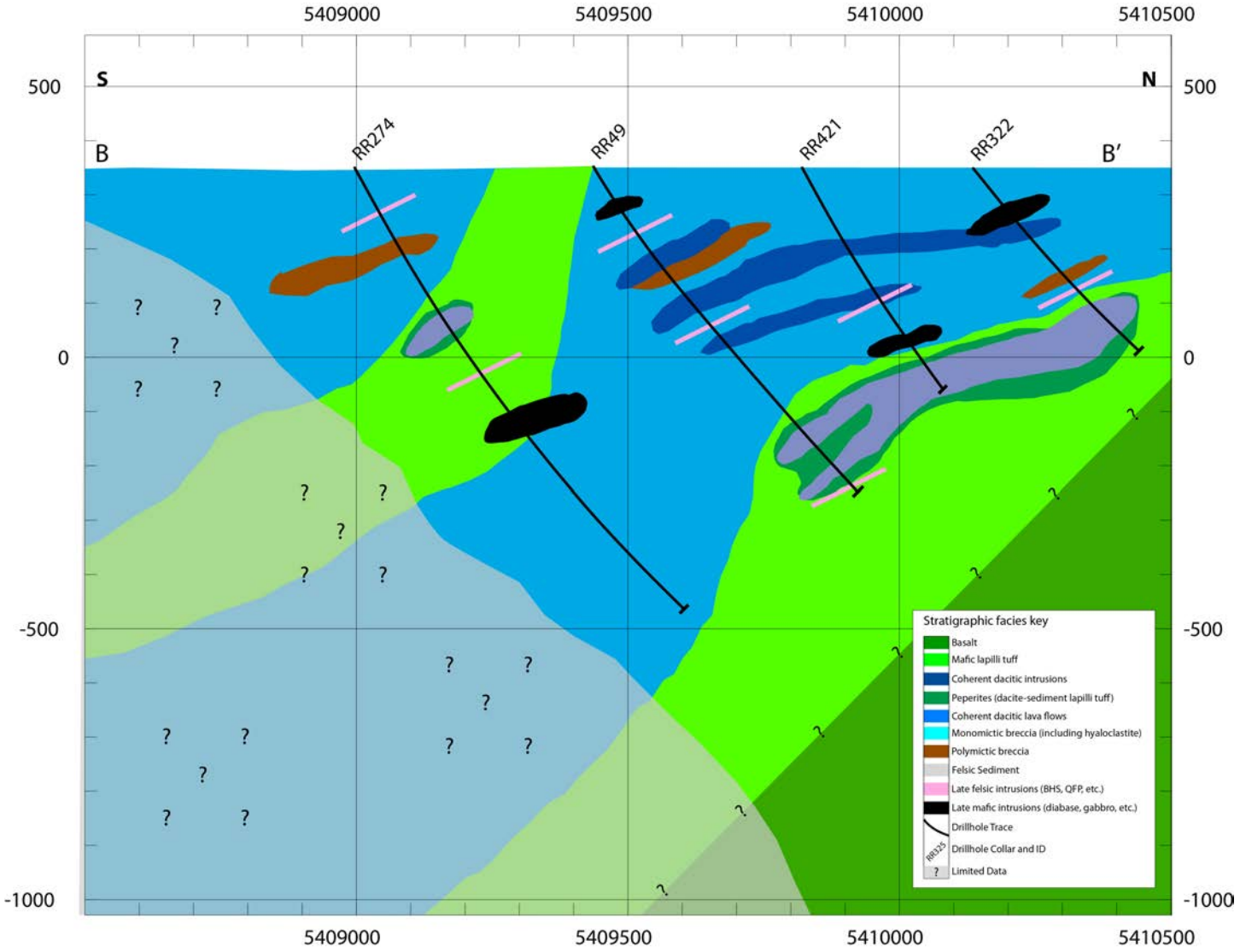

Figure 29. Lithological cross section along the central section line.

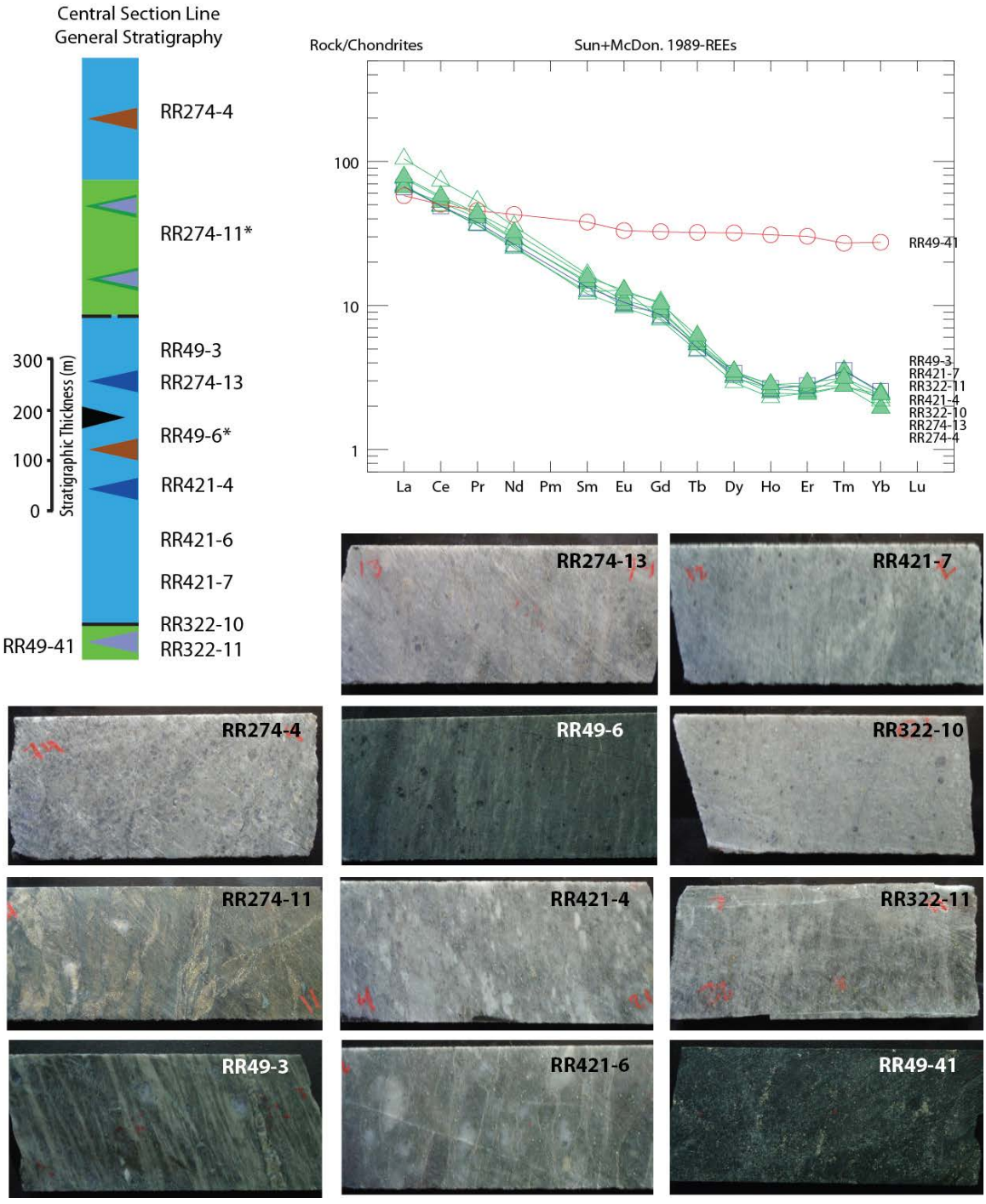

Figure 29b-Schematic diagram showing the different lithologies associated with different stratigraphic height along the central section line. Stratigraphic height corresponds to sample images and REE trace element plot. Core samples are ~5.0 cm wide.

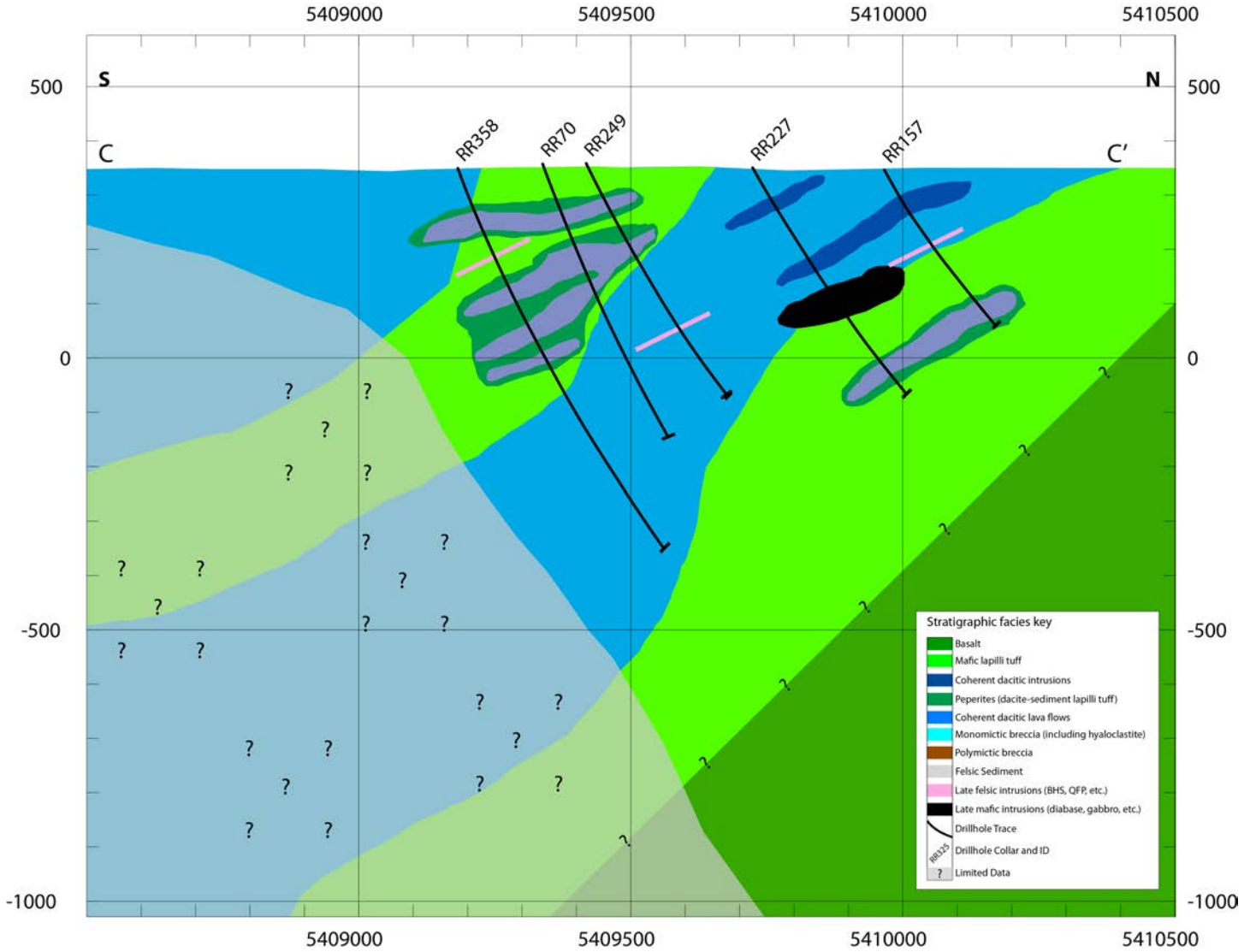

Figure 30. Lithological cross section along the central section line.

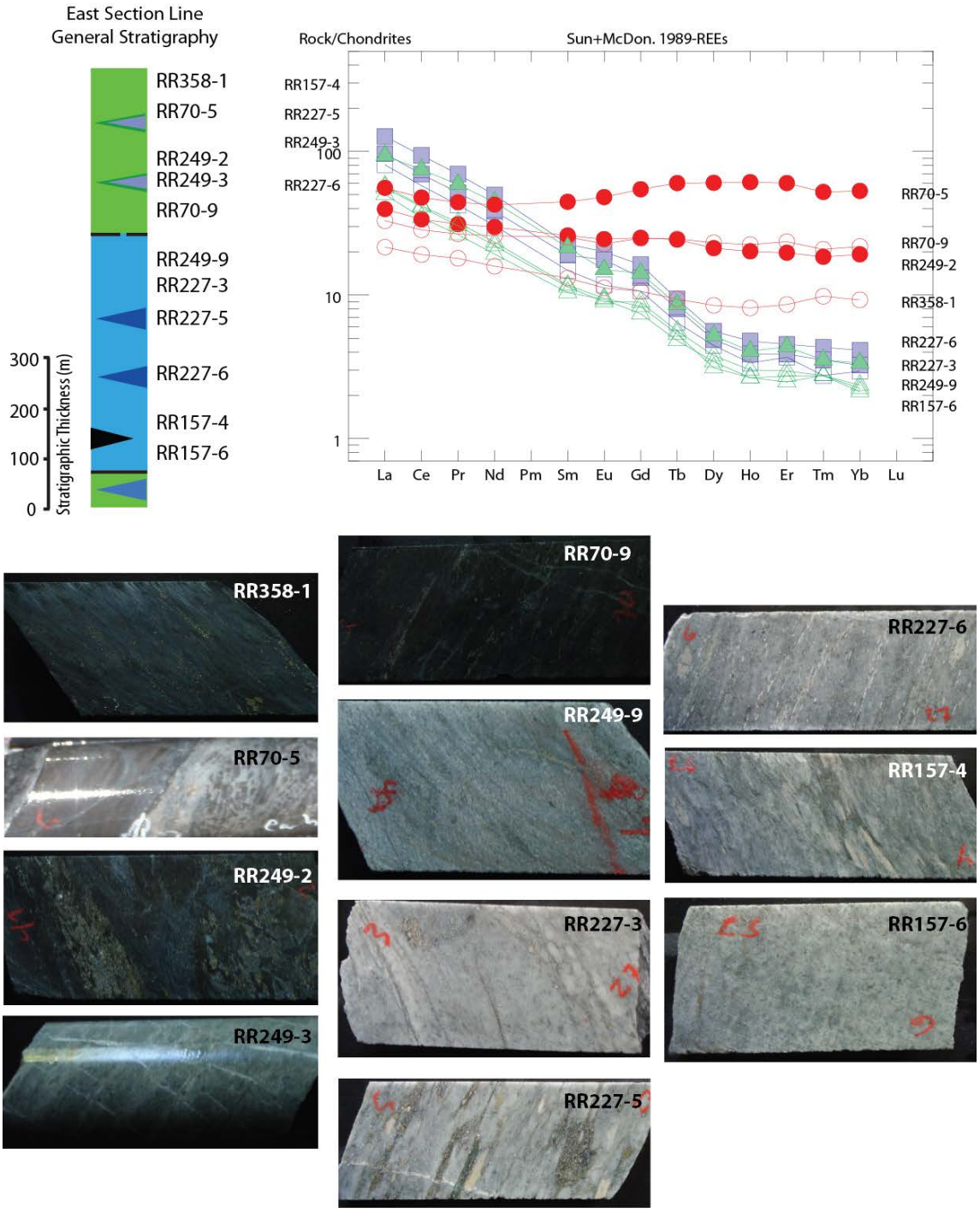

Figure 30b-Schematic diagram showing the different lithologies associated with different stratigraphic height along the east section line. Stratigraphic height corresponds to sample images and REE trace element plot. Core samples are ~5.0 cm wide.

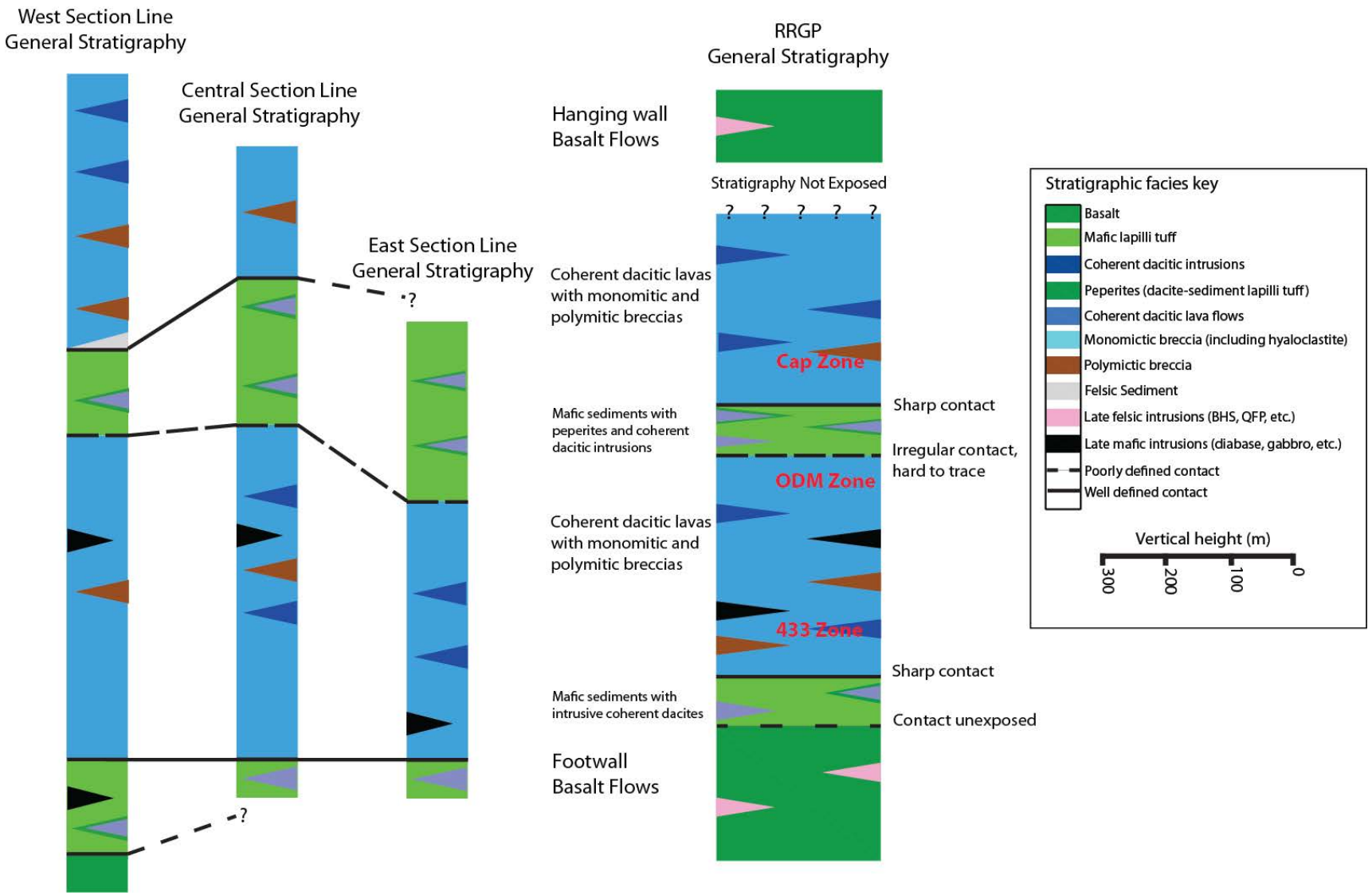

Figure 31. Generalized stratigraphic section of the volcanic succession of the RRGP.

This lower package of dacitic lava flows is in sharp contact with overlying mafic tuffs. The mafic tuffs are 150 m thick and locally contain mafic lapilli clasts set in a fine-grained matrix. The mafic tuffs were previously mapped and logged as basalt lava flows (Cullen, 2005). Thin, 3-15 m thick, dacitic intrusions occur within this mafic tuff package and are associated with peperites. These units outcrop in the center of the drilling area and was recognized in eight of the diamond drill cores logged.

Dacitic lava flows and associated lapilli tuffs overlie the mafic tuff. This package of dacitic lava flows extends ~300 m and represents the uppermost stratigraphy in the diamond drill holes. Dacitic lava flows are interbedded with 5-25 m thick breccia facies and 1-5 m thick sedimentary horizons with rare lenses of mafic tuff. In the east section, dacites are interlayered with more abundant polymict lapilli tuffs, with the abundance of polymict lapilli tuffs increasing to the north of the central and west section lines. This dacite package crops out to the east of the drilling zone and forms several large (>2 km^2) hills that are heavily forested. Most of the outcrops are composed of dacite, but there are sections that are made up of monomict to polymict lapilli tuffs—particularly further to the east (Plate 1).

2.6 Geochemistry of volcanic facies

Along with field mapping, core logging, and petrographic analysis, 69 samples underwent major and trace element analysis. Geochemical analysis was used to identify primary rock types, tectonic environment of formation, as well as the provenance of the mafic tuff and the clast population in the breccias (Rosengren et al., 2008). Because of the polyphase deformation and pervasive hydrothermal alteration, immobile trace elements are critical in distinguishing primary rock types and associated volcanic facies. The geochemistry suggests that the RRGP underwent bimodal volcanism with distinct end members composed of dacites and tholeiitic basalts (Figs. 6 and 7).

This thesis presents the first geochemical analysis utilizing trace element data to understand the original source of the mafic and felsic rocks. Mobility of major elements (in particular the alkali elements) during alteration and metamorphism results in AFM (Le Bas et al., 1986) geochemical classification spanning a wide range of rock types

inconsistent with field mapping and petrographic studies (Fig. 32). This is a result of a widespread hydrothermal alteration system and subsequent metamorphism (Winter, 2000). Some trace elements, i.e. HFSE, in comparison, are relatively immobile during hydrothermal alteration processes, and can be used to more accurately assess strongly metamorphosed and altered rocks (Jenner, 1996). Trace element geochemistry shows that the felsic and mafic components in the RRGP are derived from different crustal sources. It also establishes the provenance for the mafic tuff, the peperites, the polymict lapilli tuffs and the monomict lapilli tuffs.

Footwall pillowed and massive basalts plot as tholeiites using Nb/Y vs Zr/P_2O_5 and P_2O_5 vs Zr (Winchester and Floyd, 1976) diagrams (Fig. 33), and as arc-basalts using a tectonic discrimination diagram (Fig. 34; Woods, 1980). The basalts also display Nb, Ti, and Ta depletion on a REE spidergraph (primative mantle normalized after Sun and McDonough, 1980) indicating their arc-like nature (Winter, 2000). Arc-like basalts are related to the subduction of an oceanic plate underneath either a continental or another oceanic plate. In the subduction zone, loss of volatiles from the subducting slab starts to partial melt the overriding mantle. The magma rises and forms arcuate volcanic island chains that are typically thin (10-30 km) but can be several thousand kilometers in length (Winter, 2000).

Geochemically, the mafic tuffs have almost indistinguishable trace element geochemistry from the basalt lava flows (Fig. 35). This suggests that the mafic tuffs were derived from the basalts. While trace elements are consistent in the mafic tuffs, major element values are highly variable due to hydrothermal alteration (for example SiO_2 ranges from 37.7-71.8%; Na_2O from 0.22-2.86%, K_2O from 0.09-3.15%, MgO from 1.17-10.25%, and Fe_2O_3 from 2.8-15.9%).

Peperites are hard to classify geochemically using major and minor elements because of hydrothermal alteration and their mixed character comprising both mafic tuffs and dacitic clasts. Dacitic clasts are typically subordinate to the mafic tuff matrix and, because of this peperites, have trace element values similar to mafic tuff and basalts. However, the siliceous nature, and in particular, the amount of SiO_2 can vary widely depending on their distance from dacitic intrusions. Near contacts with dacitic intrusions,

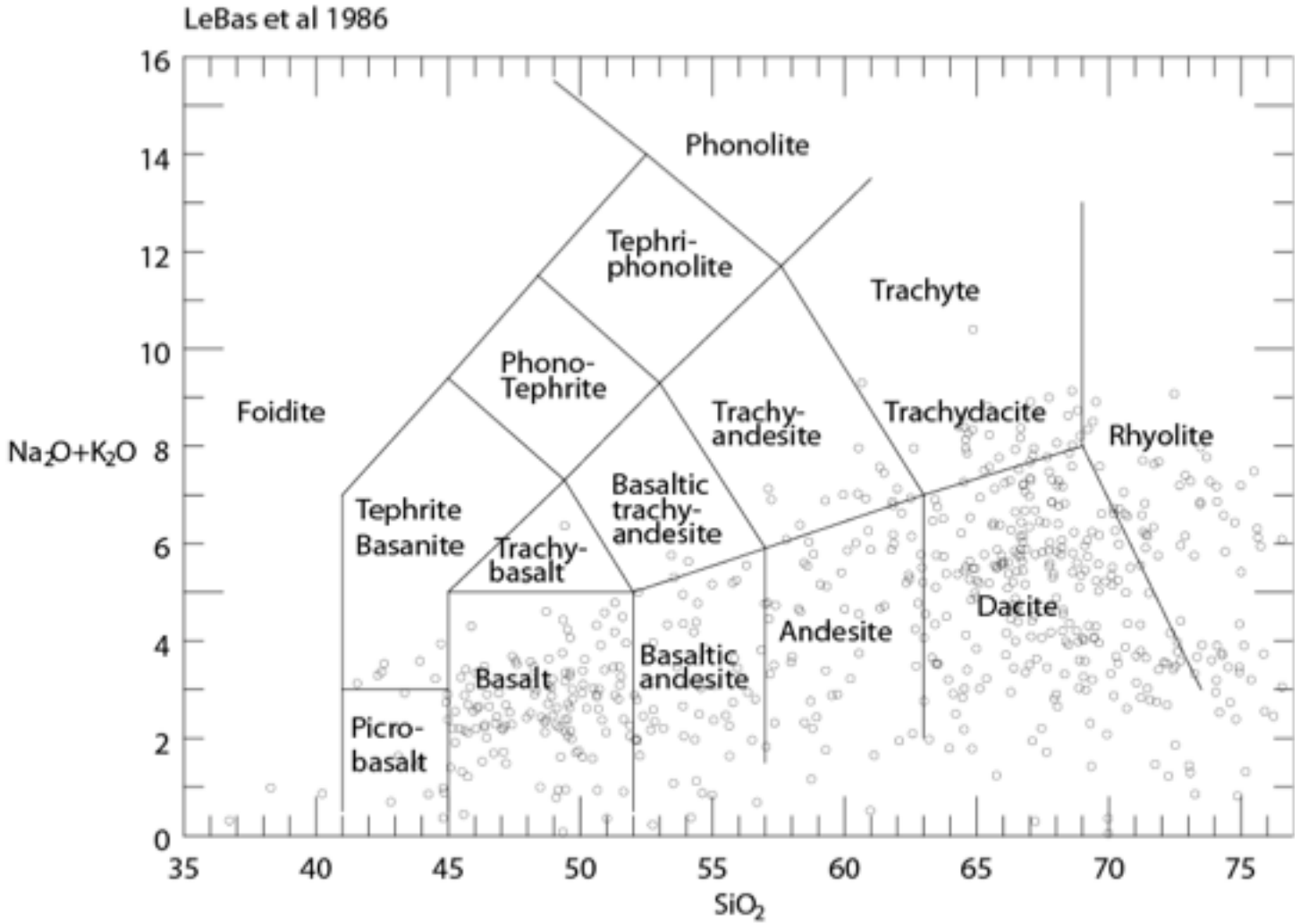

Figure 32- LeBas et al. (1986) undivided TAS diagram of 550 whole rock analyses in the RRGP area. Alteration has effectively created rocks that correspond to each rock type.

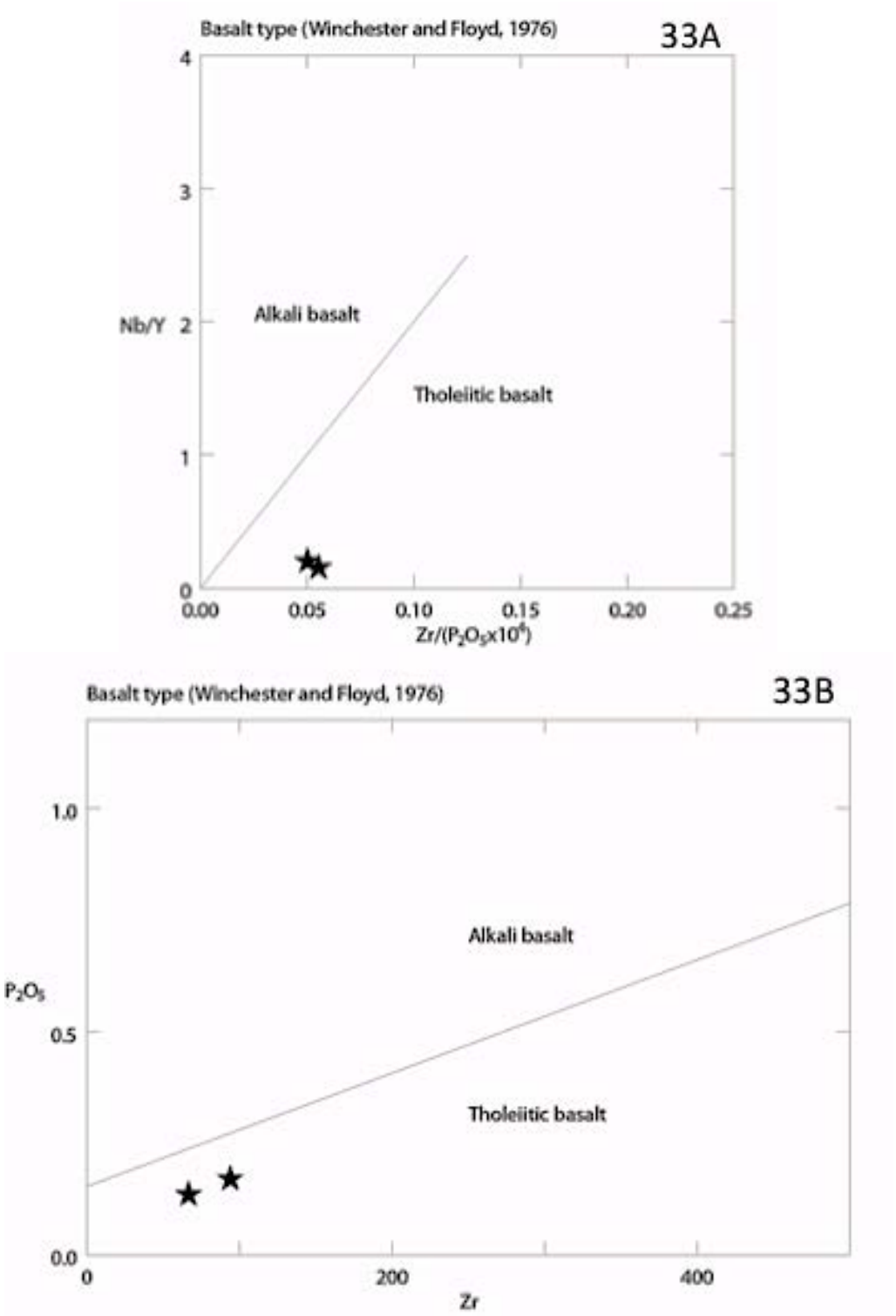

Figure 33. Basalt types based on Winchester and Floyd (1976). Fig. 33A Nb/Y vs Zr/P_2O_5 and Fig. 33B P_2O_5 vs Zr. Both plots show that the basalt sample is a tholeiitic basalt based on trace element data.

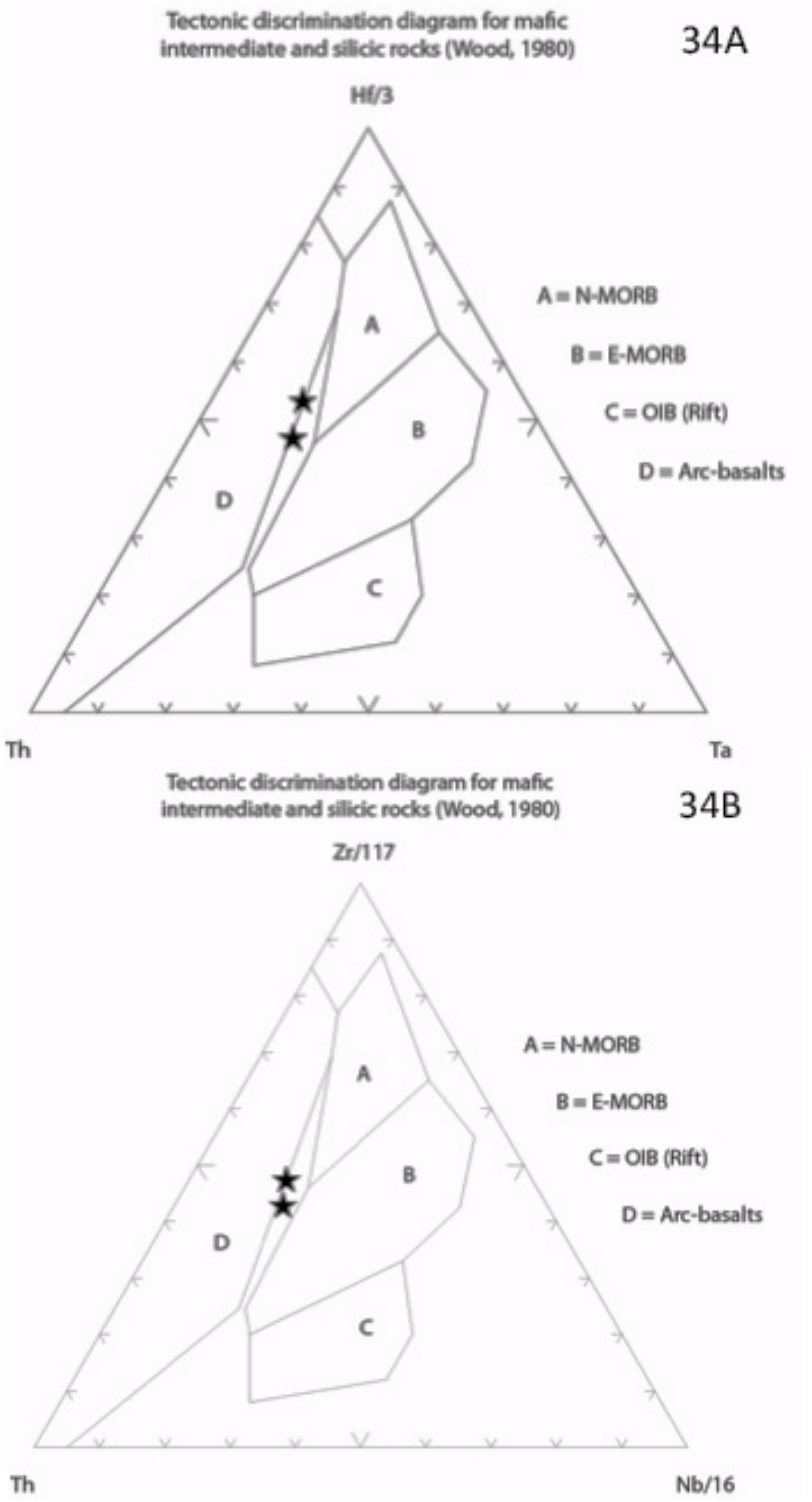

Figure 34. Tectonic discrimination diagrams from Wood (1980) Fig. 34A Hf/3 vs Th vs Ta and Fig. 34B Zr/117 vs Th vs Nb/16 of the basalt flows. The basalt samples plots as an arc-basalt in both diagrams.

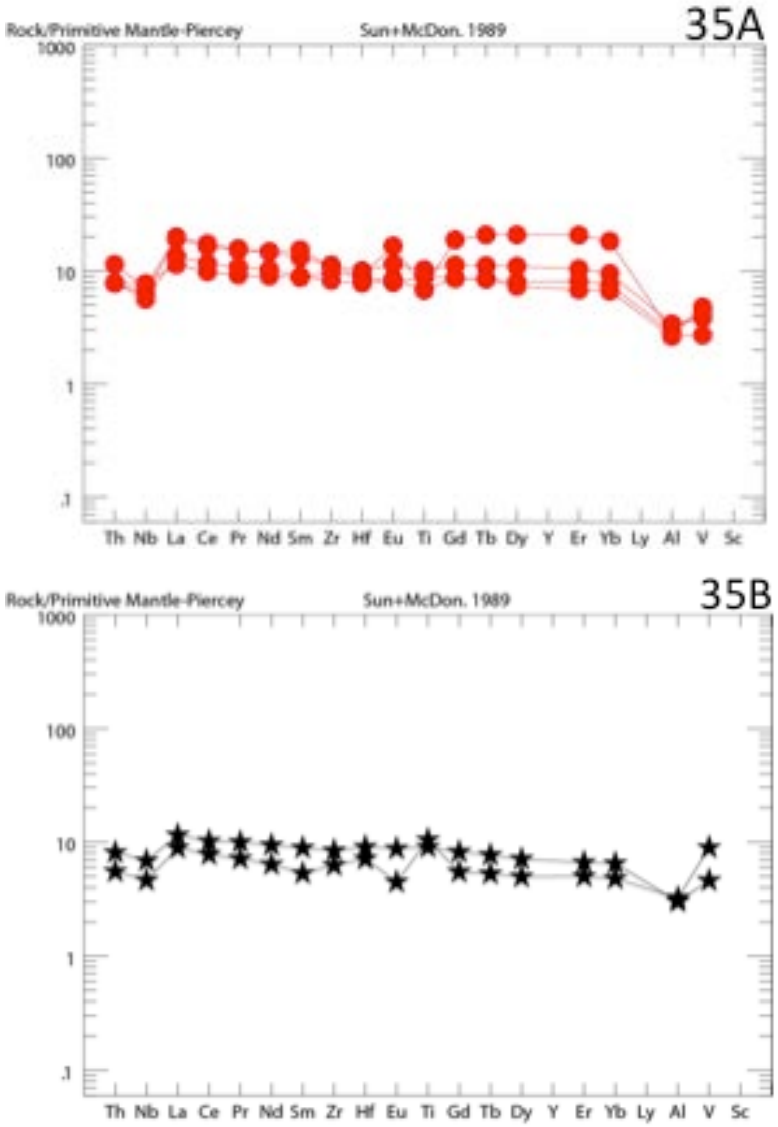

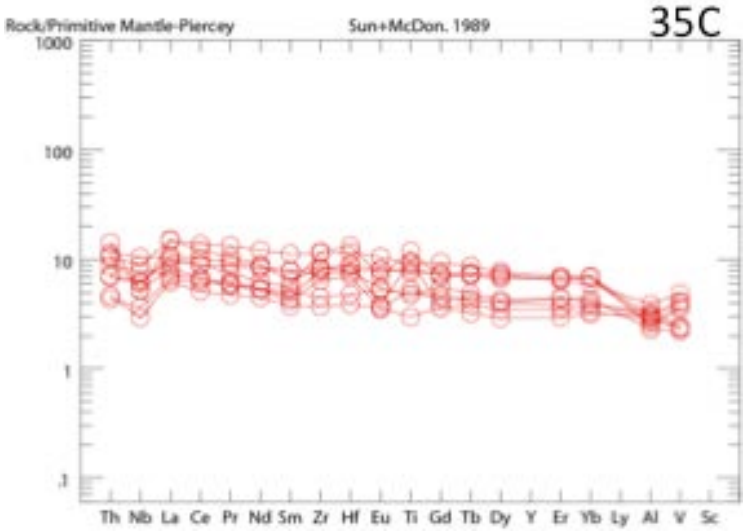

Figure 35. Comparison of the REE spider diagrams (chondite normalized-Sun and McDonough, 1989) of peperites (Fig. 35A), basalt (Fig. 35B) and mafic sediments (Fig. 35C). All three different facies show almost identical REE slopes.

the peperites have high SiO_2 values, which decrease further away from the contact (Fig. 36). This is a result of the disintegration of the felsic magma and the incorporation of the more felsic groundmass into the original mafic tuff (Busby-Spera and White, 1987). If the mafic tuff were consolidated and anhydrous, the contact between the dacitic intrusion would be sharp and would not result in the elevated values in SiO_2 (Busby-Spera and White, 1987).

Felsic units are geochemically distinct from the mafic units. The felsic units plot, with few exceptions, as dacites on a Winchester-Floyd (1977) diagram (Fig. 6), and as volcanic arc-like related rocks on a Hf-Rb/30-Ta*3 diagram (Fig. 37; Harris et al., 1986). The dacites have trace element values characteristic of a more evolved magma source that is geochemically and compositionally distinct from the tholeiitic basalt (Winter, 2000; Fig. 38). Lapilli tuffs, both polymict and monomict (Fig. 38), have identical geochemistry suggesting the dacitic lava flows were their source, likely resedimented features of the carapace and flank breccias of the dacitic lava flows. The trace elements data of the felsic units indicate that they are distinct from the tholeiitic basalt and are likely the result of a more evolved portion of slab melting (Winter, 2000).

The felsic units plot as FI felsic metavolcanic rocks (Fig. 39; Lesher et al., 1986). Lesher et al. (1986) defined FI rocks as "dacites and rhyodacites characterized by steep REE patterns with weakly negative to moderately positive Eu anomalies, high Zr/Y, and low abundances of HFSE, and high abundances of Sr." FI rocks are interpreted as being derived from a deep magmatic source and lack high-level differentiation in high-level magma chambers which results in their unique geochemical signatures (Lesher et al., 1986). FI rocks are abundant throughout the rock record but are typically barren for VMS deposits (Hart et al., 2004). However as RRGP demonstrates significant gold mineralization can occur within FI group rocks.

2.7 Volcanogenic interpretation

Massive and pillowed lavas, along with mafic tuffs, make up the majority of the RRGB and form the footwall and hanging wall rocks to the felsic volcanic succession. Associated with the massive and pillowed lavas are abundant hyaloclastites, lapilli tuffs

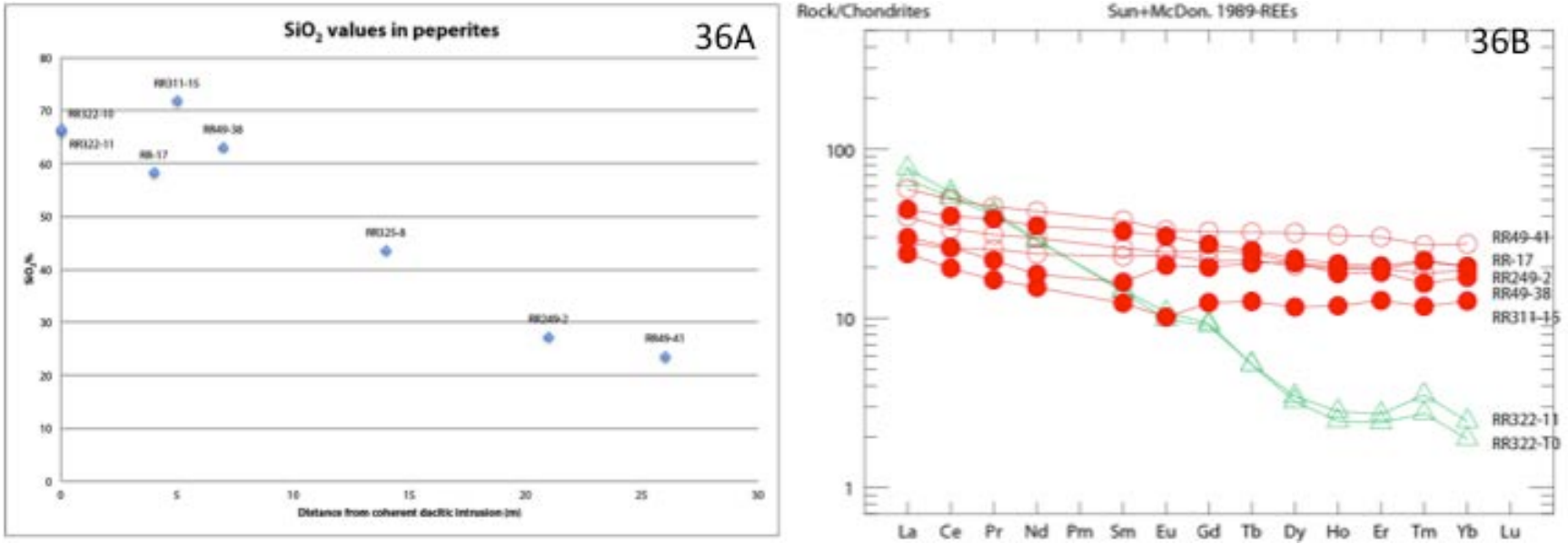

Figure 36. Fig. 36A showing the drop in SiO_2 plotted against distance from the contact with the dacitic intrusions. Fig 36B REE spider diagram showing the difference in trace element plots.

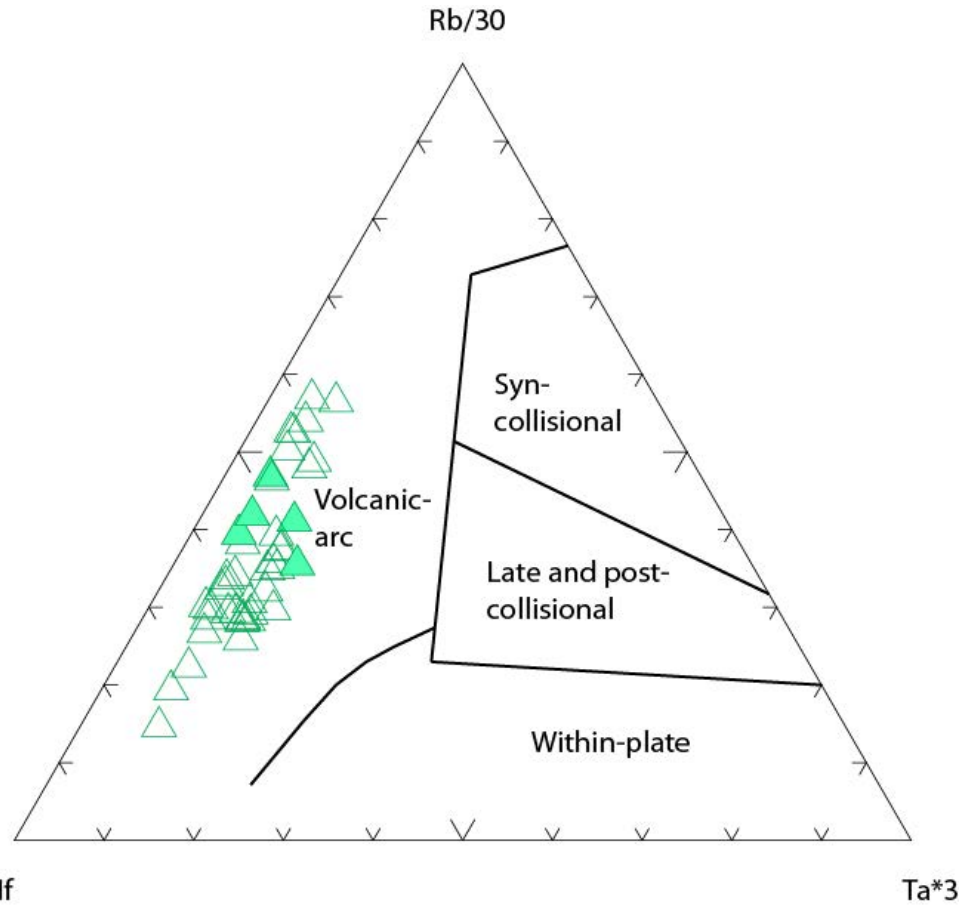

Figure 37. Hf-Rb/30-Ta*3 diagram (Harris et al., 1986) with dacite lava flows and dacitic intrusions plotting within a volcanic-arc setting.

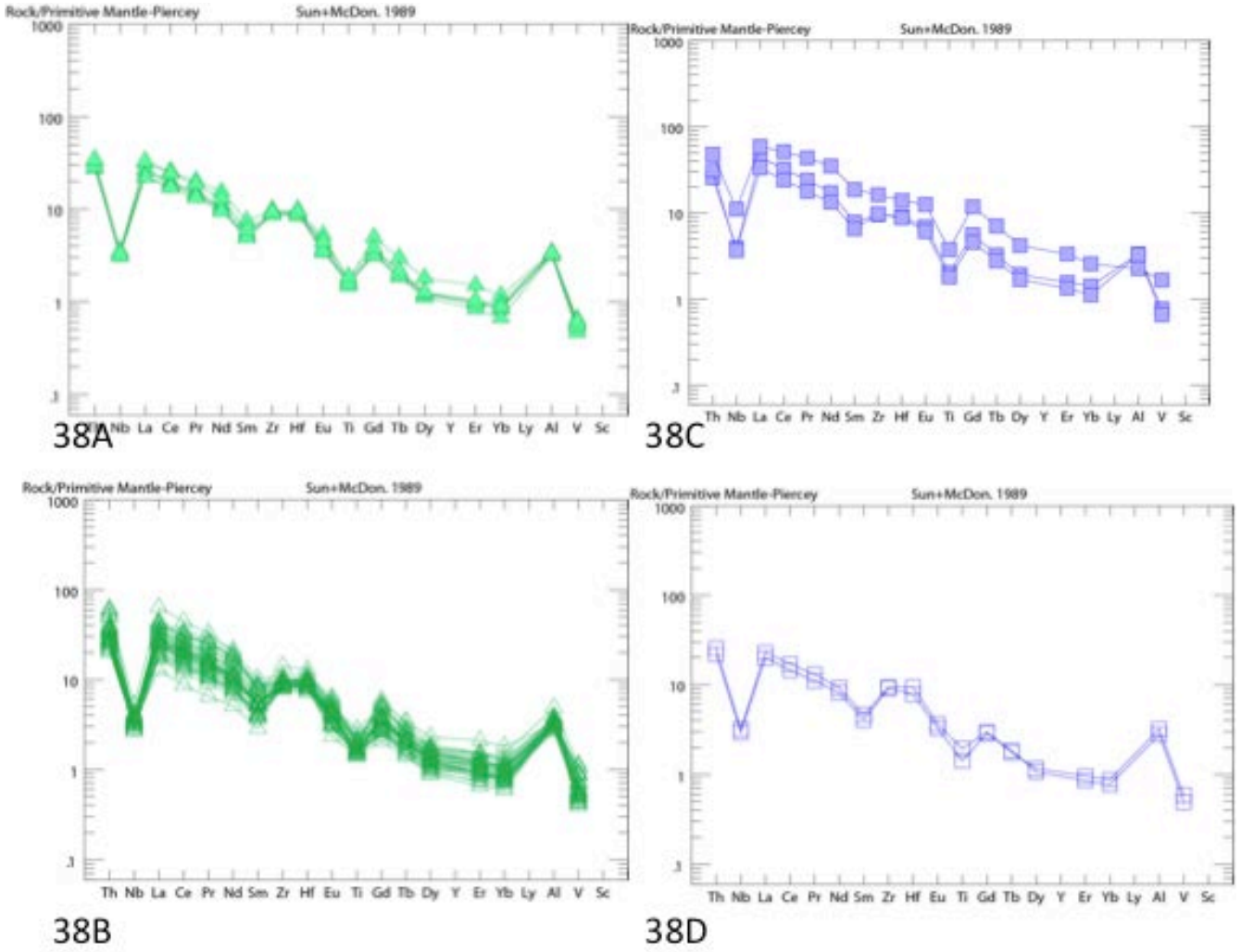

Figure 38. Comparison of the REE spider diagrams (chondite normalized-Sun and McDonough, 1989) of dacitic lava sills and dikes (Fig. 38A), dacitic lava flows (Fig. 38B), monomict breccias (Fig. 38C), and polymict breccias (Fig. 38D). Similar to the mafic facies all four felsic facies show almost identical REE slopes.

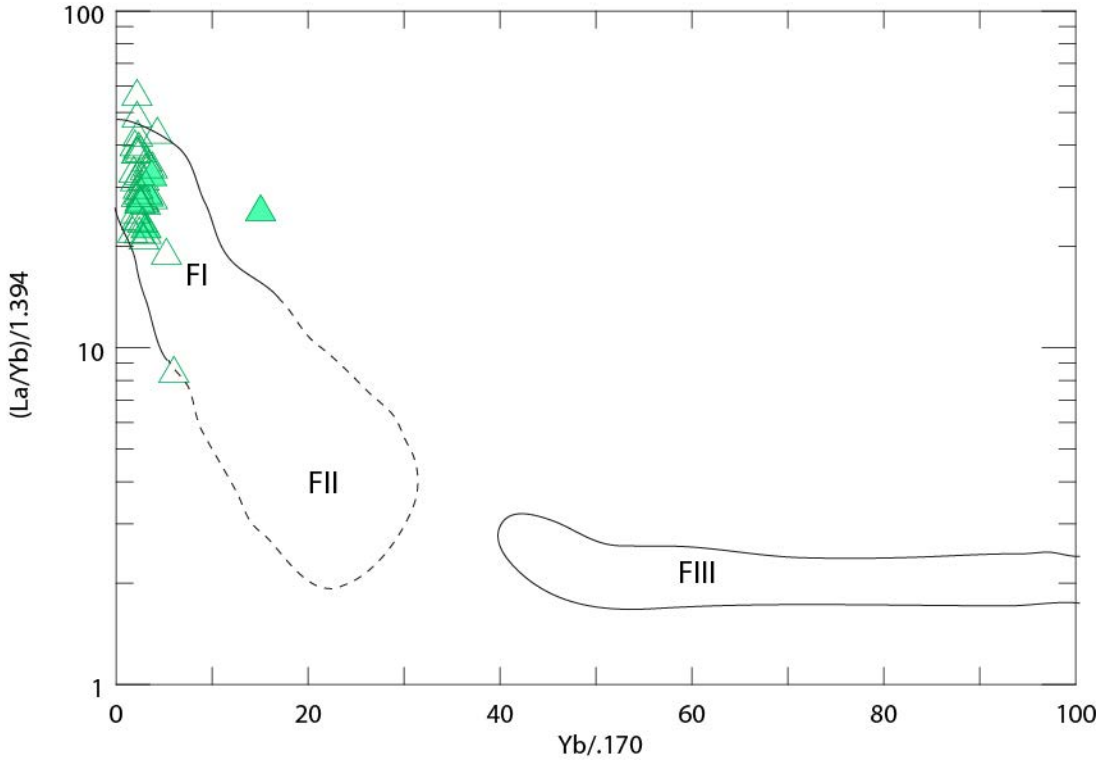

Figure 39. Plot of dacitic lava flows and intrusions that plot within the FI field of metavolcanics rocks (after Lesher et al., 1986)

and breccias related to autobrecciation which are more easily eroded and transported. Pillow selvages and pillow breccias are observed in basalt outcrops surrounding the RRGP. Basalt lavas in the RRGP are related to arc-like style volcanism and may form at a variety of water depths as seamounts or shield volcanoes creating bathymetric highs (Cas and Wright, 1992). With continued effusive eruptions the steepening of the volcanic flanks results in the resedimentation of brecciated material (Cas, 1992). It is possible that many of the mafic breccias associated with the basalt flows were eroded from bathymetric highs, creating the heterogeneous mafic tuff observed throughout the RRGP. The heterogeneity of the mafic tuff most likely the result of multiple sources involving the resedimentation of: 1) basalt lava flows; 2) pelagic sediments; and 3) clastic sediments. The occurrence of amygdaloidal mafic clasts indicates that the mafic tuffs were likely the results of mass flows and slumps that redeposited hyaloclastite and carapace breccias of the basalt lavas.

Dacites, both intrusive and extrusive, represent the majority of rocks at the RRGP. Typically volcanism is modeled as a surface process with emphasis placed on volcanic eruptions and their deposits (Gibson et al., 1999). These models commonly neglect the emplacement of magma as dikes, sills, and subvolcanic intrusions (Gibson et al., 1999). In most eruptions, the volume of magma emplaced in the near subsurface exceeds that erupted at surface (Moore, 1970). The similarities between the dacites throughout the felsic volcanic succession suggests that they were derived from the same magma chamber. Differences in quartz and feldspar crystal percentages indicates that the eruptions occurred over a time period sufficient to allow for some magma chamber crystallization.

Dacitic sills and dikes intrude the mafic tuffs and are commonly associated with peperites. The peperites are intermediate between the dacitic intrusions and the mafic tuffs. Peperites can form in a variety of settings where magmatism and sedimentation are contemporaneous, and where the host sediment is unconsolidated and wet. (Skilling et al., 2002). Peperites are most commonly associated with syn-volcanic intrusions occurring in a subaqueous setting (Busby-Spera and White, 1987). The association between dacitic intrusions, peperites, and mafic tuff, as well as chilled margins between dacite intrusions

and mafic tuff, demonstrates that portions of the dacitic magma were emplaced as sills and dikes while the mafic tuffs were still unconsolidated and wet; this allowed mixing to occur between them.

Dacitic lava flows containing amygdules are associated with hyaloclastites, lapilli tuffs, and sedimentary rocks. The homogeneity and primary textures of these dacite lava flows are interpreted as being related to effusive volcanism with emplacment as a dacitic lobe-hyaloclastite flow complex. Lobe-hyaloclastite flow complexes are fissure fed with individual flows typically traveling 2 to 5 km forming relatively broad, domal shaped (<200 m) lava shields. These flows are characterized by three facies;

1. massive lava;
2. lobe-hyaloclastite-syn-depositional peperites;
3. carapace and flank breccias (Gibson et al., 1999).

All three of these facies are present at the RRGP as dacitic crystal-rich lava flows, peperites, hyaloclastites, and polymict and monomict lapilli tuffs. The dacitic lava flows, previously interpreted as pyroclastic flows and conglomeratic units due to secondary textures resulting from alteration, are lava flows constituting the massive facies of this flow complex. This unit is composed of different flow lobes that can be distinguished by the variation in quartz and feldspar crystal content. Contacts between units are commonly difficult to establish because they have been obscured by alteration and metamorphism.

Hyaloclastites occur immediately adjacent to dacite flows. Hyaloclastites are a quenched fragmented aggregate formed by the nonexplosive shattering of lava when flowing into water, ice, or water-saturated sediments (Cas, 1992; Schmidt and Schmincke, 2000). The interaction between the hot magma and the cold fluid results in rapid heat loss which causes rapid contraction of the lava producing block-like fragments with curvi-planar surfaces; jigsaw fit textures may be common (Cas and Wright, 1992).

Lapilli tuffs can be generally divided into polymict or monomict types. Polymict units within the RRGP are poorly stratified with angular-subround lapilli-size clasts. They vary from clast-supported to matrix-supported. The units are indicative of mass flow transport processes such as a debris flows of flank and carapace breccias of the lobe/hyaloclastite flow succession (Rosengren et al., 2008). These mass flows are

compositionally variably and are made up of dominantly resedimented dacite with minor clay- and sand-sized components. Debris flows are dense, cohesive flowing mixtures of sediments and water and move downslope under the force of gravity; they are common in a volcanically active environments (Vallance, 2000). Because of this, the polymict lapilli tuffs are laterally confined and are poorly correlated throughout the RRGP area. Monomict lapilli tuffs can have rounded to angular fragments or clasts, and are dacite in composition. This indicates that the clasts are resedimented products of the hyaloclastite carapace. The monomict breccia may accumulate by the continued gravity flow of hyaloclastite and autoclastic debris down advancing flow fronts (Rosegren et al., 2008).

The thin horizons of sandstones and shales within the RRGP are interpreted to have been deposited during periods of volcanic quiescence. The units are laterally confined and poorly preserved because of overprint by dacitic lavas, mass flows, and subsequent structural deformation.

2.8 Mode of emplacement

Based on volcanological facies studies a history of the felsic succession at the RRGP can be reconstructed (Fig. 40). Volcanic rocks at the RRGP are related to bimodal volcanism of effusive tholeiitic basalt flows and dacites in a volcanic arc-like setting. From trace element data the tholeiitc basalt and dacites were likely sourced from two different magma chambers. The stratigraphy suggests that these two processes occurred contemporaneously, possibly on the flank of a large shield volcano.

Initially, large amounts of basalt lavas were emplaced on the seafloor, likely producing bathymetric highs. Large amounts of autoclastic basalt was eroded during this large-scale volcanic event resulting in the formation of the mafic tuffs. Contemporaneous with the tholeiitic basalt lava flows, low density calc-alkaline dacitic magma buoyantly rose and was emplaced below the mafic tuffs. Magma rose further, possibly through fractures and faults related to the arc-like system, and spread laterally through the mafic tuff pile as dikes and sills with some disintegration of the intrusion(s) and surrounding mafic tuff resulting in peperites.

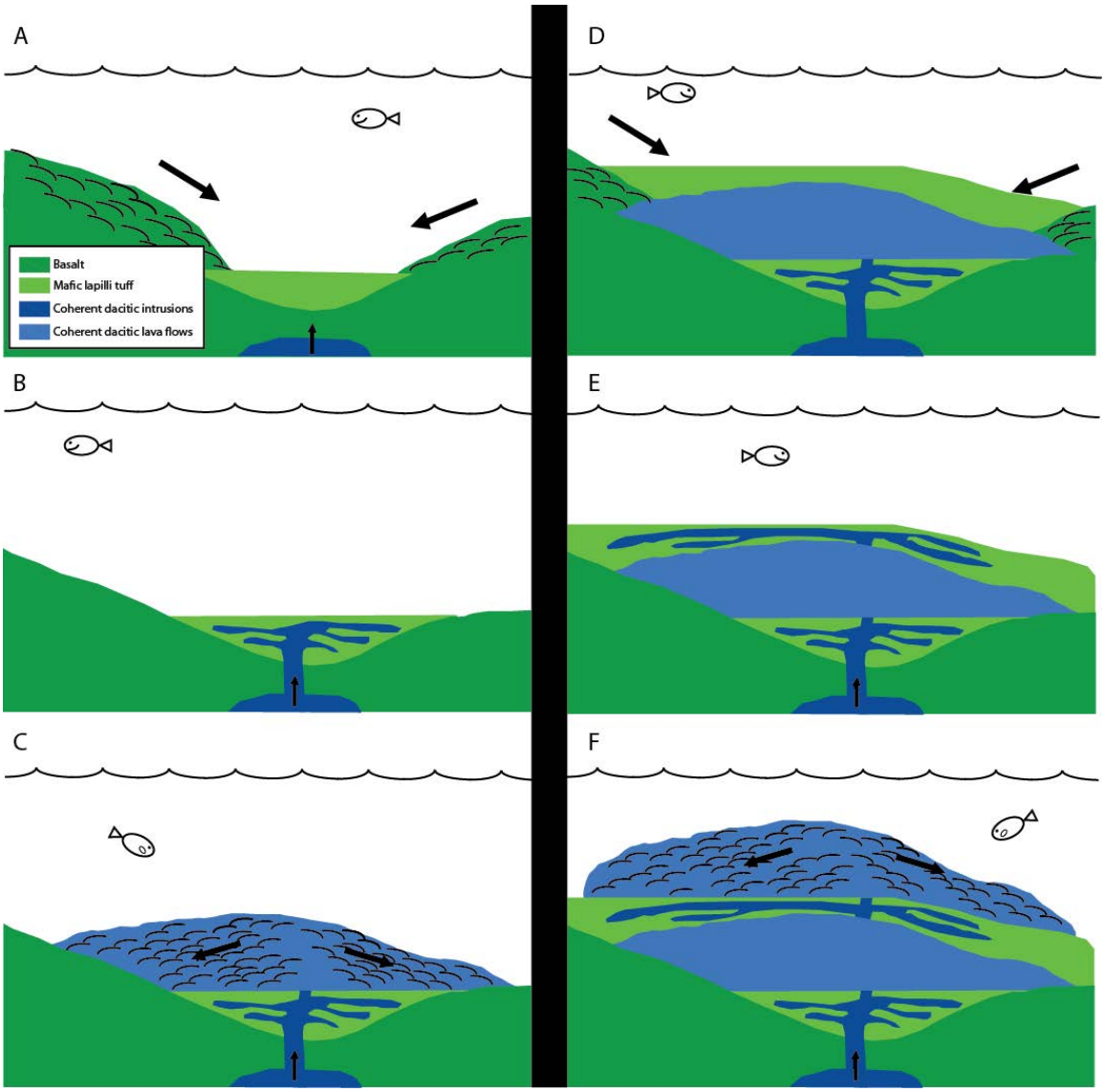

Figure 40. Schematic reconstruction of the volcanology of the RRGP. (A) Mass flow and resedimentation of hyaloclastites and breccias related to seamounts and arc building basalts. (B) Rising of dacitic magma and emplacement of dacite into fractures and voids related to arc basalt volcanism, sediments are generally dry and moderately lithified with some wet sediment dacitic lava interaction resulting in peperites. (C) Continued volcanism and breach of the surface resulting in dacitic lavas emplaced as part of a lobe-hyaloclastite flow complex. Carapace breccias and hyaloclastites result in the monomict and polymict breccias in the deposit. (D) Quiescence in the dacitic magma chamber and more mass flows and slumps from the surrounding arc basalts—possibly triggered by gravitation instabilities caused by the emplacement of the dacites. (E) Reactivation of the dacitic magma chamber resulting dacitic intrusions and peperites in the poorly lithified, wet mafic sediments. (F) Dacitic lavas again breach the surface resulting in another lobe-hyaloclastite flow with subordinate breccias.

The dacitic magma continued its ascent until it breached the surface and was erupted subaqueously as lobe-hyaloclastite flow complexes. These flows are chemically and compositionally identical to the dikes and sills but have textures indicative of subaqueous effusion. The dacite lava flows are intercalated with monomict breccias and hyaloclastites. Areas of the RRGP lacking breccias, composed almost entirely of dacite lava flows, are the result of a sustained flow-through of lava, which rapidly emplaced the dacites directly over one another. The abundance of polymict breccias towards the north and east could indicate the limits of the lobe-hyaloclastite flow complex.

During the effusive dacitic eruptions mass flows of mafic material continued to be deposited on top of the dacitic volcanic pile as thin 1-8 m thick mafic tuffs and one large 150 m thick pile of mafic tuff. This large mass flow could have been the result of gravitational instability triggered by dacitic volcanism and tectonically associated with the dacite magma chamber. Continued dacitic volcanism led to the intrusion of the still wet mafic tuff pile, which resulted in the formation of abundant peperites. Dacitic magma again reached the ocean floor and resulted in a second period of effusive dacitic volcanism. After the dacitic volcanism had terminated, the dacitic volcanic pile was covered by massive and pillowed basalt flows.

3.0 Alteration

3.1 Introduction

Hydrothermal fluids have long been recognized as a critical component for the formation of a wide variety of mineral deposits. Throughout earth history, many mineral deposits have formed or been modified directly by hot aqueous solutions flowing through the crust (Robb, 2005). These fluids are driven by a local heat source that circulates water through the crust leading to large scale interaction between the fluid and the surrounding rocks (Robb, 2005). This interaction leads to various degrees of rock alteration, which is characterized by the development of a mineral assemblage that is different than that found in the original rock (Reed, 1997). These mineralogical and chemical changes result from metasomatic changes where the composition of a rock changes as a result of the introduction or removal of chemical constituents (Gifkins et al., 2005). Secondary alteration compositions (e.g. minerals) reflect the original rock composition, as well as the properties and amount of fluid that has interacted with the rock (Reed, 1997). Hydrothermal fluids are known to have been important in the RRGP because of the presence of veins and minerals that cannot be explained by igneous and sedimentary compositions subsequently modified solely by metamorphic processes (Osterberg et al., 1987). Understanding the hydrothermal system at RRGP is important because alteration zones mark the pathways of hydrothermal fluids and may represent a useful guide for further exploration (Robb, 2005).

In addition to hydrothermal alteration, the rocks of the RRGP have undergone regional mid- to upper-greenschist grade metamorphism (Mackie et al., 2003). Metamorphism is defined as the chemical, mineralogical and textural changes in a rock in response to increasing pressure and temperature, commonly during subduction or orogenic episodes (Gifkins et al., 2005). Regional metamorphic events modified both primary and secondary minerals, resulting in metamorphic mineral assemblages consistent with post-alteration compositions. This regional metamorphic assemblage is best observed in the footwall and hanging wall basalt lava flows, which contain chlorite (25-20%), actinolite (15-20%), carbonate (10-15%), and epidote (25-35 %)—the expected greenschist facies of a mafic volcanic rock (Fig. 41; Winter, 2000).

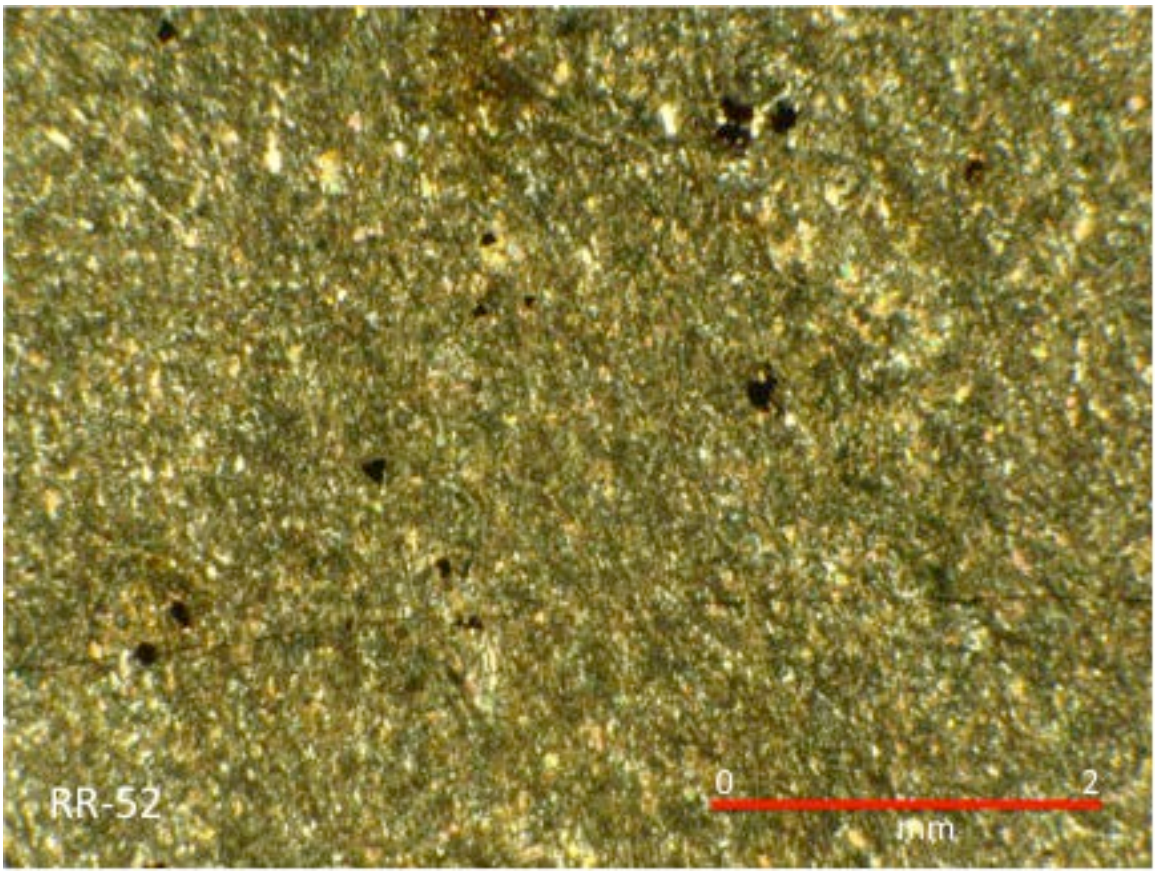

Figure 41. Photomicrograph of footwall basalt metamorphosed to greenschist facies. Crossed polars.

3.2 Alteration assemblages

Hydrothermal alteration is variable throughout the felsic rocks that host the deposit. Based on studies at other hydrothermal mineral deposits (e.g. Osterberg et al., 1987; Franklin et al., 2005; Whitford et al., 1989; Gemmell, 2007), this variability is likely dependent on many factors including: 1) permeability and composition of the host rock; 2) composition and temperature of the hydrothermal fluid; 3) hydrostatic pressure; and 4) the fluid to rock ratio, which is defined as the volume of water that passes through a given volume of rock during the period of alteration (Reed, 1997). Differences in rock properties (both within and across facies) and circulating fluids result in individual lithologies containing multiple alteration assemblages. Understanding the spatial distribution of alteration assemblages and their mineralogical and chemical characteristics can help identify the setting and type of hydrothermal system that occurred at the RRGP. Hydrothermal alteration assemblages are distinguished from regional metamorphic assemblages based on the presence and abundances of mineral that cannot be solely due to regional metamorphism (Osterberg et al., 1987). Secondary mineral assemblages and mineral textures of these secondary minerals are the primary means used to separate different hydrothermal alteration assemblages (Osterberg et al., 1987).

Alteration in the felsic succession is characterized by quartz, sericite and chlorite. Based on the abundances of these minerals five different alteration mineral assemblages have been defined within the felsic succession of the RRGP: 1) least-altered (LA); 2) moderately sericite altered (MSA); 3) strongly sericite altered (SSA); 4) epidote-bearing (EPB); and 5) chlorite/carbonate altered (CCA).

The three sericitic zones are distinguished using the modal proportion of sericite. Samples containing <20% modal sericite are defined as the least-altered assemblage, between 20-35% modal sericite are defined as the MSA, and those with >35% modal sericite are defined as the SSA. These alteration assemblages range in lateral extent and thickness; contacts between the assemblages are dominantly gradational and locally alteration assemblages can overprint one another on a meter scale.

3.2.1 Least-altered (quartz + sericite ± chlorite ± carbonate)

Least altered rocks within the felsic succession of the RRGP have compositions similar to that expected from greenschist facies metamorphism of an unaltered dacite. The unit is distinguished by a tan to white color and relative lack of pseudo-clastic or pseudo-tuffaceous textures (Fig. 42). Additionally, foliation is poorly developed and crosscutting veins are rare. The LA assemblage occurs in dacitic sills and dikes, dacitic lava flows and sedimentary rocks. Zones of LA assemblages vary in thickness from 10-150 m and commonly grade into the MSA assemblage.

The LA assemblage consists predominately of a very fine-grained matrix of 40-60% microcrystalline quartz with 5-20% very fine-grained interstitial sericite (Fig. 43). Relict fine- to medium-grained feldspars are present and are partially to totally replaced by sericite (Fig. 44). Fine-grained needle- to lath-shaped, green birefringent (Mg-rich) chlorite (0-10%) occurs within the matrix and ranges in abundance from 0-10%. Fine- to medium-grained carbonate (5-15%) occurs in two forms: 1) in aggregates of ankerite and dolomite with chlorite and pyrite; and 2) as rare late crosscutting veins of calcite. Very fine- to fine-grained biotite (0-5%) is a minor component of the assemblage and occurs near the Black Hawk Stock and below 500 m depth in several central section drill holes. Fine-grained anhedral to cubic pyrite (0-8%) occurs disseminated in the matrix, and is commonly rimmed by sericite, chlorite and carbonate.

3.2.2 Moderately sericite-altered (quartz + sericite ± chlorite ± carbonate)

MSA samples are tan white to grey in color, and can be distinguished from LA rocks based on an increase in pseudo-clastic textures and abundant patchy sericite and chlorite (Fig. 45). Increases in crosscutting veins and foliation can also be used to distinguish this unit from LA rocks. The MSA assemblage occurs in dacitic sills and dikes, dacitic lava flows and both monomict and polymict lapilli tuffs. Contacts between MSA assemblages and LA and SSA assemblages are typically gradational.

MSA rocks contain between 20-35% very fine to fine-grained sericite, both interstitially in the microcrystalline matrix, as well as in veins parallel to the foliation (Fig. 46). Pseudo-clastic textures are present and are locally associated with increases of

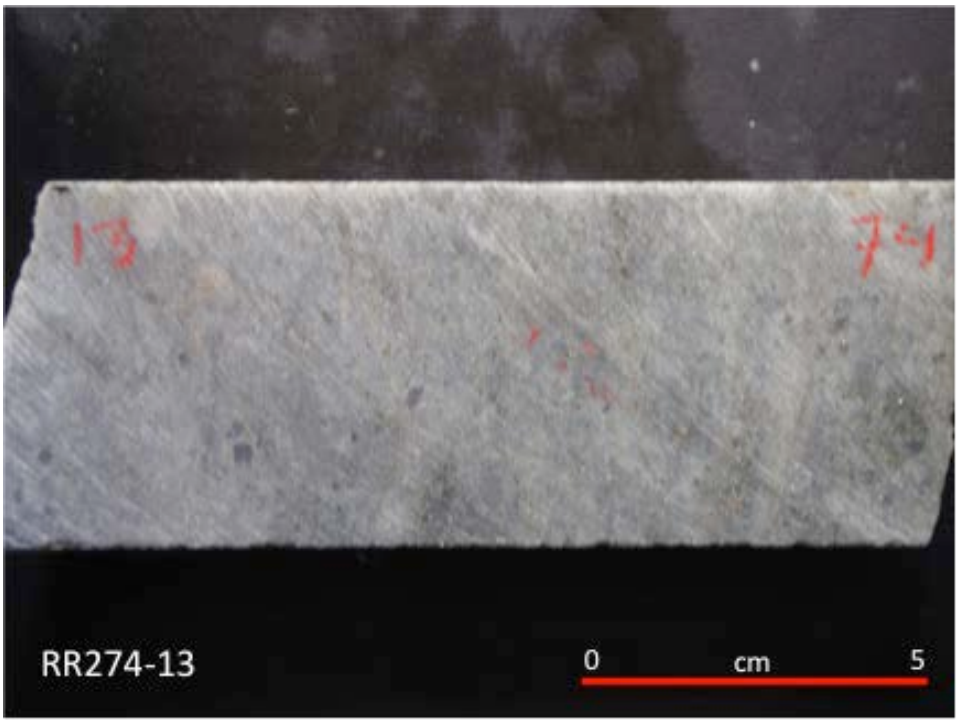

Figure 42. Weakly sericite altered drill core sample of a dacitic lava flow.

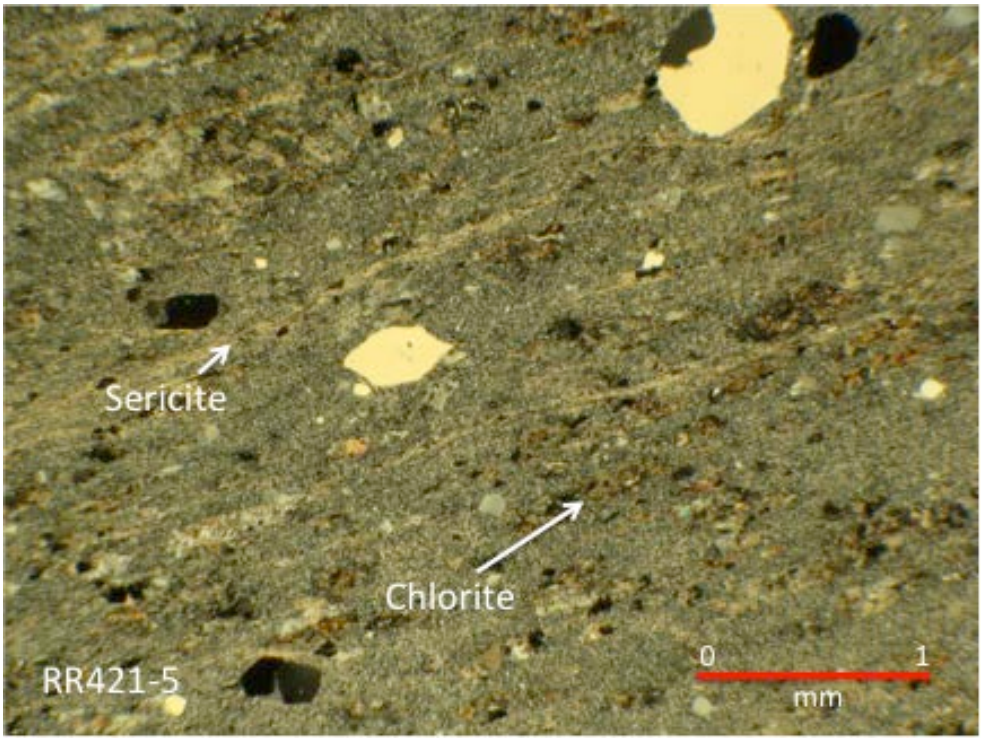

Figure 43. Weakly sericite altered sample of a dacitic lava flow, sample has 10% disseminated sericite with minor chlorite. Quartz crystals are euhedral-subround and non fragmented. Crossed polars.

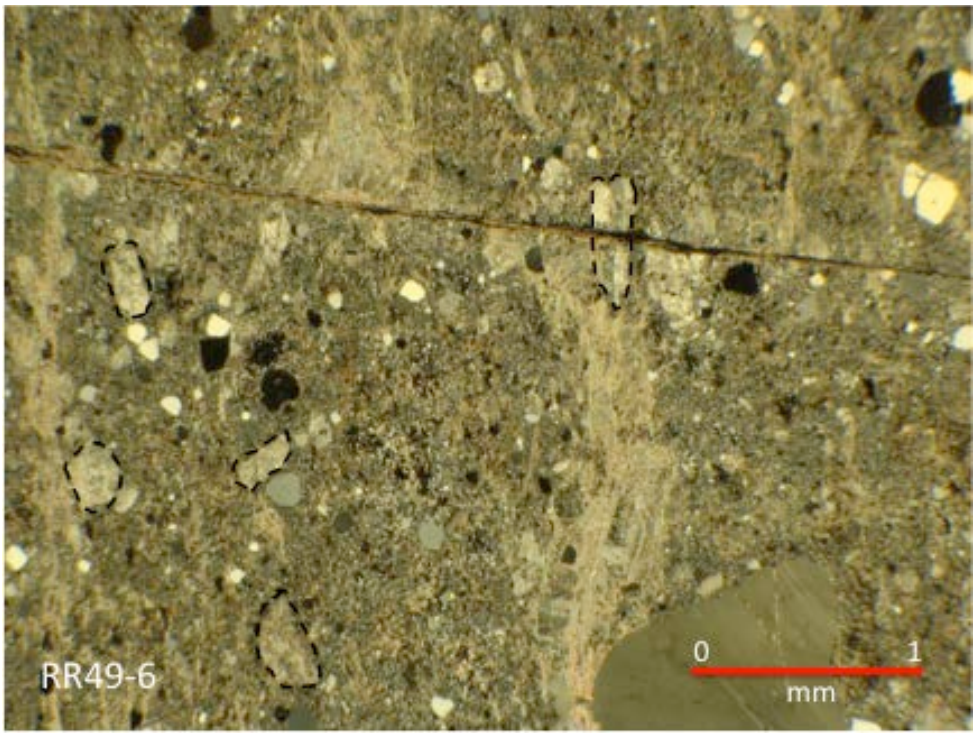

Figure 44. Sericite pseduomorphs after plagioclase feldspar (outlined) in a weakly sericite altered sample of a dacitic sill or dike. Crossed polars.

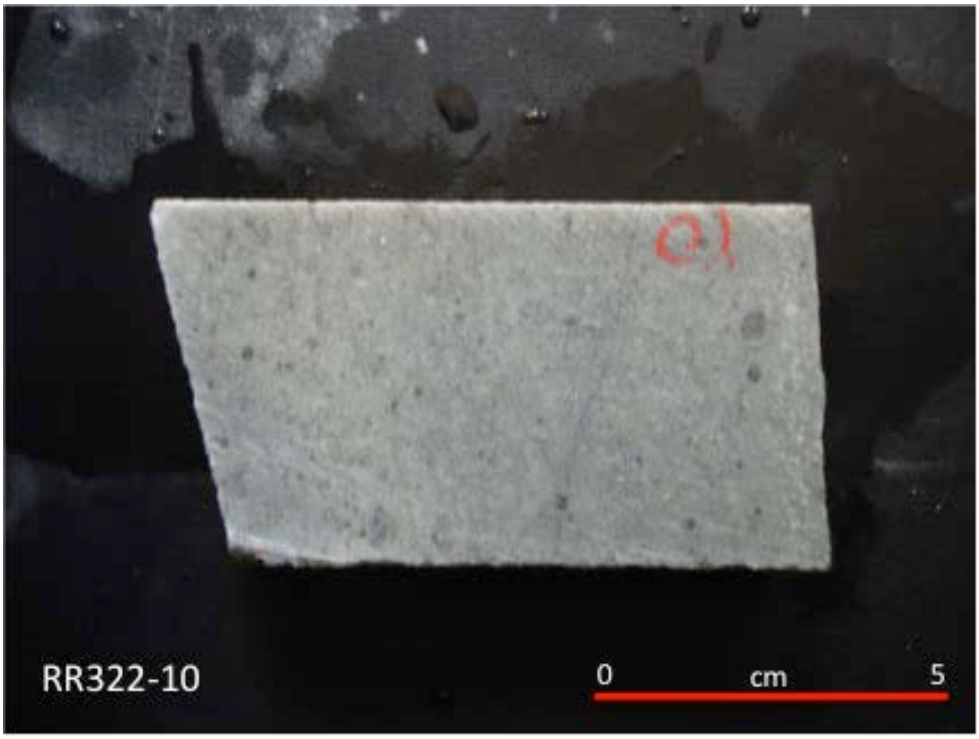

Figure 45. Moderately sericite altered drill core sample of a dacitic sill or dike.

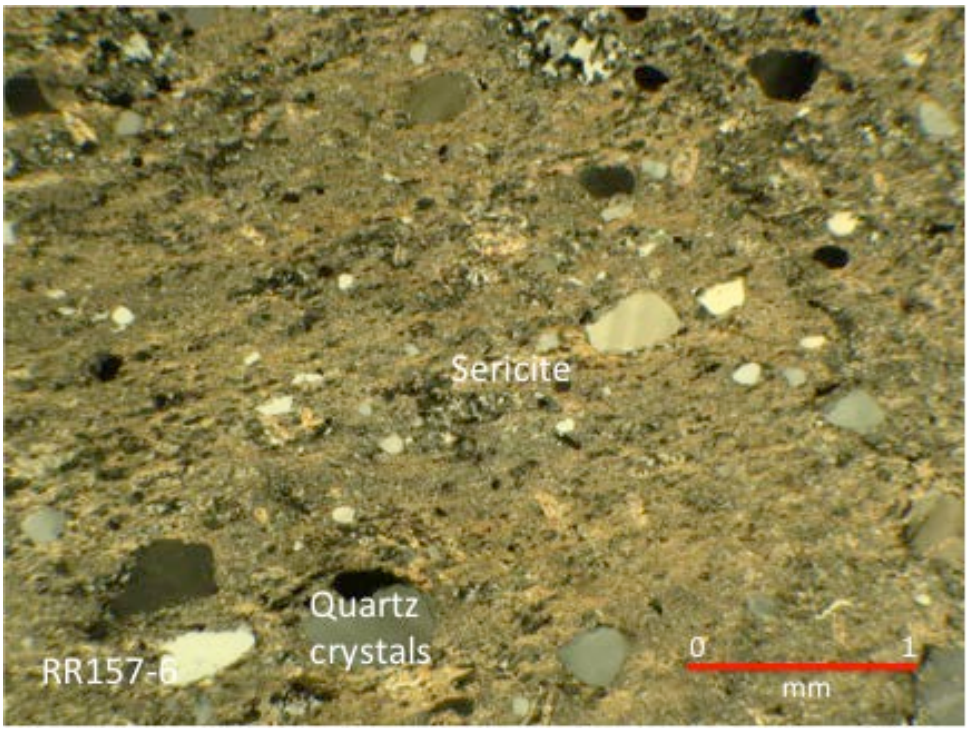

Figure 46. Moderately sericite altered sample of a dacitic lava flow. Sericite is disseminated in the matrix and defines rock foliation in veinlets. Crossed polars.

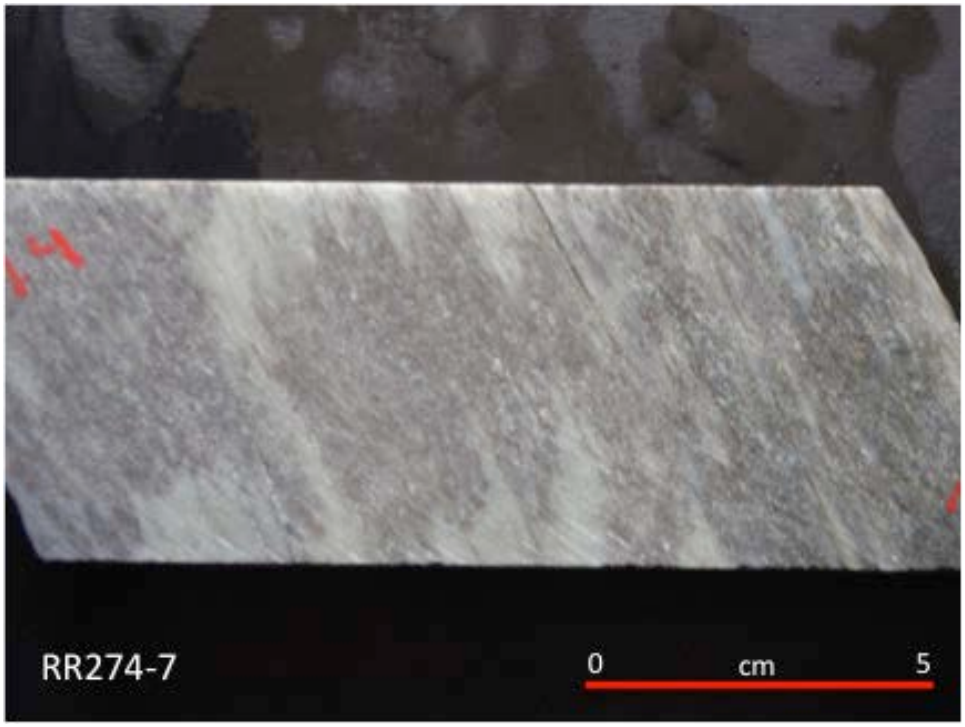

Figure 47. Strongly sericite altered drill core sample of a dacitic lava flow.

chlorite and carbonate. Fine- to medium-grained, disseminated subhedral to anhedral ankerite and dolomite occurs within the matrix. Carbonate also occurs in abundant 0.3-1.4 cm thick, crosscutting calcite veins. Fine-grained Mg-chlorite (5-35%) occurs both as interstitial grains and as discontinuous 0.2-1.3 mm thick veins that parallel foliation. Fine- to medium-grained cubic to anhedral pyrite (2-15%) occurs disseminated in the matrix, typically rimmed by chlorite and/or ankerite and dolomite.

3.2.3 Strongly sericite-altered (quartz + sericite ± chlorite ± carbonate)

The SSA assemblage is distinguished from the MSA assemblage based on its abundant pseudo-clastic and pseudo-tuffaceous textures in drill core (Fig. 47). In drill core samples of SSA rocks can be highly variable in appearance ranging in color from light green (from abundant chlorite) to dark grey, and can be locally strongly silicified with a bleached appearance. This alteration assemblage consists of intense sericite-rich domains (>50%) that, coupled with polyphase deformation, result in the appearance of many pseudo-clastic textures. SSA assemblages occur in dacitic lava flows, polymict lapilli tuffs, and mafic tuffs (rare). Crosscutting veins can be abundant and foliation can be intense. SSA rocks typically grade into MSA or LA assemblages.

The SSA assemblage is characterized by >35% very fine-grained sericite. Sericite occurs both interstitially in the microcrystalline quartz matrix (Fig. 48) and as 0.2-1.2 mm thick veins that define the rock fabric. Near areas of strong deformation, sericite can be intensely foliated (Fig. 49). Quartz crystals are increasingly elongate with an increase in the intensity of the foliation. Bladed to tabular laths of very fine- to fine-grained chlorite (15-35%) is commonly disseminated in the matrix and occurs in veins orthogonal to rock fabric or as discontinuous veinlets within sericite-rich domains. Fine- to medium-grained ankerite and dolomite is common in the matrix (10-30%), and is also observed replacing epidote group minerals. Abundant late quartz-calcite veins crosscut the assemblage. Fine- to medium-grained pyrite (5-25%) varies between samples but is more abundant in the SSA units than other alteration assemblages. Fine- to medium-grained chalcopyrite is rare (0-2%) as stringer and vein fillings and sphalerite is absent in this assemblage.

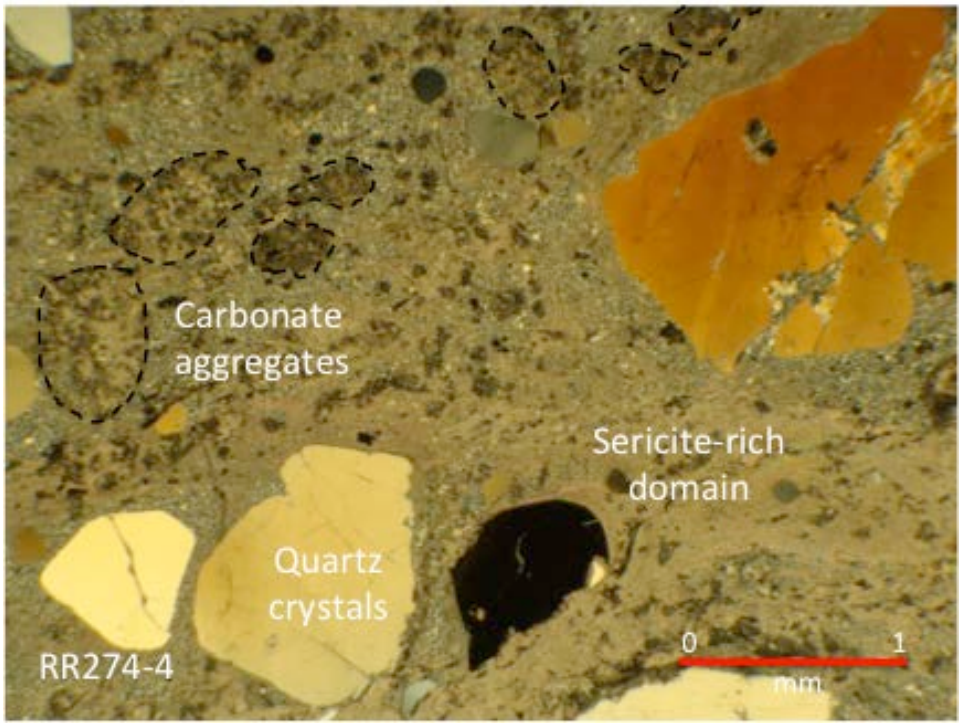

Figure 48. Strongly sericite altered sample of a dacitic lava flow with abundant grungy carbonate aggregates (outlined). Crossed polars.

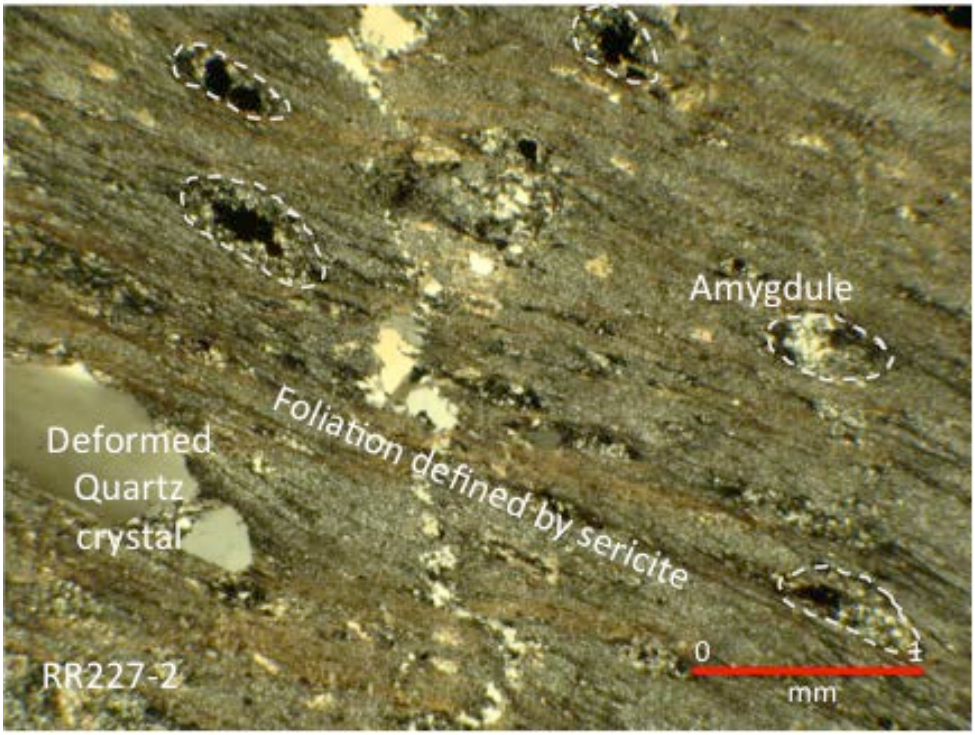

Figure 49. Strongly sericite altered and foliated sericite sample of a dacitic lava flow. Section contains amygdules parallel to foliation (outlined). Crossed polars.

3.2.4 Epidote-bearing (quartz + sericite ± chlorite ± carbonate + epidote ± zoisite/clinozoisite ± garnet)

EPB rocks are difficult to distinguish from sericite-altered rocks in hand sample because of their similarities in appearance (Fig. 50). Epidote group (epidote ± zoisite/clinozoisite) minerals are too fine-grained to be seen in hand sample, and can only be distinguished by petrographic analysis. All samples defined as EPB by petrography are confined to dacite lava flows. Because of the small sample size and the inability to distinguish the EPB assemblage in hand sample, its spatial distribution is poorly constrained.

The EPB is mineralogically similar, and in hand sample identical in appearance, to the SSA assemblage; it is distinguished petrographically by the presence of minor (1-10%) very fine-grained epidote ± zoisite/clinozoisite. The epidote ± zoisite/clinozoisite is disseminated in the groundmass, associated with sulfides (Fig. 51), and is commonly replaced by fine-grained ankerite and dolomite. Epidote ± zoisite/clinozoisite also occur as euhedral crystals in fragmented sericite veins. Rare (1-5%), fine- to medium-grained, spessartine (Mn-rich) garnets were observed in two samples of the EPB assemblage (Fig. 52). The subhedral to anhedral garnet poikiloblast contain numerous quartz, chlorite and sericite inclusions. Fine-grained pyrite (5-20%) is the most abundant sulfide, but 1-2% fine-grained chalcopyrite and sphalerite occur with sericite and/or dolomite or ankerite.

3.2.5 Chlorite/carbonate altered (quartz + (fe, mg) chlorite + carbonate)

The chlorite/carbonate alteration assemblage has a pale green to dark green color in outcrop and drill core, and has previously been interpreted as representing mafic lava flows (Fig. 54). This alteration type locally has pseudo-clastic textures due to the presence of 1-2 cm carbonate aggregates within a chloritic matrix (Fig. 55). The CCA assemblage is locally interlayed on a meter scale with the SSA assemblage. The alteration assemblage is not widespread; however, where it occurs, it is intense. The assemblage is pervasive in the mafic tuff facies and rarely observed within the felsic facies.

In thin section this assemblage comprises 25-50% fine to medium-grained ankerite and dolomite with 10-50% fine-grained chlorite. Chlorite occurs both as blue

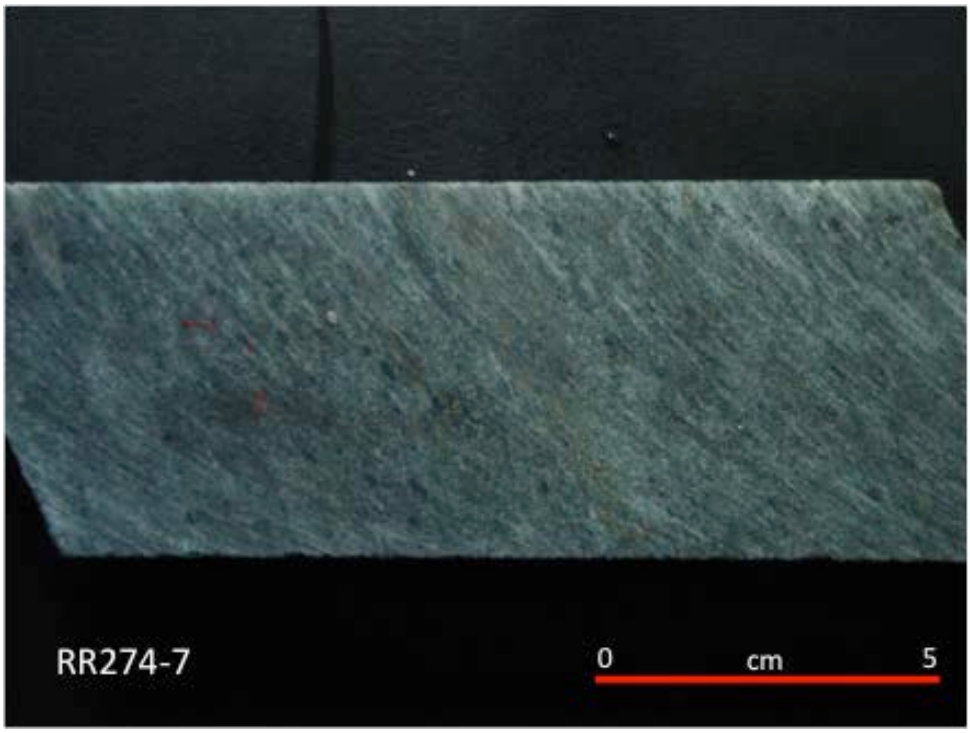

Figure 50. Epidote bearing drill core sample of a dacitic lava flow. Color is due to chlorite in the groundmass.

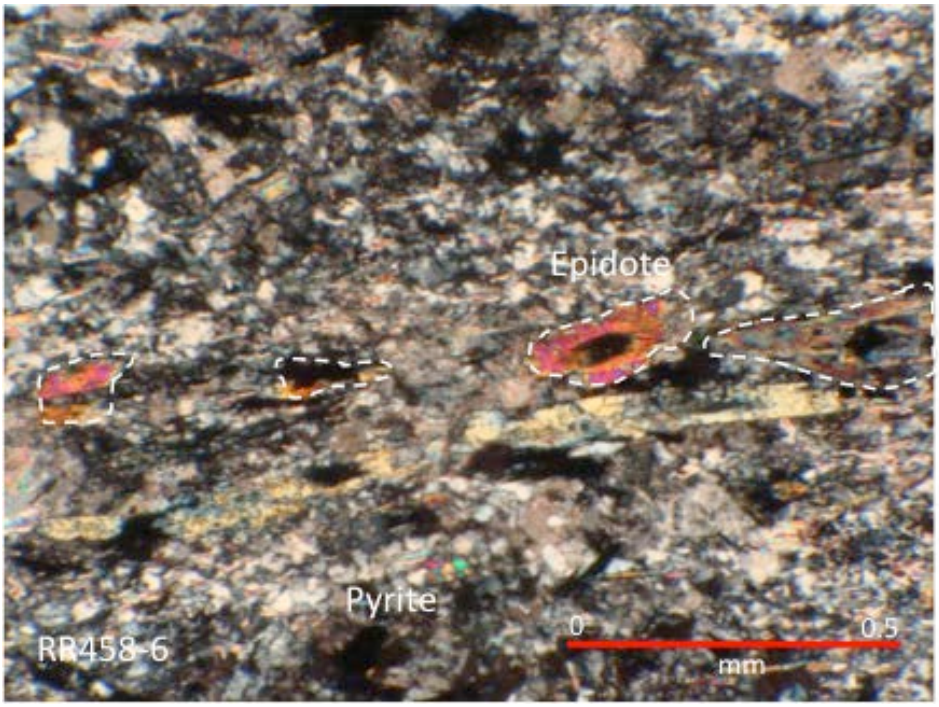

Figure 51. Epidote-bearing sample in a dacitic lava flow. Note the similarity between the strongly sericite altered sample and the epidote altered sample. Epidote is associated with abundant sericite and carbonate and makes up ~3% of the sample. Crossed polars.

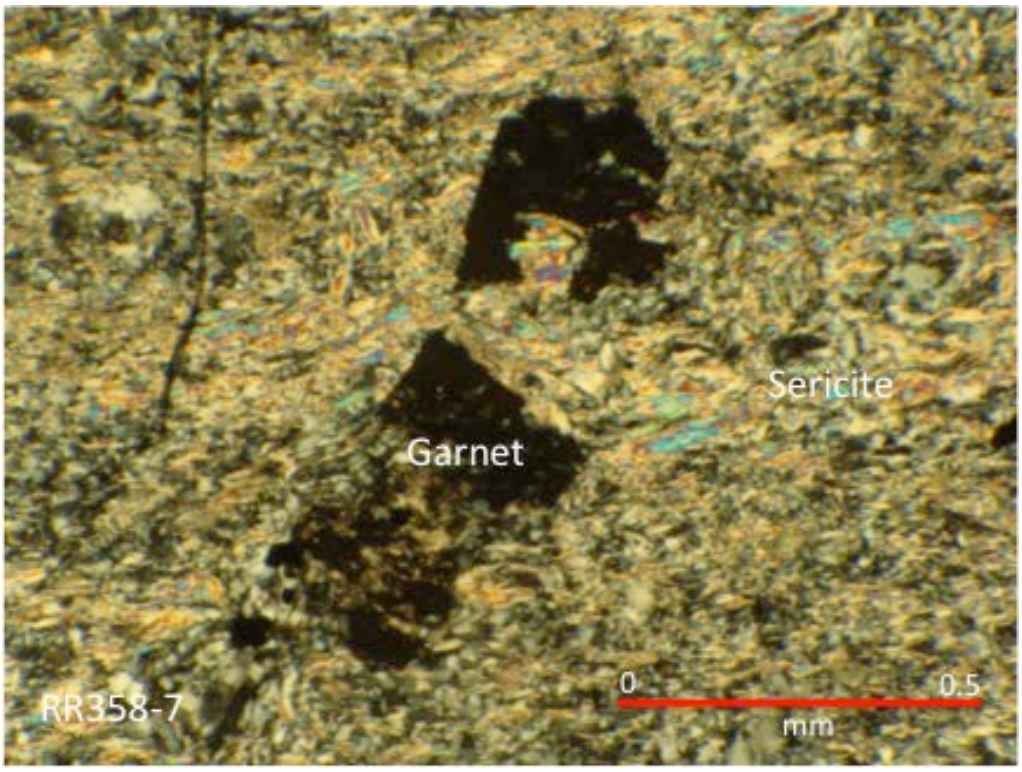

Figure 52. Garnet poikiloblast disseminated in a epidote bearing sample. Garnet is rare and was only observed in two samples. Crossed polars.

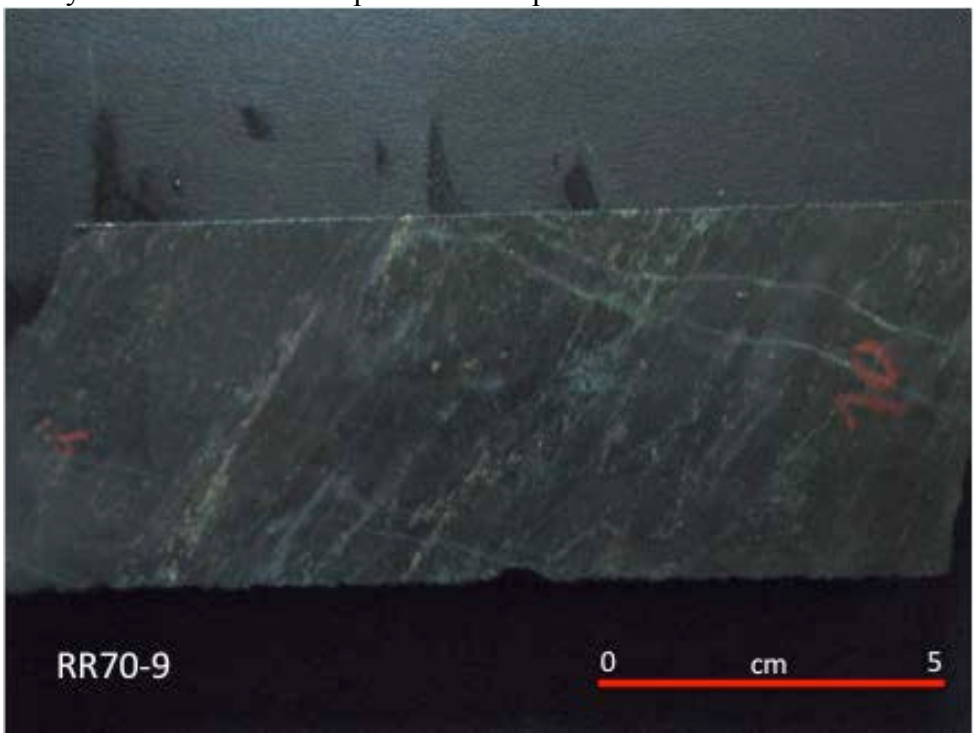

Figure 53. Chlorite/carbonate alteration of a mafic tuff.

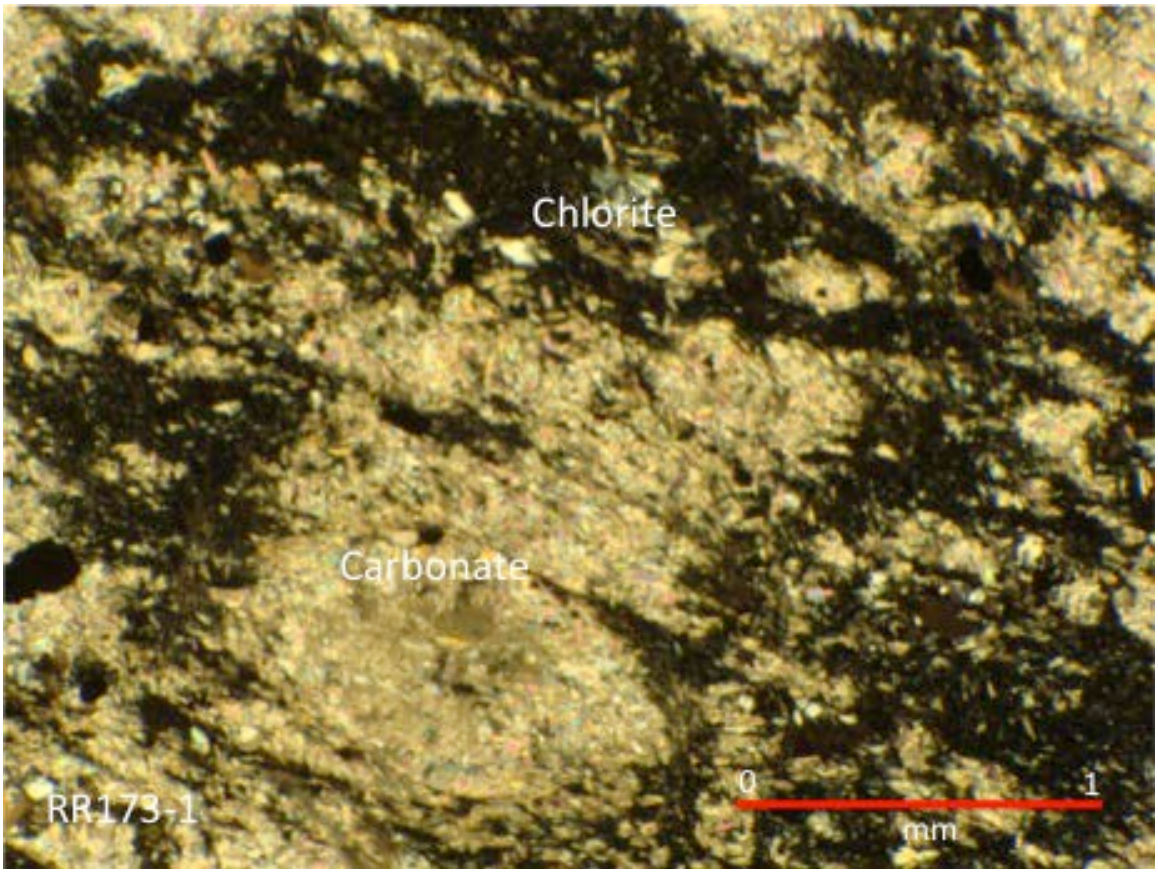

Figure 54. Carbonate/chlorite altered sample in a mafic sedimentary rock. Carbonate is patchy and occurs as 0.5-2 cm pseudo-clasts surrounded by chlorite. Crossed polars.

birefringent (Fe-rich) and green birefringent (Mg-rich) crystals (Hey, 1954). A lack of samples limits any spatial distribution of the different compositions of Mg vs. Fe chlorites. In several samples, the chlorite and carbonate have almost completely replaced all other minerals. Fine-grained sericite (5-20%) locally occurs disseminated in the matrix as well as within veinlets that are parallel to chlorite veins and 5-15% fine- to medium-grained pyrite occurs in the chlorite/carbonate groundmass.

3.3 Alteration distribution

Surficial distribution of the different alteration assemblages was compiled from outcrop mapping, petrographic analysis, and previous RRRL and NRL RC geochemistry (Plate 2). Alteration assemblages in the RRGP appear to be semiconformable (Figs. 55, 56 and 57); however, zones of originally high rock permeability and strong deformation (i.e. shear zones) are associated with increased alteration intensities from adjacent less altered rock. The SSA (and possibly the EPB) assemblage occurs in several lithologies including: dacitic lava flows, lapilli tuffs, and mafic tuffs. LA and MSA are restricted to dacitic lava flows, dacitic intrusions and sedimentary rocks. Shear zones within the dacites are typically altered to SSA and CCA assemblages. CCA is common within mafic tuffs and the matrix to the peperites. Mafic units locally contain the SSA assemblage interspersed with the CCA assemblage on a meter scale. Alteration intensities appear to increase with greater primary lithological permeability, as WSA assemblages grade into SSA assemblages approaching permeable horizons and shear zones.

3.4 Paragenesis of secondary minerals

Because of the similarities in composition (i.e. the ubiquitous nature of quartz, chlorite, sericite and carbonate) and textures across the RRGP, a parageneis of the alteration minerals within the felsic succession can be defined (Fig. 58). This parageneis is based on petrographic study of crosscutting relationships and textures in this study, as well as earlier microprobe and petrographic work by Schandl (2006).

Early stage hydrothermal alteration related to a syn-volcanic hydrothermal system is marked by quartz, sericite, and epidote. Quartz is the earliest secondary mineral and

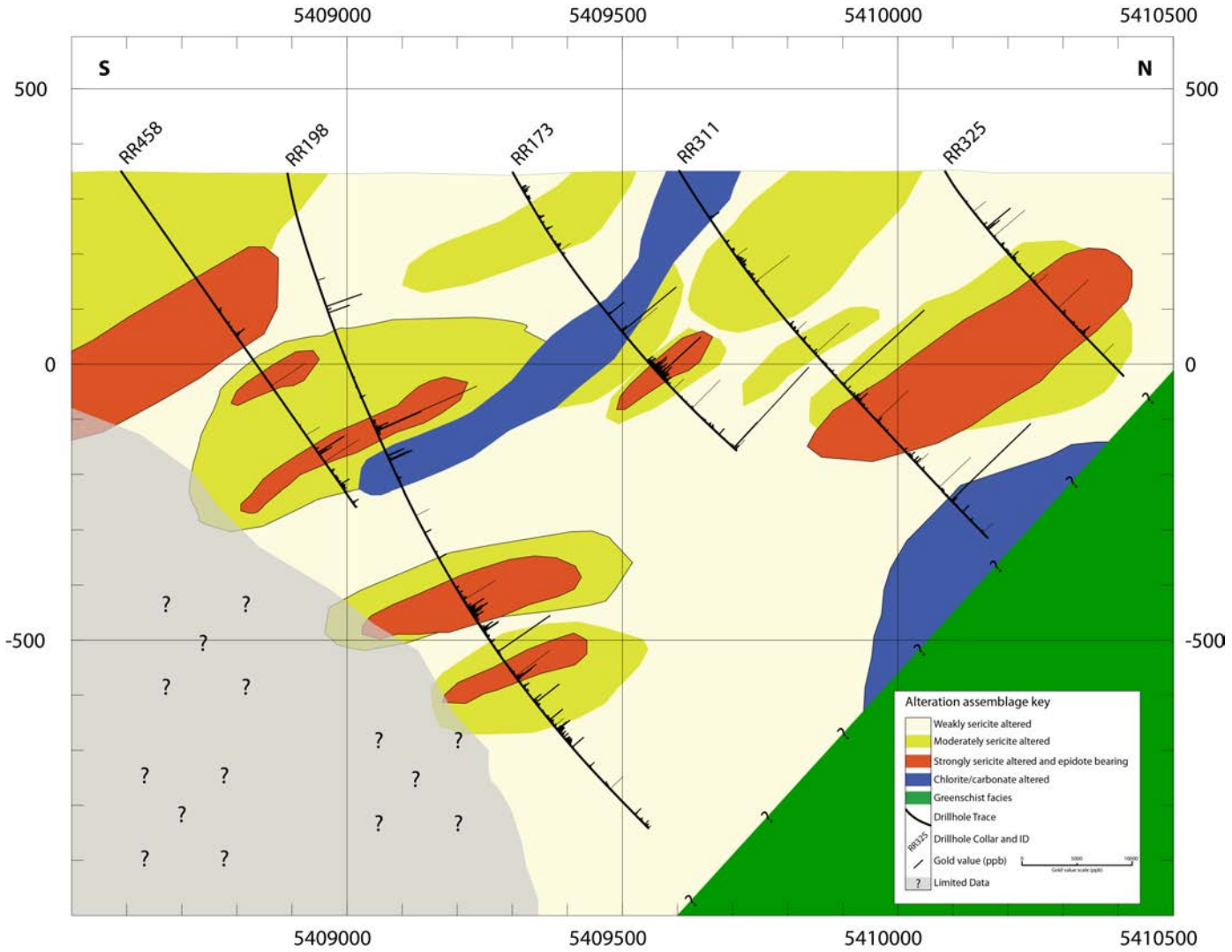

Figure 55. Alteration cross section along the west section line. Numbers at top and bottom are NAD83 UTM Northings (m). Numbers at left and right of cross section are elevation (masl).

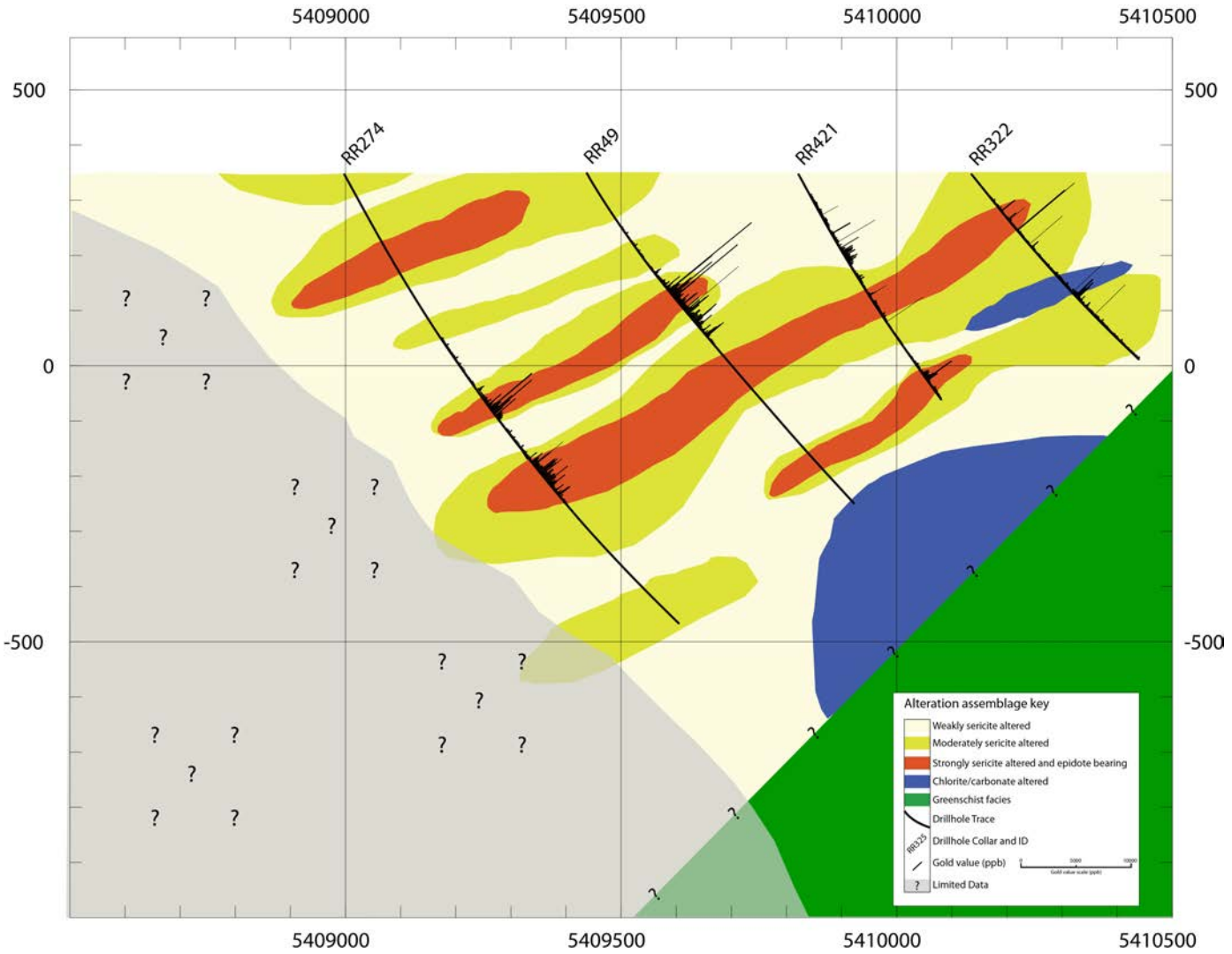

Figure 56. Alteration cross section along the central section line. Numbers at top and bottom are NAD83 UTM Northings (m). Numbers at left and right of cross section are elevation (masl).

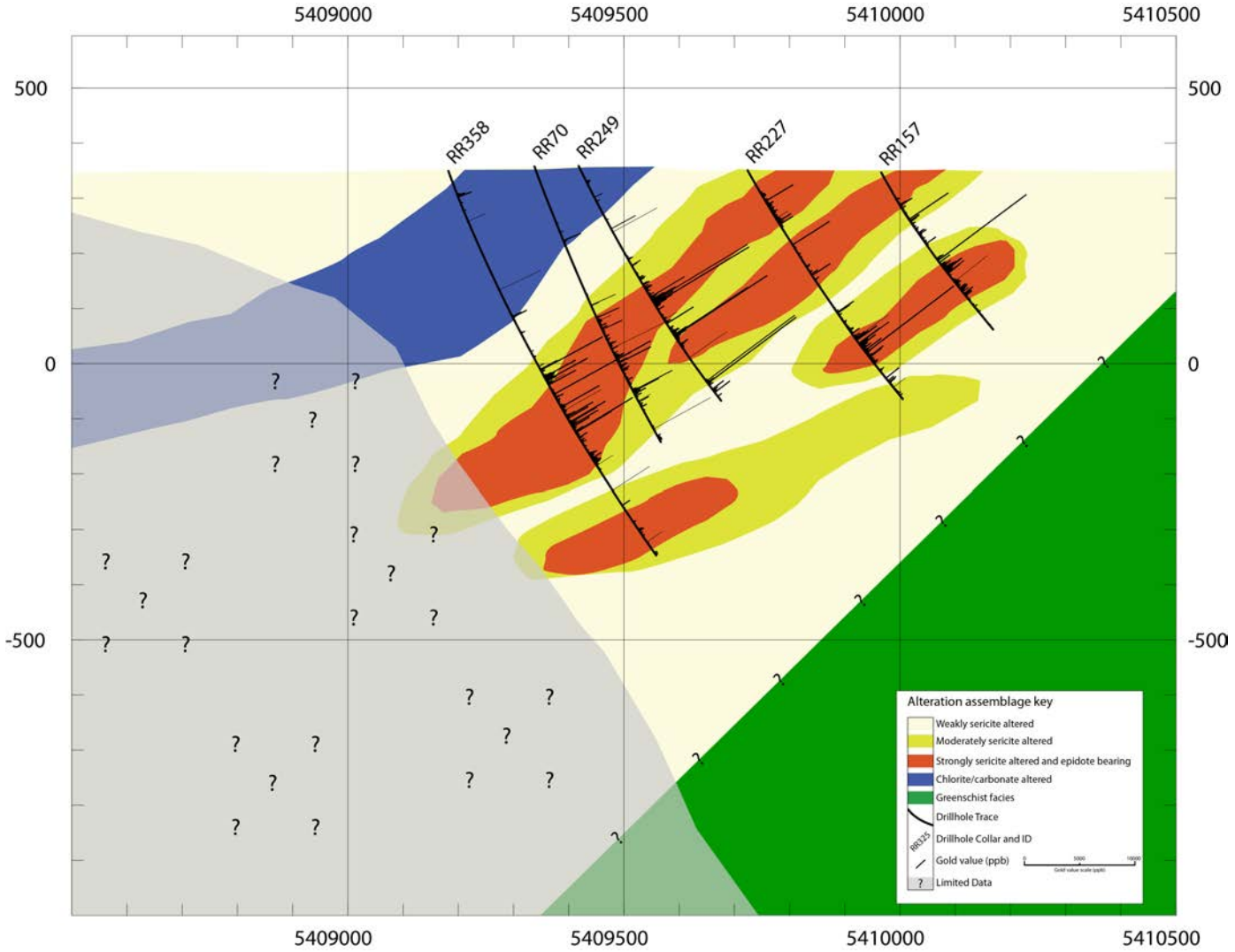

Figure 57. Alteration cross section along the east section line. Numbers at top and bottom are NAD83 UTM Northings (m). Numbers at left and right of cross section are elevation (masl).

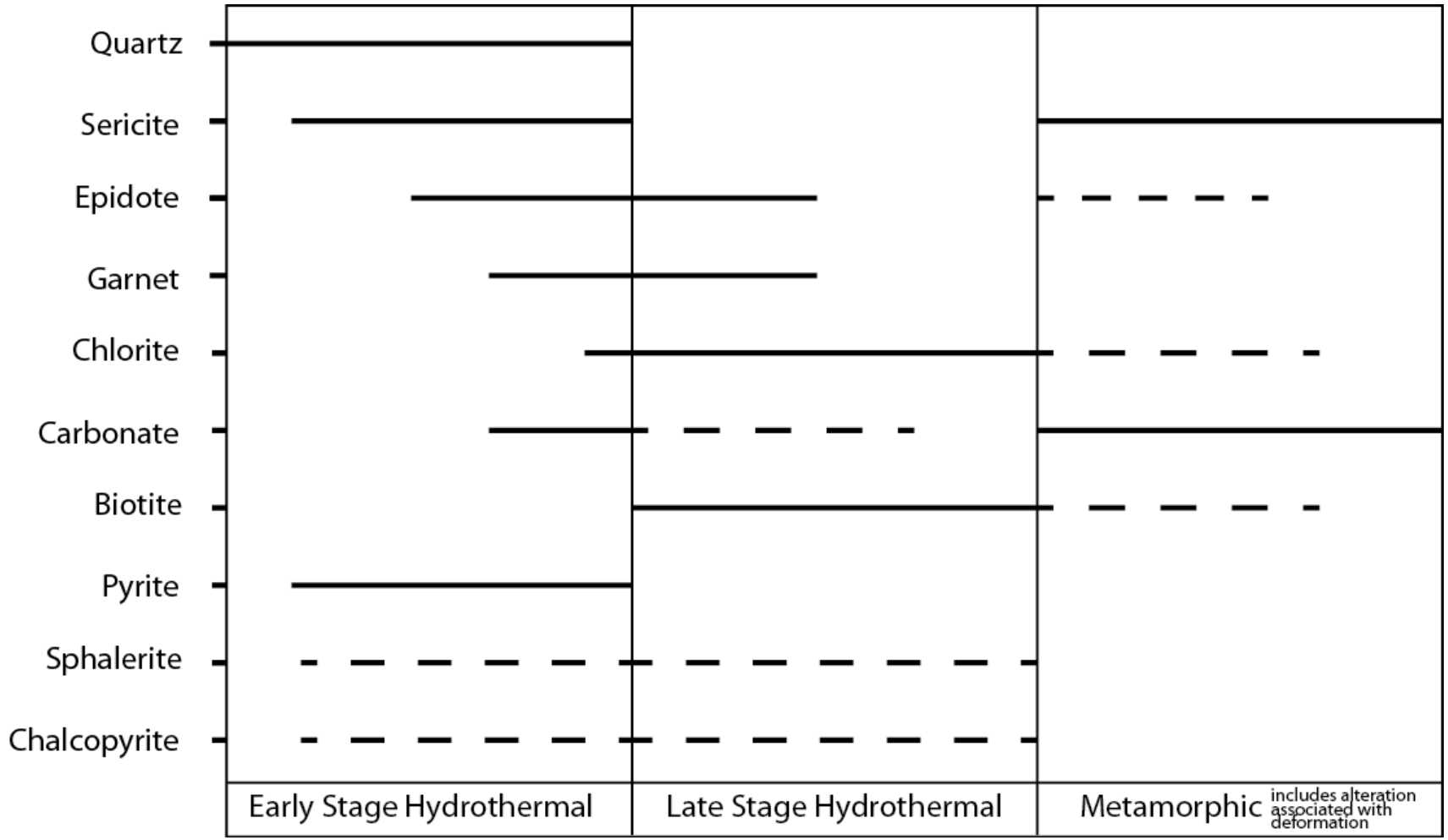

Figure 58. Proposed paragenesis of secondary minerals in the RRGP. Compiled from this thesis work and Schandl (2006).

comprises recrystallized, microcrystalline groundmass. Silicification is pervasive throughout the alteration units and could represent the devitrification of volcanic glass and silica dumping from hydrothermal fluids as glass is the most reactive component within a volcanic environment (Reed, 1997). Sericite is an early mineral observed replacing plagioclase feldspars and occurs interstitial to the microcrystalline quartz-rich matrix. Sericite suggests the further breakdown of matrix plagioclase feldspar ± glass, which can be shown chemically as:

$$\underset{\text{Albite}}{3NaAlSi_3O_8} + K_2O + 2H^+_{(aq)} = \underset{\text{Sericite}}{KAl_3Si_3O_{10}(OH)_2} + \underset{\text{Quartz}}{6SiO_2} + 3Na^+_{(aq)} \quad (1).$$

Aggregates of fine-grained, subhedral to euhedral epidote group minerals occur disseminated in the microcrystalline groundmass are likely early secondary minerals because of their crystal texture and strong replacement by later minerals.

Late stage, pre-metamorphic hydrothermal alteration is marked by chlorite, carbonate and biotite. Chlorite postdates sericite, quartz, and epidote, occurring as flaky aggregates or in thin veins parallel with rock fabric. Chlorite also occurs in limited domains in the matrix and also makes up fine-grained chlorite and quartz aggregates. Chlorite is likely a product of interaction between fluids rich in Fe and Mg and earlier sericite: (Fe5Al)(AlSi3)O10(OH)8

$$\underset{\text{Albite}}{2NaAl_3Si_3O_{10}}(OH)_2 + 3H_4SiO_{4(aq)} + 9Fe^{2+}_{(aq)} + 6Mg^{2+}_{(aq)} + 18H_2O = \underset{\text{Chlorite}}{(Mg,Fe)_5(AlSi_3)O_{10}(OH)_8} + 2Na^+_{(aq)} + 28H^+_{(aq)} \quad (2).$$

Biotite, $K(Mg, Fe)_3(AlSi_3O_{10})(F, OH)_2$, is strongly associated and interlayered with chlorite, which suggests that biotite could be a product of the reaction between sericite and chlorite. Biotite also occurs in chlorite-carbonate aggregates, which have been boudinaged by late sericite veins. In the RRGP carbonate occurs as disseminated ankerite and dolomite. Ankerite and dolomite occurs contemporaneously with chlorite forming "grungy" aggregates in the groundmass—commonly replacing epidote group minerals which suggests many of the SSA and EPB assemblages may have originally contained more abundant epidote.

Sometime after the conclusion of the hydrothermal system rocks at the RRGP were subject to mid- to upper-greenschist metamorphism. Metamorphism resulted in

mineral assemblages reflecting the secondary/hydrothermally altered composition, not original lithological compositions. This process is considered as isochemical and no new elements or compositions are added to the rocks during metamorphism. Garnet, for example, is a metamorphic mineral that is likely the result of the metamorphism of Mg, Mn, and Fe rich minerals likely formed during hydrothermal alteration (e.g. Fe and Mg rich chlorite or biotite). Late metamorphic sericite and chlorite occurs as veins that define the rock fabric crosscutting all other alteration minerals with the exception of late calcite veins. Calcite veins occur with quartz as a vein-filling mineral and mark the youngest alteration minerals within the RRPG.

3.5 Alteration geochemistry

In addition to using geochemistry as a tool to distinguish lithological facies and tectonic environments, geochemistry has particular applications for the interpretation of rocks that have undergone metasomatic changes. The chemical compositions of metasomatised rocks reflect the chemical and compositional changes of alteration and allow us to understand the alteration process (Gifkins et al., 2005). Patterns of metasomatic changes are commonly used in mineral exploration to define chemical halos and gradients, and can be used to define vectors toward mineralized zones and distinguish between prospective and non-prospective targets (Gifkins et al., 2005). Metasomatic geochemical changes not only help delineate deposit targets, but also helps to develop better genetic models and distinguish between mineral deposit types (e.g. low-sulfidation vs. high-sulfidation epithermal systems; White and Hedenquist, 1995).

3.5.1 The isocon method

Evaluation of geochemistry from different alteration assemblages within a single lithological unit (e.g. LA vs. SSA in dacitic lavas) makes it possible to quantitatively estimate changes in mass or volume resulting from hydrothermal alteration. The isocon method (Grant, 1986; Grant, 2005) is commonly used to calculate metasomatic changes resulting from hydrothermal alteration, including metasomatic changes associated with VMS deposits, sedimentary exhalative deposits, and epithermal deposits (Grant, 2005).

The isocon method is based on the method of Gresens (1967), who first recognized the relationships associated with volume and/or compositional changes of metasomatic rocks from chemical analysis.

Grant (1986) manipulated Gresens' (1967) equations by recognizing a linear relationship as a basis for the isocon method :

$$C_i^A = M^0/M^A(C_i^0 + \Delta C_i) \quad (3).$$

where:

C_i^A=concentration of component I in the altered sample,

M^0=mass of the least altered sample,

M^A=mass of the altered sample,

C_i^O=concentration of component I in the least altered sample,

ΔCi=change of concentraction of component i.

Equation 3 can be solved so that M^O / M^A is constant and immobile elements will have $\Delta C_i = 0$. After solving for the immobile elements it is possible to solve simultaneous equations where:

$$C_i^A = (M^0/M^A)\, C_i^0 \quad (4).$$

This can be done graphically by plotting C_i^A against C_i^0 in which the immobile elements will plot along a straight line through the origin representing a ratio of mass before and after alteration (this is referred to the line of best-fit). If this line has a slope=1 the alteration process occurred at constant mass. If slope < 1, mass is gained, if slope > 1, mass is lost. This line connects other points of equal geochemical concentration (where $\Delta C_i = 0$) and is referred to as an *isocon* (Grant, 2005). Quantitatively this can be solved by:

$$C^A = (M^0/M^A)\, C^0 \quad (5).$$

The general form of the equation used to quantify gains and losses from alteration can be written as:

$$\Delta C_i/C_i^O = (M^A/M^O)(C_i^A/C_i^O) - 1 \quad (6).$$

This equation, which is simply y=mx+b where m is the slope of the isocon and is equal to (M^A/M^O), yields the overall change in mass relative to M^0. The data can be compared using the a priori assumption that certain components were immobile (i.e. constant

Al_2O_3), the assumption of constant mass during alteration, or the assumption of constant volume during alteration (Grant, 2005). As well, immobility of species may also be determined using discrimination diagrams comparing elements known to be immobile in hydrothermal systems (e.g. Jenner, 1996). Species that plot above the isocon are gained during metasomatism. Those that plot below the isocon are leached. Increasingly steeper slopes indicate proportionally higher gains, and decreasing, shallow slopes indicate losses during metasomatism processes.

3.5.2 Application of the isocon method to the RRGP

The isocon method allows rocks with different metasomatic changes within the same lithological protolith to be compared. Alteration processes can be evaluated by comparing a least-altered mineral assemblage with a more altered mineral assemblage, or comparing various alteration assemblages with each other (Grant, 1986). In the RRGP, the least-altered assemblage was chosen based on the presence of metamorphic mineral assemblages and abundances consistent with greenschist facies metamorphism of a dacite. Because of the lack of gold mineralization and lack of distinguishable alteration assemblages in the mafic units, isocon analysis in this thesis has been restricted to the felsic succession, specifically the LA, MSA, SSA, and EPB assemblages within the dacitic lava flows.

In order to define a best-fit isocon, it was necessary to determine which elements were immobile during alteration. Discrimination diagrams in which historically immobile elements (Jenner, 1996; Grant, 2005) were plotted against an immobile element (e.g. HFSE) were used to determine element immobility. The most immobile elements cluster around a slope of 1 with an r^2 (coefficient of determination value) of >0.6 (Fig. 59). Within the RRGP the least mobile elements were determined to be Zr, Nb, and Hf (Table 2). An aluminum reference isocon was also plotted, because many previous studies have shown that Al_2O_3 is relatively immobile in hydrothermal systems associated with VMS and low-sulfidation epithermal Au systems (Grant, 2005). Lastly, a constant mass isocon (m=1) that results when no mass has been lost or gained during the metasomatism event was also plotted.

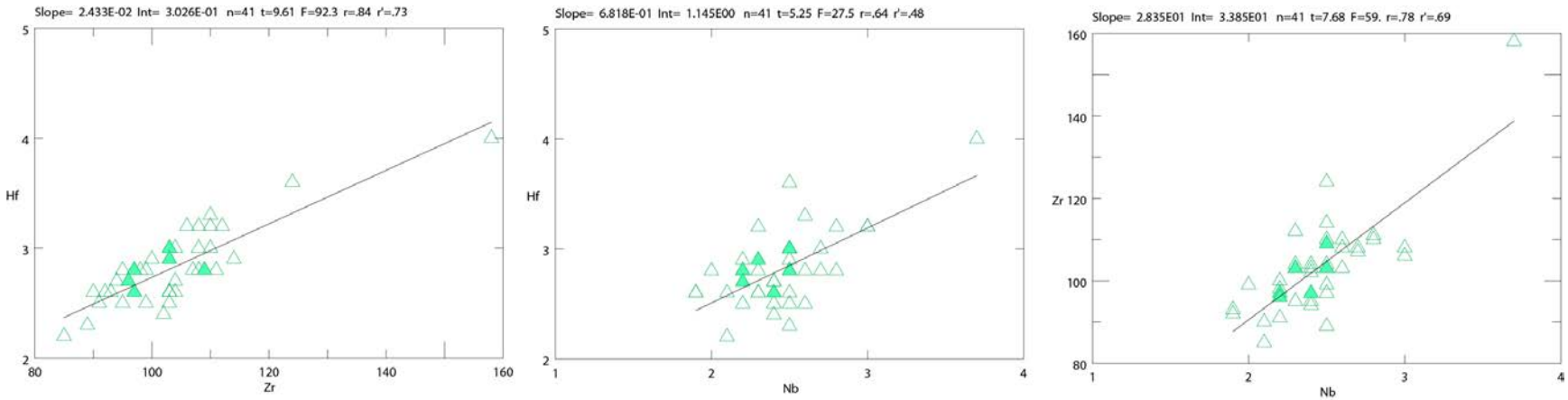

Figure 59. Immobile element discrimination diagrams of dacitic lava flows and intrusions. TiO2 is in % and trace element concentrations are in parts per million (ppm). int is the y-intercept if the best fit line is project backwards. n is the number of samples. The Coefficient of Determination (r^2) is a of the estimated regression line for the data, higher r^2 values indicate a better fit. The Spearman's Rank Correlation Coefficient (r') is a measure of the association of the two variables when rank-order data are utilized (Hudak et al., 2002).

Element 1	Element 2	r	r^2	r'
Ni	V	0.55	0.30	0.59
Cr	V	0.60	0.36	0.65
Cr	Ni	0.70	0.49	0.61
Ta	Cr	0.29	0.08	0.42
Ta	V	0.39	0.15	0.43
Ta	Ni	0.00	0.00	0.05
Nb	Ta	0.41	0.17	0.46
Nb	Cr	0.48	0.23	0.32
Nb	V	0.52	0.27	0.31
Hf	V	0.51	0.26	0.43
Hf	Ni	0.04	0.00	0.00
Hf	Cr	0.34	0.12	0.20
Hf	Ta	0.68	0.46	0.81
Hf	Nb	0.64	0.41	0.48
Zr	Hf	0.84	0.71	0.73
Zr	Nb	0.78	0.61	0.69
Zr	Ta	0.37	0.14	0.22
Zr	Cr	0.22	0.05	0.25
Zr	Ni	0.04	0.00	0.04
Zr	V	0.42	0.18	0.26
TiO_2	V	0.83	0.69	0.79
TiO_2	Ni	0.37	0.14	0.42
TiO_2	Cr	0.47	0.22	0.32
TiO_2	Ta	0.55	0.30	0.71
TiO_2	Nb	0.69	0.48	0.44
TiO_2	Hf	0.75	0.56	0.65
TiO_2	Zr	0.65	0.42	0.47

Table 2. Evaluation of immobile elements based on statistical correlation determined from variation diagrams. Coefficient (r) is a measure of the linear association between the two components from values ranging from +1 (a perfect positive correlation) to –1 (a perfect negative correlation). The Coefficient of Determination (r^2) is a of the estimated regression line for the data, higher r^2 values indicate a better fit. The Spearman's Rank Correlation Coefficient (r') is a measure of the association of the two variables when rank-order data are utilized (Hudak et al., 2002). Higher r^2 values correspond to immobile elements. Hf, Nb, and Zr (highlighted in yellow) were chosen as the most immobile elements from the RRGP.

The isocon results for the RRGP data are used to compare metasomatic changes associated with the different alteration assemblages to better understand hydrothermal processes associated with mineralization. The isocon analysis assumes that the metamorphism is isochemical, that is no new elements are introduced and the concentrations of elements remains constant during metamorphism. The different alteration assemblages are compared to the LA assemblage to understand metasomatic changes associated with hydrothermal alteration. Additionally, the alteration assemblages are compared with one another to measure progressive changes associated with more intensely altered assemblages (i.e. MSA vs. SSA). The best fit isocon is used for all these comparisons because it standardizes changes in mass based on least mobile elements. Because of the possible variations in the original rock compositions, changes in fluid chemistry and interaction times, element/component changes between -10 and +10% are too small to attribute to metasomatism related to the hydrothermal system. Moderate gains and losses are defined as values between ±10 to ±25%. Significant gains and losses are defined as anything >25% or <-25%. Significant gains and losses are highlighted in the text (gains and losses refer to % gains and losses) and all other values appear in Table 3.

3.5.3 Least altered vs. moderately sericite altered assemblages

Alteration minerals in the MSA samples are compositionally identical to, but in relatively different proportions to the LA samples. The difference between the two is the alteration intensity.

The MSA assemblage is generally enriched compared to the best fit isocon (Fig. 60) in all major elements/components with moderate gains in MgO and S and significant gains in K_2O (27.2%), CO_2 (49.2%) and MnO (35.4%) compared to the LA assemblage. Na_2O shows significant loss (-47.4%) in the moderately altered assemblage. Major elements/components that are relatively immobile include SiO_2, Al_2O_3, TiO_2, Fe_2O_3, CaO, and P_2O_5. The assemblage is enriched in metallic trace elements (Table 3) with significant gains in Au (251.9%), Hg (39.4%), Sb (152.7%) and As (36.6%) with

Major elements	*LA vs MSA*	*LA vs SSA*	*LA vs EPA*	*MSA vs SSA*	*SSA vs EPA*
SiO2	2.7	-1.9	3.3	-4.5	5.2
Al2O3	-4.1	-7.2	-0.3	-3.2	7.5
TiO2	-13.5	23.5	23.2	42.7	-0.2
Fe2O3	-7.0	-5.0	23.7	2.2	30.2
MnO	35.4	-1.6	137.0	-27.3	140.8
MgO	12.0	26.7	17.5	13.2	-7.2
CaO	-11.5	-29.7	2.9	-20.5	46.3
Na2O	-47.4	-59.6	-55.4	-23.2	10.4
K2O	27.2	41.3	55.2	11.1	9.8
P2O5	-14.9	-5.5	9.5	11.0	15.9
LOI	28.2	49.7	21.7	16.8	-18.7
Mass	0.3	-1.9	3.5	-2.1	5.5
S	1.5	75.4	-9.5	72.8	-48.4
C	48.2	37.4	8.3	-7.3	-21.1
CO2	49.2	37.5	9.5	-7.9	-20.3
H2O	9.0	15.5	53.7	5.9	33.1
H2O+	36.9	65.8	51.1	21.1	-8.8
Metallic Trace Elements					
Au	251.9	310.9	458.1	16.8	35.8
Ag	14.0	83.6	-9.8	61.0	-51.1
Cu	15.5	15.7	85.9	0.1	60.7
Zn	-11.0	296.7	3.0	345.5	-74.0
Pb	21.4	54.6	55.2	27.3	0.4
Mo	24.2	-11.4	-38.1	-28.6	-30.1
Sb	152.7	231.0	92.5	31.0	-41.8
As	36.6	113.1	57.6	56.0	-26.1
Hg	39.4	128.1	34.0	63.6	-41.2
Trace elements					
Ba	36.1	27.4	48.0	-6.4	16.2
Co	5.6	22.4	42.5	15.9	16.5
Cr	-13.8	4.2	85.5	20.8	78.2
Hf	-2.0	-1.2	0.5	0.8	1.7
Nb	1.7	1.6	5.4	-0.1	3.8
Ni	-7.4	39.6	80.3	50.7	29.2
Rb	35.5	49.5	53.0	10.4	2.4
Sn	-10.9	-0.6	-3.8	11.6	-3.3
Sr	-15.9	-31.1	-13.5	-18.1	25.5
Y	-10.3	-1.5	34.8	9.8	36.8
Zr	0.3	-0.5	-6.0	-0.8	-5.5

Table 3. Gains and losses (in percent) of components for the least altered assemblage compared to different alteration assemblages felsic units based on isocon analysis.

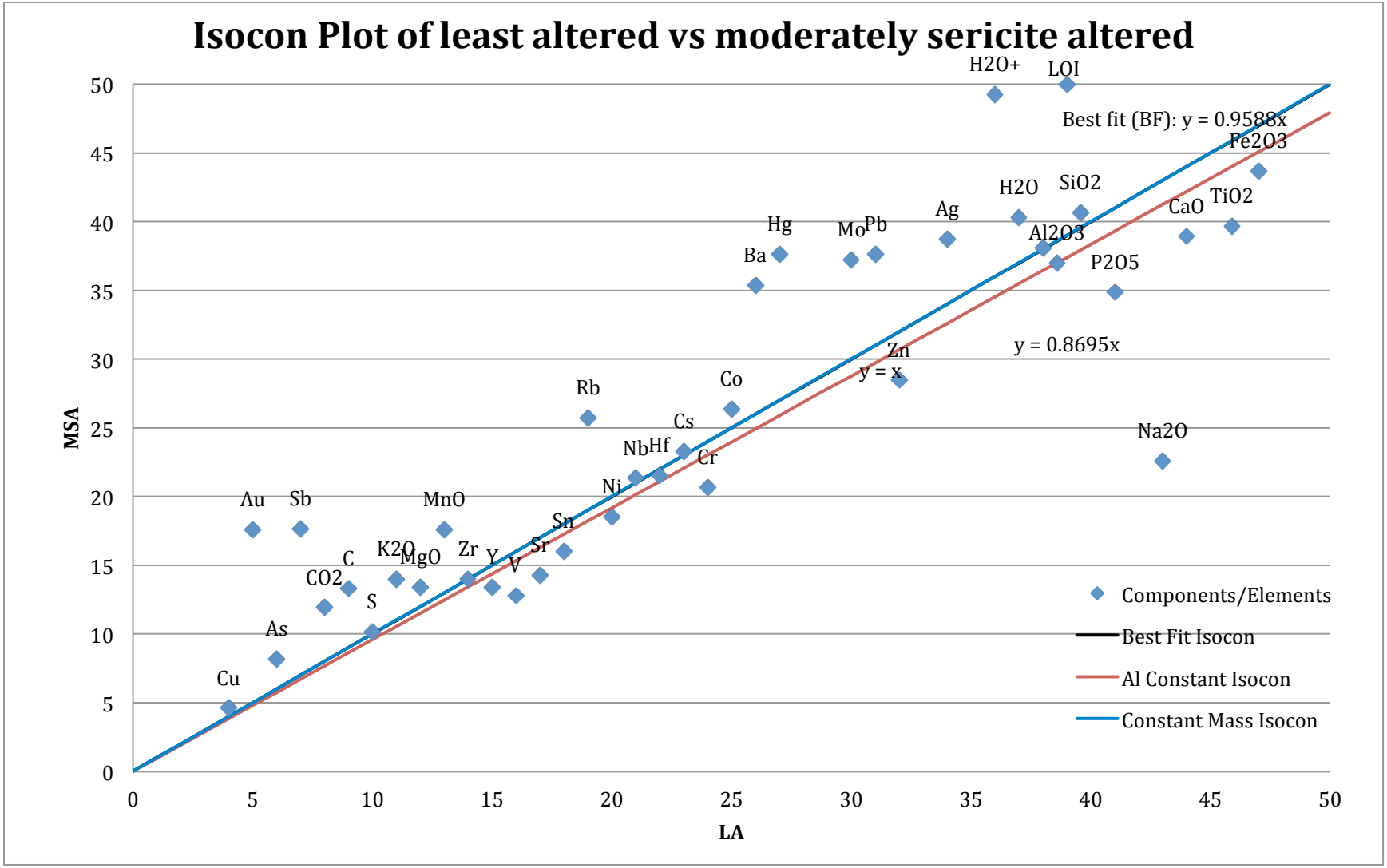

Figure 60. Isocon diagram comparing least altered with moderately sericite altered.

moderate gains in Ag, Cu, Mo, and Pb. The overall mass change compared to the best fit isocon is 0.3%.

The enrichment in K_2O and loss in Na_2O is reflected mineralogically in more pervasive sericite, which has completely replaced plagioclase feldspar in the MSA assemblage. Increases in MgO are reflected in the presence of higher abundances of chlorite disseminated in the groundmass. The large CO_2 increase is reflected in the presence of groundmass ankerite and dolomite. Gains in Au are accompanied by Ag, As, Pb, Sb, As, and Hg in compared with the LA assemblage. The MSA assemblage contains rare sphalerite and chalcopyrite disseminate in the groundmass.

3.5.4 Least altered vs. strongly sericite altered assemblages

Like the MSA assemblage, the SSA assemblage shows enrichment compared to the best fit isocon in most major elements/components with respect to the LA assemblage. Alteration minerals are compositionally identical to, but in relatively different in proportions to the LA samples.

The SSA shows significant gains compared to the best fit isocon (Fig. 61) in: MgO (26.7%), K_2O (41.3%), S (75.4%) and CO_2 (37.5%), with moderate gains in TiO_2. Major elements/components that show significant losses are CaO (-29.7%) and Na_2O (-59.6%). SiO_2, Al_2O_3, Fe_2O_3, MnO, P_2O_5 are relatively immobile. Metallic trace elements are all enriched within the SSA assemblage compared within the LA assemblage (except Mo) with significant gains in Au (310.9%), Ag (83.6%), Zn (296.7%), Pb (54.6%), Sb (231.0%), As (113.1%), and Hg (128.1%). The overall mass change compared to the best fit isocon is -1.9%.

The SSA assemblage mimics the trends of the MSA assemblage in chemical enrichment and mineralogical composition. Losses in Na_2O coupled with gains in K_2O and MgO compared with the LA assemblage are reflected mineralogically in the complete destruction of plagioclase feldspars by sericite and the addition of chlorite in the groundmass (see equations 1 and 2). Like the MSA assemblage, increases in Zn and Cu are accompanied by an increase in Au; mineralogically this is seen with more abundant sphalerite and chalcopyrite disseminated in samples in this alteration

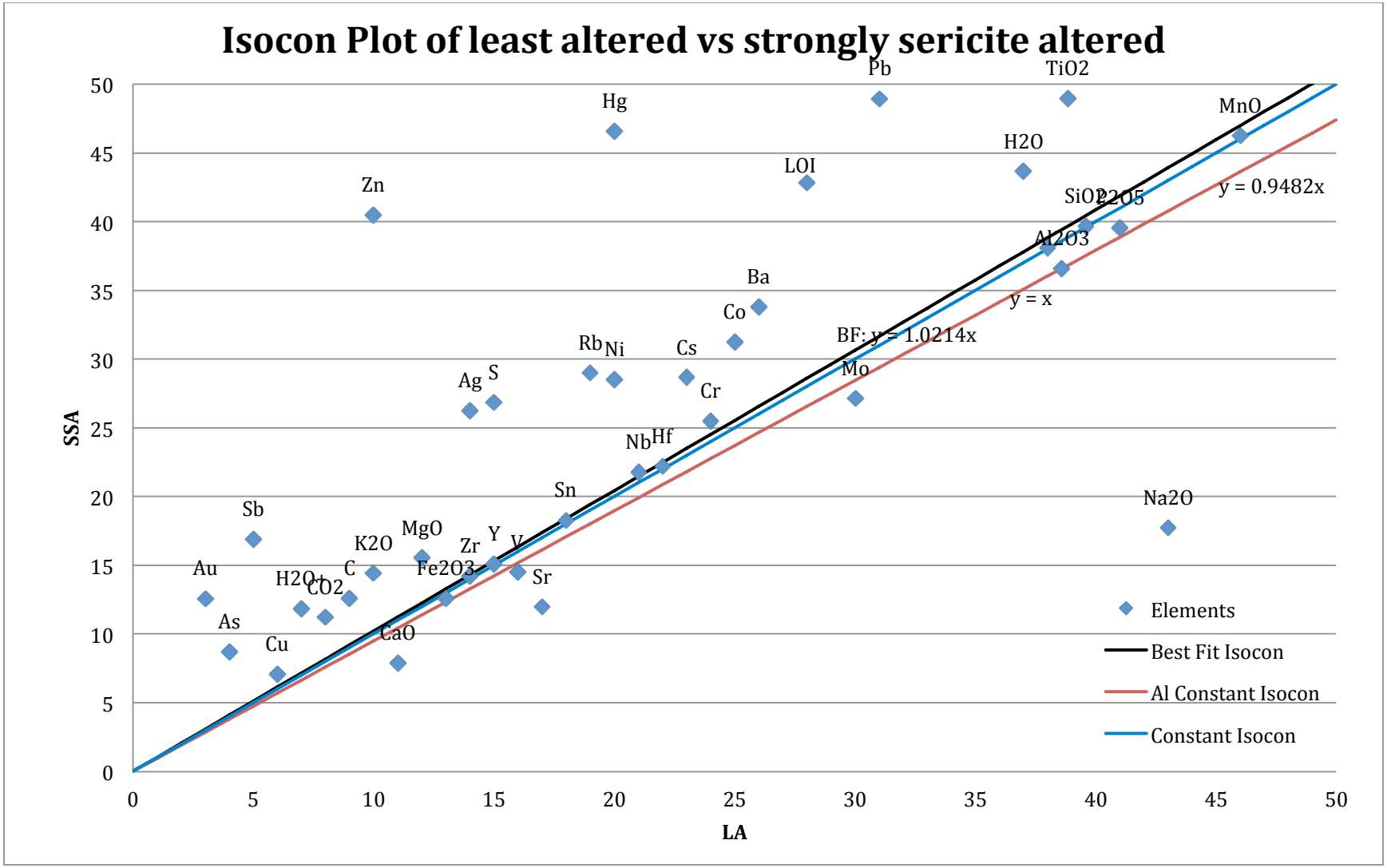

Figure 61. Isocon diagram comparing least altered with strongly sericite altered.

assemblage. The increase in CO_2 reflects the presence of carbonate in the groundmass (mostly dolomite based on the gains and losses of CaO and MgO).

3.5.5 Moderately least altered vs. strongly sericite altered assemblages

Comparing the MSA and SSA using the best fit isocon shows the progressive chemical changes associated with more intense alteration of assemblages containing the same mineral species. These assemblages are distinguished solely on the modal proportion of sericite. Because of mineralogical similarities, gains and losses between the two assemblages are less than gains and losses compared with the LA assemblage.

Significant gains in major elements/components in the SSA assemblage compared with the MSA using the best fit isocon (Fig. 62) include TiO_2 (42.7%) and S (72.8%) with moderate gains in K_2O and P_2O_5. Moderate losses include CaO and Na_2O with significant losses in MnO (-27.3%). Relatively immobile components are SiO_2, Al_2O_3 MgO, and Fe_2O_3. For the metallic trace elements the SSA assemblage shows significant gains in Zn (345.5.5%), Ag (61.0%), As (56.0%), Pb (27.3%), Sb (31.0%) and Hg (63.6%) with moderate gains in Au compared to the MSA. Cu is relatively immobile. The overall mass change compared to the best fit isocon is -2.1%.

The chemical changes, particularly the enrichment of K_2O and loss of Na_2O, between the MSA and the SSA are reflected mineralogically with the complete replacement of plagioclase feldspar and greater amount of sericite and chlorite disseminated in the matrix with the SSA samples.

3.5.6 Least altered vs. epidote-bearing assemblages

Compared to the best fit isocon (Fig. 63) the EPB assemblage shows significant enrichment in MnO (137.0%) and K_2O (55.2%) with moderate enrichment in TiO_2, Fe_2O_3, MgO, and CO_2. The EPB shows significant depletion in Na_2O (-55.4%) compared to the LA assemblage. Relatively immobile elements/components include SiO_2, Al_2O_3, P_2O_5, CaO, and S. Metallic trace elements/components significantly enriched in EPB rocks compared with LA rocks include Au (458.1%), Cu (85.9%), Pb (55.2%), Sb

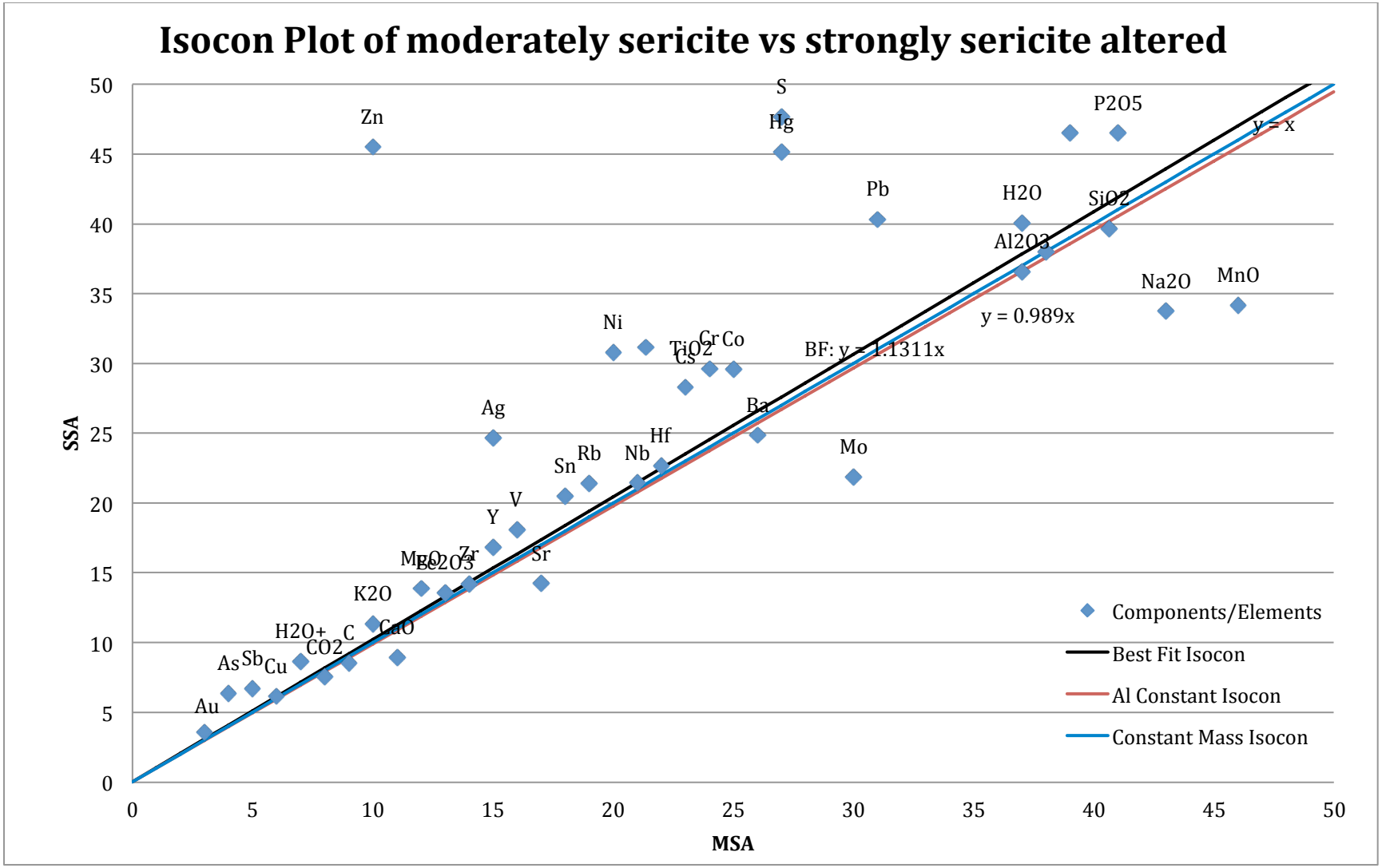

Figure 62. Isocon diagram comparing moderately sericite altered with strongly sericite altered.

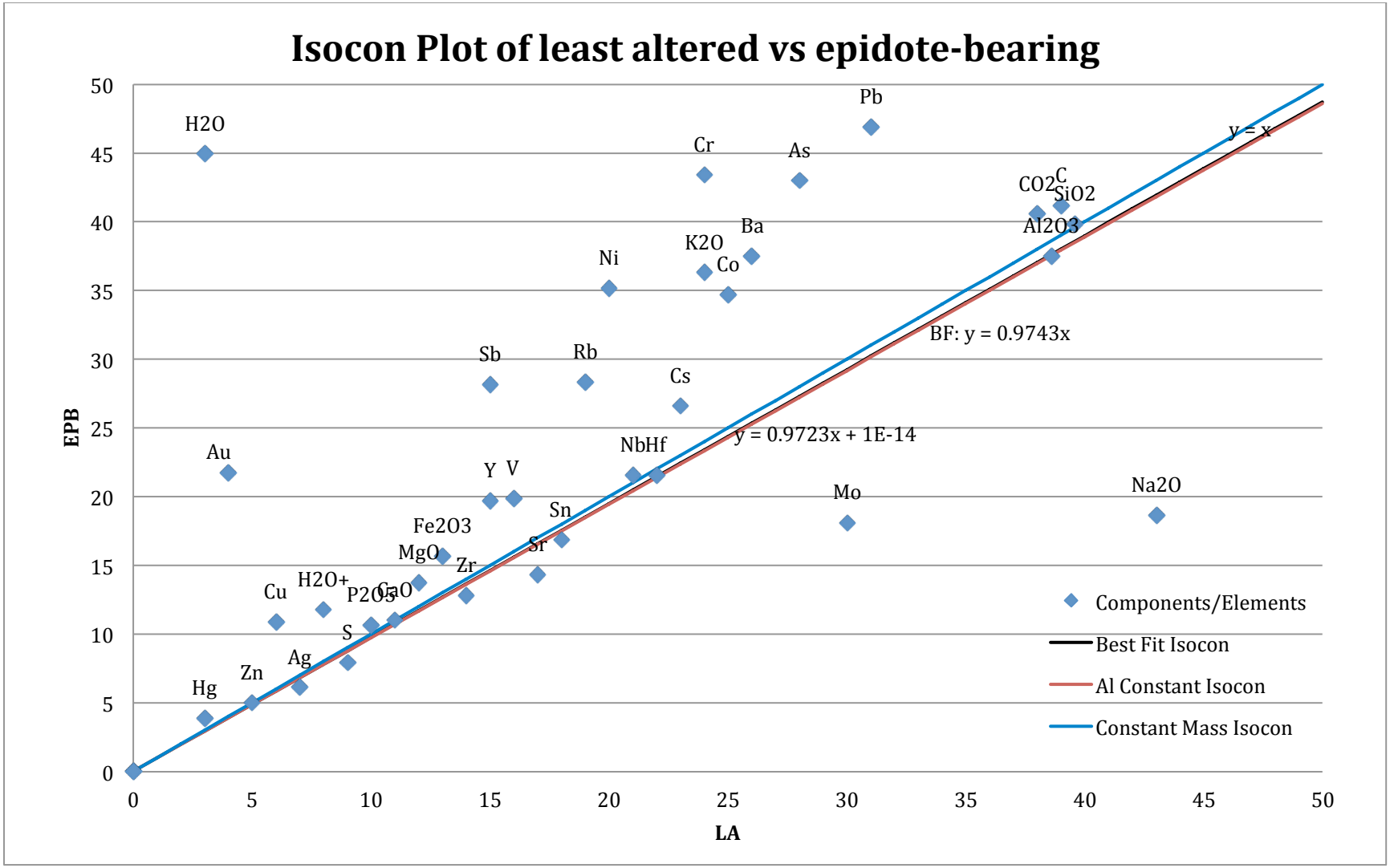

Figure 63. Isocon diagram comparing least altered with epidote-bearing.

(92.5%), As (57.6%) and Hg (34.0%) while Ag and Zn are relatively immobile. The overall mass change compared to the best fit isocon is 3.5%.

The EPB assemblage has similar trends to the SSA assemblage compared with the LA assemblage. The enrichment of MnO in these EPB samples is seen mineralogically in the presence of Mn-rich spessartine garnets (elemental composition confirmed by microprobe by Schandl, 2006) in the groundmass. The loss in Na_2O and gains in MgO and Fe_2O_3 are reflected compositionally in the replacement of feldspar by sericite and the presence of chlorite. K_2O, however, is depleted, resulting in less sericite disseminated in the groundmass. Similar to the SSA samples, both As and Hg are enriched in the EPB samples.

3.5.7 Strongly sericite altered vs. epidote-bearing assemblages

The SSA and EPB assemblage have many chemical and mineralogical similarities and are distinguished on the basis of the presence of 1-10% epidote group minerals within the EPB groundmass. Many of the epidote minerals within the EPB assemblage are strongly overprinted by carbonate, and this may indicate that epidote originally had a greater distribution, but has been replaced by carbonate during subsequent deformation, alteration and metamorphism. It is therefore likely, due to the similarities between the SSA and EPB assemblages, that both originally had epidote group secondary minerals.

Based on best fit isocon (Fig. 64) the EPB assemblage shows moderate gains in, Na_2O and P_2O_5 with significant gains in MnO (140.8%), Fe_2O_3 (30.2%) and CaO (46.3%). The EPB assemblage shows moderate losses in S (-48.4%) and in CO_2 (-20.3%). SiO_2, Al_2O_3, TiO_2, MgO, and K_2O are all relatively immobile. For metallic trace elements the EPB assemblage is significantly enriched in Au (35.8%) and Cu (60.7%) compared to the SSA assemblage and shows significant losses in Ag (-51.1%), Zn (-74.0%), Mo (-30.1%), Sb (-41.8%), As (-26.1%), and Hg (-41.2%) while Pb is relatively immobile. The overall mass change compared to the best fit isocon is 5.5%.

The chemical changes, particularly the increase in MnO and CaO, are reflected mineralogically in the occurrence of epidote group minerals in the groundmass and the

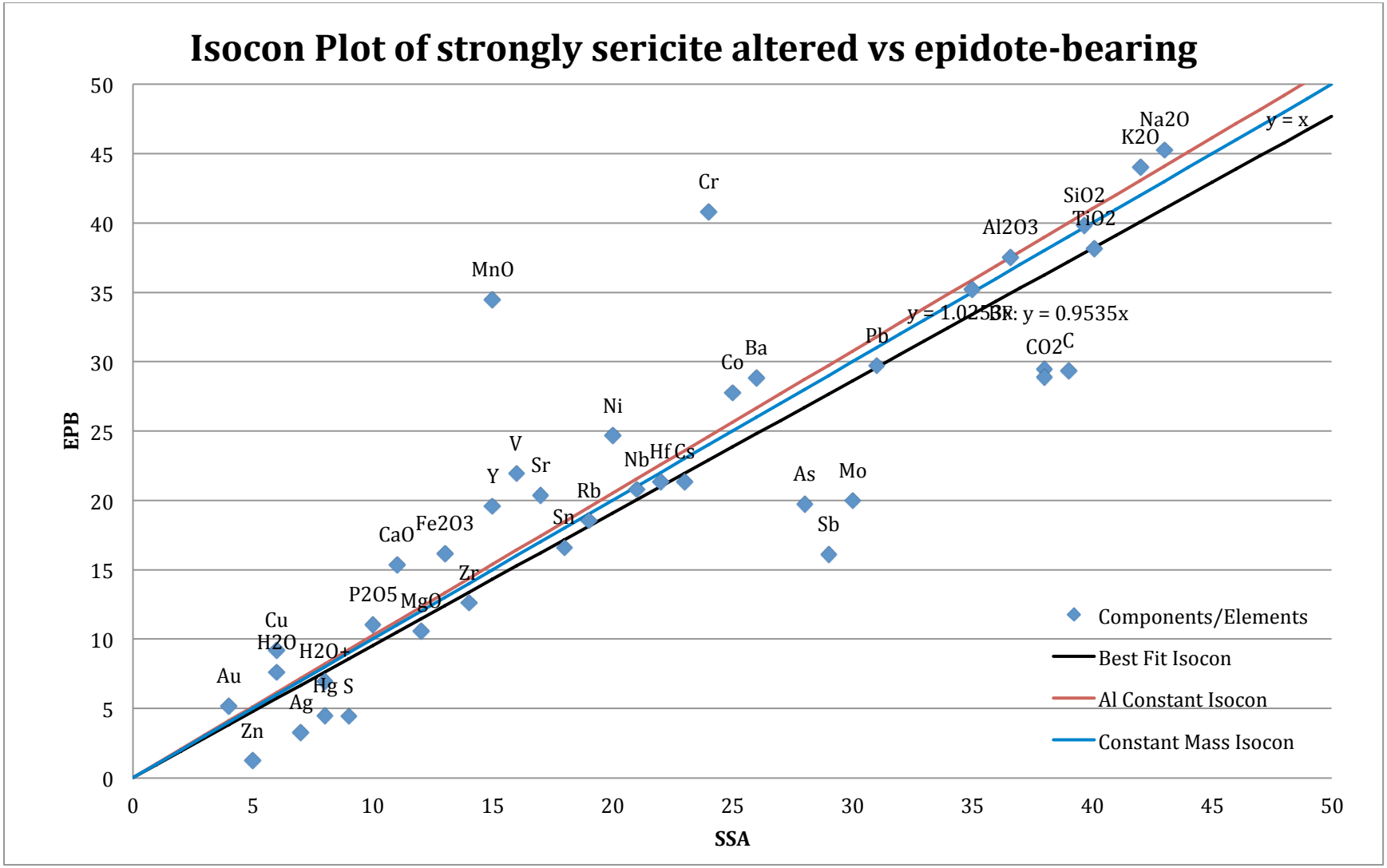

Figure 64. Isocon diagram comparing strongly sericite altered with epidote-bearing.

occurrence of Mn-rich spessartine garnet (see above). The loss in CO_2 is reflected in the relative lack of carbonate within the EPB assemblage.

3.5.8 Box plot analysis

In addition to the isocon analysis, samples were plotted using the AI-CCPI box plot developed by Large et al. (2001). This method uses the Ishikawa alteration index-(AI; Ishikawa et al., 1976) and the chlorite-carbonate-pyrite index-(CCPI; Large et al., 2001), which were developed to measure the intensity of sericite, chlorite, carbonate, and pyrite replacement of feldspars and glass, associated with hydrothermal alteration (Large et al., 2001). The AI was initially used to quantify intensities of sericite and chlorite alteration proximal to Kuroko VMS deposits based on geochemistry. The index was derived to measure the breakdown of plagioclase and volcanic glass and their replacement by sericite and chlorite (Ishikawa et al., 1976). This can be calculated:

$$\mathrm{AI} = \frac{100\,(\mathrm{K_2O+MgO})}{\mathrm{K_2O+MgO+\,Na_2O+CaO}} \qquad (7).$$

For unaltered rocks the index varies from 20 to 60 depending on the rock type. An AI of 100 represents the complete replacement of feldspars and glass by sericite and chlorite (Large et al., 2001).

A major limitation of the Ishikawa AI is that it does not take into account carbonate alteration that can be significant within hydrothermal alteration zones. To compensate for this Large et al. (2001) introduced the chlorite-carbonate-pyrite index (CCPI):

$$\mathrm{CCPI} = \frac{100\,(\mathrm{MgO+FeO})}{\mathrm{MgO+FeO+\,Na_2O+K_2O}} \qquad (8).$$

This ratio measures the increases in MgO and FeO associated with chlorite development. The formation of chlorite commonly replaces feldspars and sericite in the rock, leading to a loss of Na_2O and K_2O (Large et al., 2001).

At the RRGP intensely altered samples plot with higher values (Fig. 65). Strongly sericite and chlorite altered samples (e.g. SSA) have high AI values whereas strongly carbonate altered samples have higher CCPI values (e.g. CCA). Less altered samples (e.g. LA and MSA) typically plot in the least altered box for dacites as defined by Large

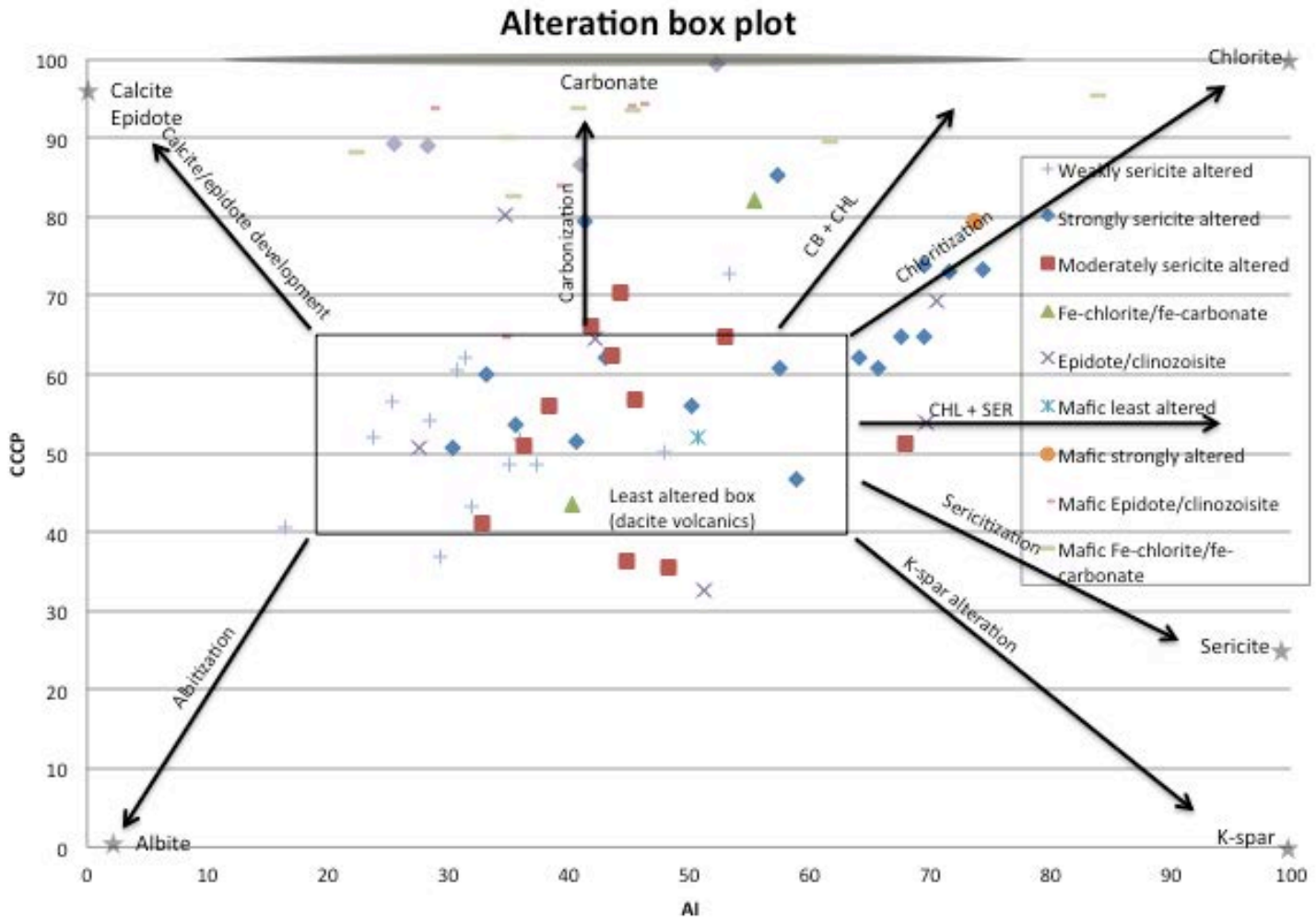

Figure 65. Alteration box plot (Large et al., 2001) based on this study's geochemistry.

et al., (2001). Many samples show higher CCPI values and show stronger enrichment of chlorite. Much of this is likely a result of pyrite (FeS) disseminated in the groundmass increasing the CCPI value and skewing the data towards chlorite. The dominate trends seen within the alteration box plots are identical to the metasomatic changes seen in the isocon analysis and are marked by sericite, sericite + chlorite + pyrite, and chlorite-carbonate alteration.

3.5.9 Alteration geochemistry summary

The alteration assemblages show progressive changes in the enrichment and depletion of major and metallic trace elements relative to the LA assemblage and relative to alteration intensity. The most intensely altered samples have the greatest metasomatic changes. This is highlighted in the gains and losses compared to the best fit isocon using the isocon analysis (Grant, 1986) as well as in the highest AI and CCPI values using the alteration box plot method (Large et al., 2001). The most obvious progressive changes from LA to SSA assemblages are: 1) the increasing depletion of Na_2O from LA→MSA (-47.4%)→SSA (-59.6%) and EPB (-55.5%), 2) the increasing enrichment of K_2O from LA→MSA (27.2%)→SSA (41.3%)→EPB (55.2%), 3) the increasing enrichment of MgO from LA→MSA (12.0%)→SSA (26.8%) and EPB (17.5%) and 4) the increasing enrichment of Au from LA→MSA (251.9%)→SSA (310.9%)→EPB (458.1%).

Other major elements/components (e.g. SiO_2, CaO, Fe_2O_3 etc.) show more variability, likely due to the similarities of the alteration assemblages and how the alteration assemblages were defined and distinguished. Metallic trace elements (particularly Pb, Sb, As, and Hg) show strong correlation with increases in Au values associated with different assemblages. This is observed in the SSA and EPB assemblages where the highest Au values are associated with the highest values in Ag, Cu, Zn, Pb, Sb, Ag, and Hg.

Most alteration minerals are stable over limited temperature and pH ranges which provides information on the thermal and geochemical structure of the hydrothermal system (White and Hedenquist, 1995). Comparing the isocon analysis and petrographic observations of the different assemblages with White and Hedenquist's (1995) data on

mineral stability from pH and temperature indicates that these different assemblages are likely the result of wall/rock with fluids of different temperature ranges at near neutral pH. Using the distribution and abundances of minerals the alteration assemblages can be classified based on the fluid temperature (e.g. White and Hedenquist, 1995): MSA is the result of low to moderate temperature alteration (100-150°C), SSA is the result of moderate temperature alteration (150-200°C) and the EPB is the result of high temperature alteration (200-300°C). The EPB assemblage was most likely originally widespread and associated with the highest gold values, but has been replaced by later carbonate and is now difficult to differentiate from other assemblages.

The variability in these alteration assemblages, particularly the differences in alteration intensities is due to the original permeability of the lithological facies. More permeable units had a higher fluid to rock ratio and were the most acidic resulting in the formation of abundant sericite by the reaction of the acidic fluid with plagioclase feldspar (eqn. 1). Later fluids enriched in Fe and Mg, possibly a result of draw down of seawater, resulted in the formation of chlorite by the reaction of the fluid and the early sericite (eqn. 2). Moving to more competent, less permeable units, fluid to rock ratios were decreased resulting in less acidic conditions and the decreased formation of sericite and chlorite.

3.6 Alteration model

Secondary minerals, style and distribution of alteration and mineralization at the RRGP including:

a. presence of ubiquitous quartz, sericite, carbonate, chlorite, epidote and pyrite;
b. zonation of alteration assemblages;
c. mineralization associated with highly permeable units—i.e. flow tops, lapilli tuffs, shear zones;
d. style of mineralization dominantly as open space filling and stringer veins;
e. alteration associated with the most altered mineral assemblages;
f. relationship of base metals to Au and Au:Ag ratio around 0.5; and

g. mineralization and alteration associated with intrusive and silicic volcanism;

are characteristics (with the exception of mineralization in shear zones at the RRGP) typical of low-sulfidation epithermal gold deposits (Simmons et al., 2005). Because of these similarities the RRGP is interpreted to represent a metamorphosed, low-sulfidation epithermal gold deposit in which local gold values have been enriched during post-volcanic structural deformation. Many of the textures indicative of epithermal systems have been lost due to deformation and subsequent metamorphism, but the association of gold mineralization with permeable units and epithermal-like alteration assemblages, present striking analogies to those of Phanerozoic epithermal gold deposits.

Until recently many geologist have restricted epithermal systems to areas of Tertiary volcanism (Gemmell, 2007). Previously, these systems were almost unknown in pre-Cenozoic lithologies because of their lack of preservation due to their shallow location in the crust and their erodibility. However, while controversial, Archean epithermal deposits (Penczack, 1996; Huston et al., 2002; Robert et al., 2005; Gemmell, 2007; Kesler and Wilkinson, 2009) are beginning to be recognized, and the presence of these deposits suggest that preservation, not Archean age, is the key control on the temporal distribution of epithermal deposits (Gemmell, 2007). Low-sulfidation epithermal gold deposits are harder to recognize in ancient terrains, because their alteration mineral assemblages are not unique and are similar to greenschist facies metamorphism (Robb, 2005). Additionally, in regional metamorphic terrains, primary minerals and textures may no longer be present, depending on the grade of subsequent metamorphism (Huston et al., 2002).

Epithermal deposits were first defined by Lindgren (1933) who noted these deposits formed at shallow depths, with distinct ore and gangue mineralogy and textural features. These deposits form near the surface, and mineralization occurs usually at a depth of 600 m under temperatures from 50-300° C and moderate pressure primarily by replacement, or by open-space filling (Simmons et al., 2005). The form of deposits originating by open-space filling typically reflects that of the structural control of the hydrothermal fluids (Simmons et al., 2005).

The distinction between pre-metamorphic early stage and late stage alteration minerals is the result of overprinting of the low-sulfidation epithermal system by a later draw down of seawater. Alteration associated with the early low-sulfidation epithermal system is the result of an evolving hydrothermal system, resulting in gradational alteration intensity with the most permeable units. The later draw down of seawater through the system is more widespread and crosscuts the earlier alteration assemblages. This is seen in the distribution of late stage alteration minerals. Chlorite, for example, is widespread and occurs in relatively constant amounts within the different alteration assemblages. Chlorite is often documented as a secondary mineral that can be formed by reacting sericite with water enriched in Fe and Mg:

$$\underset{\text{Sericite}}{2KAl_3Si_3O_{10}(OH)_2} + 3H_4SiO_{4(aq)} + 9Fe^{2+}_{(aq)} + 6Mg^{2+}_{(aq)} + 18H_2O = \underset{\text{Chlorite}}{3(Mg,Fe)_5Al_2Si_3O_{10}(OH)_8} + 2K^{+}_{(aq)} + 28H^{+}_{(aq)} \quad (9).$$

These elements are the common constituents of seawater (Franklin et al., 2005) and the occurrence of chlorite throughout the RRGP is the result of seawater entering the system and reacting with the rocks at 150-200° C (White and Hedenquist, 1995). The textures and abundances of chlorite indicate that the hydrothermal system was continuously subaqueous, the result of a draw down of seawater interacting with the rock at 150-200° C. This later draw down of seawater could be related to the waning of the low-sulfidation epithermal system (Franklin et al., 2005).

The hydrothermal system associated with the RRGP also likely had a strong magmatic input. The magmatic input was related to some subvolcanic intrusion—possibly related to the emplacement of the dacite intrusions and lava flows—which contributed CO_2, SO_2, HCl and H_2S gases to the system (Simmons et al., 2005). Additionally, the magmatic input could represent the source of many of the metals within the RRGP (pers. comm. Hudak, 2011). Low-sulfidation deposits typically have less magmatic input than high-sulfidation deposits and lack many of the characteristics alteration mineralogies and sulfides associated with high-sulfidation deposits. The lack of textures and mineralogies indicative of a metamorphosed high-sulfidation deposit at the RRGP is likely the result of fluid mixing between the magmatic source and the seawater

hydrothermal system. The initially acidic magmatic fluids were stabilized by the more neutral fluids and resulted in the phyllic to propylitic assemblages seen at the RRGP.

The zonation of alteration intensities, and their association with gold mineralization, from permeable to competent rock, is typical of epithermal deposits. Within low-sulfidation epithermal systems, fluid conduits, both structurally controlled (i.e. shear zones) or lithologically-controlled (i.e. flow tops, breccias), act as focusing mechanisms for the hydrothermal fluids (Simmons et al., 2005). Reed (1997) has modeled a hydrothermal fluid interacting with surrounding rock where fluid composition and pH changes as constituents of chemical reactions are consumed and with changing fluid/rock ratios. Within a zone of high permeability, high fluid flow and initial fluid/rock ratios will be high. Unreacted fluids will be moderately acidic; over time, acid-consuming chemical reactions, mineral precipitation, and decreased flow will cause the system to evolve to one with lower fluid/rock ratios and alkaline conditions (Reed, 1997). In an ideal epithermal deposit the alteration assemblages are marked by an inner zone of silicification giving way to an outer zone of potassic-sericitic (phyllic) alteration made up of quartz + feldspar + sericite + illite ± smectite (Robb, 2005). These zones grade out into propylitically altered rocks containing quartz + albite + carbonate ± sericite ± epidote ± pyrite (Fig. 66). Along with zonation of alteration assemblages, alteration intensities within modern epithermal systems decrease with distance from the upflow zone. Commonly there is also strong overprinting of different alteration assemblages (Robb, 2005).

Polyphase deformation and regional greenschist facies metamorphism has had a strong affect at the RRGP, and has destroyed or modified most of the original mineralogy of the alteration assemblages at the RRGP. Metamorphism has led to the formation of micas (notably sericite and chlorite) from original clay minerals. The gradational change from SSA rocks in units associated with high permeabilities to less altered rocks further from permeable lithological facies likely illustrates a metamorphosed analog to an epithermal system (see Fig. 66). Silicification is pervasive throughout the deposit but is highest near gold rich zones, and likely represents the alteration zonation present in the original epithermal system. SSA and EPB assemblages are metamorphic equivalents to

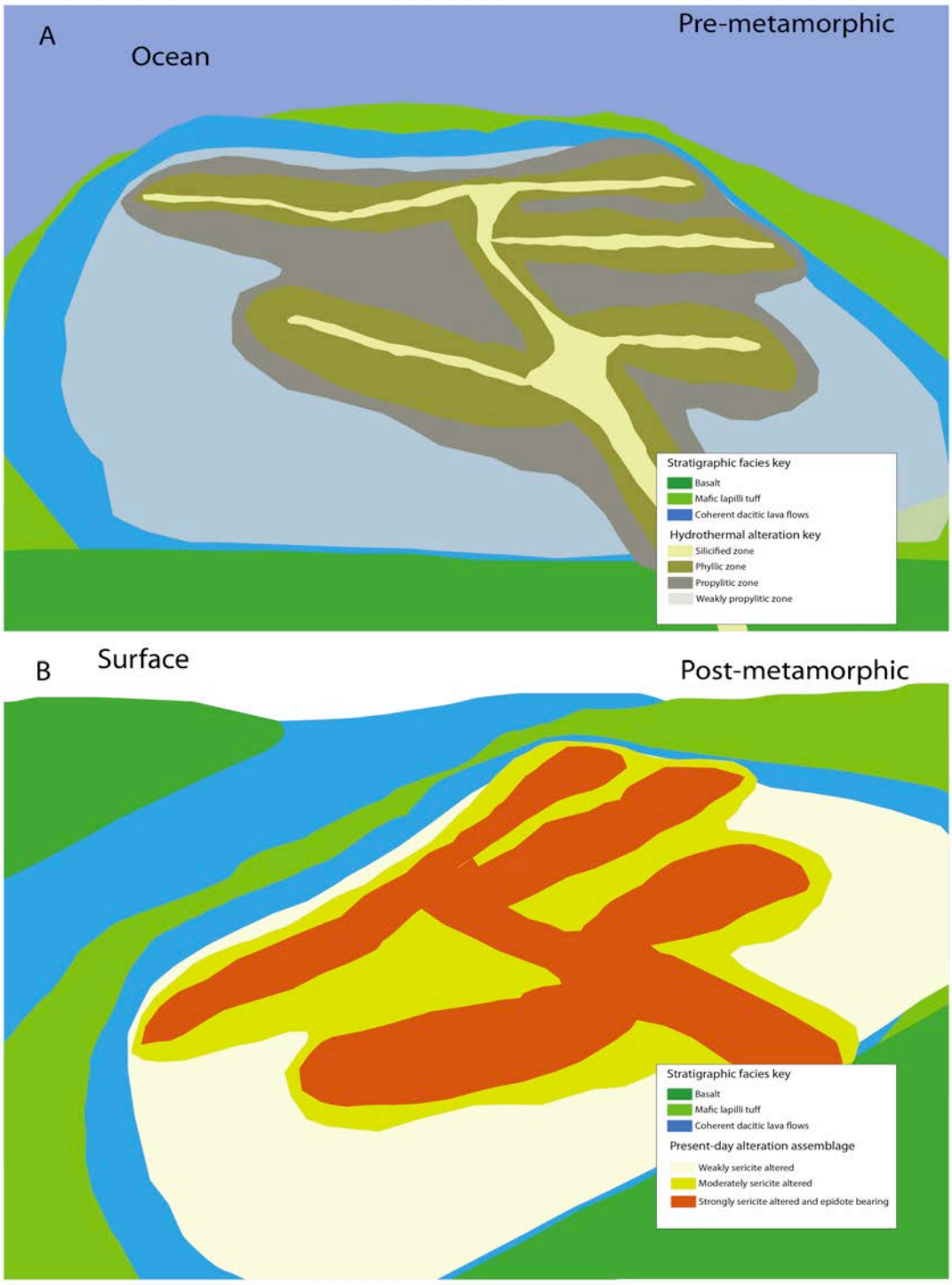

Figure 66. Comparison of the likely original hydrothermal alteration assemblage (A) grading from an inner zone of silicification to a phyllic zone and to a more regional propyllitic zone. When subjected to isochemical metamorphism these assemblages change into the assemblages seen in the RRGP today (B). Further discussion in the text.

the phyllic assemblage and the MSA and LA assemblages are possibly metamorphosed equivalents to the propyllitic assemblage.

The RRPG is believed to be the result of a syngenetic subaqueous hydrothermal system that began soon after the emplacement of the dacite intrusions and lava flows. The feeding fissure related to the volcanism provided a conduit for fluid flow and the hypabyssal intrusions provided ample heat to drive the hydrothermal system of mixed meteoric and magmatic sources at low crustal depths. Compositional changes in Na_2O_3, SiO_2, CaO, Fe_2O_3, K_2O and MgO are observed throughout the alteration assemblages and are the result of large-scale convection of seawater through permeable volcanic successions driven the emplacement of the hypabassal dacitic intrusions (Baker, 1985). This metasomatism and changes in Na_2O, SiO_2, CaO, Fe_2O_3, K_2O and MgO is common in subaqueous volcanic systems and has been previously documented (e.g. Baker, 1985 and Galley, 1993). This initial fluid was circulated through permeable units and syn-volcanic faults and reacted with the wall rock resulting in the silicification and phyllic altered assemblages associated with open space filling and stringer gold mineralization. As the system evolved and travelled distally from the fluid conduit the same rock, now infiltrated by a more alkaline fluid at lower fluid/rock ratio was altered to propyllitic assemblages. Later draw down of seawater resulted in the abundant later alteration minerals that are associated with the assemblages.

During regional greenschist metamorphism, the mineralogy of the synvolcanic alteration assemblages were modified by metamorphic reactions. This lead to the sericite altered assemblages that are preserved at the RRGP; the EPB and SSA assemblages are believed to be the metamorphic equivalents of phyllic assemblages; WSA and MSA assemblages are the metamorphic equivalents of propyllitic assemblages. Many characteristic textures were destroyed and primary alteration minerals reacted to form metamorphic equivalents. However, the secondary minerals, style and distribution of alteration and gold mineralization, as well as the correlation between Ag, As, Hg, Sb, and Pb with Au mineralization imply this deposit was the result of a syngenetic low-sulfidation gold system.

4.0 Summary and conclusions

The RRGP is situated within an Archean felsic volcanic succession, that is underlain and overlain by massive and pillowed basalt lava flows. Geochemically, rocks within the RRGP are bimodal, and represent two distinct magmatic sources—tholeiitic basalt and dacite. The felsic succession is dominated by massive dacitic lava flows with subordinate lapilli tuffs interlayered with mafic tuffs and dacitic sills and dikes. Alteration within the RRGP is dominated by sericite + chlorite + carbonate ± epidote. Alteration intensity appears to correlate well with original rock permeability. At the RRGP gold mineralization is constrained to the dacitic lava flows within areas of high permeability, which have undergone later enrichment during deformation. Types and distribution of gold mineralization suggest that the gold is related to a syn-volcanic, low-sulfidation epithermal-type system, which was likely remobilized and upgraded, in structurally deformed domains during post-volcanic deformation and greenschist facies metamorphism.

Polyphase deformation and alteration have had strong affects on the RRGP, destroying most primary textures associated with the felsic volcanic succession. However, the preserved textures suggest that dacitic volcanism was related to a subaqueous lobe-hyaloclastite flow complex. This complex was located within a volcanic arc-like setting and formed contemporaneously with massive and pillowed basalt lava flows. Thick mafic tuffs interlayered with the felsic volcanic rocks are the result of the resedimentation of hyaloclastites and associated flow breccias related to tholeiitic basalt flows. This resedimentation was likely related to gravitational collapse or instability possibly caused by the oversteppening of basalt volcanic edifice flanks and mass movement of basalt autoclastic breccias. When these wet, unconsolidated sediments were deposited over the dacitic fissure the dacitic magma was emplaced in the mafic lapilli tuff resulting in the formation of dacitic sills and dikes and associated peperites that locally occur within the RRGP. The matrix of the peperites is compositionally intermediate between the dacitic intrusions and the mafic lapilli tuffs with dacitic clasts distributed within the matrix. Once the dacitic magma had breached the mafic tuff it erupted effusively onto the ocean floor to form massive, sparsely amygdaloidal, locally

porphyritic dacite flow lobes and lava domes, with associated autoclastic breccia. Because of the subsequent deformation and alteration, it is difficult to determine the original thicknesses of individual flow lobes: however within the massive dacitic lava flows are closely associated with hyaloclastites and dacitic lapilli tuffs; and horizons containing >40% amygdules within the dacitic lava flows likely represent flow tops. Dacitic lapilli tuffs are the result of the remobilization of felsic hyaloclastite and dacitic carapace breccias related to the dacitic lobe-hyaloclastite flow complex.

Gold mineralization at the RRGP is variable and is related to open space fillings, stringers, and veins. Gold values are strongly correlated with alteration intensity. Alteration assemblages at the RRGP are dominated by sericite ± chlorite ± carbonate ± epidote with ubiquitous silicification. These alteration assemblages are consistent with propylitic and phyllic alteration assemblages that have been subject to mid- to upper-greenschist metamorphism. Permeable units, like flow tops and shear zones, contain the most intense alteration and inherently have higher gold grades. This suggests that the hydrothermal fluids containing gold were focused through the most permeable units and deposited the highest amount of gold in these rocks. Further from the fluid source alteration intensity and gold values both decrease simultaneously. Post-volcanic structural deformation and hydrothermal activity appears to have locally upgraded gold grades within shear zones.

5.0 References

Allen, R.L., 1988. False pyroclastic textures in altered silicic lavas, and implications for volcanic hosted mineralisation. Econ. Geol. 83, 1424–1446.

Ayers, L.D. 1997. A Volcanological Investigation of Rock Units, Structures, and Gold Mineralization, Rainy River Project. Unpublished company report. Nuinsco Resources Ltd., pp. 43.

Bajc, A.F., 1991. Quaternary Geology, Fort Frances-Rainy River Area. Ontario Geological Survey, Open File Report 5794, accompanied by maps P. 3065, P. 3137, P. 3138., pp. 170.

Baker, J.H., 1985. Rare earth and other trace element mobility accompanying albitization in a Proterozoic granite, west Bergslagen, Sweden. Mineralogical Magazine 49, 107–115.

Blackburn, C.E., Beard, R.C., Rivett, A.S., 1981, Kenora–Fort Frances, geological compilation series, Kenora and Rainy River districts; Ontario Geological Survey, Map 2443, scale 1:253 440.

Blackburn, C.E., John, G.W., Ayer, J., Davis, D.W., 1991. Wabigoon Subprovince. In: Thurston, P.C., Williams, H.R., Sutcliffe, R.H., Stott, G.M. (Eds.), Geology of Ontario: Ontario Geological Survey. Special Volume 4, Part 1, 303 -381.

Busby-Spera C.J., White J.D.L. 1987. Variation in peperite textures associated with differing host-sediment properties. Bull. Volcanol. 49, 765-775

Cas, R.A.F., 1992. Submarine volcanism: eruption styles, products, and relevance to understanding the host-rock successions to volcanic-hosted massive sulphide deposits. Econ. Geol. 87, 511–541.

Cas, R.A.F., Wright, J.V., 1992. Volcanic Successions, Modern and Ancient: A Geological Approach to Processes, Products and Successions. Chapman and Hall, Melbourne, p. 512.

Cole, G., El-Rassi, D., Couture, J., 2009. Mineral Resource Evaluation Rainy River Gold Project Western Ontario, Canada. Unpublished company report. Rainy River Resources Ltd., pp. 113.

Condie, Kent C., 1981. Archean greenstone belts: Development in Precambrian Geology; volume 3. Elsevier Scientific Publishing Company, The Netherlands, p. 434.

Cullen, P., Clark, J., Nelson, B., 2005. Technical Report for the Rainy River Project Kenora Mining Division, Northwest Ontario. Unpublished company report. Collingwood Capital Corporation, pp. 35.

Cooke, D.R., Simmons, S. T., 2000. Characteristics and Genesis of Epithermal Gold Deposits. In: Hagemann, S.G., Brown, P.E. (Eds.), Gold in 2000: Society of Economic Geologists, Reviews in Economic Geology, 13, 69-98.

De Rosen-Spence, A.F., Provost, D., Dimroth, E., Gochnauer, K., Owen, V., 1980. Archean Subaqueous Felsic Flows, Rouyn-Noranda, Quebec, Canada and their Quaternary equivalents. Precamb. Res. 12, 43–77.

Dimroth, E., Cousineau, P., Leduc, M., Sanschagrin, Y., 1978. Structure and organization of Archean subaqueous basalt flows, Rouyn-Noranda area, Quebec, Canada. Can. Jour. Earth Sci. 15, 902-918.

Dube, B., Dunning, G., Lauziere, K., 1995. Geology of the Hope Brook Mine, Newfoundland, Canada: A Preserved Late Proterozoic High-Sulfidation Epithermal Gold Deposit and Its Implications for Exploration. Econ. Geol., 93, 405-436.

Fisher, R.V., 1960. Classification of volcanic breccias. Geol. Society of America Bull. 71, 973-982.

Fisher, R.V., 1966. Mechanism of deposition from pyroclastic flows. Amer. J. Sci. 264, 350-363.

Franklin, J. M., Gibson, H. L., Galley, A. G., Jonasson, I. R., 2005. Volcanogenic Massive Sulfide Deposits. In: Hedenquist, J. W., Thompson, J. F. H., Goldfarb, R. J., Richards, J. P. (Eds.), Economic Geology 100th Anniversary Volume: Society of Economic Geologists, Littleton, CO, 523-560.

Galley, A.G., 1993. Characteristics of semi-conformable alteration zones associated with volcanogenic massive sulfide districts. Journal of Geochemical Exploration 48, 175–200.

Gibson, H.L., Morton R.L., Hudak, G., 1999. Submarine volcanic processes, deposits and environments favorable for the location of volcanic-associated massive sulfide deposits. Reviews in Economic Geology 8, 13–51.

Gifkins, C., Herrmann, W., Large, R., 2005. Altered Volcanic Rocks: A guide to description and interpretation. University of Tasmania, Centre for Ore Deposits and Exploration Studies, Hobart, pp. 287.

Grant, J. A., 1986. The Isocon diagram—A simple solution to Gresen's equation for metasomatic alteration. Econ. Geol. 81, 1976–1982.

Grant, J. A., 2005. Isocon analysis: A brief review of the method and applications: In: Dini, A., Corteel, C. Deyhle, A. (Eds.), Element and Isotope Mobility during Water-Rock Interaction Processes. Physics and Chemistry of the Earth 30 (17–18), 997–1004.

Gemmell, J. B., 2007. Hydrothermal alteration associated with the Gosowong epithermal Au-Ag deposit, Halmara, Indonesia: Mineralogy, geochemistry, and exploration implications. Econ. Geol. 102, 893-922.

Gresens, P. L., 1967. Composition-volume relationships of metasomatism. Chem. Geol. 2, 47–65.

Groves, D.I., Goldfarb, R.J., Robert, F., Hart, C.J.R., 2003. Gold deposits in metamorphic belts: Overview of current understanding, outstanding problems, future research, and exploration significance. Econ. Geol. 98, 1-29.

Hart, T.R., Gibson, H.L., Lesher, C.M., 2004. Trace element geochemistry and petrogenesis of felsic volcanic rocks associated with volcanogenic massive Cu-Zn-Pb sulfide deposits. Econ. Geol. 99, 1003-1013.

Hey, M.H., 1954. A New Review of the Chlorites. Mineralogical Magazine 30, 277-292.

Hildreth, W., Mahood, G.A., 1985. Correlation of ash-flow tuffs. Geological Society of America Bulletin 96, 968-974.

Hudak, G.J., Heine, J., Newkirk, T., Odette, J., and Hauck, S., 2002. Comparative geology, stratigraphy, and lithogeochemistry of the Five Mile Lake, Quartz Hill, and Skeleton Lake VMS occurrences, Vermilion District, NE Minnesota: Natural Resources Research Institute, University of Minnesota, Duluth, Technical Report, NRRI/TR-2002/03, pp. 390.

Huston, D.L., Blewett, R.S., Keillor, B., Standing, J., Smithies, R.H., Marshall, A., Mernagh, T.P., Kamprad, J., 2002. Lode gold and epithermal deposits of the Mallina basin, North Pilbara terrain, Western Australia. Econ. Geol. 97, 801–818.

Ishikawa, Y., Sawaguchi, T., Iwaya, S., Horiuchi, M., 1976. Delineation of prospecting targets for Kuroko deposits based on modes of volcanism of underlying dacite and alteration halos. Mining Geology 26, 105–117.

Jenner, G.A., 1996. Trace element geochemistry of igneous rocks: geochemical nomenclature and analytical geochemistry. In: Wyman, D.A. (Ed.), Trace Element Geochemistry of Volcanic Rocks: Applications For Massive Sulphide Exploration: Geological Association of Canada, Short Course Notes 12, 51-77.

Kesler S.E. and Wilkinson B.H., 2009. Crustal resources of gold in epithermal ore deposits. Econ. Geol. 104, 623–633.

Large, R.R., Gemmell, J.B., Paulick, H., Huston, D., 2001. The alteration box plot: A simple approach to understanding the relationship between alteration mineralogy and lithogeochemistry associated with VHMS deposits. Econ. Geol. 96, 957–972.

Lebas, M.J., Le Maître, R. W., Streckeisen, A. Zanettin, B., 1986. A chemical classification of volcanic rocks based on the total alkali-silica diagram. Journal of Petrology 27, 745-750.

Lesher, C.M., Goodwin, A.M., Campbell, I.H., Gorton, M.P., 1986. Trace-element geochemistry of ore-associated and barren, felsic metavolcanic rocks in the Superior province, Canada. Canadian Journal of Earth Sciences 23, 222–237.

Lindgren, W., 1933. Mineral Deposits, 4th Ed.. McGraw-Hill, New York, pp. 930.

Mackie, B., Puritch, E., Jones, J., 2003. Rainy River Project: Exploration Summary and Mineral Resource Estimate for the #17 Gold Zone. Unpublished company report. Nuinsco Resources Ltd., pp. 43.

Osterberg, S.A., Morton, R.L., Frankin, J.M., 1987. Hydrothermal alteration and physical volcanology of Archaean Rocks in the vicinity of the Headway- Coulee massive sulpide occurrence, Anaman Area, Northwest Ontario. Econ. Geol. 82, 1505–1520.

Paulick, H., Mcphie, J., 1999. Facies architecture of the felsic lava-dominated host sequence to the Thalanga massive sulfide deposit, lower Ordovician, northern Queensland. Austr. J. Earth Sci. 46 (3), 391–405.

Penczak, R, .S., Mason R., 1997. Metamorphose Archean Epithermal Au-As-Sb-Zn-(Hg) vein mineralization at the Campbell mine, northwestern Ontario. Econ. Geol. 92, 696-719.

Percival, J.A., 2007, Geology and metallogeny of the Superior Province, Canada. In: Goodfellow, W.D.,(Ed.), Mineral Deposits of Canada: A Synthesis of Major Deposit-Types, District Metallogeny, the Evolution of Geological Provinces, and Exploration Methods: Geological Association of Canada, Mineral Deposits Division. Special Publication No. 5, 903-928.

Reed, M.H., 1997. Hydrothermal Alteration and Its Relationship to Ore Fluid Composition. In: Barnes, H.L. (Ed.), Geochemistry of Hydrothermal Ore Deposits. John Wiley and Sons, New York, pp. 303–366.

Robb, L., 2005. Introduction to Ore-Forming Processes. Blackwell Science, Malden, MA, p. 373.

Robert F., Poulsen K.H., Cassidy K.F., Hodgson C.J., 2005, Gold Metallogeny of the Superior and Yilgarn Cratons. In: Hedenquist, J. W., Thompson, J. F. H., Goldfarb, R. J., Richards, J. P. (Eds.), Economic Geology 100th Anniversary Volume: Society of Economic Geologists, Littleton, CO, 1001-1034.

Rosengren, N.M., Cas, R.A.F., Beresford, S.W., and Palich, B.M., 2008, Reconstruction of an extensive Archaean dacitic submarine volcanic complex associated with the

komatiite-hosted Mt Keith nickel deposit, Agnew-Wiluna Greenstone Belt, Yilgarn Craton, Western Australia. Precamb. Res. 161, 34-52.

Schandl, E., 2006. Petrographic and mineralogical study of the Rainy River Au prospect, Richardson TP. Ontario. Unpublished company report. Rainy River Resources Ltd., pp. 157.

Schmidt, R., H.U. Schmincke. 2000. Seamounts and island building. In Sigurdsson, H., Houghton, B.F., McNutt, S.R., Rymer, H., Stix, J. (Eds.), Encyclopedia of volcanoes. Academic Press, San Diego, pp.. 383–402.

Siddorn, J., 2007. Structural investigations, Rainy River Project, Ontario, Canada. Internal presentation by SRK Consulting (Canada) presented to Rainy River personnel, October 2007.

Simmons, S.F., White, N.C., John, D.A., 2005. Geological characteristics of epithermal precious and base metal deposits. In: Hedenquist, J. W., Thompson, J. F. H., Goldfarb, R. J., Richards, J. P. (Eds.), Economic Geology 100th Anniversary Volume: Society of Economic Geologists, Littleton, CO, 485–522.

Skilling, I.P., White, J.D.L., McPhie, J., 2002. Peperite: a review of magma-sediment mingling. Journal of Volcanology and Geothermal Research 114, 1-17.

Stott, G., Corkery, T., Leclair, A., Boily, M., Percival, J., 2007. A revised terrane map for the Superior Province as interpreted from aeromagnetic data [abstract]. Institute on Lake Superior Geology Proceedings, 53rd Annual Meeting, Lutsen, MN, 53 (1), 74-76.

Vallance, J.W., 2000, Lahars. In Sigurdsson, H., Houghton, B.F., McNutt, S.R., Rymer, H., Stix, J. (Eds.), Encyclopedia of volcanoes. Academic Press, San Diego, pp. 601-616.

White, N.C., and Hedenquist, J.F., 1995. Epithermal Gold Deposits: styles, characteristics, and exploration. SEG Newsletter 23, 1 & 9-13

Whitford, D.J., McPherson, W.P., Wallace, D.B., 1989. Geochemistry of the host rocks of the volcanogenic massive sulfide deposit at Que River, Tasmania. Econ. Geol. 84, 1–21.

Winchester, J.A., Floyd, P.A., 1977. Geochemical discrimination of different magma series and their differentiation products using immobile elements. Chem. Geol. 20, 325-343.

Winchester JA, Floyd PA, 1976. Geochemical magma type discrimination; application to altered and metamorphosed basic igneous rocks. Earth Planet Sci. Lett. 28, 459-469.

Wood, D. A., 1980. The application of a Th-Hf-Ta diagram to problems of tectonomagmatic classification and to establishing the nature of crustal contamination of basaltic lavas of the British Tertiary volcanic province. Earth Planet. Sci. Lett. 50, 11–30.

Appendix I: Petrographic Analyses of RRGP samples

The following tables are a summary of the abbreviation used in Appendix I for the petrographic analysis.

Samples denoted with a * have an accompanying geochemical analysis.

Abbreviations:

Volcanic Textures
1-massive, 2-phyric, 3-fragmental, 4-amygdaloidal, 5-spherulitic

Crystals
eu-euhedral, sub-subhedral, frg-fragmented, emb-embayed

Amygdule fillings
qcc-quartz+carbonate+chlorite, qccp-quartz+carbonate+chlorite+pyrite, q-quartz, qc-quartz+chlorite

Fragments
FC-felsic clasts, MC-mafic clasts, lp-lapilli-sized

Groundmass
equi-equigranular groundmass, inequi-inequigranular groundmass, vfg-very-fine grained (<125 μm), fg-fine grained (125–250 μm), mg-medium grained (0.25–0.5 mm), cg-coarse grained (0.5–1 mm), vcg-very-coarse grained (>1 mm)

Minerals
QFM-quartz/feldspar matrix, SM-sericite mica, MC-magnesium-rich chlorite, IC-iron-rich chlorite, CB-carbonate minerals, AC-actinolite group minerals, EP-epidote, CL-clinozoisite, BI-biotite, SF-sulfides

Alteration
SER-sericite alteration, CHL-chlorite alteration, CAR-carbonate alteration, EPD-epidote alteration, ACT-actinolite alteration, BIO-biotite alteration
For CHL, CAR, EPD, ACT and BIO: rare=<5%, weak=5-10%, mod-moderate=10-20%, int-intense=>20%
For SER: weak=<20%, mod-moderate=20-35%, int=>35% for sericite

Appendix I: Table 1
Basalts

Sample		RR-44	RR-53*	RR325-16*
Drill hole depth (m)		otc	otc	351.3
Groundmass	*QFM*	15	15	12
	SM	0	0	10
	MC	10	5	3
	IC	10	15	0
	CB	10	5	18
	AC	35	37	22
	EP	15	20	30
	CL	0	0	0
	BI	0	0	0
	SF	5	3	5
	Total	100	100	100
	Distribution	equi	equi	inequi
	Size	mg	vfg	mg
	Foliation	poor	non	non
Amygdules	*Amygdule %*	0	0	0
	Fililng	0	0	0
Alteration	*SER*	none	none	weak
	CHL	int	int	rare
	CAR	mod	weak	mod
	BIO	none	none	none
	EPD	mod	int	int
	ACT	int	int	none
Additional Volcanic Textures		1	1	1

Appendix I: Table 2
Mafic tuffs

Sample		RR-17*	RR49-1	RR49-37	RR49-38*	RR49-40	RR70-1	RR70-10	RR173-5	RR198-8*
Drill hole depth (m)		otc	226.5	671.8	690.15	747.65	52.4	273.4	145.3	458.9
Groundmass	*QFM*	55	35	1	35	23	35	26	33	15
	SM	5	22	56	25	41	0	20	23	10
	MC	0	5	22	10	12	5	0	23	25
	IC	15	20	5	0	5	0	0	9	15
	CB	2	3	0	0	0	15	10	9	0
	AC	0	0	0	0	0	25	12	0	20
	EP	10	0	tr	15	0	5	0	0	15
	CL	0	0	0	10	3	0	0	0	0
	BI	6	0	0	0	0	0	10	0	0
	SF	7	15	15	5	16	15	22	3	0
	Total	100	100	99	100	100	100	100	100	100
	Distribution	inequi	inequi	inequi	inequi	inequi	inequi	inequi	inequi	inequi
	Size	fg-mg	vfg	fg	vfg	vfg	mg	vfg	fg	fg
	Foliation	poor	moderate	moderate	mod	non	poor	moderate	non	poor
Fragments	*FC*	0	0	0	0	0	0	0	0	0
	MC	0	0	0	0	0	0	0	0	65
	Size (cm)	0	0	0	0	0	0	0	0	1-4.5
Alteration	*SER*	weak	mod	int	mod	int	none	mod	mod	weak
	CHL	mod	int	int	mod	mod	weak	none	int	int
	CAR	rare	rare	none	none	none	mod	mod	weak	none
	BIO	weak	none	none	none	none	none	mod	none	none
	EPD	int	none	rare	int	rare	weak	none	none	mod
	ACT	none	none	none	none	none	int	weak	none	none
Additional Volcanic Textures		1, 3	1, 3	1, 3	1, 3	1, 3	1, 3	1, 3	1, 3	1, 4

Appendix I: Table 2 cont.
Mafic tuffs cont.

Sample		RR198-10*	RR249-1	RR249-6	RR274-11	RR311-11*	RR311-15*	RR325-10	RR325-8*	RR358-1*
Drill hole depth (m)		492.3	46.3	152	468.5	550.3	806.4	246.7	207.4	48.8
Groundmass	*QFM*	31	14	12	16	49	40	24	17	28
	SM	12	0	11	8	29	0	37	2	52
	MC	16	4	16	29	7	21	5	12	0
	IC	25	4	27	12	0	0	25	40	5
	CB	10	18	22	25	0	5	0	21	0
	AC	0	31	0	0	0	5	0	0	0
	EP	0	9	0	0	0	20	0	0	0
	CL	0	0	1	0	0	2	0	0	0
	BI	0	13	11	6	0	1	0	0	3
	SF	6	7	0	4	15	6	9	8	12
	Total	100	100	100	100	100	100	100	100	100
	Distribution	inequi	inequi	inequi	inequi	inequi	inequi	inequi	inequi	inequi
	Size	fg	vfg	fg	fg	fg	fg-mg	fg	fg-mg	vfg
	Foliation	poor	moderate	poor	poor	mod	poor	non	non	moderate
Fragments	*FC*	0	0	0	0	0	0	0	0	0
	MC	0	0	0	0	0	0	0	0	0
	Size (cm)	0	0	0	0	0	0	0	0	0
Alteration	*SER*	weak	none	weak	weak	mod	none	int	rare	int
	CHL	int	weak	int	int	weak	moderate	int	int	weak
	CAR	mod	mod	int	int	none	weak	none	int	none
	BIO	none	mod	mod	weak	none	rare	none	none	rare
	EPD	none	weak	rare	none	none	int	none	none	none
	ACT	none	int	none	none	none	none	none	none	none
Additional Volcanic Textures		1, 3	1, 3	1, 3	1, 3	1, 3	1, 3	1, 3	1, 3	1, 3

Appendix I: Table 2 cont.
Mafic tuffs cont.

Sample		RR358-3
Drill hole depth (m)		98
Groundmass	*QFM*	43
	SM	13
	MC	22
	IC	0
	CB	6
	AC	0
	EP	0
	CL	0
	BI	6
	SF	10
	Total	100
	Distribution	inequi
	Size	fg
	Foliation	poor
Fragments	*FC*	0
	MC	0
	Size (cm)	0
Alteration	*SER*	weak
	CHL	int
	CAR	weak
	BIO	weak
	EPD	none
	ACT	none
Additional Volcanic Textures		1, 3

Appendix I: Table 3
Dacitic dikes and sills

Sample		RR49-34	RR49-35	RR49-36	RR49-42	RR49-43	RR70-3	RR70-4	RR157-10	RR157-11
Drill hole depth (m)		661.58	664.45	668.15	754.65	783.65	105.2	116.3	278.3	340.3
Crystals	*QTZ*	11	11	11	0	1	0	9	8	2
	FSP	0	0	0	0	0	0	6	6	2
	Min. size	0.3	0.4	0.5	0.5	0.2	0	0.5	0.3	0.3
	Max. size	1.8	2	2.5	1.6	0.6	0	1.5	2	0.6
	Shape	sub-frg	sub	sub-frg	frg-frg	frg-frg	0	sub	sub	sub-frg
Groundmass	*QFM*	45	58	53	25	55	32	39	49	30
	SM	17	16	24	5	25	0	28	9	54
	MC	17	6	8	30	10	13	3	4	8
	IC	0	0	0	15	0	0	0	0	0
	CB	8	7	2	0	2	32	0	9	0
	AC	0	0	0	0	0	0	2	0	0
	EP	0	0	0	15	3	0	0	0	0
	CL	0	0	0	0	0	0	0	0	0
	BI	0	0	0	5	0	2	9	13	0
	SF	2	2	2	5	4	21	3	2	4
	Total	100	100	100	100	100	100	99	100	100
	Distribution	equi	equi	equi	inequi	inequi	inequi	equi	equi	equi
	Size	vfg	vfg	vfg	fg	fg	fg	vfg	vfg	vfg
	Foliation	poor	mod	non	mod	mod	poor	non	poor	poor
Alteration	*SER*	weak	weak	mod	weak	mod	none	mod	weak	int
	CHL	mod	weak	weak	int	mod	mod	rare	rare	weak
	CAR	weak	weak	rare	none	rare	int	none	weak	none
	BIO	none	none	none	weak	none	rare	weak	mod	none
	EPD	none	none	none	mod	rare	none	none	none	none
	ACT	none	none	none	none	none	none	none	none	none
Additional Volcanic Textures		1, 2	1, 2	1, 2	1, 2	1, 2	1	1, 2	1, 2	1, 2

Appendix I: Table 3 cont.
Dacitic dikes and sills cont.

Sample		RR173-1*	RR173-2	RR227-9	RR249-3*	RR249-5	RR274-9	RR274-10	RR311-3*	RR311-14
Drill hole depth (m)		38.3	72.5	427.5	88.9	103.4	322.4	343.3	113.5	724
Crystals	*QTZ*	0	7	12	5	0	3	2	5	10
	FSP	0	0	0	5	0	0	0	31	25
	Min. size	0	0.5	0.6	0.7	0	0.3	0.3	1	1.5
	Max. size	0	2	1.5	1.5	0	1.6	1	3.5	3.5
	Shape	0	sub	eu	sub-eu	0	sub-frg	eu	sub	sub
Groundmass	*QFM*	24	39	59	43	53	43	33	44	40
	SM	10	39	6	27	28	0	0	10	5
	MC	19	10	9	4	3	34	30	5	10
	IC	0	0	0	0	0	0	0	0	0
	CB	43	2	2	0	2	16	30	2	0
	AC	0	0	0	0	0	0	0	0	0
	EP	0	0	0	13	5	0	0	0	4
	CL	0	0	0	0	0	0	0	0	0
	BI	0	0	0	0	6	2	0	0	5
	SF	4	3	12	3	3	2	5	3	0
	Total	100	100	100	100	100	100	100	100	99
	Distribution	inequi	equi	inequi	equi	equi	inequi	inequi	inequi	equi
	Size	fg	fg	vfg	vfg	vfg	vfg	fg	vfg	vfg
	Foliation	poor	mod	int	poor	mod	mod	mod	non	non
Alteration	*SER*	weak	int	weak	mod	mod	none	none	weak	weak
	CHL	mod	mod	weak	rare	rare	int	int	weak	weak
	CAR	int	rare	rare	none	rare	mod	int	rare	none
	BIO	none	none	none	none	weak	rare	none	none	weak
	EPD	none	none	none	mod	weak	none	none	none	rare
	ACT	none	none	none	none	none	none	none	none	none
Additional Volcanic Textures		1	1, 2	1, 2	1, 2	1, 2	1, 2	1, 2	1, 2	1, 2

Appendix I: Table 3 cont.
Dacitic dikes and sills cont.

Sample		RR322-10*	RR322-11*	RR322-12	RR325-11	RR325-14	RR325-15	RR358-2	RR358-5	RR393-5*
Drill hole depth (m)		359.3	417.3	432.6	252.3	276.4	289.3	69.8	308.6	323.1
Crystals	*QTZ*	2	4	0	0	13	3	6	2	8
	FSP	0	9	0	5	2	6	0	2	10
	Min. size	1	1	0	0.4	1.5	0.4	0.5	0.5	0.5
	Max. size	3.5	2.5	0	2	3.5	2	1.5	1	2.4
	Shape	sub-frg	sub	0	sub	sub	sub	eu	sub-frg	sub-eu
Groundmass	*QFM*	42	45	35	37	45	39	28	31	30
	SM	33	31	0	26	25	33	23	26	40
	MC	5	2	15	11	10	0	0	15	3
	IC	0	0	0	0	0	0	15	0	0
	CB	15	4	15	16	3	17	14	0	6
	AC	0	0	0	0	0	0	0	0	0
	EP	0	0	0	0	0	0	14	13	0
	CL	0	0	15	0	0	0	0	0	0
	BI	0	3	0	3	2	0	0	7	0
	SF	3	2	20	2	0	2	0	4	3
	Total	100	100	100	100	100	100	100	100	100
	Distribution	equi	equi	inequi	equi	equi	equi	inequi	inequi	inequi
	Size	vfg	vfg	fg	vfg	fg	fg	fg	fg	fg
	Foliation	poor	mod	non	mod	non	non	non	non	mod
Alteration	*SER*	mod	mod	none	mod	mod	mod	mod	mod	int
	CHL	weak	rare	mod	mod	mod	none	mod	mod	rare
	CAR	mod	rare	mod	mod	rare	mod	mod	none	weak
	BIO	none	rare	none	rare	rare	none	none	weak	none
	EPD	none	none	mod	none	none	none	mod	mod	none
	ACT	none	none	none	none	none	none	none	none	none
Additional Volcanic Textures		1, 2	1, 2	1	1, 2	1, 2	1, 2	1, 2	1, 2	1, 2

Appendix I: Table 3 cont.
Dacitic dikes and sills cont.

Sample		RR458-8
Drill hole depth (m)		461.7
Crystals	*QTZ*	3
	FSP	0
	Min. size	0.2
	Max. size	0.8
	Shape	eu
Groundmass	*QFM*	43
	SM	29
	MC	0
	IC	13
	CB	10
	AC	0
	EP	0
	CL	0
	BI	0
	SF	2
	Total	100
	Distribution	inequi
	Size	vfg
	Foliation	int
Alteration	*SER*	mod
	CHL	mod
	CAR	mod
	BIO	none
	EPD	none
	ACT	none
Additional Volcanic Textures		1, 2

Appendix I: Table 4
Peperites

Sample		RR49-39	RR49-41*	RR70-5*	RR70-9*	RR198-21	RR249-2*	RR249-7	RR358-3	RR358-4
Drill hole depth (m)		697.2	749.32	134.5	262.3	1376.3	71.3	182.5	98	235.2
Groundmass	*QFM*	20	19	27	30	35	30	16	43	39
	SM	46	43	24	4	5	0	7	13	39
	MC	15	0	4	0	40	0	0	22	0
	IC	0	0	0	0	0	0	0	0	0
	CB	0	2	30	0	15	53	0	6	7
	AC	0	0	0	36	0	0	51	0	0
	EP	0	0	0	14	0	0	0	0	0
	CL	4	5	0	4	0	5	0	0	0
	BI	0	0	9	8	0	0	22	6	10
	SF	15	31	6	4	5	12	4	10	5
	Total	100	100	100	100	100	100	100	100	100
	Distribution	inequi	inequi	inequi	inequi	inequi	inequi	inequi	inequi	inequi
	Size	vfg	mg	fg	vfg	fg-mg	fg	fg	fg	vfg
	Foliation	poor	poor	poor	mod	mod	non	mod	poor	non
Fragments	*FC*	3	5	65	55	15	15	10	20	15
	MC	0	0	0	0	0	0	0	0	0
	Size	lp	lp	lp	lp	lp	lp	lp	lp	lp
Alteration	*SER*	int	int	mod	rare	weak	none	weak	weak	int
	CHL	mod	none	rare	none	int	none	none	int	none
	CAR	none	rare	int	none	mod	int	none	weak	weak
	BIO	none	none	weak	weak	none	none	int	weak	mod
	EPD	rare	weak	none	mod	none	weak	none	none	none
	ACT	none	none	none	int	none	none	int	none	none
Additional Volcanic Textures		3	3	3	3	3	3	3	3	3

Appendix I: Table 5
Dacitic lava flows

Sample		RR-46*	RR-47*	RR-48	RR-49*	RR-50*	RR-51*	RR-54*	RR-56*	RR-57*
Drill hole depth (m)		otc	otc	otc	otc	otc	otc	otc	otc	otc
Crystals	*QTZ*	2	10	4	2	0	11	3	0	8
	FSP	3	5	3	0	0	3	0	2	2
	Min. size	1	1	0.5	0.5	0	1	0.2	0.4	0.5
	Max. size	1.8	2.5	1.3	1.4	0	2.3	0.5	0.7	1.3
	Shape	sub	sub	sub	sub	0	sub	sub	sub	sub-frg
Groundmass	*QFM*	65	40	55	50	55	57	37	52	55
	SM	15	30	15	24	35	17	40	38	25
	MC	7	5	5	5	2	3	2	6	4
	IC	0	0	0	0	0	0	0	0	0
	CB	0	0	0	3	0	0	6	0	3
	AC	0	0	0	0	0	0	0	0	0
	EP	0	0	2	7	5	0	7	0	0
	CL	0	0	0	0	0	0	0	0	0
	BI	5	6	13	7	0	6	0	0	0
	SF	3	4	3	2	3	3	5	2	3
	Total	100	100	100	100	100	100	100	100	100
	Distribution	equi	equi	equi	equi	equi	equi	equi	equi	equi
	Size	fg	fg	mg	mg	fg	fg	vfg-fg	fg	fg
	Foliation	non	non	poor	non	non	non	non	poor	int
Amygdules	*Amygdule %*	0	0	0	5	0	2	0	0	2
	Filling	0	0	0	qcc	0	q	0	0	qc
Alteration	*SER*	weak	mod	weak	mod	int	weak	int	int	mod
	CHL	weak	weak	weak	weak	rare	rare	rare	weak	rare
	CAR	none	none	none	rare	none	none	weak	none	rare
	BIO	weak	weak	mod	weak	none	weak	none	none	none
	EPD	none	none	rare	weak	weak	none	weak	none	none
	ACT	none	none	none	none	none	none	none	none	none
Additional Volcanic Textures		1, 2, 5	1, 2	1, 2	1, 2, 4	1, 3	1, 2, 4	1, 2	1, 2	1, 2, 4

Appendix I: Table 5 cont.
Dacitic lava flows cont.

Sample Drill hole depth (m)		RR-46* otc	RR-47* otc	RR-48 otc	RR-49* otc	RR-50* otc	RR-51* otc	RR-54* otc	RR-56* otc	RR-57* otc
Crystals	*QTZ*	2	10	4	2	0	11	3	0	8
	FSP	3	5	3	0	0	3	0	2	2
	Min. size	1	1	0.5	0.5	0	1	0.2	0.4	0.5
	Max. size	1.8	2.5	1.3	1.4	0	2.3	0.5	0.7	1.3
	Shape	sub	sub	sub	sub	0	sub	sub	sub	sub-frg
Groundmass	*QFM*	65	40	55	50	55	57	37	52	55
	SM	15	30	15	24	35	17	40	38	25
	MC	7	5	5	5	2	3	2	6	4
	IC	0	0	0	0	0	0	0	0	0
	CB	0	0	0	3	0	0	6	0	3
	AC	0	0	0	0	0	0	0	0	0
	EP	0	0	2	7	5	0	7	0	0
	CL	0	0	0	0	0	0	0	0	0
	BI	5	6	13	7	0	6	0	0	0
	SF	3	4	3	2	3	3	5	2	3
	Total	100	100	100	100	100	100	100	100	100
	Distribution	equi	equi	equi	equi	equi	equi	equi	equi	equi
	Size	fg	fg	mg	mg	fg	fg	vfg-fg	fg	fg
	Foliation	non	non	poor	non	non	non	non	poor	int
Amygdules	*Amygdule %*	0	0	0	5	0	2	0	0	2
	Filling	0	0	0	qcc	0	q	0	0	qc
Alteration	*SER*	weak	mod	weak	mod	int	weak	int	int	mod
	CHL	weak	weak	weak	weak	rare	rare	rare	weak	rare
	CAR	none	none	none	rare	none	none	weak	none	rare
	BIO	weak	weak	mod	weak	none	weak	none	none	none
	EPD	none	none	rare	weak	weak	none	weak	none	none
	ACT	none	none	none	none	none	none	none	none	none
Additional Volcanic Textures		1, 2, 5	1, 2	1, 2	1, 2, 4	1, 3	1, 2, 4	1, 2	1, 2	1, 2, 4

Appendix I: Table 5 cont.
Dacitic lava flows cont.

Sample		RR49-8	RR49-9	RR49-11	RR49-13	RR49-14	RR49-15	RR49-18	RR49-19	RR49-20
Drill hole depth (m)		187.1	235	272.15	345.5	347.2	368.2	404.25	415.25	423.1
Crystals	*QTZ*	15	5	4	5	10	1	0	0	4
	FSP	0	0	0	0	0	0	0	0	0
	Min. size	0.4	0.2	0.8	0.2	0.2	0.4	0	0.3	0.3
	Max. size	5	0.6	1.3	2.5	0.8	0.7	0	1.8	1.8
	Shape	sub	sub-frg	frg	frg	frg	sub-frg	0	sub-frg	sub-frg
Groundmass	*QFM*	56	43	58	43	49	54	57	57	45
	SM	21	19	25	45	28	30	16	33	40
	MC	4	2	4	2	0	0	0	2	7
	IC	0	0	0	0	0	0	15	0	0
	CB	3	24	0	0	0	0	0	5	0
	AC	0	0	0	0	0	0	0	0	0
	EP	0	0	0	0	3	5	2	0	0
	CL	0	0	0	0	0	0	0	0	0
	BI	0	0	0	0	0	0	0	0	0
	SF	1	7	9	5	10	10	10	3	4
	Total	100	100	100	100	100	100	100	100	100
	Distribution	equi	equi	equi	equi	equi	equi	equi	inequi	equi
	Size	vfg	mg	vfg	vfg	vfg	fg	vfg	vfg	vfg
	Foliation	mod	mod	mod	mod	poor	poor	mod	poor	poor
Amygdules	*Amygdule %*	0	0	2	7	2	0	0	0	0
	Filling	0	0	q	q	qccp	0	0	0	0
Alteration	*SER*	mod	weak	mod	int	mod	mod	weak	mod	int
	CHL	rare	rare	rare	rare	none	none	mod	rare	weak
	CAR	rare	int	none	none	none	none	none	weak	none
	BIO	none	none	none	none	none	none	none	none	none
	EPD	none	none	none	none	rare	weak	rare	none	none
	ACT	none	none	none	none	none	none	none	none	none
Additional Volcanic Textures		1, 2	1, 2	1, 2, 4	1, 2, 4	1, 2, 4	1, 2	1, 3	1, 2	1, 2, 5

Appendix I: Table 5 cont.
Dacitic lava flows cont.

Sample		RR49-21	RR49-22	RR49-23	RR49-24	RR49-25	RR49-26	RR49-27	RR49-28	RR49-32
Drill hole depth (m)		414.35	433.7	467.58	478.72	490.6	504	512.4	548	629.35
Crystals	*QTZ*	2	0	2	0	0	6	2	2	3
	FSP	0	0	0	0	0	0	0	0	13
	Min. size	0.2	0.3	0.2	0	0	0.5	0.3	0.2	0.4
	Max. size	0.7	0.3	0.7	0	0	4	0.7	0.5	2
	Shape	sub-frg	frg	sub-frg	0	0	sub-frg	frg	frg	sub-frg
Groundmass	*QFM*	53	61	55	51	61	43	52	52	49
	SM	29	31	30	31	36	38	29	29	22
	MC	7	4	0	10	1	4	11	12	11
	IC	0	0	0	0	0	0	0	0	0
	CB	6	2	0	0	0	0	0	0	0
	AC	0	0	0	0	0	0	0	0	0
	EP	0	0	3	0	0	0	0	0	0
	CL	0	0	0	0	0	3	0	0	0
	BI	0	0	0	5	1	0	0	0	0
	SF	3	2	10	3	1	6	6	5	2
	Total	100	100	100	100	100	100	100	100	100
	Distribution	inequi	inequi	inequi	inequi	inequi	inequi	inequi	equi	equi
	Size	mg	mg	fg	fg	vfg	mg	mg	vfg	fg
	Foliation	poor	mod	poor	non	poor	non	non	mod	poor
Amygdules	*Amygdule %*	0	0	0	0	0	0	3	0	0
	Filling	0	0	0	0	0	0	qccp	0	0
Alteration	*SER*	mod	mod	mod	mod	int	int	mod	mod	mod
	CHL	weak	rare	none	mod	rare	rare	mod	mod	mod
	CAR	weak	rare	none	none	none	none	none	none	none
	BIO	none	none	none	weak	rare	none	none	none	none
	EPD	none	none	rare	none	none	rare	none	none	none
	ACT	none	none	none	none	none	none	none	none	none
Additional Volcanic Textures		1, 2	1, 2	1, 2	1, 3	1, 3	1, 2, 5	1, 2, 4	1, 2	1, 2

Sample		RR49-33	RR70-6	RR70-8*	RR70-12	RR157-2*	RR157-3	RR157-5	RR157-6*	RR157-7
Drill hole depth (m)		638.57	158.2	241.3	328.4	128.6	136.2	150.3	185.4	238.5
Crystals	*QTZ*	9	6	3	4	1	14	0	16	2
	FSP	0	3	10	0	0	0	0	0	0
	Min. size	0.5	0.3	0.2	0.5	0.7	1	0	0.7	0.2
	Max. size	4.5	1	0.7	1.3	0.5	5	0	4.5	0.5
	Shape	sub-frg	sub-eu	sub	sub-eu	sub	sub	0	sub-eu	sub-emb
Groundmass	*QFM*	43	34	39	50	40	42	41	54	61
	SM	28	29	19	25	36	32	34	18	12
	MC	11	2	4	4	10	7	11	11	4
	IC	0	0	0	0	0	0	0	0	0
	CB	0	17	6	12	0	0	5	0	17
	AC	1	0	0	0	0	0	0	0	0
	EP	0	0	0	0	1	0	0	0	0
	CL	3	0	0	0	2	2	0	0	0
	BI	0	4	14	0	0	0	4	0	0
	SF	5	5	5	5	10	3	5	1	4
	Total	100	100	100	100	100	100	100	100	100
	Distribution	equi	equi	equi	inequi	equi	inequi	equi	equi	inequi
	Size	fg	vfg	vfg	vfg	vfg	vfg	fg	vfg	vfg
	Foliation	poor	int	poor	poor	mod	mod	non	mod	poor
Amygdules	*Amygdule %*	2	0	0	0	3	2	0	0	0
	Fililng	q	0	0	0	q	qccp	0	0	0
Alteration	*SER*	mod	mod	weak	mod	int	mod	mod	weak	weak
	CHL	mod	rare	rare	rare	mod	weak	mod	mod	rare
	CAR	none	mod	weak	mod	none	none	weak	none	mod
	BIO	none	rare	mod	none	none	none	rare	none	none
	EPD	rare	none	none	none	rare	rare	none	none	none
	ACT	none	none	none	none	none	none	none	none	none
Additional Volcanic Textures		1, 2, 4	1, 2	1, 2	1, 2	1, 2, 4	1, 2, 4	1, 3	1, 2, 5	1, 2

Appendix I: Table 5 cont.
Dacitic lava flows cont.

Sample		RR157-9	RR173-7	RR173-8*	RR173-9	RR173-10*	RR198-1	RR198-2	RR198-5*	RR198-11*
Drill hole depth (m)		262.3	175	225	312.5	473.2	96.4	140.3	378.2	608.4
Crystals	*QTZ*	0	3	20	0	2	2	0	7	20
	FSP	0	0	8	0	0	0	0	0	0
	Min. size	1.5	1	0	0	1	0.2	0	0.2	0.1
	Max. size	2.5	2.5	2.5	0	1.5	2	0	2.5	5
	Shape	sub	sub	sub	0	sub-frg	sub	0	sub	sub
Groundmass	*QFM*	41	38	28	25	48	29	38	39	32
	SM	52	35	29	25	33	38	27	39	18
	MC	6	11	8	12	3	2	22	5	5
	IC	0	0	0	30	0	0	0	0	0
	CB	0	11	6	3	10	0	11	10	7
	AC	0	0	0	0	0	0	0	0	0
	EP	0	0	0	0	0	19	0	0	15
	CL	1	0	0	0	0	0	0	0	0
	BI	0	0	0	5	0	0	0	0	0
	SF	0	2	1	0	4	10	2	0	3
	Total	100	100	100	100	100	100	100	100	100
	Distribution	inequi	equi	equi	inequi	inequi	equi	inequi	equi	equi
	Size	fg	fg	vfg	fg-mg	fg	vfg	vfg	vfg	vfg
	Foliation	poor	poor	mod	poor	poor	mod	int	mod	poor
Amygdules	*Amygdule %*	6	3	0	25	1	3	<1	0	0
	Fililng	qcp	qccp	0	q	q	qccp	q	0	0
Alteration	*SER*	int	mod	mod	none	mod	int	mod	int	weak
	CHL	weak	mod	weak	int	rare	rare	int	weak	weak
	CAR	none	mod	weak	rare	mod	none	mod	mod	weak
	BIO	none	none	none	weak	none	none	none	none	none
	EPD	rare	none	none	none	none	mod	none	none	mod
	ACT	none	none	none	none	none	none	none	none	none
Additional Volcanic Textures		1, 2, 4	1, 2, 4	1, 2	1, 3, 5	1, 2, 4	1, 2, 4	1, 3, 5	1, 2	1, 2, 5

Appendix I: Table 5 cont.
Dacitic lava flows cont.

Sample		RR198-13*	RR198-14	RR198-15	RR198-16	RR227-1	RR227-2	RR227-6*	RR249-9*	RR249-12
Drill hole depth (m)		806	847.2	943.2	1024.5	66.3	133.4	305.7	312.4	484.3
Crystals	*QTZ*	15	1	5	6	5	5	2	1	5
	FSP	0	0	0	0	0	0	0	0	0
	Min. size	0.3	1	0.5	0.6	0.3	0.4	0.3	0.4	0.4
	Max. size	1.7	1.8	1.5	1.7	1	1.5	0.5	0.8	1.2
	Shape	sub	sub-frg	frg-frg	sub	sub	frg-sub	eu	sub-emb	sub-frg
Groundmass	*QFM*	50	45	45	51	16	68	35	66	54
	SM	22	37	5	35	66	16	40	26	31
	MC	8	9	2	0	8	5	4	3	5
	IC	0	0	0	0	0	0	0	0	0
	CB	1	1	35	0	0	0	15	0	0
	AC	0	0	0	0	0	0	0	0	0
	EP	0	5	3	6	0	2	1	2	0
	CL	0	0	0	0	0	0	0	0	1
	BI	0	0	0	0	0	0	0	0	0
	SF	4	2	5	2	5	4	3	2	4
	Total	100	100	100	100	100	100	100	100	100
	Distribution	inequi	inequi	equi	equi	equi	equi	equi	equi	equi
	Size	fg	fg	fg	fg	vfg	vfg	vfg	fg	vfg
	Foliation	poor	poor	non	mod	int	int	int	poor	mod
Amygdules	*Amygdule %*	2	0	0	2	2	10	15	1	1
	Filling	q	0	0	q	qc	qcp	qcp	q	q
Alteration	*SER*	mod	int	weak	int	int	weak	int	mod	mod
	CHL	weak	weak	rare	none	weak	rare	rare	rare	weak
	CAR	rare	rare	int	none	none	none	mod	none	none
	BIO	none	none	none	none	none	none	none	none	none
	EPD	none	weak	rare	weak	none	rare	rare	rare	rare
	ACT	none	none	none	none	none	none	none	none	none
Additional Volcanic Textures		1, 2, 4	1, 2	1, 2	1, 2, 4	1, 2, 4	1, 2, 4	1, 2, 4	1, 2, 4	1, 2, 5

Appendix I: Table 5 cont.
Dacitic lava flows cont.

Sample		RR274-4*	RR274-7	RR274-8	RR274-13*	RR274-15	RR306-2*	RR306-8*	RR311-4	RR311-5
Drill hole depth (m)		150.7	200.4	210	692.3	931.2	34.4	309.4	176.3	263.4
Crystals	*QTZ*	20	2	5	2	3	3	7	4	3
	FSP	0	0	0	0	0	0	0	0	0
	Min. size	0.5	0.5	1	0.8	0.2	0.3	0.4	0.2	0.3
	Max. size	6	1.5	1.5	4.5	0.8	2	2.3	0.5	0.7
	Shape	sub	sub-eu	sub-frg	frg	frg	sub-emb	sub-eu	eu	sub-eu
Groundmass	*QFM*	25	35	62	61	69	51	55	32	45
	SM	40	35	22	19	20	20	13	43	34
	MC	1	0	5	8	0	5	18	0	0
	IC	0	0	0	0	0	0	0	0	0
	CB	10	18	2	5	3	10	0	15	12
	AC	0	0	0	0	0	0	0	0	0
	EP	1	0	0	0	0	1	3	1	0
	CL	0	0	1	0	0	0	0	0	0
	BI	0	5	0	0	0	6	0	0	0
	SF	3	5	3	5	5	4	4	5	6
	Total	100	100	100	100	100	100	100	100	100
	Distribution	equi	equi	equi	equi	equi	equi	equi	inequi	equi
	Size	vfg	vfg	vfg	fg	vfg	vfg	fg	vfg	fg
	Foliation	poor	int	int	non	mod	poor	poor	int	poor
Amygdules	*Amygdule %*	0	1	0	4	3	<1	2?	0	0
	Filling	0	q	0	q	q	q	q	0	0
Alteration	*SER*	int	int	mod	weak	mod	mod	weak	int	mod
	CHL	rare	none	weak	weak	none	weak	Problemo!	none	none
	CAR	mod	mod	rare	weak	rare	mod	none	mod	mod
	BIO	none	weak	none	none	none	weak	none	none	none
	EPD	none	none	rare	none	none	rare	rare	rare	none
	ACT	none	none	none	none	none	none	none	none	none
Additional Volcanic Textures		1, 2	1, 2, 4	1, 2	1, 2, 4	1, 2, 4	1, 2	1, 2, 4	1, 2	1, 2

Appendix I: Table 5 cont.
Dacitic lava flows cont.

Sample		RR311-7	RR322-1	RR322-2	RR322-5	RR322-7	RR322-8	RR322-9	RR325-1	RR325-2
Drill hole depth (m)		385.3	63.4	103.4	240.6	273.2	279.6	292.3	55.3	83.1
Crystals	*QTZ*	10	5	1	3	1	0	0	1	2
	FSP	6	7	0	5	0	7	0	0	0
	Min. size	0.3	0.2	0.5	0.8	0.5	0.8	0	0.2	0.3
	Max. size	1.5	2	0.8	1.2	0.8	1.3	0	0.5	0.6
	Shape	sub-frg	sub	frg-sub	sub-frg	frg-sub	sub-frg	0	sub	sub-eu
Groundmass	*QFM*	39	57	39	44	24	63	47	40	37
	SM	33	18	45	14	0	24	37	35	43
	MC	9	5	8	11	30	4	5	14	12
	IC	0	0	0	0	2	0	0	0	0
	CB	0	4	4	16	15	0	5	5	2
	AC	0	0	0	0	20	0	0	0	0
	EP	0	0	0	0	0	0	0	2	0
	CL	0	0	0	0	5	0	2	0	0
	BI	0	0	0	3	3	0	0	0	0
	SF	3	4	3	4	0	2	4	3	4
	Total	100	100	100	100	100	100	100	100	100
	Distribution	inequi	inequi	inequi	equi	inequi	equi	equi	equi	equi
	Size	fg	vfg	vfg	vfg	fg	fg	vfg	vfg	vfg
	Foliation	poor	poor	mod	poor	non	non	poor	poor	mod
Amygdules	*Amygdule %*	0	0	4	20	7	0	4	0	0
	Filling	0	0	qccp	qc	qccp	0	qccp	0	0
Alteration	*SER*	int	weak	int	weak	none	mod	int	int	int
	CHL	weak	rare	weak	mod	int	rare	rare	mod	mod
	CAR	none	rare	rare	mod	mod	none	weak	weak	rare
	BIO	none	none	none	rare	rare	none	none	none	none
	EPD	none	none	none	none	weak	none	rare	rare	none
	ACT	none	none	none	none	none	none	none	none	none
Additional Volcanic Textures		1, 2, 5	1, 2	1, 2, 4	1, 2, 4	1, 2, 4	1, 2	1, 3, 5	1, 2	1, 2, 5

Appendix I: Table 5 cont.
Dacitic lava flows cont.

Sample		RR325-3	RR325-4	RR325-5	RR325-7*	RR325-9	RR358-6	RR358-7*	RR358-8	RR393-2*
Drill hole depth (m)		112.4	146.3	147	162.3	230.1	493	608.4	656.6	161.3
Crystals	*QTZ*	0	2	5	0	0	6	1	6	8
	FSP	0	0	0	0	0	0	0	0	0
	Min. size	0	0.5	0.4	0	0	1.5	0.8	0.4	0.4
	Max. size	0	0.7	2	0	0	2.5	1.3	0.8	2
	Shape	0	sub	sub	0	0	sub	sub-eu	sub-frg	sub-frg
Groundmass	*QFM*	45	29	38	10	46	48	41	36	35
	SM	39	43	39	65	27	35	42	42	40
	MC	10	10	0	10	0	0	7	3	5
	IC	0	0	0	0	0	0	0	0	0
	CB	3	15	16	10	26	7	4	6	10
	AC	0	0	0	0	0	0	0	0	0
	EP	0	0	0	0	0	0	0	0	0
	CL	0	0	0	0	1	0	0	1	0
	BI	0	0	0	0	0	0	0	1	0
	SF	3	1	2	5	0	4	5	5	2
	Total	100	100	100	100	100	100	100	100	100
	Distribution	inequi	equi	equi	inequi	equi	inequi	inequi	inequi	equi
	Size	vfg	vfg	vfg	vfg	vfg	vfg	vfg	fg	fg
	Foliation	mod	mod	poor	int	poor	poor	poor	poor	poor
Amygdules	*Amygdule %*	0	0	0	10?	0	5	1	0	0
	Filling	0	0	0	qccp	0	q	q	0	0
Alteration	*SER*	int	int	int	int	mod	int	int	int	int
	CHL	mod	mod	none	mod	none	none	weak	rare	weak
	CAR	rare	mod	mod	mod	int	weak	rare	weak	mod
	BIO	none	none	none	none	none	none	none	rare	none
	EPD	none	none	none	none	rare	none	none	rare	none
	ACT	none	none	none	none	none	none	none	none	none
Additional Volcanic Textures		1, 3	1, 2	1, 2	1, 3, 5	1, 3	1, 2, 4	1, 2, 4	1, 2	1, 2

Appendix I: Table 5 cont.
Dacitic lava flows cont.

Sample		RR421-2*	RR421-5*	RR421-6*	RR421-7*	RR456-3*	RR458-1	RR458-2	RR458-3	RR458-5
Drill hole depth (m)		112.5	252.8	261.4	295.4	176	62.3	158.3	258.3	312.7
Crystals	*QTZ*	2	4	10	1	3	12	3	1	8
	FSP	9	8	2	0	0	0	0	0	6
	Min. size	0.6	0.6	0.6	1	0.6	0.8	0.2	0.5	0.3
	Max. size	1.8	2.5	1.8	1.5	1.8	4.5	0.5	0.8	0.5
	Shape	frg	sub	sub	sub-frg	sub	sub	eu-frg	sub	sub-frg
Groundmass	*QFM*	39	49	53	39	40	41	45	51	51
	SM	45	18	18	40	30	33	26	20	9
	MC	2	8	5	17	7	10	0	0	0
	IC	0	0	0	0	13	0	0	10	6
	CB	0	5	5	0	0	2	26	15	13
	AC	0	0	0	0	0	0	0	0	0
	EP	0	0	0	0	0	0	0	0	0
	CL	0	1	4	1	0	0	0	1	0
	BI	0	2	0	0	0	2	0	0	4
	SF	3	5	3	2	7	0	0	2	3
	Total	100	100	100	100	100	100	100	100	100
	Distribution	inequi	equi	inequi	equi	equi	equi	inequi	equi	equi
	Size	fg	vfg	fg	fg	fg	vfg	fg	vfg	vfg
	Foliation	poor	poor	poor	non	non	non	mod	poor	poor
Amygdules	*Amygdule %*	0	0	5	0	5	0	4	0	0
	Filling	0	0	qc	0	qccp	0	qcb	0	0
Alteration	*SER*	int	weak	weak	int	mod	mod	mod	mod	weak
	CHL	rare	weak	weak	mod	Problemo!	mod	none	mod	weak
	CAR	none	weak	weak	none	none	rare	int	mod	mod
	BIO	none	rare	none	none	none	rare	none	none	rare
	EPD	none	rare	rare	rare	none	none	none	rare	none
	ACT	none	none	none	none	none	none	none	none	none
Additional Volcanic Textures		1, 2	1, 2	1, 2, 4	1, 2, 5	1, 2, 4	1, 2	1, 2, 4	1, 2	1, 2

Appendix I: Table 5 cont.
Dacitic lava flows cont.

Sample		RR458-6*	RR458-7*
Drill hole depth (m)		352.3	403.3
Crystals	*QTZ*	2	6
	FSP	0	0
	Min. size	0.4	0.5
	Max. size	0.8	1.5
	Shape	sub	sub
Groundmass	*QFM*	61	39
	SM	17	24
	MC	0	10
	IC	11	0
	CB	6	19
	AC	0	0
	EP	0	0
	CL	0	0
	BI	0	0
	SF	3	2
	Total	100	100
	Distribution	equi	equi
	Size	vfg	fg
	Foliation	mod	poor
Amygdules	*Amygdule %*	0	0
	Fililng	0	0
Alteration	*SER*	weak	mod
	CHL	mod	mod
	CAR	weak	mod
	BIO	none	none
	EPD	none	none
	ACT	none	none
Additional Volcanic Textures		1, 2	1, 2, 4

Appendix I: Table 6
Monomict lapilli tuffs

Sample		RR70-15	RR198-17	RR227-3*	RR249-11	RR458-4	RR421-4*
Drill hole depth (m)		473.2	1177.4	226.3	430.2	280.3	155.3
Crystals	*QTZ*	3	6	0	2	2	5
	FSP	0	0	0	0	0	0
	Min. size	0.4	0.5	0	0.4	0.4	0.6
	Max. size	0.7	1	0	0.8	0.8	1.8
	Shape	sub-frg	sub-frg	0	sub-frg	sub	sub
Groundmass	*QFM*	33	44	65	51	42	48
	SM	42	33	27	34	28	30
	MC	14	11	3	6	9	12
	IC	0	0	0	0	0	0
	CB	2	0	0	4	14	5
	AC	0	0	0	0	0	0
	EP	0	0	0	0	0	0
	CL	0	6	2	0	0	0
	BI	0	0	0	0	0	0
	SF	6	0	3	3	5	0
	Total	100	100	100	100	100	100
	Distribution	inequi	inequi	equi	inequi	inequi	inequi
	Size	fg	fg	vfg	fg	vfg	fg
	Foliation	poor	mod	poor	mod	non	poor
Fragments	*FL*	50	50	2	25	55	25
	CL	fl	fl	fl	fl	fl	fl, cl
	Size	lapi	lapi	lapi	lapi	lapi	lapi
Alteration	*SER*	int	mod	mod	mod	mod	mod
	CHL	mod	mod	rare	weak	weak	mod
	CAR	rare	none	none	rare	mod	weak
	BIO	none	none	none	none	none	none
	EPD	none	weak	rare	none	none	none
	ACT	none	weak	rare	none	none	none
Additional Volcanic Textures		2, 3, 5	2, 3	2, 3	2, 3	2, 3	2, 3, 5

Appendix I: Table 7
Polymict lapilli tuffs

Sample		RR49-29	RR49-31	RR157-4*	RR227-5*	RR227-6*
Drill hole depth (m)		586.5	603.8	147.2	250.4	305.7
Crystals	*QTZ*	<1	2	3	2	1
	FSP	0	0	0	0	0
	Min. size	0.5	0.2	0.2	0.2	0.5
	Max. size	0.5	0.6	0.4	0.6	1
	Shape	eu-frg	sub-frg	sub-frg	eu-frg	eu-frg
Groundmass	*QFM*	38	38	44	45	26
	SM	33	34	38	20	39
	MC	19	19	5	15	5
	IC	0	0	0	0	0
	CB	5	0	0	10	13
	AC	0	0	0	0	0
	EP	0	0	3	2	4
	CL	1	3	1	0	2
	BI	0	0	1	1	0
	SF	4	4	5	5	9
	Total	100	100	100	100	99
	Distribution	equi	inequi	inequi	inequi	inequi
	Size	vfg	vfg	fg	fg	fg
	Foliation	int	mod	mod	mod	mod
Fragments	*FC*	5	2?	70	55	10
	MC	0	0	0	0	0
	Size	lp	lp	lp	lp	lp
Alteration	*SER*	mod	mod	int	mod	int
	CHL	mod	mod	weak	mod	weak
	CAR	weak	none	none	mod	mod
	BIO	none	none	rare	rare	none
	EPD	rare	rare	rare	rare	weak
	ACT	none	none	none	none	none
Additional Volcanic Textures		2, 3	2, 3	2, 3	2, 3	2, 3

Appendix I: Table 8
Felsic sedimentary rocks

Sample		RR198-7*	RR274-6*
Drill hole depth (m)		428	163.2
Groundmass	*QFM*	45	20
	SM	35	15
	MC	7	0
	IC	0	0
	CB	7	0
	AC	0	0
	EP	0	0
	CL	0	0
	BI	0	0
	SF	6	5
	Total	0	60
	Distribution	100	100
	Size	equi	inequi
	Foliation	fg	vfg
Alteration	*SER*	int	int
	CHL	int	mod
	CAR	weak	none
	BIO	none	none
	EPD	none	none
	ACT	none	none
Additional Volcanic Textures		1	1

Appendix II: Geochemical analysis

Sixty-nine samples collected from RRGP were selected for lithogeochemical analysis by ALS Chemex in Thunder Bay, Ontario. 25-60 g samples were cut and cleaned at UMD and selected based on both volcanic facies and alteration assemblages. 67 different properties including major oxide and trace elements were analyzed at ALS Chemex and are outlined below. Au values were taken from assay data compiled by RRRL to avoid redundancies. Samples not assayed by RRRL are marked N/A and were not assayed because of their low potential to host Au.

Volatiles were run using aqua regia digestion method and analyzed using ICP-MS:

Analytes	As	Bi	Hg	Sb	Se	Te
Range (ppm)	0.1-250	0.01-250	0.005-25	0.05-250	0.2-250	0.01-250

Trace elements were run using a lithium borate fusion method and analyzed using ICP-MS:

Analytes	Ba	Ce	Cr	Cs	Dy
Range (ppm)	0.5-10,000	0.5-10,000	10-10,000	0.01-10,000	0.05-1,000
Analytes	Er	Eu	Ga	Gd	Hf
Range (ppm)	0.03-1,000	0.03-1,000	0.1-1,000	0.05-1,000	0.2-10,000
Analytes	Ho	La	Lu	Nb	Nd
Range (ppm)	0.01-1,000	0.5-10,000	0.01-1,000	0.2-2,500	0.1-10,000
Analytes	Pr	Rb	Sm	Sn	Sr
Range (ppm)	0.03-1,000	0.2-10,000	0.03-1,000	1-10,000	0.1-10,000
Analytes	Ta	Tb	Tl	Tm	U
Range (ppm)	0.1-2,500	0.01-1,000	0.5-1,000	0.01-1,000	0.05-1,000
Analytes	V	W	Y	Yb	Zr
Range (ppm)	5-10,000	1-10,000	0.5-10,000	0.03-1,000	2-10,000

Base metals were run using a four acid "near-total" digestion and analyzed using ICP-AES:

Analytes	Ag	Co	Cu	Mo	Ni
Range (ppm)	0.2-100	1-10,000	1-10,000	1-10,000	1-10,000
Analytes	Pb	Zn	Cd		
Range (ppm)	1-10,000	1-10,000	0.5-1,000		

Total C and total S were calculated using a Leco furnace:

Analytes	C (total)	S (total)
Range (%)	0.01-50	0.01-50

Major Elements: Si, Al, Fe, Ca, Mg, Na, K, Ti, Mn, P, LOI were processed using a lithium metaborate fusion and analyzed by ICP-AES:

Analytes	SiO2	MgO	TiO2	BaO	Al2O3
Range (%)	0.01-100	0.01-100	0.01-100	0.01-100	0.01-100
Analytes	Na2O	MnO	LOI	Fe2O3	K2O
Range (%)	0.01-100	0.01-100	0.01-100	0.01-100	0.01-100
Analytes	P2O5	CaO	Cr2O3	SrO	
Range (%)	0.01-100	0.01-100	0.01-100	0.01-100	

Inorganic carbon (carbonate) was measured using a coulometer yielding a range of 0.2-15%.

H2O- (moisture) was run using a gravimetric procedure after drying at 105°C yielding a range of 0.01-100%. H2O+ (water of crystallization) was analyzed by Leco yielding a range of 0.01-100%.

Units: dlf-dacitic lava flow, dsd-dacitic dikes and sills, ppr-peperite, ms-mafic sedimentary rock, fs-felsic sedimentary rock pbx-polymict breccia, mbx-monomict breccia, bhs-Black Hawk Stock, blt-basalt, gbr-gabbro, db-diabase dike.

Appendix II: Table 1
Major oxide and trace element geochemistry

Sample	Unit	SiO2 (%)	Al2O3 (%)	Fe2O3 (%)	CaO (%)	MgO (%)	Na2O (%)	K2O (%)	Cr2O3 (%)	TiO2 (%)	MnO (%)	P2O5 (%)	SrO (%)	BaO (%)	C (%)	S (%)
RR-17	ms	58.2	14.1	12.2	4.42	2.65	1.62	1.21	0.02	1.94	0.15	0.21	0.03	0.03	0.05	3.35
RR-46	dlf	64.6	15.4	3.6	3.25	2.28	1.88	1.69	<0.01	0.37	0.08	0.09	0.03	0.04	0.08	0.54
RR-47	dlf	68.4	15.7	3.1	3.43	1.26	2.61	2.00	<0.01	0.37	0.06	0.10	0.03	0.06	0.18	0.20
RR-49	dlf	67.3	15.1	3.2	3.98	1.20	2.86	1.40	<0.01	0.37	0.05	0.13	0.04	0.05	0.08	0.12
RR-50	dlf	64.3	17.9	3.9	3.20	2.04	1.68	2.40	<0.01	0.51	0.06	0.17	0.06	0.10	0.02	0.04
RR-51	dlf	67.3	15.2	2.6	3.14	1.43	3.56	1.71	<0.01	0.33	0.05	0.12	0.05	0.05	0.21	0.44
RR-52	gbr	45.9	15.6	16.4	6.61	6.66	3.33	0.24	0.02	1.66	0.24	0.16	0.01	0.01	0.04	0.07
RR-53	blt	47.8	14.0	16.5	7.87	4.00	2.47	0.06	0.01	1.96	0.18	0.17	0.02	0.01	0.28	0.08
RR-54	dlf	67.5	15.4	4.6	4.08	2.01	1.55	2.09	<0.01	0.46	0.08	0.13	0.05	0.08	0.04	0.03
RR-56	dlf	67.5	17.0	3.0	2.65	0.98	2.13	1.75	<0.01	0.44	0.05	0.13	0.09	0.05	0.02	0.01
RR-57	dlf	72.4	16.4	1.4	1.78	0.70	1.64	2.07	<0.01	0.40	0.04	0.15	0.04	0.06	0.02	0.01
RR-58	bhs	61.7	14.2	5.1	4.28	2.79	4.41	4.47	0.02	0.54	0.10	0.48	0.17	0.18	0.02	<0.01
RR-59	dlf	64.1	15.6	3.1	5.55	1.14	1.85	1.38	<0.01	0.38	0.05	0.12	0.06	0.04	0.37	0.05
RR-60	dlf	57.9	22.3	3.7	5.00	1.30	2.79	2.09	0.01	0.60	0.04	0.19	0.08	0.05	0.03	0.16
RR49-3	dlf	68.0	15.3	2.3	3.12	0.90	3.56	1.88	<0.01	0.34	0.06	0.09	0.03	0.05	0.55	0.15
RR49-38	dsd	63.1	18.1	2.8	2.76	1.92	1.70	2.66	0.01	2.58	0.04	0.26	0.04	0.07	0.07	0.62
RR49-41	ppr	23.6	15.7	32.4	1.09	6.21	0.37	1.44	0.01	2.23	0.30	0.22	0.01	0.03	0.07	14.30
RR70-5	ppr	27.7	12.8	19.0	13.50	5.18	0.40	2.29	0.01	1.51	0.52	0.17	0.03	0.03	3.61	1.40
RR70-8	dlf	62.6	14.6	5.3	5.44	2.54	3.62	1.48	<0.01	0.46	0.11	0.15	0.07	0.06	0.85	0.30
RR70-9	ppr	49.5	13.3	19.7	7.75	3.10	1.05	0.42	0.01	1.93	0.51	0.20	0.02	0.01	0.24	1.79
RR157-2	dlf	67.8	13.8	4.4	1.77	1.45	0.67	2.90	<0.01	0.33	0.08	0.09	0.02	0.07	0.15	2.11
RR157-4	pbx	66.4	15.4	4.5	1.66	2.26	0.66	3.01	<0.01	0.44	0.11	0.11	0.02	0.07	0.07	1.37
RR157-6	dlf	69.3	14.8	4.5	2.75	1.43	0.96	1.52	<0.01	0.32	0.03	0.03	0.05	0.04	0.10	1.67
RR173-1	dsd	38.3	20.8	12.5	5.55	4.68	0.68	3.06	0.01	0.68	0.38	0.46	0.02	0.08	2.00	2.71
RR173-8	dlf	60.7	13.7	3.1	2.64	1.08	2.47	1.97	<0.01	0.30	0.05	0.08	0.02	0.05	0.54	0.41
RR173-10	dlf	64.7	14.0	3.6	4.34	2.26	0.26	2.93	<0.01	0.35	0.27	0.11	0.01	0.05	1.20	1.62
RR198-5	dlf	64.5	14.7	3.6	3.56	1.92	1.28	1.55	<0.01	0.36	0.06	0.11	0.03	0.04	1.26	0.26

Appendix II: Table 1 cont.
Major oxide and trace element geochemistry

Sample	Unit	Ba (ppm)	Ce (ppm)	Cr (ppm)	Cs (ppm)	Dy (ppm)	Er (ppm)	Eu (ppm)	Ga (ppm)	Gd (ppm)	Hf (ppm)	Ho (ppm)	La (ppm)	Lu (ppm)	Nb (ppm)	Nd (ppm)
RR-17	ms	216	24.5	120	10.50	5.72	3.37	1.77	24.2	5.62	3.6	1.19	10.4	0.54	6.3	16.4
RR-46	dlf	401	40.0	20	9.95	1.03	0.56	0.68	21.8	1.92	3.0	0.19	21.3	0.07	2.7	15.4
RR-47	dlf	502	34.1	30	7.67	0.95	0.50	0.61	20.7	1.90	2.7	0.17	17.9	0.07	2.4	14.1
RR-49	dlf	406	40.3	30	6.44	0.86	0.45	0.65	21.0	2.00	3.0	0.16	22.3	0.06	2.5	15.4
RR-50	dlf	874	56.0	30	10.70	1.23	0.64	0.91	25.0	2.84	3.2	0.22	27.6	0.09	3.0	23.8
RR-51	dlf	410	39.2	40	6.95	0.90	0.47	0.78	19.8	2.16	2.6	0.15	18.7	0.07	2.1	17.6
RR-52	gbr	75	18.3	150	0.71	4.85	2.94	1.33	20.4	4.53	2.6	1.02	7.7	0.47	4.4	12.5
RR-53	blt	44	18.1	80	0.18	5.22	3.18	1.47	21.1	4.88	2.8	1.13	7.9	0.51	4.9	12.7
RR-54	dlf	626	48.0	30	7.72	1.29	0.71	0.81	21.0	2.65	2.8	0.24	24.5	0.10	2.5	21.0
RR-56	dlf	390	37.5	40	4.91	0.87	0.42	0.71	24.9	2.02	3.2	0.15	19.9	0.06	2.8	14.5
RR-57	dlf	516	52.0	30	3.22	0.94	0.44	1.00	22.3	3.02	3.2	0.16	28.7	0.06	2.3	25.4
RR-58	bhs	1490	183.0	120	8.87	4.07	1.70	2.72	20.0	10.20	7.1	0.63	81.1	0.18	19.8	74.1
RR-59	dlf	369	47.2	30	10.50	1.16	0.57	0.66	20.7	2.36	3.0	0.21	24.3	0.09	2.5	18.0
RR-60	dlf	384	78.0	40	9.58	1.29	0.73	0.84	28.1	2.96	4.0	0.23	43.7	0.11	3.7	28.3
RR49-3	dlf	436	36.4	30	5.65	1.06	0.54	0.70	19.9	2.09	2.9	0.19	14.2	0.08	24.5	15.1
RR49-38	dsd	633	16.1	100	7.66	5.44	3.09	1.19	25.9	4.11	4.1	1.04	7.1	0.42	7.5	8.5
RR49-41	ppr	236	30.8	80	12.20	8.10	5.00	1.92	28.7	6.68	3.1	1.75	13.7	0.71	5.1	20.0
RR70-5	ppr	299	29.2	100	17.30	15.35	9.96	2.79	22.6	11.20	2.8	3.46	13.2	1.44	4.5	19.9
RR70-8	dlf	537	48.0	30	17.80	1.69	1.00	1.00	19.4	3.24	2.5	0.33	23.3	0.14	2.4	22.7
RR70-9	ppr	82	17.4	90	3.72	5.87	3.89	1.32	20.9	5.10	2.7	1.27	7.8	0.59	5.5	12.1
RR157-2	dlf	561	32.4	20	15.30	0.94	0.54	0.71	19.0	2.10	2.5	0.18	17.1	0.06	2.5	12.9
RR157-4	pbx	582	57.4	30	11.35	1.42	0.75	1.16	21.0	3.34	2.8	0.27	30.2	0.10	2.8	23.2
RR157-6	dlf	302	21.2	20	5.97	0.87	0.45	0.54	21.1	1.52	2.6	0.15	11.9	0.06	2.5	9.0
RR173-1	dsd	680	191.0	50	11.05	4.27	2.77	2.95	29.1	9.92	3.1	0.86	90.2	0.41	3.1	86.7
RR173-8	dlf	357	28.6	20	6.84	0.74	0.45	0.51	16.1	1.69	2.3	0.15	15.8	0.07	2.5	10.9
RR173-10	dlf	441	33.2	20	7.11	0.94	0.53	0.67	18.9	2.13	2.6	0.17	17.6	0.08	2.3	13.8
RR198-5	dlf	308	34.8	30	7.80	0.92	0.56	0.61	19.5	2.10	2.7	0.19	18.4	0.08	2.4	14.7

Appendix II: Table 1 cont.
Major oxide and trace element geochemistry

Sample	Unit	Pr (ppm)	Rb (ppm)	Sm (ppm)	Sn (ppm)	Sr (ppm)	Ta (ppm)	Tb (ppm)	Th (ppm)	Tl (ppm)	Tm (ppm)	U (ppm)	V (ppm)	W (ppm)	Y (ppm)	Yb (ppm)
RR-17	ms	3.67	39.7	4.99	1	282	0.50	0.94	0.91	<0.5	0.56	0.22	342	<1	32.6	3.44
RR-46	dlf	4.48	44.3	2.45	1	255	0.20	0.22	2.51	<0.5	0.07	0.55	32	4	5.2	0.49
RR-47	dlf	4.10	53.2	2.26	1	284	0.20	0.21	2.38	<0.5	0.09	0.55	47	1	5.1	0.48
RR-49	dlf	4.59	37.5	2.38	1	354	0.20	0.21	3.05	<0.5	0.08	0.65	40	<1	4.7	0.38
RR-50	dlf	6.91	50.2	3.62	1	464	0.20	0.30	4.35	<0.5	0.11	0.87	76	5	6.7	0.58
RR-51	dlf	4.93	44.1	2.80	1	398	0.10	0.22	2.78	<0.5	0.08	0.64	46	1	4.8	0.46
RR-52	gbr	2.78	4.2	3.69	1	115	0.30	0.77	0.77	<0.5	0.48	0.17	291	<1	29.6	3.02
RR-53	blt	2.76	1.5	3.95	1	160	0.30	0.83	0.69	<0.5	0.53	0.16	377	<1	31.8	3.20
RR-54	dlf	5.93	48.1	3.32	1	409	0.20	0.29	3.55	<0.5	0.12	0.71	71	1	7.1	0.64
RR-56	dlf	4.32	44.6	2.35	1	717	0.20	0.21	2.24	<0.5	0.08	0.41	47	1	4.3	0.38
RR-57	dlf	7.05	45.0	3.95	1	302	0.20	0.28	2.94	<0.5	0.08	0.59	70	1	4.3	0.37
RR-58	bhs	21.40	149.5	12.65	1	1470	0.80	1.04	29.40	0.8	0.20	6.47	84	1	18.1	1.29
RR-59	dlf	5.32	42.5	2.77	1	526	0.20	0.26	3.26	<0.5	0.08	0.72	69	1	5.5	0.52
RR-60	dlf	9.04	57.1	3.35	1	697	0.20	0.29	5.28	<0.5	0.11	1.02	93	1	6.0	0.73
RR49-3	dlf	4.08	41.4	2.39	3	255	1.70	0.23	4.17	<0.5	0.07	1.33	47	2	4.8	0.49
RR49-38	dsd	2.09	72.6	2.50	4	323	0.40	0.79	0.98	0.5	0.41	0.67	401	10	24.2	2.97
RR49-41	ppr	4.33	46.1	5.80	1	82	0.30	1.20	0.97	<0.5	0.69	0.19	314	1	45.0	4.67
RR70-5	ppr	4.20	61.0	6.82	1	239	0.20	2.25	0.66	<0.5	1.33	0.21	392	16	95.2	9.03
RR70-8	dlf	6.04	41.0	3.63	1	597	0.10	0.37	2.82	<0.5	0.14	0.59	88	1	9.1	0.89
RR70-9	ppr	2.53	8.5	3.87	1	219	0.30	0.92	0.66	<0.5	0.53	0.15	354	2	35.7	3.70
RR157-2	dlf	3.66	84.7	2.18	1	167	0.10	0.24	2.12	0.5	0.08	0.41	35	2	4.9	0.44
RR157-4	pbx	6.60	89.9	3.46	1	210	0.10	0.35	2.17	<0.5	0.11	0.57	63	3	6.8	0.70
RR157-6	dlf	2.50	53.7	1.59	1	393	0.10	0.18	1.91	<0.5	0.07	0.59	38	2	3.9	0.36
RR173-1	dsd	23.20	66.3	12.25	1	176	0.10	1.01	11.75	0.5	0.36	1.21	256	1	19.9	2.56
RR173-8	dlf	3.13	40.3	1.70	1	205	0.10	0.18	1.72	<0.5	0.07	0.61	34	1	3.8	0.42
RR173-10	dlf	3.89	96.0	2.24	1	92	0.10	0.24	2.11	0.8	0.07	0.46	43	3	4.6	0.46
RR198-5	dlf	4.10	38.2	2.34	1	286	0.10	0.23	2.29	<0.5	0.08	0.52	50	3	4.8	0.49

Appendix II: Table 1 cont.
Major oxide and trace element geochemistry

Sample	Unit	Zr (ppm)	As (ppm)	Bi (ppm)	Hg (ppm)	Sb (ppm)	Se (ppm)	Te (ppm)	LOI (%)	Total (%)	Au (ppb)	Ag (ppm)	Cd (ppm)	Co (ppm)	Cu (ppm)	Mo (ppm)
RR-17	ms	127	5.7	0.68	0.01	0.12	0.90	0.15	2.99	99.8	N/A	<0.5	<0.5	45	19	<1
RR-46	dlf	108	10.5	0.27	0.02	0.17	0.20	0.01	2.39	95.7	N/A	<0.5	<0.5	7	2	<1
RR-47	dlf	94	3.3	0.02	0.02	0.18	<0.2	<0.01	1.50	98.6	N/A	<0.5	<0.5	7	4	<1
RR-49	dlf	104	3.2	0.08	0.01	0.23	<0.2	0.03	1.09	96.7	N/A	<0.5	<0.5	7	31	<1
RR-50	dlf	108	1.5	0.02	0.02	0.14	0.20	0.06	1.70	98.0	N/A	<0.5	<0.5	7	28	<1
RR-51	dlf	90	2.9	0.15	0.02	0.17	<0.2	0.01	1.99	97.5	N/A	<0.5	<0.5	4	1	<1
RR-52	gbr	89	1.6	0.01	0.02	0.08	0.60	0.01	3.58	100.5	N/A	<0.5	<0.5	52	88	<1
RR-53	blt	94	0.9	0.01	0.02	0.05	0.50	0.01	4.30	99.3	N/A	<0.5	<0.5	41	47	<1
RR-54	dlf	97	1.1	0.01	0.01	0.16	0.20	<0.01	2.30	100.5	N/A	<0.5	<0.5	10	15	<1
RR-56	dlf	110	3.1	0.01	0.02	0.52	<0.2	<0.01	1.80	97.6	N/A	<0.5	<0.5	6	<1	<1
RR-57	dlf	112	0.8	0.03	0.02	0.13	<0.2	<0.01	2.80	99.9	N/A	<0.5	<0.5	2	7	<1
RR-58	bhs	306	5.1	0.32	0.01	0.19	0.30	<0.01	0.30	98.7	N/A	<0.5	<0.5	15	3	<1
RR-59	dlf	110	3.8	0.02	0.02	0.46	<0.2	<0.01	2.30	95.6	N/A	<0.5	<0.5	7	20	<1
RR-60	dlf	158	4.9	0.04	<0.005	0.73	<0.2	0.01	2.00	98.1	N/A	0.5	<0.5	8	48	<1
RR49-3	dlf	114	10.4	0.18	0.02	0.17	<0.2	0.09	3.10	98.7	N/A	<0.5	<0.5	5	19	1
RR49-38	dsd	132	9.3	0.48	0.02	0.69	0.60	0.13	3.49	99.6	N/A	<0.5	<0.5	11	15	<1
RR49-41	ppr	126	27.6	3.88	0.03	0.45	4.10	1.00	13.50	97.1	N/A	2.1	0.5	74	718	<1
RR70-5	ppr	121	7.3	0.31	0.08	0.56	0.70	0.41	12.40	95.5	54	2.2	0.5	47	423	1
RR70-8	dlf	95	2.4	0.15	0.02	0.09	0.20	0.03	4.19	100.5	N/A	<0.5	<0.5	12	31	1
RR70-9	ppr	110	5.6	0.17	0.04	0.41	0.80	0.46	2.10	99.5	38	0.7	<0.5	51	148	<1
RR157-2	dlf	99	13.1	1.88	0.28	0.19	1.10	3.00	4.10	97.4	643	3.5	14.7	9	150	<1
RR157-4	pbx	107	17.0	1.77	0.05	1.35	0.80	0.78	3.70	98.4	220	0.6	1.7	13	44	1
RR157-6	dlf	103	9.3	2.44	0.03	0.31	1.00	0.25	3.30	99.0	518	<0.5	1.0	11	126	2
RR173-1	dsd	126	8.8	0.50	0.06	0.18	1.10	0.79	8.64	95.8	270	<0.5	0.7	6	34	2
RR173-8	dlf	89	11.5	0.36	0.02	0.21	0.20	0.22	3.80	90.0	41	<0.5	<0.5	6	30	1
RR173-10	dlf	104	20.9	0.28	0.08	0.24	0.30	0.14	6.26	98.3	261	1.1	0.8	9	92	2
RR198-5	dlf	104	13.4	0.04	0.04	3.00	<0.2	0.01	6.19	97.9	N/A	<0.5	<0.5	9	19	1

Appendix II: Table 1 cont.
Major oxide and trace element geochemistry

Sample	Unit	Ni (ppm)	Pb (ppm)	Zn (ppm)	C (%)	CO2 (%)	H2O (%)	H2O+ (%)	Recvd Wt. (kg)
RR-17	ms	44	3	99	<0.05	<0.2	0.11	2.15	0.12
RR-46	dlf	2	19	105	0.07	0.20	0.15	2.14	0.05
RR-47	dlf	8	11	68	0.14	0.50	0.11	1.31	0.12
RR-49	dlf	4	8	61	0.07	0.30	0.11	0.97	0.10
RR-50	dlf	13	9	142	<0.05	<0.2	0.15	1.92	0.07
RR-51	dlf	5	16	118	0.19	0.70	0.08	0.67	0.06
RR-52	gbr	115	<2	120	<0.05	<0.2	0.15	5.25	0.06
RR-53	blt	52	2	138	0.24	0.90	0.15	4.43	0.10
RR-54	dlf	12	5	58	<0.05	<0.2	0.17	2.31	0.03
RR-56	dlf	12	9	36	<0.05	<0.2	0.10	2.02	0.10
RR-57	dlf	1	8	8	<0.05	<0.2	0.10	1.80	0.15
RR-58	bhs	40	33	78	<0.05	<0.2	0.11	0.13	0.10
RR-59	dlf	6	12	59	0.35	1.30	0.09	1.55	0.13
RR-60	dlf	8	19	54	<0.05	<0.2	0.17	2.91	0.03
RR49-3	dlf	9	5	36	0.42	1.60	0.08	1.58	0.06
RR49-38	dsd	23	4	70	0.09	0.30	0.08	2.64	0.06
RR49-41	ppr	101	6	294	0.08	0.30	0.19	7.74	0.05
RR70-5	ppr	77	10	402	3.56	13.10	0.09	3.03	0.07
RR70-8	dlf	18	9	99	0.81	3.00	0.11	1.49	0.05
RR70-9	ppr	61	7	529	0.25	0.90	0.04	1.81	0.06
RR157-2	dlf	4	5	4490	0.16	0.60	0.12	2.97	0.04
RR157-4	pbx	8	5	562	0.07	0.30	0.12	1.67	0.04
RR157-6	dlf	6	3	326	0.11	0.40	0.11	2.30	0.03
RR173-1	dsd	33	6	418	1.90	7.00	0.12	5.84	0.04
RR173-8	dlf	10	<2	62	0.53	1.90	0.12	2.20	0.03
RR173-10	dlf	10	51	254	1.17	4.30	0.07	2.48	0.05
RR198-5	dlf	14	8	82	1.21	4.50	0.09	2.54	0.03

Appendix II: Table 1 cont.
Major oxide and trace element geochemistry

Sample	Unit	SiO2 (%)	Al2O3 (%)	Fe2O3 (%)	CaO (%)	MgO (%)	Na2O (%)	K2O (%)	Cr2O3 (%)	TiO2 (%)	MnO (%)	P2O5 (%)	SrO (%)	BaO (%)	C (%)	S (%)
RR198-7	fs	62.4	11.2	12.0	2.03	1.22	0.33	1.95	0.01	0.28	0.11	0.09	0.01	0.04	0.59	7.13
RR198-8	ms	44.8	10.5	10.3	9.33	9.11	1.02	0.15	0.13	0.81	0.20	0.49	0.04	0.01	2.20	1.81
RR198-10	ms	54.0	13.8	12.3	3.58	4.39	0.22	1.71	0.01	1.04	0.29	0.14	0.01	0.05	0.87	1.92
RR198-11	dlf	65.9	15.2	4.0	3.55	1.74	1.69	2.63	0.01	0.35	0.10	0.10	0.03	0.08	0.90	0.46
RR198-12	db	43.0	12.9	14.1	14.90	5.64	2.15	0.21	0.03	1.18	0.30	0.12	0.04	<0.01	1.72	0.30
RR198-13	dlf	68.3	15.7	3.9	3.47	1.26	3.80	1.00	0.01	0.37	0.05	0.11	0.06	0.04	0.26	0.33
RR227-3	mbx	70.0	13.0	5.3	1.42	2.39	0.47	2.38	<0.01	0.31	0.06	0.09	0.02	0.05	0.07	2.37
RR227-5	pbx	66.4	15.2	6.3	1.36	2.54	0.47	2.75	<0.01	0.39	0.06	0.13	0.02	0.06	0.06	3.55
RR227-6	dlf	68.3	14.7	3.6	2.75	2.39	1.07	2.77	<0.01	0.35	0.15	0.08	0.02	0.06	0.24	0.98
RR249-2	ppr	27.3	12.2	29.5	5.05	2.90	0.51	1.70	0.01	1.46	0.23	0.21	0.01	0.04	0.80	14.65
RR249-3	dsd	67.1	15.7	3.4	3.74	1.86	1.11	3.03	<0.01	0.36	0.07	0.13	0.04	0.07	0.75	0.26
RR249-9	dlf	73.1	13.3	1.9	1.85	1.42	0.20	2.93	<0.01	0.35	0.11	0.13	0.02	0.05	0.35	0.79
RR274-4	dlf	69.7	15.2	2.3	1.49	1.54	1.55	2.81	<0.01	0.32	0.02	0.09	0.02	0.08	0.32	0.11
RR274-6	fs	67.4	7.6	10.6	2.13	1.25	0.26	1.30	<0.01	0.18	0.06	0.06	0.01	0.03	2.18	7.35
RR274-12	gbr	48.9	16.5	19.5	4.13	2.50	1.97	0.86	0.01	2.36	0.57	0.21	0.05	0.03	0.07	0.74
RR274-13	dlf	72.6	12.3	5.0	1.48	1.38	0.19	2.61	<0.01	0.33	0.19	0.08	0.02	0.08	0.23	2.18
RR306-2	dlf	69.7	14.8	2.9	3.44	1.26	1.70	2.25	<0.01	0.37	0.03	0.12	0.03	0.06	0.41	0.02
RR306-8	dlf	71.9	14.9	1.5	2.29	0.91	1.64	2.75	<0.01	0.31	0.04	0.08	0.02	0.15	0.17	0.40
RR311-3	dsd	68.7	14.9	3.1	2.88	1.10	5.56	0.56	<0.01	0.32	0.03	0.09	0.04	0.02	0.53	0.37
RR311-11	pbx	49.1	13.1	12.5	11.30	10.25	1.33	0.09	0.10	0.65	0.22	0.07	0.02	<0.01	0.04	0.01
RR311-15	ms	71.8	10.7	4.5	3.99	1.17	1.41	1.67	0.01	1.16	0.05	0.12	0.03	0.04	0.35	1.35
RR322-10	dsd	66.2	14.5	3.6	3.01	1.28	1.72	3.08	<0.01	0.37	0.11	0.10	0.03	0.05	0.90	1.65
RR322-11	dsd	66.6	14.8	4.5	2.70	1.26	3.31	2.11	<0.01	0.34	0.04	0.11	0.02	0.03	0.31	2.18
RR325-7	dlf	66.4	14.7	3.6	4.11	1.53	1.96	1.49	<0.01	0.36	0.07	0.08	0.04	0.04	0.69	0.09
RR325-8	ms	43.6	12.6	15.9	7.44	4.90	0.67	0.69	0.01	1.66	0.45	0.15	0.03	0.02	1.97	2.00
RR325-16	blt	37.2	15.0	19.8	7.79	8.63	0.13	0.06	0.02	2.27	0.29	0.12	0.03	<0.01	0.58	0.73
RR358-1	ms	58.9	14.5	11.1	1.68	2.42	0.31	3.15	0.02	2.08	0.21	0.10	0.01	0.05	0.28	1.91

Appendix II: Table 1 cont.
Major oxide and trace element geochemistry

Sample	Unit	Ba (ppm)	Ce (ppm)	Cr (ppm)	Cs (ppm)	Dy (ppm)	Er (ppm)	Eu (ppm)	Ga (ppm)	Gd (ppm)	Hf (ppm)	Ho (ppm)	La (ppm)	Lu (ppm)	Nb (ppm)	Nd (ppm)
RR198-7	fs	337	24.0	50	7.70	1.04	0.62	0.58	14.0	1.87	2.3	0.20	12.3	0.09	2.7	10.6
RR198-8	ms	43	90.8	840	3.40	3.09	1.59	2.10	13.7	7.03	4.3	0.57	40.5	0.19	7.9	47.2
RR198-10	ms	373	21.6	100	6.75	3.14	2.14	0.92	18.0	3.36	2.4	0.70	10.2	0.32	3.7	12.2
RR198-11	dlf	688	32.7	40	8.01	1.07	0.58	0.61	20.2	2.11	2.8	0.18	16.6	0.08	2.6	13.5
RR198-12	db	44	19.9	220	0.76	5.24	3.46	1.12	18.9	4.42	2.7	1.17	9.2	0.57	5.0	12.9
RR198-13	dlf	329	36.2	40	7.43	1.05	0.58	0.64	21.9	2.23	2.5	0.19	19.1	0.08	2.6	15.4
RR227-3	mbx	445	25.6	20	9.00	0.79	0.41	0.55	20.4	1.71	2.4	0.15	13.6	0.07	2.1	10.9
RR227-5	pbx	475	42.5	40	6.15	1.24	0.64	1.02	20.7	2.72	2.7	0.22	22.9	0.09	2.6	17.9
RR227-6	dlf	498	35.4	20	5.53	1.13	0.61	0.68	20.1	2.19	2.6	0.19	19.1	0.08	2.4	14.2
RR249-2	ppr	345	20.6	50	17.40	5.38	3.26	1.42	19.0	5.14	2.4	1.14	9.4	0.50	4.0	13.9
RR249-3	dsd	553	45.7	30	12.10	1.32	0.72	0.87	20.1	2.92	2.8	0.23	22.2	0.08	2.5	20.7
RR249-9	dlf	380	25.1	30	7.92	0.96	0.49	0.52	18.2	1.83	2.4	0.17	13.2	0.06	2.4	10.3
RR274-4	dlf	683	30.2	30	14.50	0.74	0.41	0.56	20.9	1.63	2.8	0.13	16.0	0.07	2.7	12.1
RR274-6	fs	206	20.8	30	4.00	0.95	0.51	0.46	11.4	1.52	1.8	0.18	10.9	0.09	2.3	8.6
RR274-12	gbr	280	18.9	110	13.80	6.44	4.34	1.51	26.2	5.26	3.2	1.45	8.3	0.69	6.3	12.4
RR274-13	dlf	686	29.9	20	7.10	0.80	0.46	0.74	16.8	1.67	2.2	0.15	16.2	0.07	2.1	11.7
RR306-2	dlf	529	38.7	30	5.41	0.84	0.45	0.64	20.8	2.15	2.8	0.16	21.6	0.06	2.8	14.7
RR306-8	dlf	1255	15.5	20	7.35	0.64	0.31	0.39	19.3	1.22	2.6	0.11	8.8	0.05	2.3	6.8
RR311-3	dsd	140	35.1	40	2.87	0.88	0.48	0.74	19.2	2.11	2.6	0.16	18.5	0.07	2.4	15.0
RR311-11	pbx	25	9.1	730	0.29	2.56	1.68	0.61	13.6	2.18	1.2	0.57	4.3	0.26	2.1	6.1
RR311-15	ms	326	12.1	100	2.40	2.96	2.11	0.59	13.8	2.54	2.2	0.67	5.7	0.35	3.8	7.1
RR322-10	dsd	413	34.0	20	5.75	0.82	0.40	0.57	20.8	1.86	2.8	0.14	18.1	0.05	2.2	13.6
RR322-11	dsd	216	31.8	30	4.30	0.88	0.45	0.63	19.8	1.92	2.7	0.16	15.6	0.07	2.2	13.4
RR325-7	dlf	296	26.2	30	5.36	0.71	0.34	0.56	20.4	1.54	3.0	0.13	14.2	0.05	2.0	10.2
RR325-8	ms	138	15.8	80	2.90	5.20	3.23	1.37	20.2	4.48	2.7	1.11	6.6	0.56	4.5	11.2
RR325-16	blt	10	13.8	110	0.48	3.66	2.40	0.75	26.9	3.26	2.2	0.81	6.1	0.38	3.3	8.6
RR358-1	ms	408	11.7	120	8.83	2.15	1.42	0.65	22.1	2.18	2.8	0.46	5.1	0.27	5.6	7.4

Appendix II: Table 1 cont.
Major oxide and trace element geochemistry

Sample	Unit	Pr (ppm)	Rb (ppm)	Sm (ppm)	Sn (ppm)	Sr (ppm)	Ta (ppm)	Tb (ppm)	Th (ppm)	Tl (ppm)	Tm (ppm)	U (ppm)	V (ppm)	W (ppm)	Y (ppm)	Yb (ppm)
RR198-7	fs	2.90	52.8	1.97	2	86	0.20	0.21	1.89	0.5	0.09	0.50	32	1	5.4	0.58
RR198-8	ms	11.95	6.1	8.31	1	330	0.30	0.76	4.07	<0.5	0.19	0.75	136	1	14.8	1.26
RR198-10	ms	2.93	45.0	2.82	1	61	0.20	0.53	1.20	<0.5	0.29	0.27	194	2	17.4	2.01
RR198-11	dlf	3.73	66.8	2.24	1	242	0.10	0.24	2.41	<0.5	0.08	0.74	50	2	4.8	0.53
RR198-12	db	2.80	3.7	3.78	1	369	0.20	0.81	0.79	<0.5	0.49	0.18	298	1	30.7	3.56
RR198-13	dlf	4.21	30.6	2.40	1	483	0.10	0.26	2.33	<0.5	0.08	0.51	54	3	5.2	0.52
RR227-3	mbx	3.03	70.0	1.79	1	226	0.10	0.20	1.84	0.5	0.07	0.42	40	2	4.0	0.38
RR227-5	pbx	4.90	84.5	2.90	1	216	0.10	0.30	2.65	0.6	0.09	0.64	54	3	6.0	0.55
RR227-6	dlf	4.03	81.4	2.27	1	168	0.10	0.24	2.23	<0.5	0.07	0.47	44	2	5.2	0.50
RR249-2	ppr	2.96	55.7	3.97	1	137	0.20	0.91	0.67	<0.5	0.47	0.21	221	11	30.2	3.26
RR249-3	dsd	5.59	82.0	3.28	1	355	0.10	0.32	2.92	0.7	0.09	0.68	53	1	6.2	0.57
RR249-9	dlf	2.88	106.5	1.74	<1	184	0.10	0.21	2.11	1.1	0.07	0.49	42	2	4.8	0.40
RR274-4	dlf	3.45	97.1	1.84	1	210	0.20	0.18	2.52	0.5	0.07	0.67	43	<1	3.8	0.39
RR274-6	fs	2.44	33.8	1.64	2	100	0.10	0.20	1.80	<0.5	0.08	0.44	28	1	4.7	0.48
RR274-12	gbr	2.76	41.7	3.55	1	423	0.30	1.00	0.84	<0.5	0.61	0.19	423	2	36.7	4.24
RR274-13	dlf	3.42	87.8	1.91	1	165	0.10	0.20	2.25	0.6	0.07	0.53	41	3	4.1	0.41
RR306-2	dlf	4.25	60.5	2.34	1	287	0.20	0.22	2.92	<0.5	0.07	0.54	42	<1	4.1	0.40
RR306-8	dlf	1.78	75.2	1.26	1	224	0.10	0.15	1.91	<0.5	0.05	0.42	36	2	3.5	0.29
RR311-3	dsd	4.15	14.9	2.40	<1	378	0.10	0.23	2.35	<0.5	0.08	0.54	38	1	4.2	0.41
RR311-11	pbx	1.31	1.2	1.66	1	147	0.10	0.42	0.40	<0.5	0.23	0.08	194	1	14.4	1.65
RR311-15	ms	1.60	54.2	1.88	1	241	0.20	0.47	0.89	<0.5	0.30	0.20	182	6	16.0	2.15
RR322-10	dsd	4.03	103.0	2.19	1	224	0.10	0.20	2.79	0.7	0.07	0.64	43	2	4.1	0.33
RR322-11	dsd	3.85	68.9	2.25	1	196	0.20	0.20	2.43	0.5	0.09	0.55	48	1	4.6	0.42
RR325-7	dlf	3.02	42.5	1.76	1	300	0.10	0.16	1.76	<0.5	0.07	0.36	44	2	3.6	0.31
RR325-8	ms	2.44	22.3	3.55	1	207	0.30	0.82	0.61	<0.5	0.55	0.15	308	1	32.2	3.43
RR325-16	blt	1.97	1.6	2.36	1	260	0.20	0.57	0.47	<0.5	0.40	0.10	732	1	24.2	2.36
RR358-1	ms	1.71	64.3	2.01	2	79	0.40	0.35	0.75	<0.5	0.25	0.24	334	4	13.1	1.57

Appendix II: Table 1 cont.
Major oxide and trace element geochemistry

Sample	Unit	Zr (ppm)	As (ppm)	Bi (ppm)	Hg (ppm)	Sb (ppm)	Se (ppm)	Te (ppm)	LOI (%)	Total (%)	Au (ppb)	Ag (ppm)	Cd (ppm)	Co (ppm)	Cu (ppm)	Mo (ppm)
RR198-7	fs	96	107.5	0.28	0.11	3.78	1.60	0.49	7.19	98.8	120	<0.5	1.7	19	109	2
RR198-8	ms	182	7.4	1.46	0.03	0.15	1.10	0.47	10.50	97.3	N/A	<0.5	<0.5	52	55	1
RR198-10	ms	94	25.7	0.30	0.11	0.56	0.80	3.03	5.59	97.1	575	5.4	1.8	32	65	1
RR198-11	dlf	108	18.6	0.23	0.03	0.53	0.20	0.36	4.50	99.9	N/A	<0.5	<0.5	11	14	2
RR198-12	db	104	6.8	0.20	0.03	0.34	0.30	0.10	6.71	101.0	82	<0.5	<0.5	37	70	2
RR198-13	dlf	103	8.7	0.12	0.03	0.16	0.20	0.12	2.30	100.5	38	<0.5	<0.5	14	54	2
RR227-3	mbx	102	45.7	2.20	0.02	0.23	0.40	0.29	4.40	99.9	14	<0.5	<0.5	9	21	<1
RR227-5	pbx	109	4.2	2.51	0.02	0.10	1.90	0.28	5.21	101.0	37	<0.5	<0.5	10	12	1
RR227-6	dlf	103	10.3	1.82	0.06	0.15	0.20	0.16	3.10	99.3	1342	<0.5	3.2	6	33	<1
RR249-2	ppr	92	165.0	1.63	0.10	0.93	3.10	3.33	11.10	92.2	60	3.2	<0.5	79	217	1
RR249-3	dsd	109	17.8	0.08	0.02	2.13	<0.2	0.05	4.90	101.5	N/A	<0.5	<0.5	10	14	1
RR249-9	dlf	102	43.1	0.04	0.03	0.56	<0.2	0.03	3.50	98.8	155	0.7	<0.5	6	9	1
RR274-4	dlf	107	1.6	0.02	0.03	0.10	<0.2	<0.01	3.00	98.1	N/A	<0.5	<0.5	3	3	2
RR274-6	fs	73	225.0	0.84	0.13	12.50	3.20	0.88	8.40	99.3	N/A	3.8	<0.5	33	104	3
RR274-12	gbr	123	3.4	0.18	0.02	0.31	0.50	0.20	1.40	98.9	N/A	<0.5	<0.5	43	58	1
RR274-13	dlf	85	23.8	0.95	0.07	0.40	0.70	0.16	3.70	99.9	N/A	0.5	1.1	9	13	1
RR306-2	dlf	111	4.4	0.01	0.02	0.17	<0.2	<0.01	2.50	99.2	N/A	<0.5	<0.5	6	2	1
RR306-8	dlf	103	1.4	0.17	0.02	0.11	0.30	0.03	2.60	99.0	N/A	<0.5	<0.5	5	2	2
RR311-3	dsd	97	1.9	0.20	0.02	0.32	0.20	0.17	2.61	99.9	N/A	0.5	<0.5	3	37	1
RR311-11	pbx	42	8.1	0.07	0.02	0.79	<0.2	0.03	2.50	101.0	50	<0.5	<0.5	47	12	1
RR311-15	ms	73	5.2	0.74	0.01	0.27	0.80	0.32	2.30	98.9	851	<0.5	<0.5	8	37	3
RR322-10	dsd	97	64.5	0.84	0.07	0.24	0.20	0.09	4.60	98.6	N/A	<0.5	4.2	6	34	2
RR322-11	dsd	96	9.7	5.44	0.01	0.13	1.40	3.32	3.10	98.9	35	<0.5	<0.5	11	11	<1
RR325-7	dlf	107	6.9	0.06	0.02	0.16	<0.2	0.01	4.50	98.9	5	<0.5	<0.5	9	18	<1
RR325-8	ms	93	36.2	2.62	0.03	1.11	0.80	0.79	8.22	96.2	124	1.4	1.6	44	137	<1
RR325-16	blt	70	2.0	0.45	0.03	0.21	0.50	0.05	6.41	97.7	114	<0.5	<0.5	24	117	<1
RR358-1	ms	90	40.5	0.51	0.39	3.15	1.00	12.05	4.50	99.0	627	18.1	<0.5	32	139	<1

Appendix II: Table 1 cont.
Major oxide and trace element geochemistry

Sample	Unit	Ni (ppm)	Pb (ppm)	Zn (ppm)	C (%)	CO2 (%)	H2O (%)	H2O+ (%)	Recvd Wt. (kg)
RR198-7	fs	36	34	527	0.58	2.10	0.07	2.67	0.04
RR198-8	ms	255	7	301	2.17	8.00	0.11	6.54	0.07
RR198-10	ms	66	7	880	0.84	3.10	0.10	5.81	0.04
RR198-11	dlf	14	4	85	0.86	3.20	0.10	2.50	0.03
RR198-12	db	67	8	272	1.66	6.10	0.05	2.07	0.05
RR198-13	dlf	12	6	40	0.27	1.00	<0.01	1.35	0.04
RR227-3	mbx	9	4	92	0.09	0.30	0.09	2.90	0.03
RR227-5	pbx	11	5	69	0.08	0.30	0.10	3.31	0.04
RR227-6	dlf	4	3	1155	0.22	0.80	0.14	3.36	0.04
RR249-2	ppr	54	13	412	0.76	2.80	0.10	4.17	0.06
RR249-3	dsd	18	6	76	0.73	2.70	0.09	3.25	0.05
RR249-9	dlf	7	8	50	0.35	1.30	0.08	2.48	0.05
RR274-4	dlf	2	2	23	0.32	1.20	0.06	2.84	0.06
RR274-6	fs	58	50	205	0.70	2.60	0.21	1.37	0.06
RR274-12	gbr	68	11	251	0.09	0.30	0.12	2.96	0.07
RR274-13	dlf	8	23	462	0.24	0.90	0.13	2.22	0.06
RR306-2	dlf	4	6	43	0.41	1.50	0.11	1.46	0.07
RR306-8	dlf	4	6	24	0.19	0.70	0.12	2.11	0.07
RR311-3	dsd	11	4	24	0.55	2.00	0.10	1.56	0.06
RR311-11	pbx	224	3	90	0.06	0.20	0.21	3.95	0.08
RR311-15	ms	30	2	32	0.35	1.30	0.06	1.35	0.08
RR322-10	dsd	11	32	973	0.88	3.20	0.10	1.78	0.05
RR322-11	dsd	13	10	50	0.28	1.00	0.09	1.15	0.06
RR325-7	dlf	9	6	125	0.68	2.50	0.12	2.63	0.06
RR325-8	ms	74	5	793	1.92	7.00	0.11	5.75	0.07
RR325-16	blt	71	4	155	0.54	2.00	0.12	8.60	0.08
RR358-1	ms	82	6	276	0.25	0.90	0.14	3.74	0.04

Appendix II: Table 1 cont.
Major oxide and trace element geochemistry

Sample	Unit	SiO2 (%)	Al2O3 (%)	Fe2O3 (%)	CaO (%)	MgO (%)	Na2O (%)	K2O (%)	Cr2O3 (%)	TiO2 (%)	MnO (%)	P2O5 (%)	SrO (%)	BaO (%)	C (%)	S (%)
RR358-7	dlf	66.5	15.7	3.2	2.18	2.11	0.49	4.03	0.01	0.42	0.34	0.13	0.01	0.05	0.42	1.52
RR393-2	dlf	62.9	15.4	4.3	1.50	2.44	0.96	2.69	0.01	0.45	0.04	0.17	0.05	0.06	0.31	0.04
RR393-5	dsd	65.6	15.7	2.8	2.55	1.12	3.72	1.94	<0.01	0.34	0.03	0.09	0.05	0.05	0.68	1.03
RR393-9	dsd	64.6	15.4	4.5	1.19	1.65	1.15	2.81	<0.01	0.40	0.04	0.14	0.03	0.05	0.33	2.90
RR421-2	dlf	70.3	13.3	2.0	3.41	1.85	1.69	1.33	<0.01	0.33	0.06	0.10	0.05	0.05	0.21	1.06
RR421-3	dlf	64.3	12.5	5.0	4.49	3.19	1.26	0.85	<0.01	0.32	0.12	0.13	0.03	0.02	0.80	3.39
RR421-4	mbx	65.2	14.9	5.9	2.04	2.21	1.34	1.66	<0.01	0.42	0.05	0.09	0.04	0.05	0.03	2.77
RR421-5	dlf	67.7	13.9	3.2	3.85	1.74	3.16	1.05	<0.01	0.32	0.12	0.11	0.05	0.04	0.31	0.78
RR421-6	dlf	65.3	14.2	4.2	3.16	2.12	3.11	0.75	<0.01	0.36	0.06	0.10	0.05	0.02	0.10	1.79
RR421-7	dlf	65.5	14.5	4.6	1.54	3.70	0.96	2.00	<0.01	0.34	0.06	0.11	0.03	0.04	0.06	1.61
RR456-2	ms	37.7	11.6	15.5	12.25	4.28	2.62	0.02	0.01	1.78	0.19	0.19	0.06	<0.01	2.72	1.54
RR456-3	dlf	62.9	14.7	3.9	3.86	1.88	1.42	2.11	<0.01	0.37	0.06	0.10	0.05	0.06	1.56	0.93
RR458-6	dlf	67.1	16.8	1.9	1.98	0.46	1.61	3.32	<0.01	0.43	0.02	0.16	0.07	0.09	0.12	0.18
RR458-7	dlf	68.2	16.5	2.7	2.81	0.68	1.89	2.50	<0.01	0.43	0.03	0.18	0.08	0.07	0.12	0.27
RR511-7	ms	43.2	15.7	11.5	7.92	5.27	2.86	0.66	0.02	1.05	0.21	0.13	0.02	0.01	1.76	0.50

Appendix II: Table 1 cont.
Major oxide and trace element geochemistry

Sample	Unit	Ba (ppm)	Ce (ppm)	Cr (ppm)	Cs (ppm)	Dy (ppm)	Er (ppm)	Eu (ppm)	Ga (ppm)	Gd (ppm)	Hf (ppm)	Ho (ppm)	La (ppm)	Lu (ppm)	Nb (ppm)	Nd (ppm)
RR358-7	dlf	437	43.4	40	10.90	1.10	0.59	0.81	21.7	2.37	2.8	0.20	21.8	0.09	2.3	19.4
RR393-2	dlf	616	54.1	60	11.75	1.19	0.60	0.80	21.8	2.87	3.2	0.20	26.7	0.08	3.0	23.9
RR393-5	dsd	436	29.9	30	5.40	0.91	0.49	0.59	22.1	1.89	3.0	0.17	15.3	0.08	2.5	12.7
RR393-9	dsd	430	43.2	30	6.59	0.93	0.49	0.74	21.5	2.23	2.9	0.17	22.7	0.06	2.3	17.5
RR421-2	dlf	421	23.8	20	8.53	0.67	0.36	0.53	19.2	1.42	2.6	0.12	11.8	0.05	1.9	10.5
RR421-3	dlf	194	37.3	20	3.76	0.92	0.44	0.89	19.1	2.07	2.5	0.16	18.8	0.05	2.2	15.1
RR421-4	mbx	392	30.0	30	6.93	0.86	0.46	0.61	21.0	1.77	2.9	0.15	15.8	0.06	2.3	12.4
RR421-5	dlf	335	26.3	30	9.06	0.78	0.39	0.49	19.0	1.59	2.6	0.14	14.0	0.05	1.9	10.9
RR421-6	dlf	201	23.4	30	3.53	0.80	0.43	0.53	19.0	1.53	2.8	0.15	12.4	0.06	2.0	9.7
RR421-7	dlf	346	44.8	20	5.40	0.88	0.42	0.71	19.8	2.18	2.9	0.15	24.7	0.06	2.2	16.6
RR456-2	ms	4	18.0	60	0.22	4.93	3.22	1.34	20.1	4.36	2.4	1.07	7.5	0.54	4.3	11.6
RR456-3	dlf	502	31.7	30	6.69	0.99	0.53	0.65	19.8	1.98	2.8	0.18	16.0	0.09	2.2	13.7
RR458-6	dlf	718	57.3	20	12.30	1.24	0.69	0.92	23.4	3.03	3.3	0.22	28.2	0.09	2.6	25.1
RR458-7	dlf	579	62.0	20	9.60	1.38	0.74	1.07	22.6	3.52	3.6	0.24	30.2	0.10	2.5	28.1
RR511-7	ms	116	10.9	170	2.33	2.96	1.82	0.89	18.4	2.76	1.5	0.62	4.6	0.30	2.6	7.4

Appendix II: Table 1 cont.
Major oxide and trace element geochemistry

Sample	Unit	Pr (ppm)	Rb (ppm)	Sm (ppm)	Sn (ppm)	Sr (ppm)	Ta (ppm)	Tb (ppm)	Th (ppm)	Tl (ppm)	Tm (ppm)	U (ppm)	V (ppm)	W (ppm)	Y (ppm)	Yb (ppm)
RR358-7	dlf	5.35	132.0	3.04	1	117	0.20	0.26	2.62	1.3	0.11	0.69	74	2	6.0	0.55
RR393-2	dlf	6.75	73.6	3.52	1	432	0.20	0.30	3.13	0.5	0.10	0.62	86	3	6.0	0.54
RR393-5	dsd	3.63	57.5	2.16	1	402	0.20	0.21	2.45	<0.5	0.09	0.64	46	1	5.1	0.47
RR393-9	dsd	5.13	96.7	2.63	1	224	0.20	0.23	2.91	0.7	0.08	0.69	50	2	5.1	0.43
RR421-2	dlf	2.97	41.5	1.74	1	399	0.10	0.16	2.32	<0.5	0.07	0.52	47	2	3.7	0.34
RR421-3	dlf	4.49	24.1	2.43	1	282	0.10	0.22	2.83	<0.5	0.08	0.70	42	2	4.9	0.36
RR421-4	mbx	3.58	52.7	2.04	1	331	0.20	0.19	2.18	<0.5	0.09	0.60	48	4	4.6	0.43
RR421-5	dlf	3.13	34.6	1.85	<1	387	0.10	0.17	2.03	<0.5	0.08	0.49	39	1	4.2	0.36
RR421-6	dlf	2.78	22.3	1.72	1	434	0.10	0.18	1.94	<0.5	0.08	0.51	43	2	4.5	0.41
RR421-7	dlf	5.04	58.4	2.51	1	215	0.20	0.21	3.00	<0.5	0.08	0.71	35	3	4.9	0.37
RR456-2	ms	2.65	0.5	3.48	1	465	0.30	0.77	0.59	<0.5	0.55	0.17	292	1	31.2	3.38
RR456-3	dlf	3.88	61.2	2.26	1	400	0.20	0.22	2.20	<0.5	0.10	0.61	57	2	5.6	0.53
RR458-6	dlf	7.15	69.2	3.80	1	585	0.30	0.30	4.75	<0.5	0.11	1.15	60	<1	6.8	0.63
RR458-7	dlf	7.93	52.3	4.54	1	699	0.20	0.35	4.98	<0.5	0.12	1.14	58	<1	7.5	0.64
RR511-7	ms	1.64	17.6	2.24	1	139	0.20	0.47	0.37	<0.5	0.31	0.09	199	<1	17.7	1.86

Appendix II: Table 1 cont.
Major oxide and trace element geochemistry

Sample	Unit	Zr (ppm)	As (ppm)	Bi (ppm)	Hg (ppm)	Sb (ppm)	Se (ppm)	Te (ppm)	LOI (%)	Total (%)	Au (ppb)	Ag (ppm)	Cd (ppm)	Co (ppm)	Cu (ppm)	Mo (ppm)
RR358-7	dlf	95	53.2	0.16	0.04	0.44	<0.2	0.13	4.10	99.3	102	<0.5	<0.5	10	18	<1
RR393-2	dlf	106	1.1	0.03	0.03	0.09	<0.2	0.08	4.49	95.4	N/A	<0.5	<0.5	4	29	<1
RR393-5	dsd	103	1.4	0.12	0.02	0.12	0.60	0.10	3.90	97.9	N/A	<0.5	<0.5	7	79	<1
RR393-9	dsd	103	9.9	2.22	0.03	0.49	0.80	0.81	4.70	96.6	N/A	0.8	<0.5	9	25	<1
RR421-2	dlf	92	9.3	0.72	0.03	0.25	0.20	0.18	2.20	96.7	85	<0.5	<0.5	5	23	<1
RR421-3	dlf	91	4.2	2.29	0.70	0.35	2.40	1.48	5.01	97.2	N/A	1.8	36.9	6	462	<1
RR421-4	mbx	105	10.9	9.61	0.02	0.18	1.50	0.48	3.80	97.7	121	1.0	<0.5	9	74	2
RR421-5	dlf	93	2.9	0.35	0.03	0.13	0.20	0.11	1.90	97.2	122	<0.5	0.6	6	29	<1
RR421-6	dlf	99	5.3	2.15	0.02	0.15	0.50	0.41	2.90	96.3	36	<0.5	<0.5	8	77	1
RR421-7	dlf	100	13.7	5.83	0.02	0.31	0.80	0.38	3.90	97.3	49	0.6	<0.5	7	28	<1
RR456-2	ms	83	1.4	0.34	0.04	0.08	1.60	0.33	10.30	96.4	N/A	0.5	<0.5	28	1940	<1
RR456-3	dlf	98	49.9	0.07	0.03	0.40	<0.2	0.01	6.50	97.9	N/A	<0.5	<0.5	13	15	<1
RR458-6	dlf	110	5.4	0.07	0.02	0.39	<0.2	0.01	2.10	96.1	N/A	<0.5	<0.5	6	12	<1
RR458-7	dlf	124	10.5	0.08	0.02	0.41	<0.2	0.03	1.99	98.0	75	<0.5	<0.5	6	11	<1
RR511-7	ms	51	8.1	0.13	0.02	0.11	1.30	0.01	9.61	98.2	N/A	<0.5	<0.5	21	18	<1

Appendix II: Table 1 cont.
Major oxide and trace element geochemistry

Sample	Unit	Ni (ppm)	Pb (ppm)	Zn (ppm)	C (%)	CO2 (%)	H2O (%)	H2O+ (%)	Recvd Wt. (kg)
RR358-7	dlf	16	37	88	0.38	1.40	0.12	3.08	0.06
RR393-2	dlf	31	4	115	0.28	1.00	0.21	3.94	0.06
RR393-5	dsd	7	3	46	0.62	2.30	0.08	1.71	0.06
RR393-9	dsd	12	9	159	0.30	1.10	0.08	2.64	0.06
RR421-2	dlf	3	12	162	0.20	0.70	0.07	1.48	0.06
RR421-3	dlf	5	8	7750	0.76	2.80	0.09	2.77	0.06
RR421-4	mbx	6	9	63	<0.05	<0.2	0.07	2.31	0.05
RR421-5	dlf	5	4	237	0.28	1.00	0.06	0.86	0.05
RR421-6	dlf	5	6	81	0.09	0.30	0.05	1.34	0.08
RR421-7	dlf	3	5	119	0.05	0.20	0.12	3.84	0.04
RR456-2	ms	38	<2	68	2.67	9.80	0.10	4.50	0.07
RR456-3	dlf	10	13	63	1.51	5.50	0.06	2.18	0.09
RR458-6	dlf	4	7	11	0.11	0.40	0.13	1.84	0.11
RR458-7	dlf	4	8	26	0.11	0.40	0.14	1.86	0.11
RR511-7	ms	89	4	120	1.68	6.20	0.15	5.76	0.07